Investigation of Soft Lewis Acid Function in Supported Noble Metal Nano-catalysts for Sustainable Synthesis

黄, 啓安

KYUSHU UNIVERSITY
GRADUATE SCHOOL OF SCIENCE

A THESIS SUBMITTED FOR THE DEGREE OF

DOCTOR OF PHILOSOPHY

Investigation of Soft Lewis Acid Function in Supported Noble Metal Nano-catalysts for Sustainable Synthesis

HUANG QIAN

Department of Chemistry

December 2022

Abstract

Metal oxide supported noble metal catalysts show many significant advantages such as low cost, high durability, and mass-producibility. In research on supported catalysts, investigating and determining the real active species and sites on the inorganic solids in various reactions were important. However, the supported noble metals are distributed rather than single species, and the reaction mechanism has not been well elucidated compared to molecular catalysts. Therefore, their research was inadequate, which hindered their industrialization. In this research, study on the development and analysis of soft Lewis acid functions of metal oxide supported noble metal catalysts was performed, and the application of these reusable soft Lewis acid catalysts can offer new opportunities for industrial processes and syntheses.

In the hard-soft acid-base (HSAB) principle, Lewis acids can be classified into hard and soft acids which can activate corresponding hard or soft bases. In industrial catalytic reactions, zeolites, typical hard acids, have been widely used. However, most reactions over soft Lewis acids were still using homogeneous catalysts. The low-valent noble metals have soft characteristics and thus should function as a soft Lewis acid to activate soft bases, such as π electrons of C–C double and triple bonds, which easilt undergo nucleophilic attack with various nucleophiles. Because Au and Pt are the soft transition metals according to the HSAB principle, the supported Au and Pt catalysts were mainly discussed in this thesis.

It was demonstrated for the first time that supported Pt catalysts with residual chloride can act as a heterogeneous soft Lewis acid. For the application to isomerization of allylic esters, high turnover numbers were realized under solvent-free conditions. X-ray photoelectron spectroscopy (XPS) and X-ray absorption fine structure (XAFS) analyses reveal that the highly dispersed Pt clusters with Pt–Cl bonds play a key role in the high activity. In addition, DFT calculation and controlling tests verify the reaction mechanism and the enhancement effect in Lewis acidity owing to the residual chloride.

Additionally, reusability of Pt-Cl/CeO_2 was investigated, and the activity was proven to be recovered. XAFS was used to understand the deactivation mechanism of

the catalysts. The reduction of PtO_xCl_y species should be the main reason for deactivation. A relatively stable state may occur during the reusing of Pt-Cl/CeO_2.

To develop a more stable soft Lewis catalysts, research on the catalytic isomerization of allylic esters with zirconia supported Au nanoparticles (NPs) succeed. It offers a practical application in the transformation between but-3-ene-1,2-diyl diacetate (3,4-DABE) and but-2-ene-1,4-diyl acetate (1,4-DABE), valuable intermediates of butanediol or THF. Furthermore, a total turnover number (TON) of more than 38,000 are available by flow reaction with the total scale up to kilogram. Meanwhile, there is no obvious deactivation despite slight agglutination of Au NPs.

Moreover, supported sodium-salt-modified Au NPs catalyst was developed, and it was stable and recyclable in the intramolecular cyclization of alkynoic acids. The effect of sodium species, which has been overlooked in previous studies, was studied, and they were found to play an essential role. In addition, the relationship between the kinetics and size of Au NPs revealed that the active sites of the catalyst are located on the surface of Au NPs. Detailed kinetic studies revealed that the cyclization was a zero-order reaction with respect to substrate concentration, and the rate-determining step of the reaction is presumed to be protodeauration.

Furthermore, a practical method for regulating and optimizing the activities of metal-oxide supported Au NP catalysts was discovered. Its effect was investigated in the multiple reactions based on the soft Lewis acid function of Au NPs. By comparing the relationship between specific surface areas and catalytic activities of the prepared metal-oxide supported Au NP catalysts, the catalysts with smaller specific surface area showed better catalytic activity. This tread was obtained in the soft Lewis acid reactions, including isomerization, cyclization, and hydroamination reactions. XPS spectra reveal that the Au NPs supported by the metal-oxides with low specific surface areas tend to have higher binding energy, revealing that more $Au^{\delta+}$ species form on their surfaces.

Finally, to further enhance the sustainability of the C4 synthesis process, one-pot synthesis of THF from 1,4-DABE was also developed by preparing bi-functional Rh/Al-MCM-41catalysts. In addition, a yield around 60% was obtained using the optimized catalysts.

Content

Abstract

Chapter 1. General Introduction

1.1. Soft Lewis Acid Catalysis……..…….2

1.2. Supported Noble Metal Catalysts……..…….4

1.3. Sustainable Synthesis and Catalysis....……..……5

1.4. This research…… ……..……8

1.5. References……..……9

Chapter 2. Pt/CeO_2 with residual chloride as reusable soft Lewis acid catalysts: Application to highly efficient isomerization of allylic esters

2.1. Introduction……12

2.2. Experimental……..……16

2.3. Results and Discussion…….……..……19

2.4. Conclusion…….…….……43

2.5. References…….…….……43

Chapter 3. Investigation of reusability and deactivation mechanism of supported Pt catalysts in the practical isomerization of allylic esters

3.1. Introduction……49

3.2. Experimental……..……51

3.3. Results and Discussion…….……..……52

3.4. Conclusion…….…….……61

3.5. References…….…….……62

Chapter 4. Engineering active and stable Au/ZrO_2 catalysts for isomerization of allylic esters: a practical application of gold catalysis

4.1. Introduction……65

4.2. Experimental……..……68

4.3. Results and Discussion…….……..……70

4.4. Conclusion…….…….……86

4.5. References……87

Chapter 5. Intramolecular cyclization of alkynoic acid catalyzed by Na-salt-modified Au nanoparticles supported on metal oxides

5.1. Introduction……91

5.2. Experimental……94

5.3. Results and Discussion……97

5.4. Conclusion……122

5.5. References……123

Chapter 6. Effect of the structure of metal oxide support on the activity of supported Au nanoparticles in soft Lewis acid catalysis

6.1. Introduction……129

6.2. Experimental……131

6.3. Results and Discussion……134

6.4. Conclusion……160

6.5. References……161

Chapter 7. One-pot synthesis of THF from but-2-ene-1,4-diyl acetate (1,4-DABE) over bifunctional rhodium silica-alumina catalysts

6.1. Introduction……164

6.2. Experimental……166

6.3. Results and Discussion……168

6.4. Conclusion……173

6.5. References……174

Concluding Remarks……176

Acknowledgments……177

List of Publication……178

Chapter 1.
General Introduction

1.1. Soft Lewis Acid Catalysis

The Lewis acid-base theory is well known as that Lewis acids accept electrons and Lewis bases donate electrons, and this is more general than the Bronsted acid-base theory, since the Lewis acids may contain halides in higher oxidation states of metals. The hard-soft acid-base (HSAB) theory was later developed by Pearson and describes the stability of acid-base adducts by classifying both acids and bases as hard and soft. Hard acids are characterized by small atomic radii, highly positive charges, and generally no unshared electron pairs in their valence shells. These correspond to the properties of hard bases. Soft acids, on the other hand, have large atomic radii, low positive charge, and contain unshared electron pairs (p or d electrons) in their valence shells. These correspond to the characteristics of soft bases [1–3]. According to the concept of HSAB, metals prefer ligands of the same kind (soft–soft or hard–hard) when forming coordinated bonds. Cations act as Lewis acids by accepting non-bonding electrons from ligands to form coordinative bonds[4]. A plot of the softness of a range of cations and anions of different valency, with respect to H^+ and OH^- ions of zero softness, was summarized (Fig. 1). In addition, the anions of higher softness have lower Lewis basicity; however, divalent cations have higher Lewis acidity compared to monovalent cations[5].

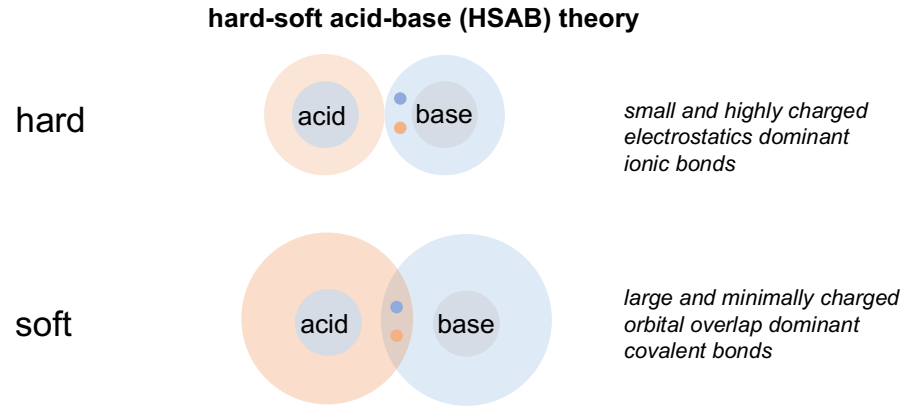

hardness of anions/cations

anions:

$PO_4^{3-} > F^- > CO_3^{2-} > SO_4^{2-} > Cl^- > OH^- > NO_3^- > Br^- > CN^- > I^- > HS^- > SO_3^{2-} > S^{2-}$

cations:

$Ca^{2+} > NH_4^+ > Na^+ > K^+ > Mg^{2+} > Cu^+ > H^+ > Ag^+ > Fe^{3+} > Zn^{2+} > Cu^{2+} > Pb^{2+} > Au^+$

Figure 1. Illustration of HSAB theory and hardness of partial anions and cations[5].

The great attraction of Lewis acid catalysts is their activity, reactivity, and selectivity in organic and inorganic synthesis, and the selectivity of Lewis acid catalysts is one of the important issues in modern catalytic chemistry. Metal catalysts that activate the π-electrons of alkenes, alkynes, aromatics (soft bases), etc. to promote attack by oxygen or nitrogen nucleophiles are called soft Lewis acid catalysts[6]. Solid acid catalysts are widely used in petrochemical reactions, synthesis of fine chemicals, and biomass conversion in industry. However, as solid acid catalysts, protonic acids such as zeolite and cation exchange resins are hard Lewis acids. The reaction tends to be complicated due to rearrangement of carbocation. That is, the selectivity tends to be low. Unlike hard Lewis acids, soft Lewis acids can coexist with water and alcohols. Au and Pt are the soft transition metals according to the HSAB principle. The low-valent noble metals have soft functions and thus should act as a soft Lewis acid to activate soft bases, such as, π-electrons of C–C double and triple bonds, to undergo nucleophilic attack with nucleophiles. Despite these catalysts provide many useful synthetic applications, the poor reusabilities and small turnover numbers (TONs) hinder their practical application. Therefore, their applications are still limited.

For soft Lewis acid catalysts, there are many examples of homogeneous catalysts. To satisfy the principles of green sustainable synthesis, the development of heterogeneous soft Lewis acid catalysts become meaningful. Over the last decades, several reactions using supported noble metal nanoparticles (NPs) as a soft Lewis acid catalysts were reported. Corma et al. reported catalytic hydroamination using supported Au catalysts[7]. In general, monovalent Au species exhibit soft Lewis acidity, but when they are immobilized on a support, reduction to stable zero-valent Au NPs and aggregation should occurr. In addition, Somorjai et al. also successfully used supported Au NPs with N-heterocyclic carbenes (NHCs) for lactonization[8]. However, exhaustion of the ligand becomes a problem. Moreover, our team have also reported hydroamination[9], direct C–H arene homocoupling[10], and Wacker oxidation[11] using supported Au and Pd catalysts with soft Lewis acid functions.

In Lewis acid-base catalysis, the counter-anion is significant to expand the Lewis acid function. The stronger the conjugated acid of the counter-anion promote better Lewis acidity. Besides, the Lewis acidity could also be enhanced by isolated cation, such as frustrated Lewis pairs. However, soft cations are easily reduced to zero-valences and easily aggregate, making it difficult to maintain activity. In addition, the systematization of heterogeneous soft Lewis acid catalysts is still insufficient, and their active sites, stabilities, and industrial applications need to be further discussed.

1.2.Supported Noble Metal Catalysts

In recent decades, supported noble metal catalysts have been widely researched, and most of them were prepared in the form of supported nanoparticles, nanolayers, clusters and single atoms[12]. In the catalytic reactions, different supported structures often cause different catalytic activities. Meanwhile, the main target of structure design or optimization is to improve the atomic efficiency of noble metal[13].

Supported Pt catalysts have been well researched in the fields of fuel cells[14], oxygen reduction reaction[15], and automobile industry[16]. In the catalytic reaction of the sustainable synthesis, dispersion of Pt species on the surface of supports is an important factor that may control the activity. Many efforts have been focused on this field in recent years, and single-atom catalysts provide a new frontier in heterogeneous catalysis due to the improved atom efficiency. On the other hand, atomically dispersed Pt species can be synthesized simply by calcination treatment when using the CeO_2 as support[17]. In fact, current applications of supported Pt catalysts are mainly based on the redox function. Despite homogenous Pt(II) complexes have been employed in the reactions, such as hydration of alkynes and nitriles[18], cyclization of alkynes[19]. However, there are no reports on the supported Pt catalysts with soft Lewis acidity; thus, supported Pt catalysts with soft Lewis acid function would be a promising heterogeneous catalysts.

Supported Au NPs catalysts are usually considered as the main form of heterogeneous Au catalysts, and the synthesis of small Au NPs on the supports should

be an important target when optimizing the activity of Au catalysts[20]. Nowadays, the most general preparation method used for the synthesis of Au NPs on metal oxides are known as deposition-precipitation, and it was proved as a convenient way to synthesize Au NPs with a diameter around of 3 nm on the support[21]. Normally, the activity of the metal NPs catalysts increased when the diameters of the particles decreased. Regarding the redox function of Au NP catalysts, the oxidation of CO to CO_2 was firstly developed by Haruta et al[22]. However, studies on π-activating reactions of alkenes, alkynes, and aromatics as soft Lewis acid catalysts are insufficient. On the other hand, gold complex catalysts have been greatly developed mainly for application to sustainable synthesis, but their application is insufficient due to problems in activity and stability. In several reports, zero-valent Au NPs have been demonstrated to be able to use as soft Lewis acid catalysts, which should be promising stable catalysts; therefore, further systematic research on soft Lewis acidic reactions catalyzed by supported gold NPs is expected to develop active and stable gold catalysts that can be industrialized.

1.3. Sustainable Synthesis and Catalysis

Supported noble metal catalysts have been developed in the synthesis of several valuable compounds. Because these catalysts can avoid energy-intensive separation processes and have a long lifetime during the application, they are considered important tools for achieving sustainable synthesis.

Catalytic reaction based on the C4 compounds, such as buta-1,3-diene, was of great significance to the development of the chemical industry. The application of supported noble metal catalysts in this field can even help realize emissions reduction, which is consistent with the concept of sustainable development goals. Tetrahydrofuran (THF) is a solvent with excellent properties and an important raw material for the synthesis of several polyurethane elastic fibers, and about million tons of THF are produced annually. In this synthesis route, byproduct but-3-ene-1,2-diyl diacetate (3,4-DABE) formed during the unit reaction of catalytic acetoxylation[23]. Thousand tons of 3,4-DABE were treated by burning every year (scheme 1). Transformation of 3,4-

DABE into its isomer but-3-ene-1,2-diyl diacetate (1,4-DABE) could be proceeded by soft Lewis acid catalysts; therefore, the isomerization of 3,4-DABE should be a practical reaction to study the performance of heterogeneous soft Lewis acid catalysts.

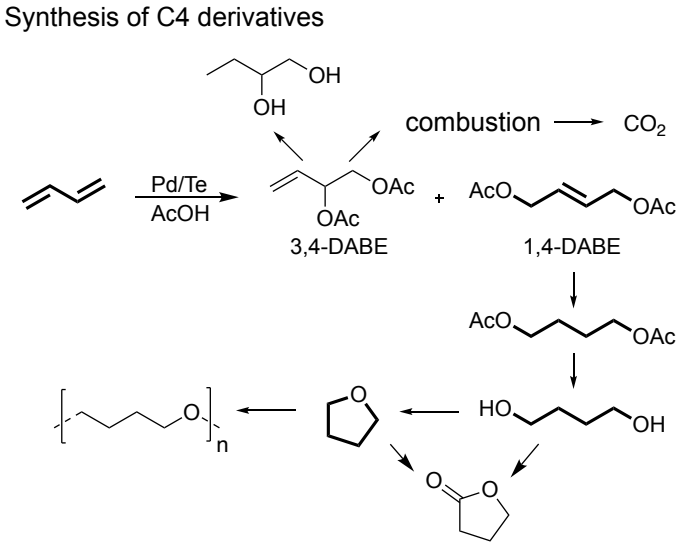

Scheme 1. Catalytic reaction and the C4 derivatives from buta-1,3-diene.

Producing methyl methacrylate (MMA) from *tert*-butyl alcohol was another significant industrial synthesis route. In the past, the plant usually used a three-step process, including the oxidation to methacrolein, subsequent oxidation to methacrylic acid, and the final esterification with methanol[24].This process needed high investment costs, and the catalyst in the second oxidation step showed short lifetime[25]. To solve this problem, a short process where methacrolein was oxidatively esterifies with methanol to produce the MMA directly, called Direct-Metha Process (Scheme 2)[26]. In this new process, Au-NiO/SiO_2-Al_2O_3-MgO with a core-shell structure was identified as the best catalyst. In addition, the practical applicability of this catalytic system was verified in a 100,000 ton/year plant, and high selectivity, high activity, and long lifetime of the optimized Au catalysts were demonstrated. Thus, the developed catalysts help save energy and resources, and make the process become highly economical in the chemical synthesis.

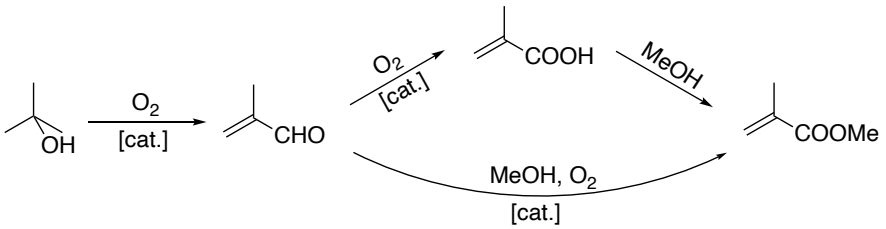

Scheme 2. The old Asahi process (upper route) and the new Direct-MethaProcess (lower route) to methyl methacrylate[25].

Heterogeneous catalysts due to the insolubility in the solvents or liquid substrates are usually evaluated in batch reactors. However, with the benefits of continuous flow reactors, the application of heterogeneous catalysts in flow reaction gradually becomes prevalent with the development of a column reactor. When the heterogeneous catalysts are filled in the column reactor, the continuous product formation, long lifetime of catalysts and high turnover frequency could be achieved. This technology can bring environmental and economic benefits.

Suzuki-Miyaura cross-coupling reaction was an important catalytic reaction, and the continuous flow synthesis with this reaction was also of great significance. Qu et al. rationally designed a novel noble metal/graphene/nylon rope to act as a highly efficient catalyst for the continuous-flow organic reactions, and they showed that different noble metal (Pd, Pt, Au and Ag) nano-catalysts and graphene can be readily assembled by a one-step hydrothermal method[27]. The high catalytic activity and stability of the catalysts developed were demonstrated in the 4-nitrophenol reduction reaction, as well as the Suzuki-Miyaura cross-coupling reaction.

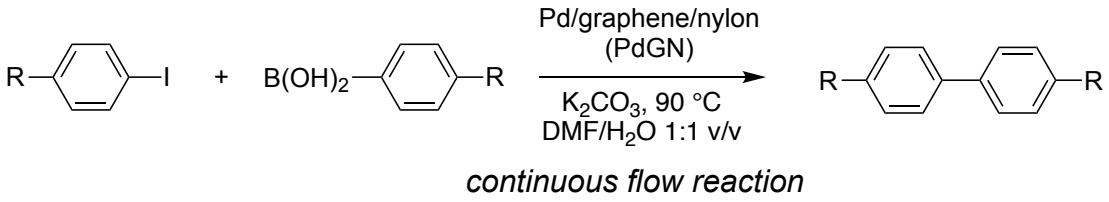

Figure 2. Schematic representation of continuous-flow system of Suzuki-Miyaura cross-coupling reaction catalyzed by the supported Pd catalysts[27].

In addition, it was also reported that supported AuNPs are suitable for being employed as catalysts in the oxidation of alcohols in continuous-flow packed bed reactors[28]. In this research, Au NPs were anchored on alkynyl carbamate-

functionalized support materials, which should be the suitable features for application as catalysts in continuous-flow reaction. Moreover, Au/SiO_2@Yne was demonstrated as an efficient catalyst, both in batch and continuous-flow conditions, and it could be applied in the oxidation of several alcohols using H_2O_2 as the oxidizing agent. Furthermore, under flow conditions, no significant decrease in the catalytic activity was observed when the catalyst worked for over 50 h. It was also found that the flow approach plays a strategic role in preserving the physical and chemical integrity of the heterogeneous catalysts during the reaction, with remarkable consequences for the reaction conversion (from 2% in batch to 80% in flow).

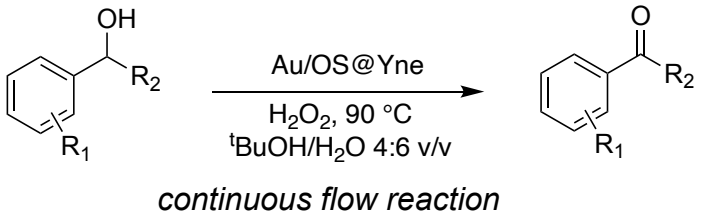

Figure 3. Illustration of supported Au NPs for alcohols oxidation in continuous flow heterogeneous systems[28].

1.4. This research

Herein, the soft Lewis acid function of supported noble metal catalysts were mainly discussed, and the active and stable catalysts were used to realize several sustainable syntheses. Pt/CeO_2 with residual chloride was proved to act as soft Lewis acids and facilitate the efficient isomerization of allylic esters. Meanwhile, reusability and deactivation mechanism of this Pt catalysts was investigated, and a great reactivation method was also developed. Moreover, a facile solvent-free methodology was developed for isomerization of allylic esters with supported Au NPs catalysts, which showed superior catalytic activity and stability. Lifetime and stability of the optimized catalyst were evaluated by a 14-day flow reaction in the scale of kilogram, and no obvious deactivation occurred. In addition, a sustainable catalytic system for the intramolecular cyclization of alkynoic acids by using Na-salt-modified Au NPs supported on monoclinic ZrO_2 was realized, and the positive and significant role of the

Na salt in this reaction was disclosed. Furthermore, a practical method for regulating and optimizing the activities of metal-oxide supported Au NP catalysts was well investigated. The catalysts with smaller specific surface area showed better catalytic activity, and this tread was obtained in the soft Lewis acid reactions, including isomerization, cyclization, and hydroamination reactions. Finally, to further enhance the sustainability of the C4 synthesis process, one-pot synthesis of THF was also developed.

1.5. Reference

[1] R. G. Pearson, J. Am. Chem. Soc. 85 (1963) 3533–3539.

[2] R. G. Pearson, J. Songstad, J. Am. Chem. Soc. 89 (1967) 1827–1836.

[3] R. G. Pearson, J. Am. Chem. Soc. 107 (1985) 6801–6806.

[4] R. D. Hancock, A. E. Martell, J. Chem. Educ. 73 (1996) 654–661.

[5] G. Senanayake, Hydrometallurgy 115–116 (2012) 1–20.

[6] A. Corma, H. García, Chem. Rev. 103 (2003) 4307–4366.

[7] A. Corma, P. Concepción, I. Domínguez, V. Forné, M.J. Sabater, J. Catal. 251 (2007) 39–47.

[8] R. Ye, A. V. Zhukhovitskiy, R. V. Kazantsev, S.C. Fakra, B.B. Wickemeyer, F.D. Toste, G.A. Somorjai, J. Am. Chem. Soc. 140 (2018) 4144–4149.

[9] Y. Yamane, X. Liu, A. Hamasaki, T. Ishida, M. Haruta, T. Yokoyama, M. Tokunaga, Org. Lett 11 (2009) 5162–5165.

[10] T. Ishida, R. Tsunoda, Z. Zhang, A. Hamasaki, T. Honma, H. Ohashi, T. Yokoyama, M. Tokunaga, Appl. Catal. B Environ. 150–151 (2014) 523–531.

[11] Z. Zhang, Y. Kumamoto, T. Hashiguchi, T Mamba, H. Murayama, E. Yamamoto, T. Ishida, T. Honma, M. Tokunaga, ChemSusChem 10 (2017) 3482–3489.

[12] L. Wang, R. Tang, A. Kheradmand, Y. Jiang, H. Wang, W. Yang, Z. Chen, X. Zhong, S.P. Ringer, X. Liao, W. Liang, J. Huang, Appl. Catal. B Environ. 284 (2021) 119759.

[13] Z. Jiang, M. Jing, X. Feng, J. Xiong, C. He, M. Douthwaite, L. Zheng, W. Song, J. Liu, Z. Qu, Appl. Catal. B Environ. 278 (2020) 119304.

[14] P. Mardle, X. Ji, J. Wu, S. Guan, H. Dong, S. Du, Appl. Catal. B Environ. 260 (2020) 118031.

[15] K. Ding, A. Gulec, A.M. Johnson, N.M. Schweitzer, G.D. Stucky, L.D. Marks, P.C. Stair, Science 350 (2015) 189–192.

[16] R.H. Nibbelke, A.J.L. Nievergeld, J.H.B.J. Hoebink, G.B. Marin, Appl. Catal. B Environ. 19 (1998) 245–259.

[17] N. Daelman, M. Capdevila-Cortada, N. López, Nat. Mater. 18 (2019) 1215–1221.

[18] X. Xing, C. Xu, B. Chen, C. Li, S.C. Virgil, R.H. Grubbs, J. Am. Chem. Soc. 140 (2018) 17782–17789.

[19] B. A. B. Prasad, F. K. Yoshimoto, R. Sarpong, J. Am. Chem. Soc. 127 (2005) 12468–12469.

[20] T. Ishida, T. Murayama, A. Taketoshi, M. Haruta, Chem. Rev. 120 (2020) 464–525.

[21] R. Zanella, L. Delannoy, C. Louis, Appl. Catal. 291 (2005) 62–67.

[22] M. Haruta, T. Kobayashi, H. Sano, N. Yamada, Chem. Lett. 16 (1987) 405–408.

[23] M. Misono, Appl. Catal. 64 (1990) 1–30.

[24] K. Suzuki, Petrotech 37 (2014) 642–646.

[25] R. Ciriminna, E. Falletta, C. D. Pina, J. H. Teles, M. Pagliaro, Angew. Chem. Int. Ed. 55 (2016) 14210–14217.

[26] K. Suzuki, T. Yamaguchi, K. Matsushita, C. Iitsuka, J. Miura, T. Akaogi, H. Ishida, ACS Catal. 3 (2013) 1845–1849.

[27] S. Zhang, X. Shen, Z. Zheng, Y. Ma, Y. Qu, J. Mater. Chem. A 3 (2015) 10504–10511.

[28] B. Ballarin, D. Barreca, E. Boanini, M. C. Cassani, P. Dambruoso, A. Massi, A. Mignani, D. Nanni, C. Parise, A. Zaghi, ACS Sustainable Chem. Eng. 5 (2017) 4746–4756.

Chapter 2.

Pt/CeO_2 with residual chloride as reusable soft Lewis acid catalysts: Application to highly efficient isomerization of allylic esters

2.1. Introduction

Supported Pt catalysts have been extensively researched and proven to play crucial roles in multiple applications, such as fuel cells[1], three-way catalysts[2], catalytic redox reactions[3], and value-added fine chemical reactions[4]. However, most applications of supported Pt catalysts are based on the redox function. On the other hand, to the best of our knowledge, there are no reports on the supported Pt catalysts using soft Lewis acidity, although homogenous Pt(II) complexes have been applied in the hydration of alkynes and nitriles[5], isomerization of allylbenzenes[6], cyclization of alkynes[7], etc. Therefore, a heterogeneous supported platinum catalyst with soft Lewis acidity would be a promising, practical, and environmental catalyst, which can be easily separated from the reaction mixture and reused.

For the Lewis acid-base catalysis, the counter-anion is important to the Lewis acid function. The stronger the conjugated acid of the counter-anion is, the greater the Lewis acidity showed by the central metal. In addition, Lewis acidity can also be increased when the cation is isolated, like the function of frustrated Lewis pairs. Whereas, soft cations such as Au(I) and Pd(II) are easily reduced and aggregate, which makes it difficult to keep their activity when apply them as immobilized catalysts.

Considering the goal of atom efficiency and the price of platinum, platinum catalysts that contain highly dispersed Pt or even single-atom Pt catalysts have attracted wide interest[8]. Besides, a special metal-support interaction between Pt and CeO_2 was discovered and studied, revealing that the trapping of platinum on the CeO_2 surface can facilitate and atomic dispersion[9,10]. Because of the properties of supported Pt in current applications, it is significant to develop supported Pt catalysts as soft Lewis acids.

Sustainable synthesis of C4 chemicals is significant in the chemical industry. During

the current catalytic reactions for C4 chemicals, there are still unusable byproducts, such as but-3-ene-1,2-diyl diacetate (3,4-DABE) (Fig. 1a). The minor product 3,4-DABE, an isomer of but-2-ene-1,4-diyl diacetate (1,4-DABE) which is an important intermediate to produce tetrahydrofuran (THF). THF is produced million tons/year for polyesters and polyethers, and thousand tons/year of 3,4-DABE is incinerated. Thus, the efficient transformation of 3,4-DABE into 1,4-DABE will be valuable in chemical industry and environmental protection, and will be conducive to a low-carbon society. Recently, we developed a direct transformation of but-1,3-diene into but-2-ene-1,4-diol with O_2 and H_2O with supported Pd catalysts [11]. It is an alternative route to THF; however. the selectivity should to be further improved[12]

In the recent decades, several kinds of homogeneous catalysts were developed for this reaction via the π-allyl[13,14] or soft Lewis acid mechanism[15,16] (Fig. 1b). Additionally, only low activity was obtained when using hard Lewis acid catalysts like montmorillonite and ZSM-5; therefore, we devote to developing active soft Lewis acid catalysts and thus choose the isomerization of 3,4-DABE as the benchmark reaction.

Here, we for the first-time report that Pt/CeO_2 with residual chloride can act as soft Lewis acids and can facilitate the isomerization of allylic esters efficiently (Fig. 1c). Interestingly, the active species in this reaction are demonstrated as highly dispersed Pt clusters consisting of Pt–Cl and Pt–O bonds. The residual chloride anion could enhance the Lewis acidity of the Pt metal center. In addition, this should be the first example of the supported Pt soft Lewis acid catalysts. Moreover, this is also the first example of applying supported noble catalysts in the practical isomerization of allylic esters. This reaction can be realized under solvent-free conditions, and the TON of the catalyst reaches 5400. Furthermore, the role of Pt–Cl bonds in the isomerization reaction was also studied

by the density functional theory (DFT) calculations. Our findings introduce a new approach for the transformation of unsaturated compounds over high-performance supported Pt soft Lewis acid catalysts as well as provide a strategy to control the acidity of supported metal Lewis acid catalysts.

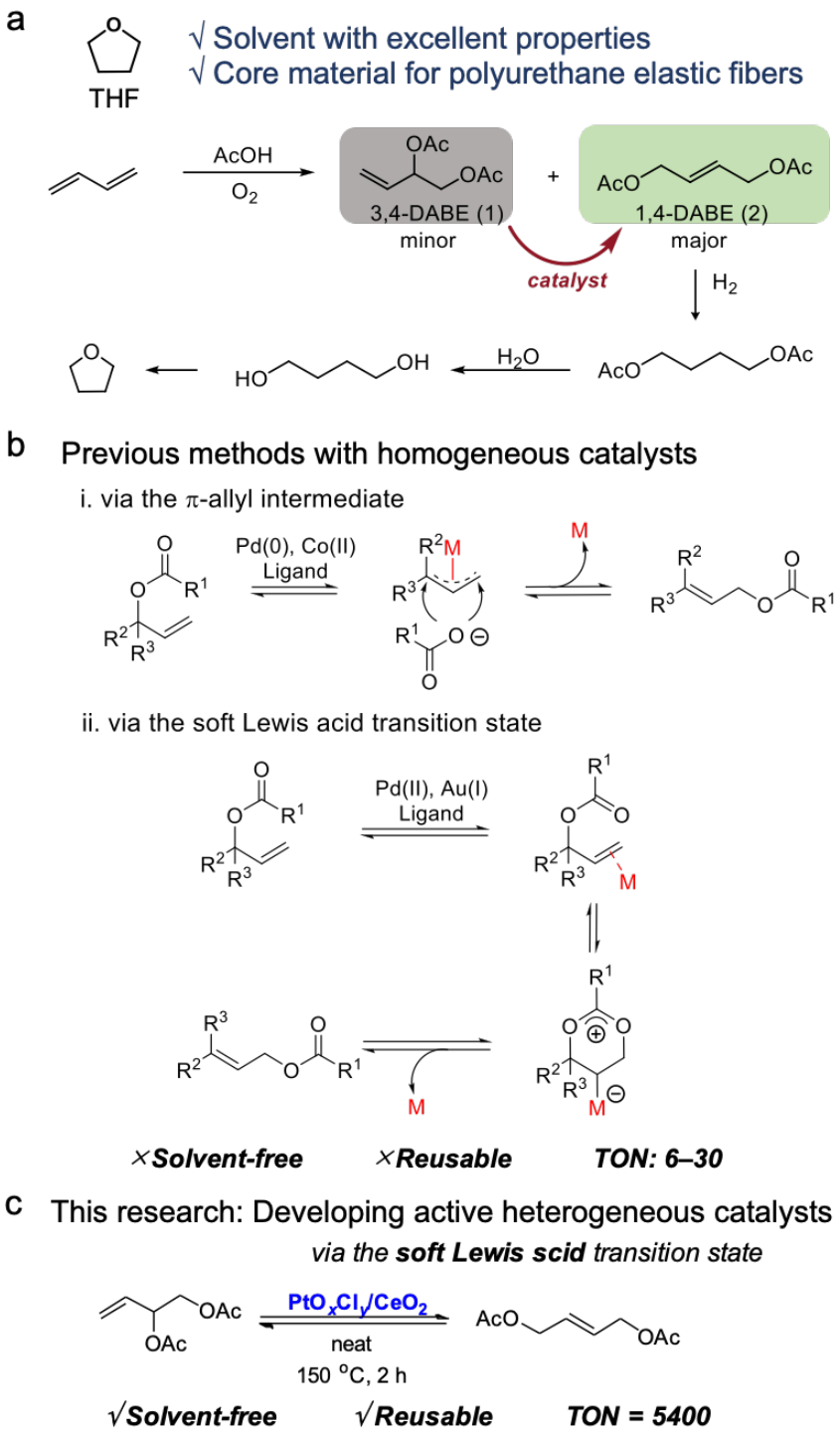

Figure 1. (a) A C4 chemical reaction process from buta-1,3-diene; (b) Reaction mechanism with homogeneous catalysts; (c) Research of efficient supported soft Lewis acid catalysts (this research).

2.2. Experimental

2.2.1. Materials

Chloroplatinic acid hexahydrate ($H_2PtCl_6 \cdot 6H_2O$) was purchased from Furuya Metal Co., Ltd. Palladium nitrate ($Pd(NO_3)_2$) and hydrogen tetrachloroaurate tetrahydrate ($HAuCl_4 \cdot 4H_2O$) were purchased from Tanaka Precious Metals Co., Ltd. Platinum acetylacetonate ($Pt(acac)_2$), tetraammineplatinum(II) nitrate ($Pt(NH_3)_4(NO_3)_2$) and hydrogen hexachloroiridate(IV) n-hydrate ($H_2IrCl_6 \cdot nH_2O$) were purchased from FUJIFILM Wako Pure Chemical Corp. CeO_2 (JRC-CEO-3) and ZrO_2 (JRC-ZRO-4) were reference catalysts supplied by the Catalysts Society of Japan. Al_2O_3 with a specific surface area of 179 m^2/g was purchased from Mizusawa Industrial Chemicals, Ltd. MgO with a specific surface area of 8 m^2/g was purchased from Ube Industries, Ltd. TiO_2 (PC-101) was purchased from Titan Kogyo, Ltd. 3,4-DABE was purchased from Sigma Aldrich, Ltd., and used as received. All chemicals were used without further purification.

2.2.2. Preparation of catalysts

Pt/CeO_2, Pt/ZrO_2, Pt/Al_2O_3, Pt/TiO_2, and Pt/MgO catalysts with a Pt loading of 1 wt% were prepared by the impregnation method. H_2PtCl_6 aqueous solution (Pt: 19.75 g/L; 511 μL) was diluted in 1.5 mL distilled water. A metal oxide support (1.0 g) was added to the aqueous solution, and then stirred at room temperature for 30 min. After the impregnation process, the catalysts were dried by a vacuum freeze method overnight. The obtained catalysts were calcined in a furnace at 300 °C for 4 h. Pt/CeO_2 Cl-free catalysts were also prepared by the impregnation method from $Pt(acac)_2$ and $Pt(NH_3)_4(NO_3)_2$ and were named Pt/CeO_2_A and Pt/CeO_2_N, respectively. $Pt(acac)_2$ (20.4 mg) was dissolved in 2 mL dehydrated toluene, and the following procedures were as described above. $Pt(NH_3)_4(NO_3)_2$ (20.1 mg) was dissolved in 0.5 M HNO_3 (2 mL). The following

procedures were the same as described above.

Ir/CeO_2 catalysts were also prepared by the impregnation method. $H_2IrCl_6 \cdot nH_2O$ (Ir: 36.5 wt%; 27.7 mg) was diluted in 1.5 mL distilled water, and the following procedures were the same as those of Pt/CeO_2.

Pd/CeO_2 and Pd/ZrO_2 catalysts were prepared by the impregnation method. $Pd(NO_3)_2$ aqueous solution (Pd: 200 g/L) was diluted in 1 mL distilled water. ZrO_2 or CeO_2 (1.0 g) was added to the aqueous solution and stirred for 30 min. After the impregnation was completed, residual distilled water was removed by freeze-drying. The catalysts were calcined at 550 °C for 4 h. Then they were reduced in a flow of H_2 (20 mL/min) at 200 °C for 2 h. The obtained Pd/CeO_2 and Pd/ZrO_2 catalysts were directly used for catalytic reactions without further treatment.

Au/ZrO_2 was prepared by deposition precipitation method. ZrO_2 (1.0 g) was added to an aqueous solution (100 mL) of urea (7.6 g) and $HAuCl_4 \cdot 4H_2O$ (21.1 mg). Then the mixture was stirred at 90 °C for 10 h. After collecting by filtration, the obtained catalyst was washed with water and dried in air at 70 °C overnight. Finally, the catalyst was calcined in air at 300 °C for 4 h and directly used for catalytic reactions without further treatment.

HCl treatment was performed with Pt/CeO_2 catalysts prepared from Cl-free precursors, and the treated catalysts were named Pt/CeO_2_A_HCl and Pt/CeO_2_N_HCl. The prepared catalysts (0.1 g) were added to 1.5 mL HCl solution (0.1 M) and stirred at 90 °C for 6 h. Then, the solid was collected by filtration and vacuum freeze-dried for 4 h. Finally, the obtained catalysts were calcined again at 300 °C for 1 h.

2.2.3. Characterization

High-angle annular dark-field scanning transmission electron microscopy (HAADF-

STEM) images were performed with a JEOL JEM-ARM200F. The loading amount of Pt in the prepared catalysts was determined by microwave plasma-atomic emission spectrometry (MP-AES) via an Agilent 4100 MP-AES. X-ray diffraction (XRD) was performed using a Rigaku MiniFlex600 instrument equipped with a Cu K_α radiation source. The properties of the surface species was analyzed by X-ray photoelectron spectroscopy (XPS) using a Shimadzu AXIS-165 spectrometer equipped with Al K_α radiation at a pressure lower than 10^{-8} Pa. The obtained binding energies were calibrated to the C1s peak at 284.8 eV. XPS spectra were analyzed by XPS PEAK41 software. The local structures of Pt species were analyzed by Pt L_{III}-edge and L_I-edge X-ray absorption fine structure (XAFS) spectra collected at the BL14B2 beamline of SPring-8 (Hyogo, Japan). XAFS measurement experiments were conducted in fluorescence mode. The specific spectral analysis was conducted with the XAFS analysis software Athena and REX2000. Temperature-programmed reduction of H_2 (H_2-TPR) was performed by a BELCAT instrument equipped with a thermal conductivity detector (TCD).

Conversions and yields of the compounds discussed were detected by gas chromatography (GC) using an Agilent GC 6850 Series II instrument equipped with a flame ionization detector (FID) and a J&W HP-1 column. ^1H and ^{13}C NMR spectra were collected on a JEOL JNM-ECS400 or JEOL JNM-ECA600 spectrometer.

2.2.4. General Procedure for the Catalytic Reactions

A screw cap vial was charged with catalysts, but-3-ene-1,2-diyl diacetate, and a magnetic stirring bar. Then, the reaction mixture was stirred at 150 ℃ under an N_2 or air atmosphere. After reaction, the mixture was filtered, and the filtrate was analyzed by GC with tridecane as an internal standard. In the scale-up reaction of 10 mmol, same procedures were performed, and the catalytic activity was evaluated by the same method

described above. In a recycling experiment, A screw cap vial was also charged with catalysts, but-3-ene-1,2-diyl diacetate and a magnetic stirring bar. The catalytic activity was tested through the same method described above. The screw cap vial was cooled in an ice bath for approximately 20 min after reacting for 2 h. The used Pt catalysts were washed with Et_2O, collected by centrifugation, and dried under vacuum conditions. Then, the obtained Pt catalysts were used for the next run.

2.2.5. Computational Methods

DFT calculations for the model cluster systems were carried out using Gaussian 09[17]. For the model clusters, a 6-31+G(d) basis set for C, O, and H atoms and LANL2DZ for Pt atoms were used, and hybrid DFT (PBE0 functional) was applied. First-principles calculations using DFT for the structures and electronic states of the slab models were carried out with the Vienna Ab initio Simulation Package (VASP)[18,19]. The projector-augmented-wave (PAW)[20] method was utilized for the calculation of the ionic core electrons. The Perdew-Burke-Ernzerhof (PBE)[21] functional with a cutoff energy of 400 eV was set for the determination of the exchange correlation term. To confirm the possible behavior of electrons in the supported Pt catalysts, the DFT + U method (U (Ce, 4f) = 5.0 eV) was used[22].

2.3. Results and Discussion

2.3.1. Isomerization of 3,4-DABE

The direct transformation of 3,4-DABE to 1,4-DABE was selected as the benchmark reaction for the isomerization of allylic esters with various heterogeneous catalysts, and the equilibrium between 3,4-DABE and 1,4-DABE was reported to be 37/63[13], as shown in Fig. 2a. In fact, the distillation separation of 3,4-DABE and 1,4-DABE is

established in chemical industry of THF production. Catalyst screening was carried out with various metal oxide-supported Pd, Ir, Au, Pt catalysts, which may act as soft Lewis acids and facilitate the reaction, according to the previsou reports with the Pd complex[16] and Au complex catalysts[15], in which the highest TON is only 33.

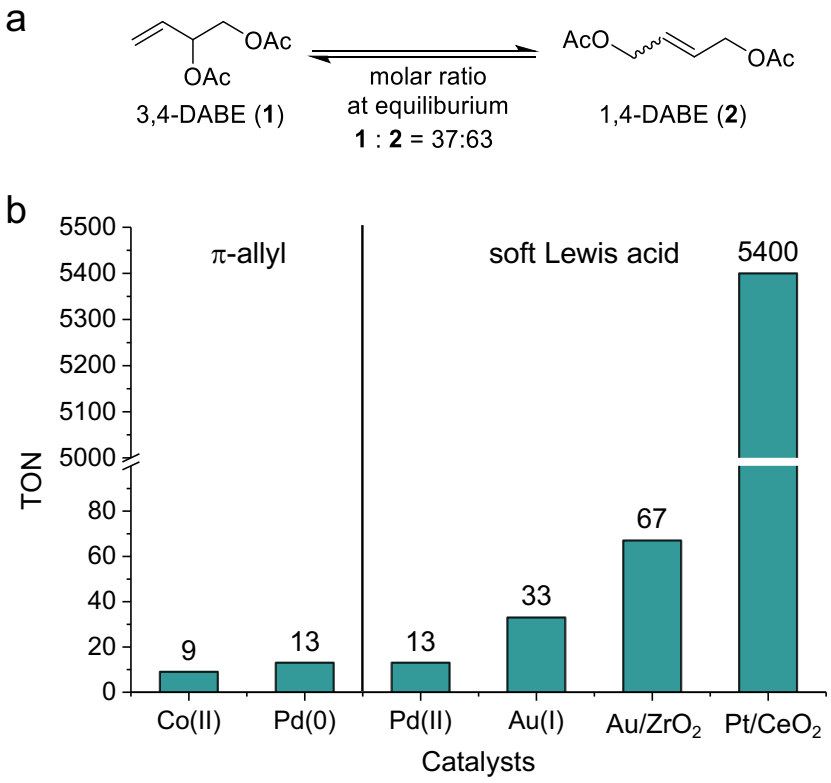

Figure 2. (a) Equilibrium of 3,4-DABE and 1,4-DABE; (b) TON for the catalyst prepared in this study and the maximum TON of discussed allylic esters substrates in the previous reports[13–16].

To develop active catalysts for the direct isomerization of allylic esters, we chose ZrO_2 and CeO_2 as supports, which could promote the high dispersion of noble metal species, owing to the strong metal-support interaction[23,24]. Among the discussed supported noble metal catalysts, Au/ZrO_2 and Pt/CeO_2 catalysts produced (2) in the yields of 11% and 52%, respectively (Table 1).

Table 1. Support effect of metal oxide-supported Pt catalysts in the catalytic isomerization of 3,4-DABE.

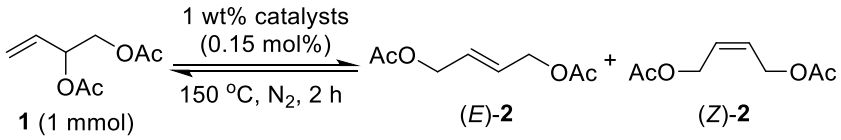

1 (1 mmol) (*E*)-**2** (*Z*)-**2**

Entry	Catalyst	Conv./%[a]	Yield/%[a]		TON
			(*E*)-2	(*Z*)-2	
1[b]	Pd/ZrO_2	0	0	0	0
2[c]	Pd/CeO_2	18	0	0	0
3	Ir/CeO_2	0	0	0	0
4	Au/ZrO_2	14	10	1	67
5	Pt/CeO_2	63	51	1	347
6	Pt/ZrO_2	57	49	2	327
7	Pt/TiO_2	63	47	1	320
8	Pt/Al_2O_3	49	40	0	267
9	Pt/MgO	39	27	0	180
10[d]	Pt/CeO_2	55	52	1	5300
11[d,e]	Pt/CeO_2	56	51	1	5200
12[d,e,f]	Pt/CeO_2	60	53	1	5400
13[g]	Mont-K10	18	12	1	–
14[g]	ZSM-5	27	7	1	–

[a]Determined by GC analysis using tridecane as an internal standard. [b]Using 10 wt% Pd/ZrO_2 (2 mol%), THF used as the solvent, and reacting for 14 h. [c]Using 5 wt% Pd/CeO_2 (2 mol%), DMSO used as the solvent, reacting for 18 h. [d]Reacting in 0.01 mol%. [e]Under an air atmosphere. [f]Reacting at the feedstock scale of 10 mmol. [c]Using 30 mg catalysts under an air atmosphere, reacting for 5 h.

In addition, a high TON of 5400 was also obtained in the reaction scale of 10 mmol. With the optimized 1 wt% Pt/CeO_2, the isomerization reaction could reach the equilibrium after 30 min and showed a turnover frequency (TOF) of 2120 h^{-1} with the catalyst amount of 0.05 mol% (Fig. 3). The time course of the isomerization of 3,4-DABE over the optimal Pt/CeO_2 catalysts was performed with a Pt amount of 0.05 mol% at 150 °C in 2 h. After reacting for 30 minutes, few changes in the conversion and yields could be observed.

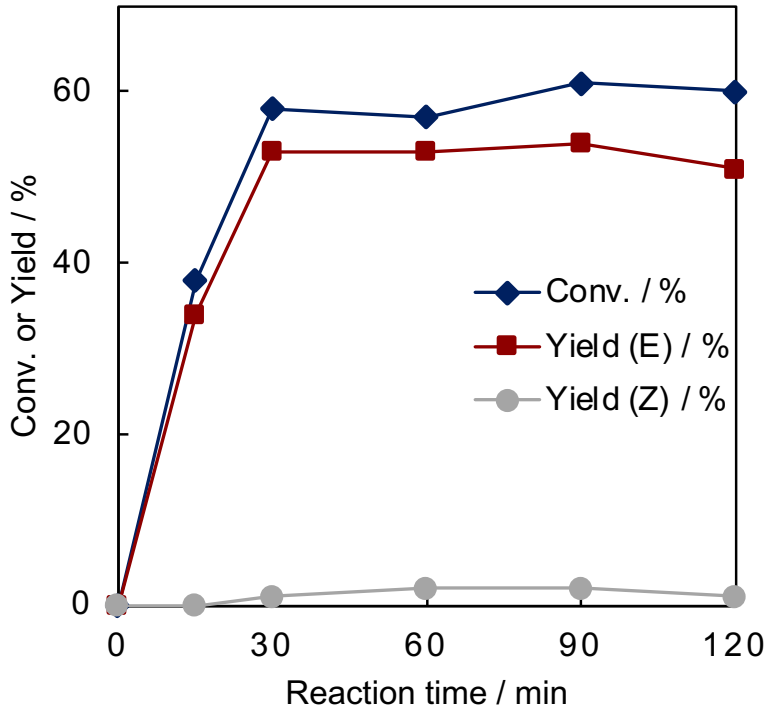

Figure 3. Reaction time course of the catalytic isomerization of allylic esters using Pt/CeO_2.

Moreover, the effect of loading amount was also investigated, and Pt/CeO_2 catalysts with Pt loadings below 3 wt% showed high activity (Table 2), which is probably related to the atomically dispersed active Pt species that was only formed with Pt loadings less than 3 wt%[25].

Table 2. Effect of the Pt loading on the catalytic isomerization of allylic esters.

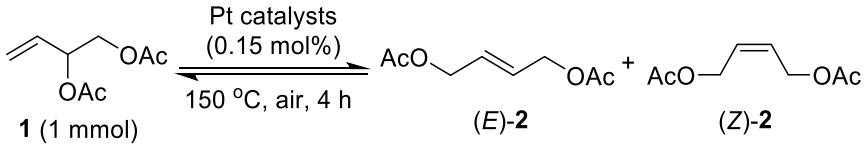

Entry	Catalyst	Conv./%[a]	Yield/%[a]	
			(*E*)-2	(*Z*)-2
1	1 wt% Pt/CeO_2	51	49	1
2	3 wt% Pt/CeO_2	57	50	1
3	5 wt% Pt/CeO_2	48	43	1
4	10 wt% Pt/CeO_2	27	18	n.d.

[a]Determined by GC analysis using tridecane as the internal standard.

The reusability of the catalysts was evaluated with the Pt catalysts supported by different metal oxide supports, and Pt/CeO_2 exhibited better reusability than the other catalysts after reacting for twice (Fig. 4). After the Pt/CeO_2 catalysts were used twice, no obvious deactivation could be observed both in the conversions or yields. However, a marked decrease in conversions and yields were observed when using the other catalysts. In addition, the reaction solution of the Pt/CeO_2 catalysts was analyzed by MP-AES, and the leaching of the Pt was only around 2 %.

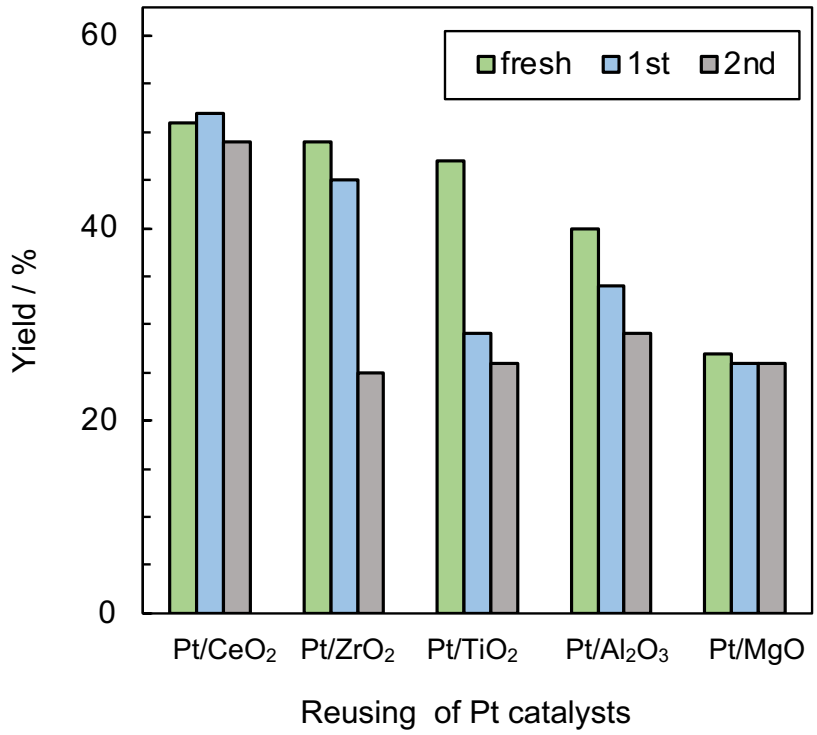

Figure 4. Reusability of Pt catalysts supported by different metal oxides for the isomerization of allylic esters.

In fact, the use of $H_2PtCl_6 \cdot 6H_2O$ as a precursor through the simple impregnation method could facilitate the formation of stable oxidized Pt species, such as $Pt(OH)_xCl_y$[26] and PtO_xCl_y[27]. Many reports on residual chloride in supported Pt catalysts showed their poisoning effect on catalytic activities[27-29]. In addition, the promoting effect of the residual chloride was also discovered in a few cases[30]. Therefore, to remove the influence of residual chloride, we also evaluated the Pt/CeO_2 prepared by Cl-free precursors, such as $Pt(acac)_2$ and $Pt(NH_3)_4(NO_3)_2$ (Table 3). The existence of chloride species was investigated by XPS spectra (Fig. 6a). Interestingly, Cl-free Pt/CeO_2 showed no catalytic activities (Table 3, entries 2 and 3). In contrast, Pt/CeO_2 prepared from $H_2PtCl_6 \cdot 6H_2O$ and HCl-treated catalysts showed high catalytic activity, and produced 1,4-DABE in approximately 60% yield (Table 3, entries 1, 4, and 5). Furthermore, the same

effect was also observed over the Pt/CeO_2-containing bromide anion. The reaction with CeO_2 treated by HCl (without Pt loading) was also discussed (Table 3, entry 6), and no yield of target compounds was detected. Considering the above results, the chloride anion should enhance the Lewis acidity of the Pt metal center, which is important for the catalytic activity in this reaction.

Table 3. Chloride effect over the supported Pt catalyst in the catalytic isomerization of allylic esters.

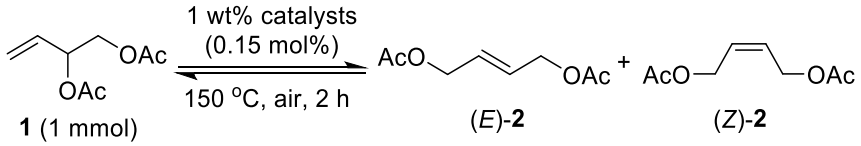

Entry	Catalyst	Precursor	Conv./%[b]	Yield/%[b]	
				(E)	(Z)
1	Pt/CeO_2_Cl	$H_2PtCl_6 \cdot 6H_2O$	63	51	1
2	Pt/CeO_2_A	$Pt(acac)_2$	4	1	n.d.
3	Pt/CeO_2_N	$Pt(NH_3)_4(NO_3)_2$	3	1	n.d.
4[a]	Pt/CeO_2_A_HCl	$Pt(acac)_2$	64	50	7
5[a]	Pt/CeO_2_N_HCl	$Pt(NH_3)_4(NO_3)_2$	65	52	8
6[a]	CeO_2_HCl	/	3	n.d.	n.d.

[a]Treated by 0.1 M HCl after the catalysts were prepared. [b]Determined by GC analysis using tridecane as an internal standard.

2.3.2. Characterization of the Catalysts

HAADF-STEM coupled with EDS mapping was used to determine the existence and morphology of supported Pt species on the prepared Pt/CeO_2 catalysts. The formation of Pt particles was not observed, which should be due to the high dispersion of Pt species

or the high atomic weight of Ce in the support[24]. Notably, EDS mapping of Pt element revealed the high dispersity (Fig. 5), and the existence and fine dispersion of Cl element could also be confirmed by the EDS mapping.

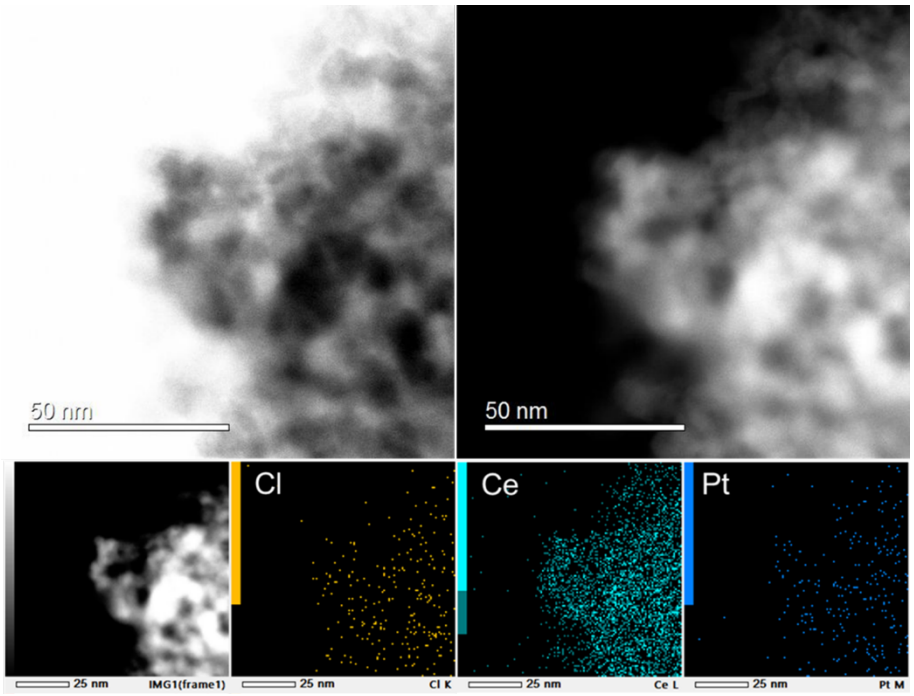

Figure 5. HADDF-STEM images coupled with EDS mapping of 1 wt% Pt/CeO_2 prepared from $H_2PtCl_6 \cdot 6H_2O$.

XPS spectra of the prepared catalysts were analyzed to investigate the chemical states of the supported Pt species (Fig. 6). In the Cl 2p spectra, a couple of peaks at 198.3 eV and 200 eV with a spin-orbit separation of 2 eV corresponding to $2p_{1/2}$ and $2p_{2/3}$ were observed from the catalysts Pt/CeO_2_Cl, Pt/CeO_2_A_HCl, and Pt/CeO_2_N_HCl (Fig. 6a). The results uncover the existence of residual chloride for the catalysts prepared by $H_2PtCl_6 \cdot 6H_2O$ and Cl-free catalysts with HCl post-treatment. In addition, according to the reaction results in Table 3, the essential positive effect of chloride in Pt/CeO_2 catalysts was further proved.

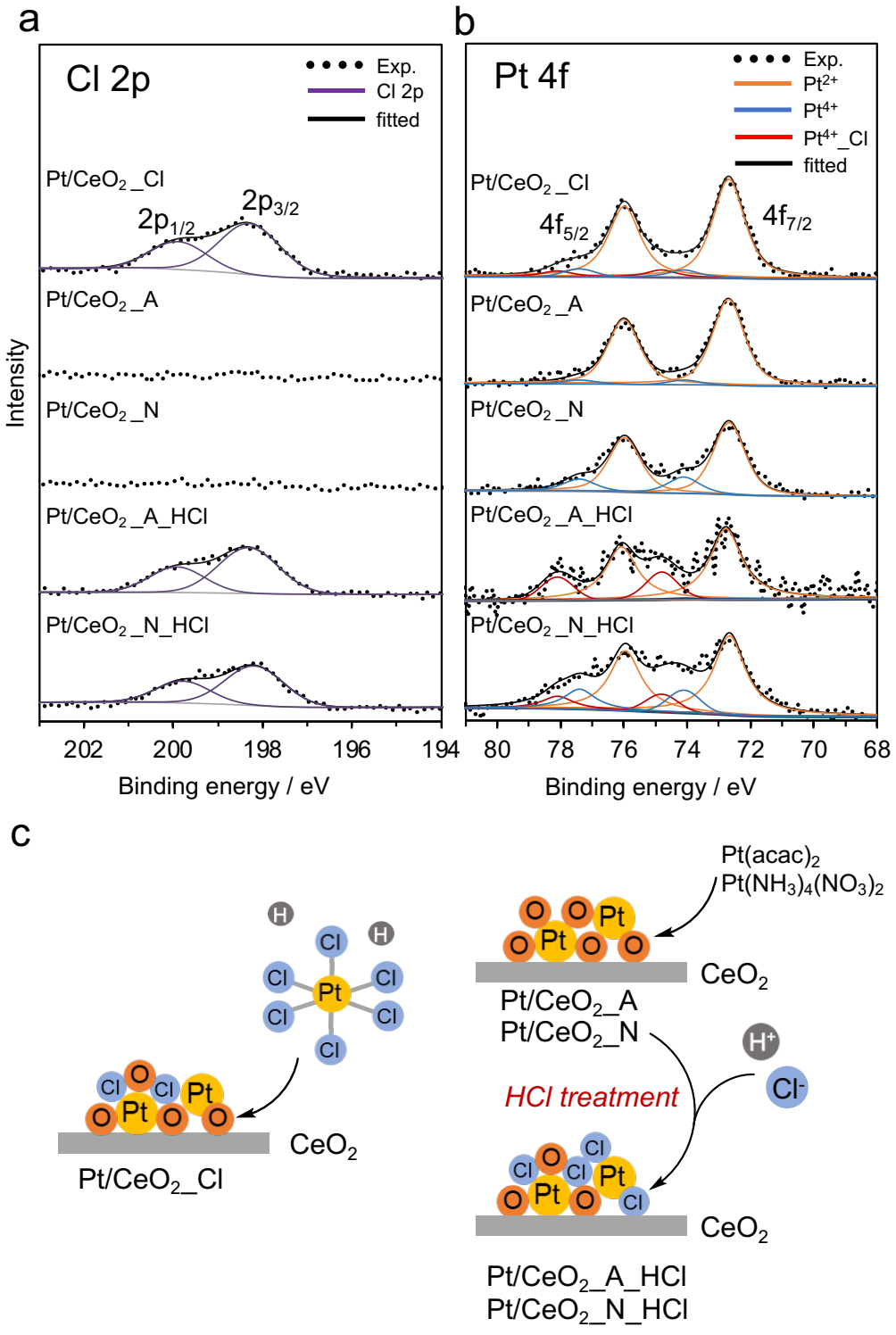

Figure 6. XPS spectra of 1wt% Pt/CeO_2 prepared from different precursors or Cl-free catalysts with HCl post-treatment. (a) XPS spectra of Cl 2p; (b) XPS spectra of Pt 4f; (c) Simple structural model correlates the XPS spectra.

XPS spectra in the Pt 4f regions of Pt/CeO_2 catalysts prepared by different precursors and Cl-free catalysts with HCl post-treatment were further analyzed by peak deconvolution (Fig. 6b). From the XPS spectra, Pt species supported on CeO_2 were mainly in the Pt^{2+} state (72.7 eV, Pt $4f_{7/2}$, $Pt(OH)_2$, yellow curves) with a component from Pt^{4+} (74.1 eV, Pt $4f_{7/2}$, PtO_2, blue curves)[31]. Meanwhile, XPS spectra in the Ce 3d regions were also collected (Fig. 7). The Ce 3d peaks of the catalysts prepared from Cl-contianing precursor and HCl-treated catalysts prepared from Cl-free precursors shifted by 0.2 eV to higher binding energies, when compared with those of the catalysts containing no chloride species. The peak shift can be considered as the positive charge effect with the existence of chlorine.

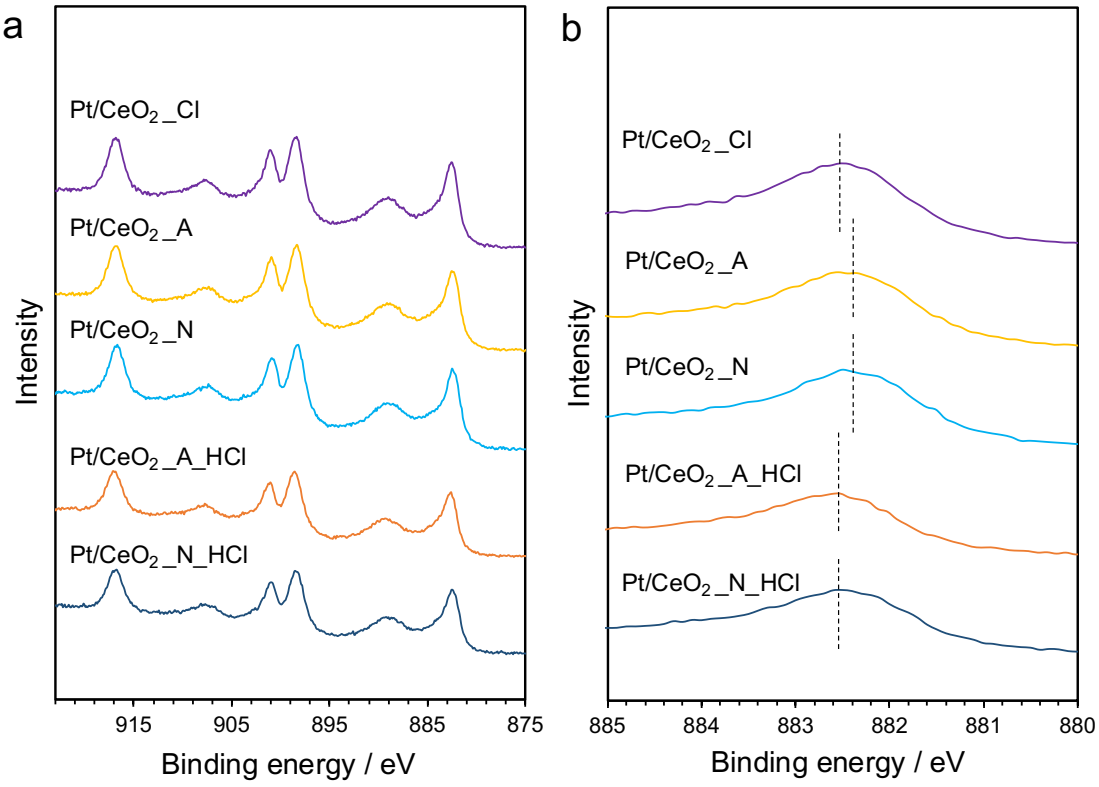

Figure 7. Ce 3d XPS spectra of (a) 1 wt% Pt/CeO_2 prepared from different precursors or as-prepared catalysts after HCl post-treatment and (b) amplification of the peaks.

The unobservable Pt nanoparticles in the HAADF-STEM images and the dominant Pt^{2+} oxidation state reveal that most of the Pt atoms on the support may be trapped and strongly bound on the CeO_2(111) facet by forming a 4-fold coordination[32]. For the catalysts containing chloride ions, Pt^{4+}(Cl) components (74.8 eV, Pt $4f_{7/2}$, red curves) were also observed (Fig. 6b), and they were considered as the Pt species with Pt–Cl bonds[26]. In addition, after HCl post-treatment, peaks attributed to Pt^{4+}(Cl) also emerged, and they appeared simultaneously with the peaks of Cl 2p (198.3 eV, Cl $2p_{3/2}$). In conclusion, Pt/CeO_2 prepared from $H_2PtCl_6 \cdot 6H_2O$ and HCl-treated Cl-free catalysts containing residual chloride ions could provide high catalytic activity (Fig. 6c).

Pt L_{III}-edge X-ray absorption near edge structure (XANES) spectra of Pt/CeO_2 catalysts prepared by different precursors were measured in an air atmosphere with the reference of Pt foil (Fig. 8a). Characteristic peak, the white lines, at around 11568 eV were observed, which indicate that the Pt species in the catalysts were in high oxidation states[33]. In addition, the intensity of the white line of Pt/CeO_2_Cl was higher than those of Pt/CeO_2_A and Pt/CeO_2_N. After HCl post-treatment, increased intensities of the white lines were detected in the spectra of Pt/CeO_2_A_HCl and Pt/CeO_2_A_HCl, uncovering the increased oxidation state along with the formation of chloride (Fig. 8c).

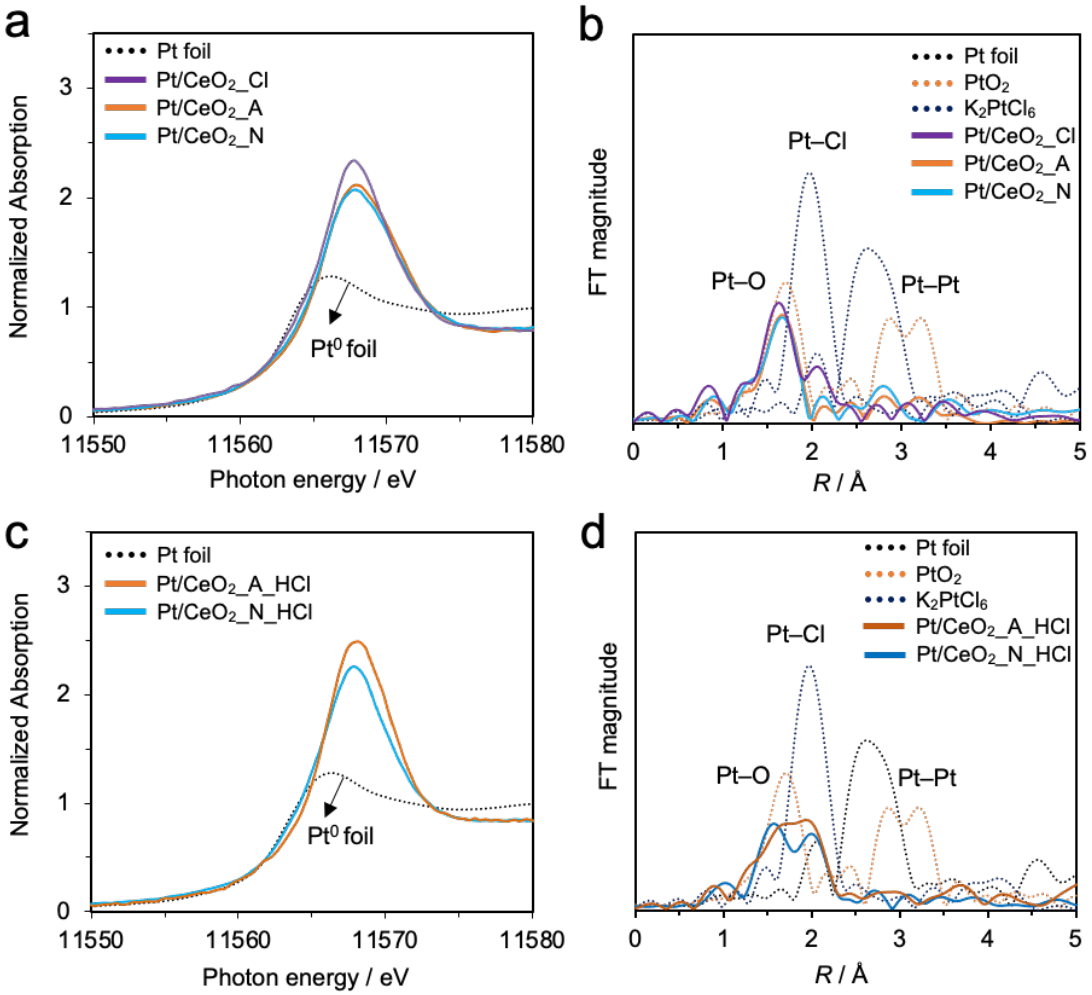

Figure 8. Pt L_{III}-edge XANES spectra and radial structure functions of Pt/CeO_2 (k = 3–13 $Å^{-1}$). (a) (b) prepared from various precursors; (c) (d) HCl-treated Pt/CeO_2 prepared from Cl-free precursors.

In addition, phase-uncorrected radial structure functions (RSFs) of Pt/CeO_2 prepared by different precursors were also analyzed (Fig. 8b), and two peaks were mainly observed at approximately 1.65 Å and 1.95 Å in Pt/CeO_2_Cl. According to the peaks from the reference sample of Pt foil, PtO_2, and K_2PtCl_6, the peak at approximately 1.65 Å could be attributed to Pt–O coordination, and the peak at approximately 1.95 Å could be attributed to Pt–Cl coordination. Meanwhile, the weak intensities of peaks at 2.60 Å and 2.85 Å

should correspond to the Pt–Pt coordination in Pt foil and the Pt–O–Pt coordination in PtO_2, respectively, and they were much weaker than those of the reference samples, revealing the high dispersion of Pt species and the existence of Pt nanoclusters or even atomic Pt species. This result was also consistent with the finding in HAADF-TEM measurement. On the other hand, in the spectra of Pt/CeO_2_A and Pt/CeO_2_N, peaks at approximately 1.65 Å and 2.85 Å were also observed, and almost no intensities at approximately 1.95 Å were observed, uncovering the formation of PtO_x species. After HCl post-treatment, in the RSFs spectra of Pt/CeO_2_A_HCl and Pt/CeO_2_N_HCl, peaks at approximately 1.65 Å and 1.95 Å were observed as predicted (Fig. 8d), and no obvious peaks could be observed around the distances of other coordination. Considering the reaction results and the investigation of XPS spectra, the active species of Pt/CeO_2 were proven to contain both Pt–O coordination and Pt–Cl coordination that were highly dispersed. In addition, the k^3-weighted Pt L_{III}-edge extended X-ray absorption fine structure (EXAFS) oscillation patterns of Pt/CeO_2_Cl, Pt/CeO_2_A_HCl, and Pt/CeO_2_N_HCl were collected and compared with those of PtO_2, and K_2PtCl_6 (Fig. 9). In the spectra, oscillation patterns of Pt/CeO_2_Cl, Pt/CeO_2_A_HCl, and Pt/CeO_2_N_HCl were between those of K_2PtCl_6 and PtO_2, revealing the existence of both Pt–O coordination and Pt–Cl coordination in the active catalysts.

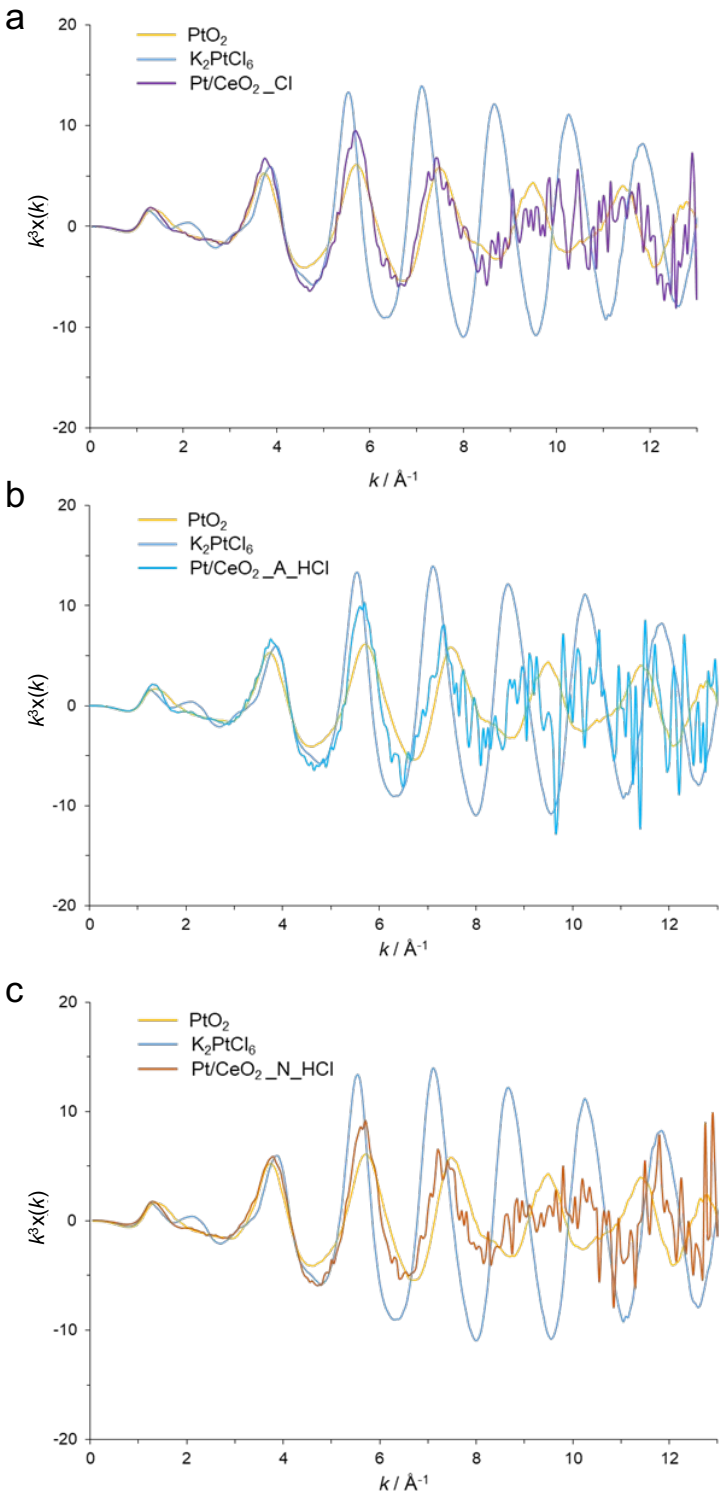

Figure 9. k^3-weighted Pt L_{III}-edge EXAFS oscillations of Pt/CeO_2_Cl, Pt/CeO_2_A_HCl, and Pt/CeO_2_N_HCl.

For a further investigation, Pt L_{III}-edge XANES spectra of Pt catalysts supported by different metal oxides were also collected in an air atmosphere. Through estimating the intensities of the white lines, the oxidation states of Pt species supported by other metal oxides were lower than those by CeO_2 (Fig. 10). Pt–O coordination and Pt–Cl coordination were also compared in the phase-uncorrected RSFs, and a relatively low intensity was observed from the catalysts with low catalytic activity.

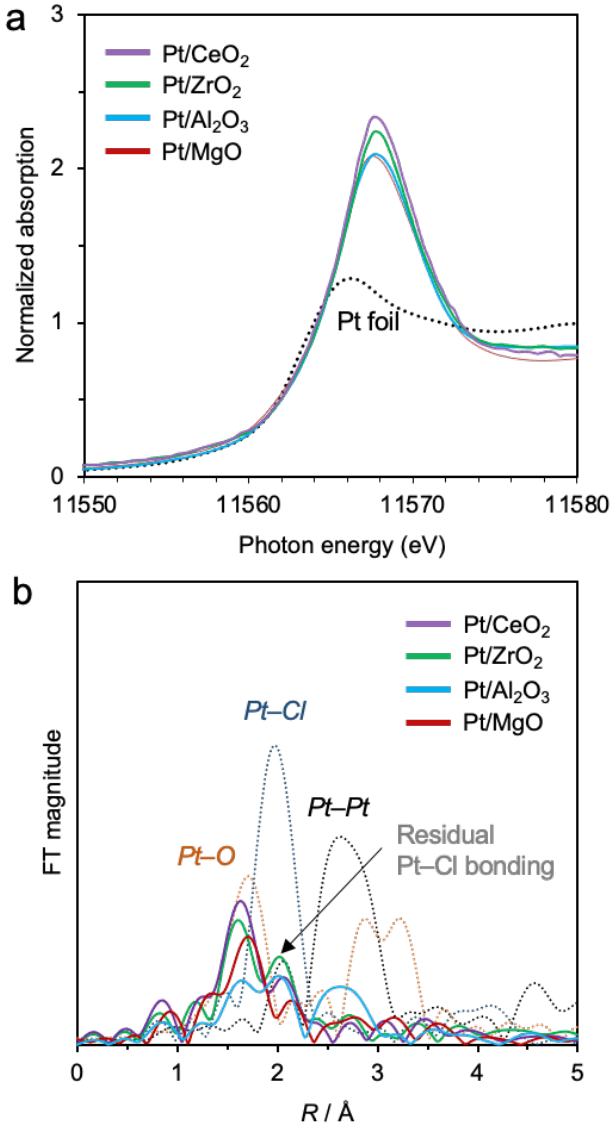

Figure 10. (**a**) Pt L_{III}-edge XANES spectra and (**b**) RSFs of Pt catalysts supported by different metal oxides (k = 3–13 $Å^{-1}$).

Furthermore, the specific oxidation states of Pt species of the catalysts were analyzed by the edge energy of Pt L_I-edge XANES spectra (Fig. 11). The energy differences from the edge energy of Pt foil are shown as *ΔEs*, and *ΔE*s are found to vary linearly with the oxidation states of Pt. The oxidation state of Pt in Pt/CeO_2_Cl was nearly 4+ and higher compared with that of Pt/Al_2O_3_Cl. These results reveal that a higher oxidation state of Pt could provide a higher catalytic activity.

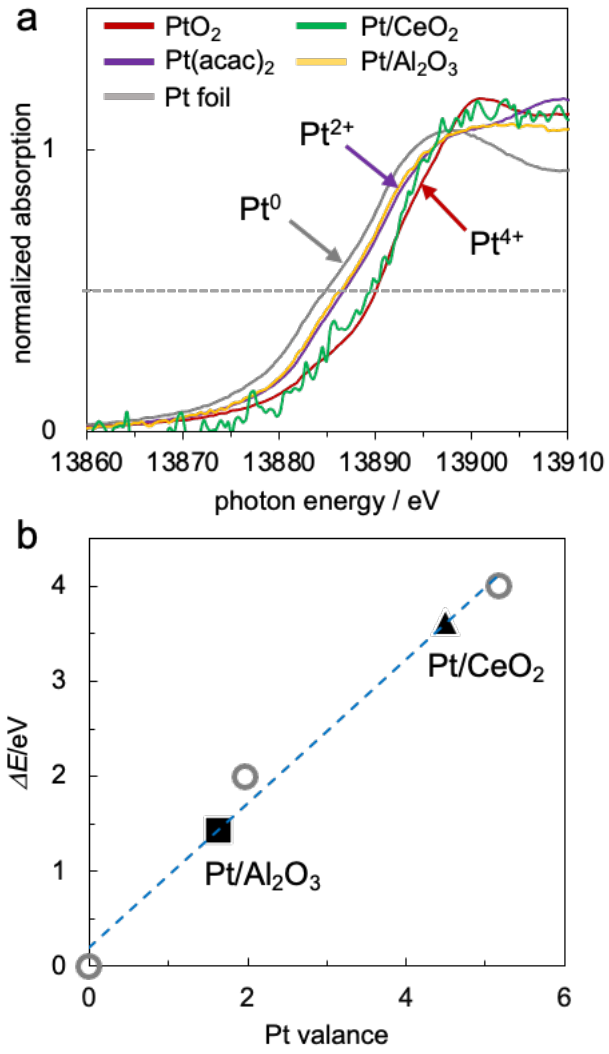

Figure 11. (a) Pt L_I-edge XANES spectra and (b) edge energy plots of Pt/CeO_2 and Pt/Al_2O_3 prepared from $H_2PtCl_6 \cdot 6H_2O$.

H_2-TPR measurement was also conducted to investigate the active Pt species, and CeO_2 gave a reduction peak at 550 ℃, which should belong to the reduction of the surface of CeO_2 (Fig. 12). However, Pt/CeO_2_Cl only showed an sharp reduction peak at 220 ℃ below 600 ℃, which might be attribute to the $Pt(OH)_xCl_y$ species directly binded to the surface of CeO_2. Moreover, the disappearance of the reduction peak of CeO_2 at 550 ℃ in the curve of the prepared catalysts also revealed a strong metal-support interaction between Pt species and CeO_2.

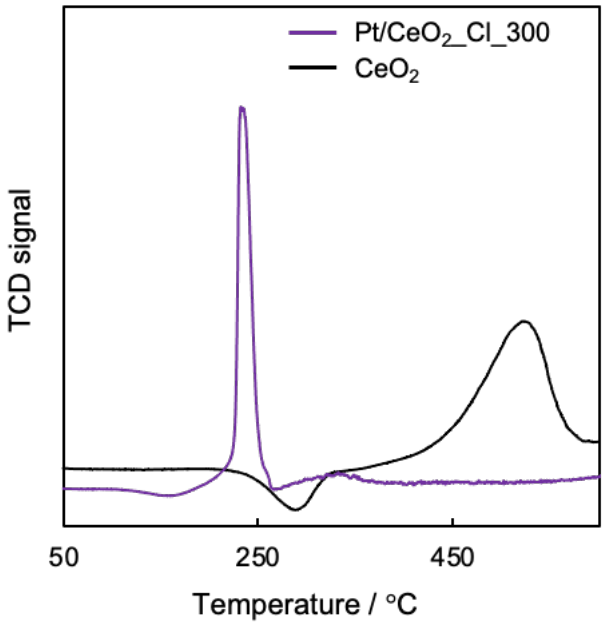

Figure 12. TPR profiles of 1 wt% Pt/CeO_2 (prepared from a $H_2PtCl_6 \cdot 6H_2O$ precursor, red line, calcination temperature: 300 ℃) and CeO_2 without treatment (black line).

Additionally, measurement of Pt/CeO_2_A showed a peak at 80 ℃, and Pt/CeO_2_N showed a peak at 190 ℃ (Fig. 13a). The difference in the reduction peaks of the prepared Cl-free catalysts might be related to the supported PtO_x in different sizes and Pt/O ratios as well as the interaction between Pt and CeO_2. In this section, Pt/CeO_2_Cl was calcined at 300 ℃ and 500 ℃ during the preparation process to obtain $Pt(OH)_xCl_y$ and PtO_xCl_y acting as references [34,35]. In addition, after HCl post-treatment, the peak of Pt/CeO_2_A_HCl was mainly showed at approximately 220 ℃ (Fig. 13b). However, the peak of Pt/CeO_2_N_HCl was observed at 250 ℃. Thus, supported Pt species after HCl post-treatment were considered as $Pt(OH)_xCl_y$ and PtO_xCl_y with the reference peaks in Fig 13a. These results were roughly consistent with the findings in the XAFS analysis,

and the shift from the different calcination temperatures may be related to the changes in the ratios of x/y of the species. The main reduction temperature should increase along with the decrease in the x/y ratio.

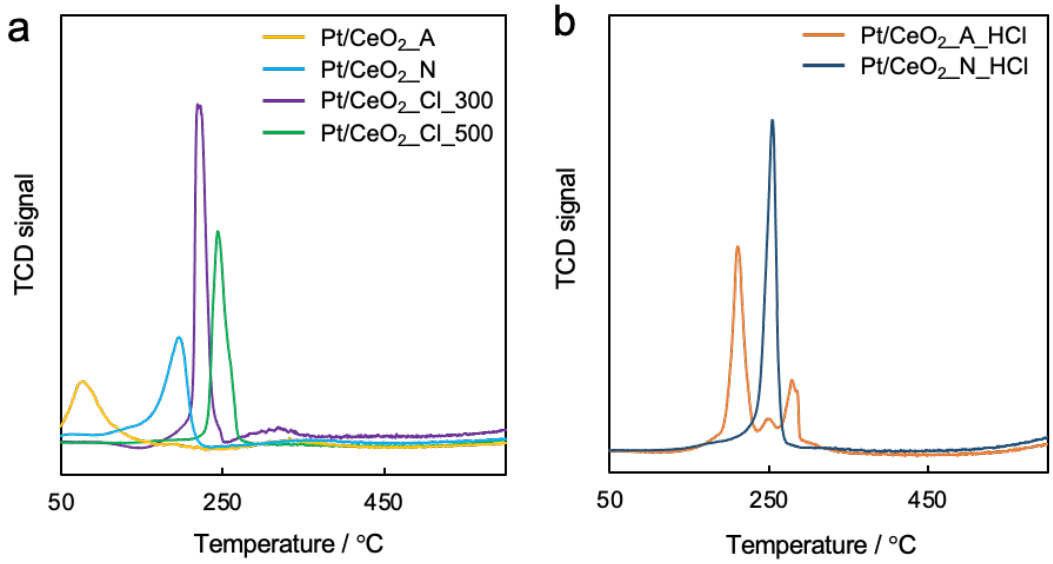

Figure 13. TPR profiles of 1 wt% Pt/CeO_2 prepared (a) from different precursors or with different calcination temperatures and (b) with HCl post-treatment.

Based on the above experimental results, the formed Pt–Cl bonds in Pt/CeO_2 catalysts can play an essential role for the high catalytic activity, which should be due to the stably enhanced acidity of Pt with the existence of chloride anions. In addition, the active species supported on CeO_2 are considered as $Pt(OH)_xCl_y$ and PtO_xCl_y, which can be prepared with a simple impregnation method or a HCl post-treatment. Furthermore, because of the strong interaction between Pt and CeO_2, the active specie can easily be highly dispersed and keep Pt in a high oxidation state.

2.3.3. Catalytic Isomerization of Allylic Esters

With the previous reports on this reaction with homogeneous catalysts, the reaction mechanism of the catalytic isomerization of allylic esters could be classified into the π-allyl mechanism and the soft Lewis acid mechanism. Thus, pentanoic acid was added to the reaction mixture to confirm the reaction mechanism using Pt/CeO_2 catalysts. Only the products of (*E*)-2a and (*Z*)-2a were detected, and no exchange between externally added pentanoic acid was observed, proving that the mechanism for the isomerization of allylic esters with Pt/CeO_2 catalysts could be a soft Lewis acid

mechanism (Fig. 14a).

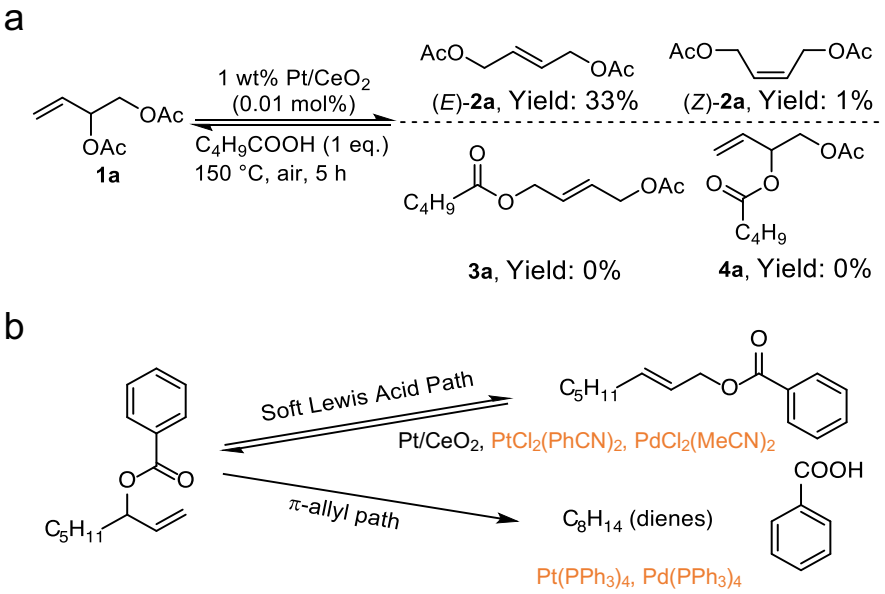

Figure 14. (a) Reaction mechanism investigation by the addition of pentanoic acid. (b) illustration of catalytic reaction paths of substrate oct-1-en-3-yl benzoate.

An investigation on substrate scope was also conducted under the optimized reaction conditions. The optimized Pt/CeO_2 catalysts also provided great reaction activities for the isomerization of other allylic acetates (Table 4). When the allylic acetate derived from tertiary alcohol was evaluated, a yield of 48% was obtained (entry 1). Meanwhile, the substrates with pentyl or cyclo-hexyl groups also showed high yields to the model reaction discussed above (entries 2 and 3). Particularly, the substrate with phenyl group even provided a higher yield than those of others, which might be due to the stable conjugated structure of the product (entry 4). However, low yield and Z-isomer formation were detected when testing linalyl acetate derived from tertiary alcohol, which might be related to the strong steric effect (entry 5). Actually, the theoretical maximum yields for the equilibria have not been discussed for each substrate, but they should be close to those values except for the result in entry 5.

Table 4. Pt/CeO_2-catalyzed isomerization of allylic acetates.

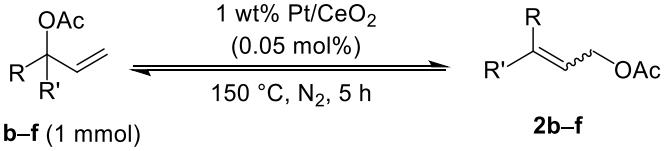

1b–f (1 mmol) **2b–f**

Entry	Substrate		Product		Conv./%[a]	Yield/%[a]
1		**1b**	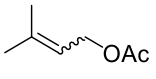	**2b**	54	48
2	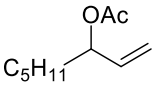	**1c**	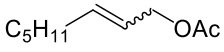	**2c**	66	62
3	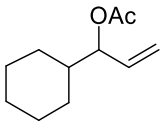	**1d**	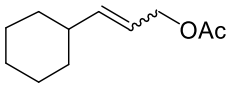	**2d**	67	55
4[b]	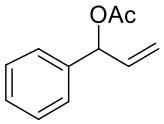	**1e**	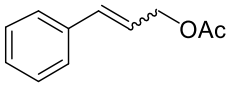	**2e**	89	87
5	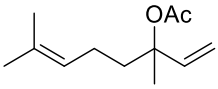	**1f**	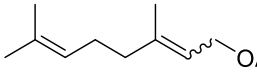	**2f**	14	10[c]

[a]Determined by GC analysis using tridecane as an internal standard. [b]0.25 mol% Pt/CeO_2. [c]71:29 ratio of *E*/*Z* isomers.

Furthermore, allylic benzoates with different groups on the phenyl moiety were also discussed and generally showed great results in the reaction with the Pt/CeO_2 catalysts (Table 5). Despite the presence of the electron-donating methoxy or electron-withdrawing nitryl group on the phenyl, the obtained yields were around 57–67% (entries 1–3), showing the weak electron effect in this reaction. In addition, allylic benzoate with a 2,4,6-trimethylphenyl group was tested to investigate the steric effect of the substrates (entry 4), and a yield of 33% revealed that the steric effect plays a more essential role than the electron effect in this reaction.

Table 5. Pt/CeO_2-catalyzed isomerization of allylic benzoates.

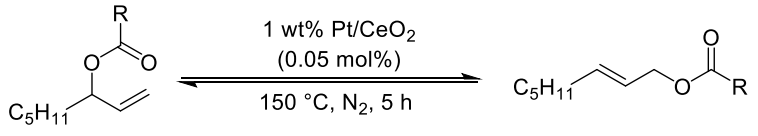

1g j (1 mmol) **2g j**

Entry	Substrate	Product	Conv./%[a]	Yield/%[a]
1	**1g** (R = Ph)	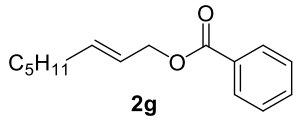 **2g**	67	63
2[b]	**1h** (R = 4-NO_2-C_6H_5)	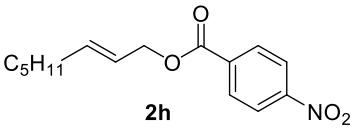 **2h**	68	57
3	**1i** (R = 4-MeO-C_6H_5)	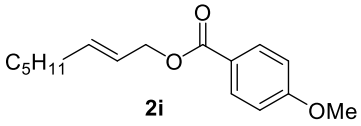 **2i**	68	67
4[b]	**1j** (R = 2,4,6-Me_3-C_6H_3)	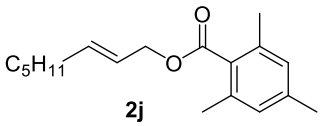 **2j**	35	33

[a]Determined by NMR analysis using mesitylene as an internal standard. [b]under an air atmosphere.

Homogeneous Pt and Pd catalysts were also discussed for the substrate of allylic benzoate (Fig. 14b). The soft Lewis acid complexes $PdCl_2(MeCN)_2$ provided the product for allylic benzoate as well as Pt/CeO_2, although TON was low (5000 for Pt/CeO_2 cf. 6 for $PdCl_2(MeCN)_2$). Then, it is noteworthy that Pd(0) and Pt(0) complexes, which catalyze the reaction via a π-allyl intermediate, could only give eliminated diene due to the low nucleophilicity of benzoate. Therefore, these results also demonstrate the soft Lewis acid mechanism using Pt/CeO_2 catalysts. In addition, the proposed catalytic cycle for the isomerization of allylic esters with Pt/CeO_2 was presented, and the hexatomic ring state over the Pt catalysts was a transition state (Fig. 15).

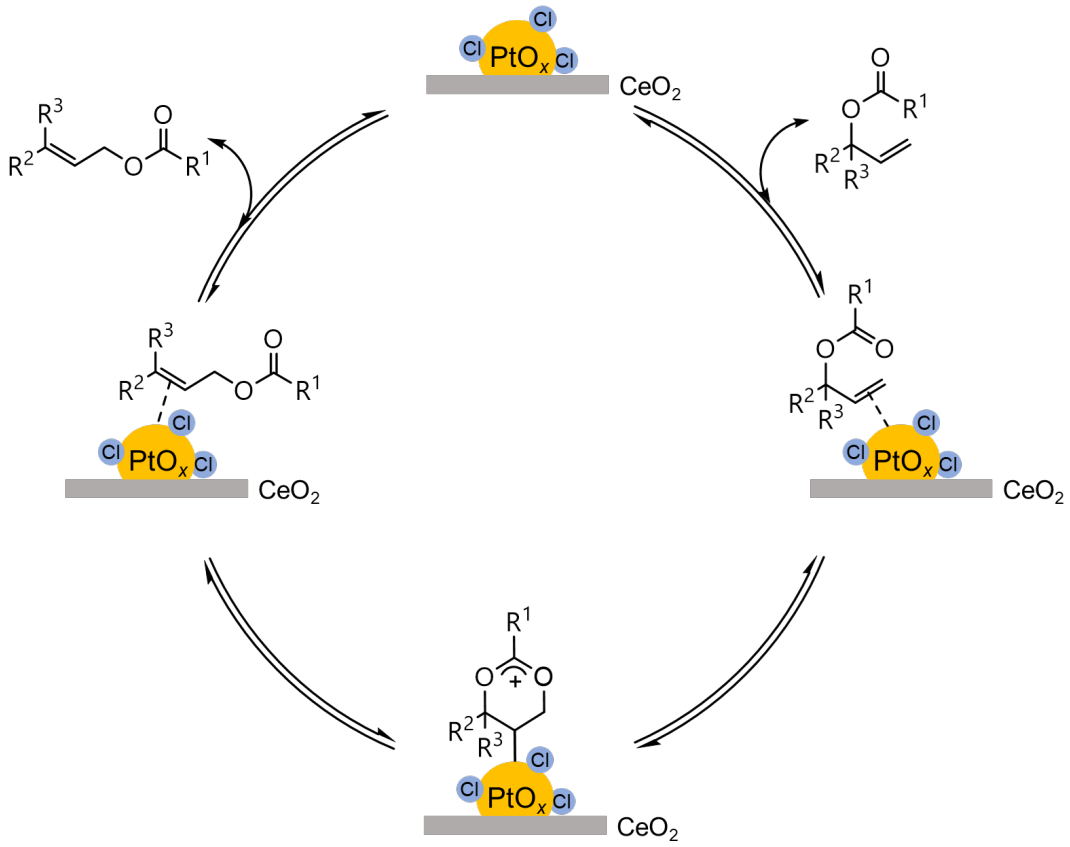

Figure 15. Proposed catalytic cycle of the isomerization of allylic esters with Pt/CeO_2.

2.3.4. Result of Calculations

Because of the Pt-Cl clusters supported by metal oxides were demonstrated as the active species for the catalytic isomerization of allylic esters, the quantum chemical calculation was conducted to investigate the role of the charges over Pt clusters.

Initially, DFT calculations on the isolated cluster model were carried out with Gaussian09 to investigate the relationship between the activation energies and the charges of the Pt clusters. The calculation results of the reaction cycle based on the cluster model were consistent with the proposed Lewis acid mechanism, and INI-TS1 was considered the activation energy barrier due to the major energy gap between TS1 and INI (Fig. 16a). In other words, the catalytic activities of cationic clusters are much higher than those of neutral clusters. In addition, the detailed results are not listed here, and the change in energy of the transition state corresponds to a reversible reaction.

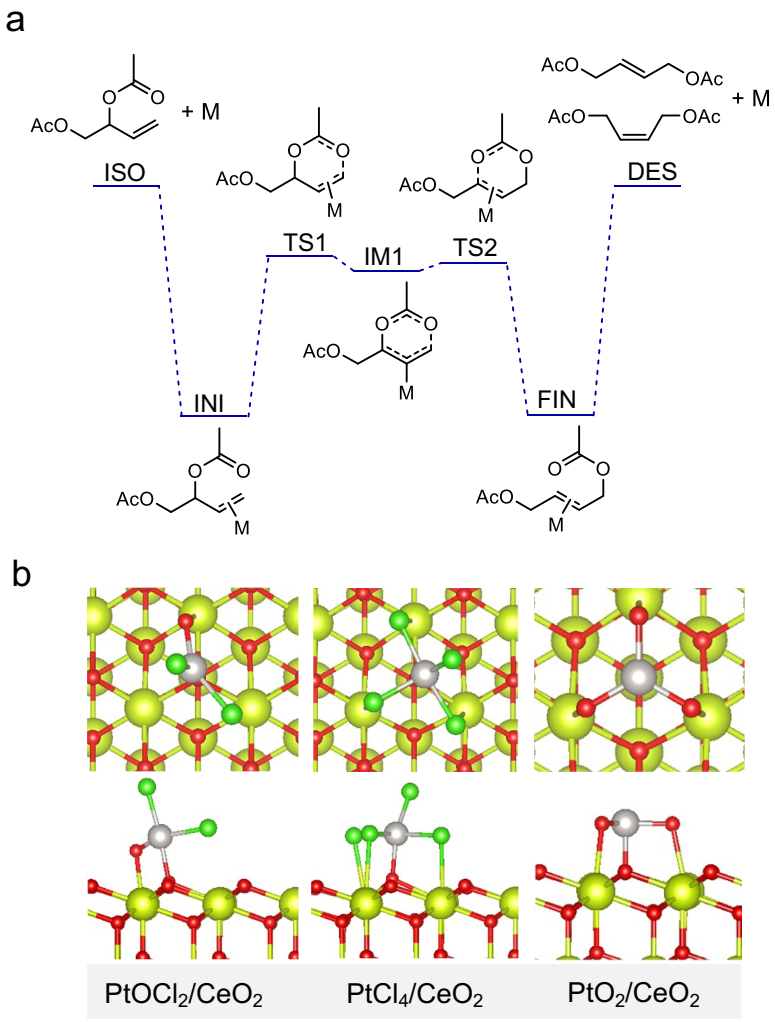

Figure 16. (a) Basic transition states of the catalytic isomerization of 3,4-DABE on the cluster model. (b) Slab models of Pt/CeO_2.

A slab model was set up with single-atom tetravalent Pt species containing Pt–Cl bonds and Pt–O bonds on $CeO_2(111)$ surfaces, such as $PtOCl_2/CeO_2$, $PtCl_4/CeO_2$, and PtO_2/CeO_2 with VASP code, to further simulate the actual reaction paths (Fig. 16b). Ce–Cl bonding was observed in the optimized model of $PtCl_4/CeO_2$, where the Ce–Cl group can also work as a Lewis acid and thus possibly increase the acidity of the Pt metal center in a Lewis acid-assisted approach[36,37].

Afterwards, the energy of each state for the catalytic process was optimized, and the diagram of the results reveals that the activation energy barrier and adsorption-desorption energy were low enough to facilitate the whole process when using Pt/CeO_2 catalysts with Pt–Cl bonds (Fig. 17a). In addition, the calculation for the reaction over

PtO_2/CeO_2 was also conducted, and the result shows that the adsorption of 3,4-DABE should be via di–σ (Pt–O) bonding between the C=C and Pt–O instead of the π-bond (Fig. 17b). Due to the large activation energy barrier (1.40 eV) and high desorption energy (2.14 eV), PtO_2/CeO_2 was demonstrated to show low activity for this reaction. The results of DFT calculations in this section are highly consistent with the actual results of the reaction and the findings in characterization experiments. Therefore, this research could promote a deep understanding of the effects of the fine structures or compositions of supported platinum catalysts on developing effect valuable catalytic reactions with olefin compounds.

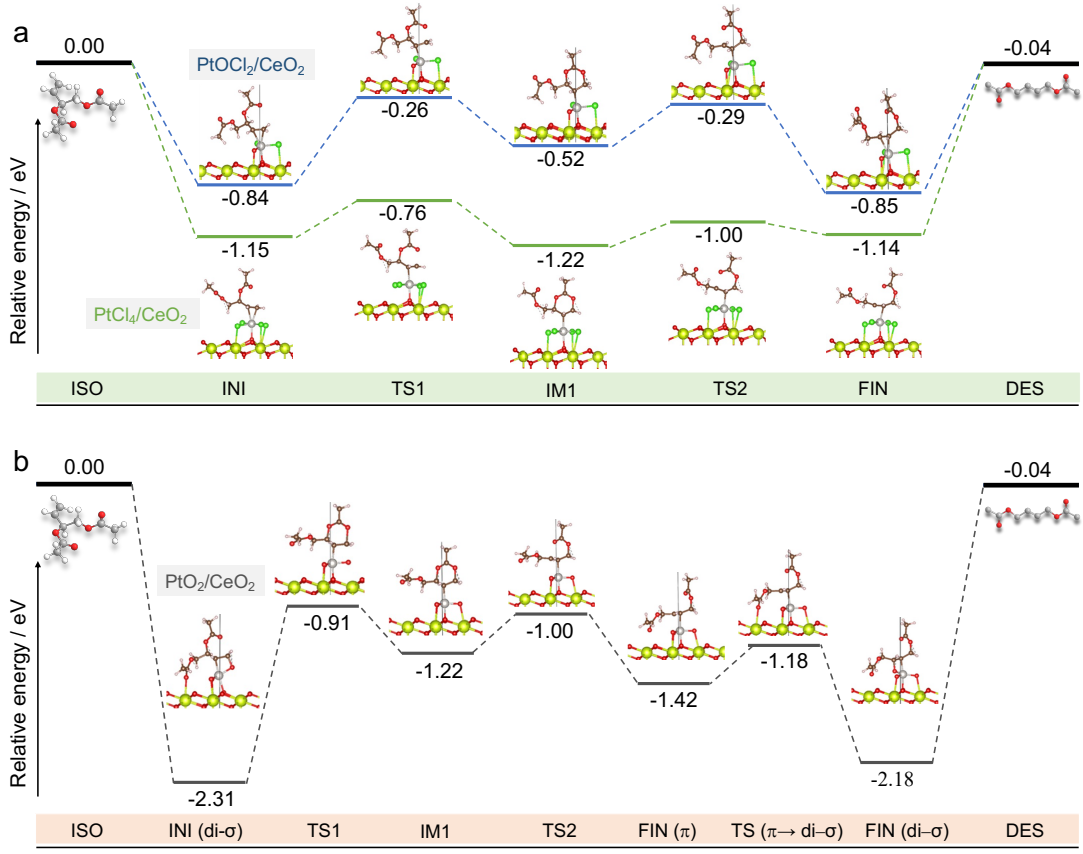

Figure 17. Calculation results for isomerization of 3,4-DABE on Pt/CeO_2 catalysts. (a) Diagram of the energy calculation of the transition states on the model catalysts $PtOCl_2/CeO_2$ and $PtCl_4/CeO_2$. (b) Diagram of the energy calculation of the transition states on the model catalyst PtO_2/CeO_2.

2.4. Conclusion

In conclusion, the efficient isomerization of allylic esters was achieved under solvent-free conditions using metal oxide-supported Pt catalysts, which can act as soft Lewis acids. great reusability, a high TON of 5400, and a wide substrate scope are available with the optimized Pt/CeO_2 catalysts. In addition, through the structural characterizations, the active species on CeO_2 were proved as highly dispersed Pt oxide clusters with Pt–Cl bonds, such as PtO_xCl_y. The reaction process with the optimized Pt catalysts was demonstrated to be via the soft Lewis acid mechanism, as proved by controlling experiments and DFT calculations. The characterization results reveal that the existence of Pt–Cl bonds, the high oxidation state of Pt species, and the strong interaction between CeO_2 and Pt play key roles in the high activity in this reaction. This research provides great reference of supported Pt soft Lewis acids that can efficiently catalyze the isomerization of allylic esters under ultra-simple reaction condition. Moreover, the enhancement effect of residual chloride on the Lewis acidity of the Pt metal center and thus the high catalytic activity could also show significance for the advanced design of heterogeneous catalyst in the future.

2.5. References

[1] P. Mardle, X. Ji, J. Wu, S. Guan, H. Dong, S. Du, Thin film electrodes from Pt nanorods supported on aligned N-CNTs for proton exchange membrane fuel cells, Appl. Catal. B Environ. 260 (2020) 118031.

[2] R.H. Nibbelke, A.J.L. Nievergeld, J.H.B.J. Hoebink, G.B. Marin, Development of a transient kinetic model for the CO oxidation by O_2 over a Pt/Rh/CeO_2/γ-Al_2O_3 three-way catalyst, Appl. Catal. B Environ. 19 (1998) 245–259.

[3] K. Ding, A. Gulec, A.M. Johnson, N.M. Schweitzer, G.D. Stucky, L.D. Marks, P.C. Stair, Identification of active sites in CO oxidation and water-gas shift over supported Pt catalysts, Science 350 (2015) 189–192.

[4] R.K.P. Purushothaman, J. van Haveren, D.S. van Es, I. Melián-Cabrera, J.D. Meeldijk, H.J. Heeres, An efficient one pot conversion of glycerol to lactic acid using

bimetallic gold-platinum catalysts on a nanocrystalline CeO_2 support, Appl. Catal. B Environ. 147 (2014) 92–100.

[5] X. Xing, C. Xu, B. Chen, C. Li, S.C. Virgil, R.H. Grubbs, Highly Active Platinum Catalysts for Nitrile and Cyanohydrin Hydration: Catalyst Design and Ligand Screening via High-Throughput Techniques, J. Am. Chem. Soc. 140 (2018) 17782–17789.

[6] A. Scarso, M. Colladon, P. Sgarbossa, C. Santo, R.A. Michelin, G. Strukul, Highly active and selective platinum(II)-catalyzed isomerization of allylbenzenes: Efficient access to (E)-anethole and other fragrances via unusual agostic intermediates, Organometallics 29 (2010) 1487–1497.

[7] A. Scarso, M. Colladon, P. Sgarbossa, C. Santo, R.A. Michelin, G. Strukul, Highly active and selective platinum(II)-catalyzed isomerization of allylbenzenes: Efficient access to (E)-anethole and other fragrances via unusual agostic intermediates, Organometallics 29 (2010) 1487–1497.

[8] L. Wang, R. Tang, A. Kheradmand, Y. Jiang, H. Wang, W. Yang, Z. Chen, X. Zhong, S.P. Ringer, X. Liao, W. Liang, J. Huang, Enhanced solar-driven benzaldehyde oxidation with simultaneous hydrogen production on Pt single-atom catalyst, Appl. Catal. B Environ. 284 (2021) 119759.

[9] N. Daelman, M. Capdevila-Cortada, N. López, Dynamic charge and oxidation state of Pt/CeO_2 single-atom catalysts, Nat. Mater. 18 (2019) 1215–1221.

[10] Z. Jiang, M. Jing, X. Feng, J. Xiong, C. He, M. Douthwaite, L. Zheng, W. Song, J. Liu, Z. Qu, Stabilizing platinum atoms on CeO_2 oxygen vacancies by metal-support interaction induced interface distortion: Mechanism and application, Appl. Catal. B Environ. 278 (2020) 119304.

[11] Z. Zhang, T. Mamba, E. Yamamoto, H. Murayama, T. Ishida, T.Honma, T. Fujitani, M. Tokunaga, Direct transformation of terminal alkenes with H_2O into primary alcohols over metal oxide-supported Pd catalysts, Appl. Catal. B Environ. 246 (2019) 100–110.

[12] Z. Zhang, T. Mamba, Q.-A. Huang, H. Murayama, E. Yamamoto, T.Honma, M.

Tokunaga, The additive effect of amines on the dihydroxylation of buta-1,3-diene into butenediols by supported Pd catalysts, Mol. Catal. 475 (2019) 110502.

[13] S. Bouquillon, J. Muzart, Palladium(0)-catalyzed isomerization of (Z)-1,4-diacetoxy-2-butene - Dependence of η1- or η3-allylpalladium as a key intermediate on the solvent polarity, European J. Org. Chem. (2001) 3301–3305.

[14] M. Mukhopadhyay, M.M. Reddy, G.C. Maikap, J. Iqbal, Cobalt(II)-Catalyzed Conversion of Allylic Alcohols/Acetates to Allylic Amides in the Presence of Nitriles, J. Org. Chem. 60 (1995) 2670–2676.

[15] N. Marion, R. Gealageas, S.P. Nolan, [(NHC)Au1]-Catalyzed Rearrangement of Allylic Acetates, Org. Lett. 9 (2007) 2653–2656.

[16] A.M. Zawisza, S. Bouquillon, J. Muzart, Palladium(II)-catalyzed isomerization of (Z)-1,4-diacetoxy-2-butene: Solvent effects, European J. Org. Chem. 2 (2007) 3901–3904.

[17] Gaussian 09, Revision A.02, M. J. Frisch, G. W. Trucks, H. B. Schlegel, G. E. Scuseria, M. A. Robb, J. R. Cheeseman, G. Scalmani, V. Barone, G. A. Petersson, H. Nakatsuji, X. Li, M. Caricato, A. Marenich, J. Bloino, B. G. Janesko, R. Gomperts, B. Mennucci, H. P. Hratchian, J. V. Ortiz, A. F. Izmaylov, J. L. Sonnenberg, D. Williams-Young, F. Ding, F. Lipparini, F. Egidi, J. Goings, B. Peng, A. Petrone, T. Henderson, D. Ranasinghe, V. G. Zakrzewski, J. Gao, N. Rega, G. Zheng, W. Liang, M. Hada, M. Ehara, K. Toyota, R. Fukuda, J. Hasegawa, M. Ishida, T. Nakajima, Y. Honda, O. Kitao, H. Nakai, T. Vreven, K. Throssell, J. A. Montgomery, Jr., J. E. Peralta, F. Ogliaro, M. Bearpark, J. J. Heyd, E. Brothers, K. N. Kudin, V. N. Staroverov, T. Keith, R. Kobayashi, J. Normand, K. Raghavachari, A. Rendell, J. C. Burant, S. S. Iyengar, J. Tomasi, M. Cossi, J. M. Millam, M. Klene, C. Adamo, R. Cammi, J. W. Ochterski, R. L. Martin, K. Morokuma, O. Farkas, J. B. Foresman, and D. J. Fox, Gaussian, Inc., Wallingford CT, 2016.

[18] G. Kresse, J. Furthmüller, Efficient iterative schemes for ab initio total-energy calculations using a plane-wave basis set, Phys. Rev. B. 54 (1996) 11169–11186.

[19] G. Kresse, J. Furthmüller, Efficiency of ab-initio total energy calculations for

metals and semiconductors using a plane-wave basis set, Comput. Mater. Sci. 6 (1996) 15–50.

[20] P.E. Blöchl, Projector augmented-wave method, Phys. Rev. B. 50 (1994) 17953–17979.

[21] J.P. Perdew, K. Burke, M. Ernzerhof, Generalized gradient approximation made simple, Phys. Rev. Lett. 77 (1996) 3865–3868.

[22] E.W. McFarland, H. Metiu, Catalysis by doped oxides, Chem. Rev. 113 (2013) 4391–4427.

[23] T. Ishida, T. Honma, K. Nakada, H. Murayama, T. Mamba, K. Kume, Y. Izawa, M. Utsunomiya, M. Tokunaga, Pd-catalyzed decarbonylation of furfural: Elucidation of support effect on Pd size and catalytic activity using in-situ XAFS, J. Catal. 374 (2019) 320–327.

[24] J. Jones, H. Xiong, A.T. DeLaRiva, E.J. Peterson, H. Pham, S.R. Challa, G. Qi, S. Oh, M.H. Wiebenga, X.I.P. Hernández, Y. Wang, A.K. Datye, Thermally stable single-atom platinum-on-ceria catalysts via atom trapping, Science 353 (2016) 150–154.

[25] D. Kunwar, S. Zhou, A. Delariva, E.J. Peterson, H. Xiong, X.I. Pereira-Hernández, S.C. Purdy, R. Ter Veen, H.H. Brongersma, J.T. Miller, H. Hashiguchi, L. Kovarik, S. Lin, H. Guo, Y. Wang, A.K. Datye, Stabilizing High Metal Loadings of Thermally Stable Platinum Single Atoms on an Industrial Catalyst Support, ACS Catal. 9 (2019) 3978–3990.

[26] Z.R. Ismagilov, S.A. Yashnik, A.N. Startsev, A.I. Boronin, A.I. Stadnichenko, V. V. Kriventsov, S. Kasztelan, D. Guillaume, M. Makkee, J.A. Moulijn, Deep desulphurization of diesel fuels on bifunctional monolithic nanostructured Pt-zeolite catalysts, Catal. Today 144 (2009) 235–250.

[27] F.J. Gracia, J.T. Miller, A.J. Kropf, E.E. Wolf, Kinetics, FTIR, and controlled atmosphere EXAFS study of the effect of chlorine on Pt-supported catalysts during oxidation reactions, J. Catal. 209 (2002) 341–354.

[28] X. Zhu, B. Cheng, J. Yu, W. Ho, Halogen poisoning effect of Pt-TiO_2 for formaldehyde catalytic oxidation performance at room temperature, Appl. Surf. Sci.

364 (2016) 808–814.

[29] K. Zhang, L. Dai, Y. Liu, J. Deng, L. Jing, K. Zhang, Z. Hou, X. Zhang, J. Wang, Y. Feng, Y. Zhang, H. Dai, Insights into the active sites of chlorine-resistant Pt-based bimetallic catalysts for benzene oxidation, Appl. Catal. B Environ. 279 (2020) 119372.

[30] H. Shi, O.Y. Gutiérrez, H. Yang, N.D. Browning, G.L. Haller, J.A. Lercher, Catalytic consequences of particle size and chloride promotion in the ring-opening of cyclopentane on Pt/Al_2O_3, ACS Catal. 3 (2013) 328–338.

[31] J. Lee, Y. Ryou, X. Chan, T.J. Kim, D.H. Kim, How Pt interacts with CeO_2 under the reducing and oxidizing environments at elevated temperature: The origin of improved thermal stability of Pt/CeO_2 compared to CeO_2, J. Phys. Chem. C. 120 (2016) 25870–25879.

[32] A. Bruix, J.A. Rodriguez, P.J. Ramírez, S.D. Senanayake, J. Evans, J.B. Park, D. Stacchiola, P. Liu, J. Hrbek, F. Illas, A new type of strong metal-support interaction and the production of H_2 through the transformation of water on $Pt/CeO_2(111)$ and $Pt/CeO_x/TiO_2(110)$ catalysts, J. Am. Chem. Soc. 134 (2012) 8968–8974.

[33] M. Brown, R.E. Peierls, E.A. Stern, White lines in x-ray absorption, Phys. Rev. B. 15 (1977) 738–744.

[34] H. Lieske, G. Lietz, H. Spindler, J. Völter, Reactions of platinum in oxygen- and hydrogen-treated Pt γ-Al_2O_3 catalysts. I. Temperature-programmed reduction, adsorption, and redispersion of platinum, J. Catal. 81 (1983) 8–16.

[35] Y. Gao, W. Wang, S. Chang, W. Huang, Morphology effect of CeO_2 support in the preparation, metal-support interaction, and catalytic performance of Pt/CeO_2 catalysts, ChemCatChem 5 (2013) 3610–3620.

[36] Z. Hu, H. Metiu, Halogen adsorption on CeO_2: The role of Lewis acid-base pairing, J. Phys. Chem. C. 116 (2012) 6664–6671.

[37] K. Futatsugi, H. Yamamoto, Oxazaborolidine-derived Lewis acid assisted Lewis acid as a moisture-tolerant catalyst for enantioselective Diels-Alder reactions, Angew. Chem. Int. Ed. 44 (2005) 1484–1487.

Chapter 3.
Investigation of reusability and deactivation mechanism of supported Pt catalysts in the practical isomerization of allylic esters

3.1. Introduction

In recent decades, supported Pt catalysts have been widely studied, and have been applied to tackle energy and environment problems, such as fuel cells[1], exhaust-gas treatment[2], and volatile organic compounds (VOCs) conversion[3]. In addition, supported Pt catalysts are also applied in the transformation of petroleum-based feedstocks or biomass derivatives into high value-added chemicals[4–7]; however, most of them acted as redox catalysts. As a matter of fact, the number of previous studies about the Lewis acid-base properties of supported Pt catalysts was infrequent. On the other hand, homogeneous Pt(II) catalysts have been well developed in many reactions by soft Lewis acid functions[8,9], based on Pearson's hard-soft acid-base (HSAB) theory[10]. To obtain further recognition of the Lewis acid properties of supported Pt catalysts, we prepared well-designed metal-oxides supported Pt catalysts, which can be applied for the isomerization of allylic esters in a soft Lewis acid mechanism[11], and it was the first example for supported Pt catalysts acting as soft Lewis acids. Meanwhile, an extremely high turnover number (TON) was also obtained, which was more than two orders of magnitude higher than those in the previous reports[12–13]. Highly dispersed Pt oxide clusters with Pt–Cl bonds were demonstrated to play an essential role for the high catalytic activity.

Currently, utilization of biomass derivatives and the captured CO_2 have become a significant field for researches of heterogeneous catalyst and resource chemicals[14,15]. However, only few attention has been paid to solving the practical issues in the production of valued chemicals of the petrochemical industry[16,17]. For instance, during the production of C4 derivatives, a byproduct but-3-ene-1,2-diyl diacetate (3,4-DABE) obtained by oxidative acetoxylation of butadiene is treated by burning, which is not environmental (Fig. 1). With the previous research on supported Pt catalysts with soft Lewis acidity for the isomerization of allylic esters, this issue can be solved with the industrialization of catalytic isomerization of 3,4-DABE[11].

Meanwhile, for the industrial heterogeneous catalysts, reusability should be one of the most significant indexes besides the catalytic activity. Normally, along with the

increase of reaction times or reusing times, ineluctable deactivation of catalysts occurred to some extend by various reasons, such as sintering, coking, and the changes in valence states[18–20]. Therefore, in-depth investigation on the reasons and mechanisms of catalyst deactivation can alleviate the deactivation and help reactivate the catalysts[21].

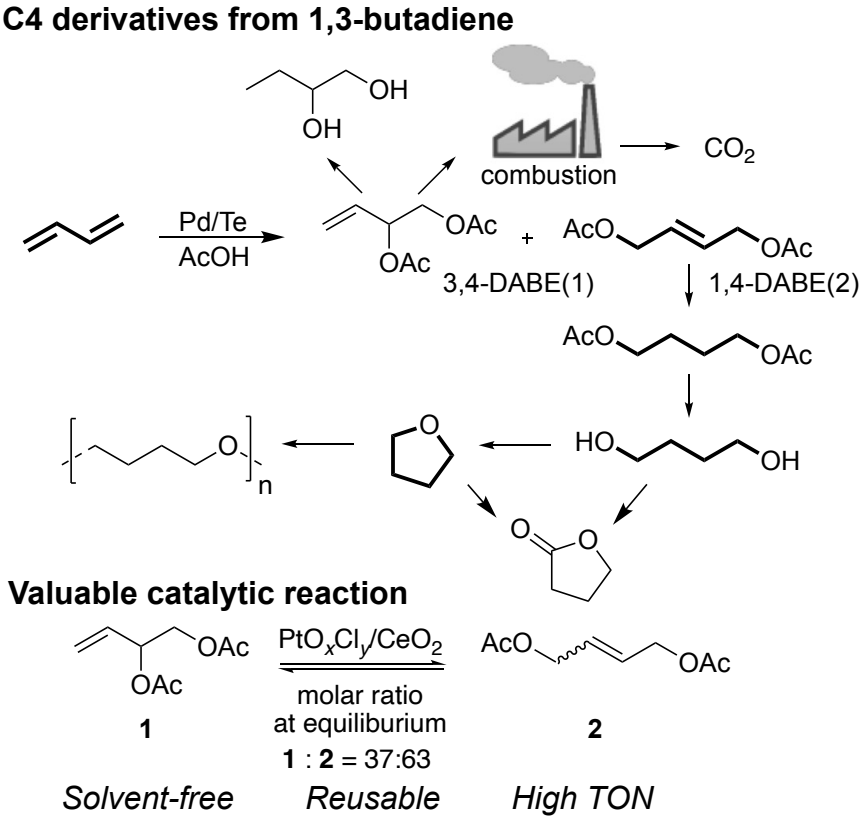

Figure 1. Illustration of a C4 derivatives production unit and the value of catalytic isomerization of 3,4-DABE.

In this research, we carried out investigation over the reusability of metal oxides supported Pt catalysts with soft Lewis acid function in the isomerization of 3,4-DABE to facilitate the industrialization of this catalytic system. Multiple used catalysts were analyzed using X-ray absorption fine structure (XAFS) to understand the states of supported Pt species and their deactivation mechanism. The results uncover that the deactivated catalysts can be easily reactivated through a method with HCl treatment, and a relatively stable state may form during the reusing of Pt-Cl/CeO_2, retarding the further deactivation.

3.2. Experimental

3.2.1. Materials

Chloroplatinic acid hexahydrate ($H_2PtCl_6 \cdot 6H_2O$) was purchased from Furuya Metal Co., Ltd. CeO_2 (JRC-CEO-3, 81 m^2/g), ZrO_2 (JRC-ZRO-4, 30 m^2/g), Al_2O_3(9) (JRC-ALO-9, γ-Al_2O_3, 204 m^2/g), and Al_2O_3(10) (JRC-ALO-10, θ-Al_2O_3 104 m^2/g) were reference catalysts obtained by the Catalysis Society of Japan. 3,4-DABE was purchased from Sigma Aldrich, Ltd.

3.2.2. Preparation of catalysts

Pt-Cl/CeO_2 catalysts with a loading of 1 wt% Pt were prepared by an impregnation method. H_2PtCl_6 aqueous solution (Pt: 19.75 g/L; 511 μL) was diluted in 1.5 mL of H_2O. 1.0 g CeO_2 was added to the solution and mixed at room temperature for 30 min. Then, the obtained slurries were dried by a vacuum freeze method overnight. Finally, the catalysts were calcined with a furnace at 300 °C for 4 h. Pt-Cl/ZrO_2 and Pt-Cl/Al_2O_3 were prepared by the same method.

The reactivation of deactivated Pt-Cl/CeO_2 was investigated with HCl treatment. The deactivated catalysts (100 mg) were added into a 0.1 M HCl solution (1.5 ml) and stirred at 80 °C for 12 h. Then, the solid was filtered and dried by a vacuum freeze method for 6 h. The obtained catalysts were then calcined at 500 °C for 4 h.

3.2.3. Characterization

The local structures of supported Pt catalysts were analyzed through Pt L_{III}-edge XAFS spectra measured at the BL14B2 beamline of SPring-8 (Hyogo, Japan). Temperature-programmed desorption (TPD) was performed by a BELCAT instrument equipped with a thermal conductivity detector (TCD). In addition, the CO-pulse were conducted to confirm the dispersion of the supported platinum species, and the samples were pretreated in a flow of He at 300 °C for 30 min.

Conversions and yields of the compounds discussed were determined by gas chromatography (GC) using an Agilent GC 6850 Series II instrument equipped with a flame ionization detector (FID) and a J&W HP-1 column with tridecane as an internal standard.

3.2.4. General Procedure for the Catalytic Reactions

A screw cap vial was charged with catalysts, 3,4-DABE, and a magnetic stirring. Then, the reaction mixture was stirred at 150 °C under an N_2 or air atmosphere (1 atm). When the reaction was finished, the mixture was filtered, and the filtrate was analyzed by GC.

Reusing tests were carried out with the Pt-Cl/MO_x prepared by an impregnation method. In one reusing cycle, the screw cap vial was cooled in an ice bath after the reaction. After collecting by the centrifugation, used Pt catalysts were washed with Et_2O twice and dried under vacuum conditions. Then, the obtained catalysts were used for the next cycle.

3.3. Results and Discussion

Pt-Cl/CeO_2 catalysts ould be easily prepared by an impregnation method using the precursor of $H_2PtCl_6{\cdot}6H_2O$. Therefore, the catalysts for reusing test were prepared by this method, and their reusability and the deactivation mechanism were investigated. Then, an 8-run reusing test for isomerization reaction of 3,4-DABE was performed, and an obvious deactivation was observed (Fig. 2).

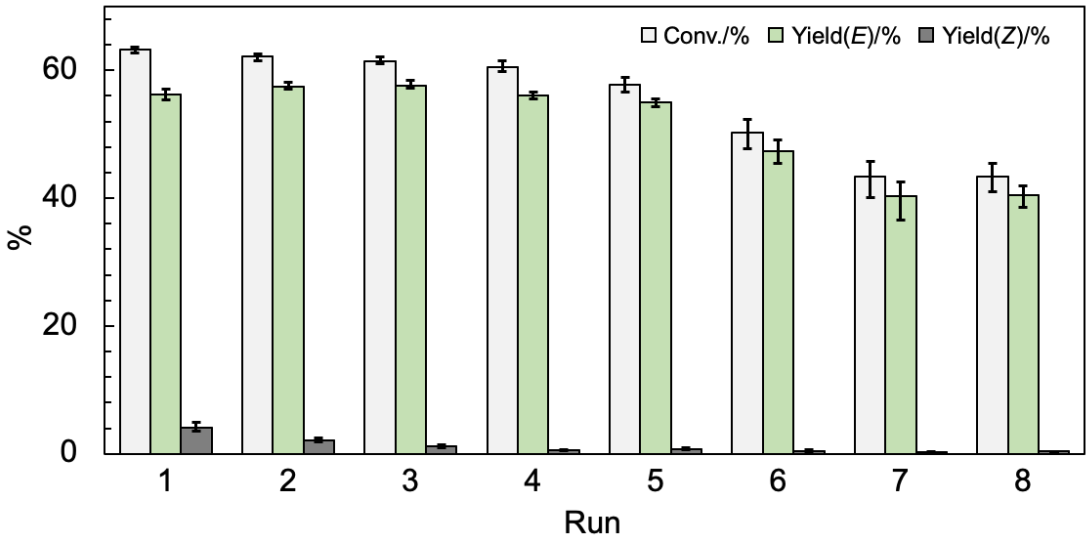

Figure 2. Reusability of Pt-Cl/CeO_2 for isomerization of 3,4-DABE.

Since it has been measured that the leaching amount of supported Pt species in this reaction was only around 2% in our previous research[11], it could be inferred that the

dominant deactivation reason of catalysts in this reaction should be reduction or agglutination of the supported Pt species. In addition, oxychlorination treatment has been demonstrated to be an effective method for reactivation of supported Pt catalysts [22]. Thus, calcination treatment and HCl-treatment are performed to discuss the reactivation of the catalysts. TPD is used to identify residual organic matter on the surface of the catalysts, and desorption peak of organic compounds from the deactivated catalysts was observed extended to above 400 °C (Fig. 3); therefore, the used and the HCl-treated catalysts after the 8th run were calcinated at 500 °C.

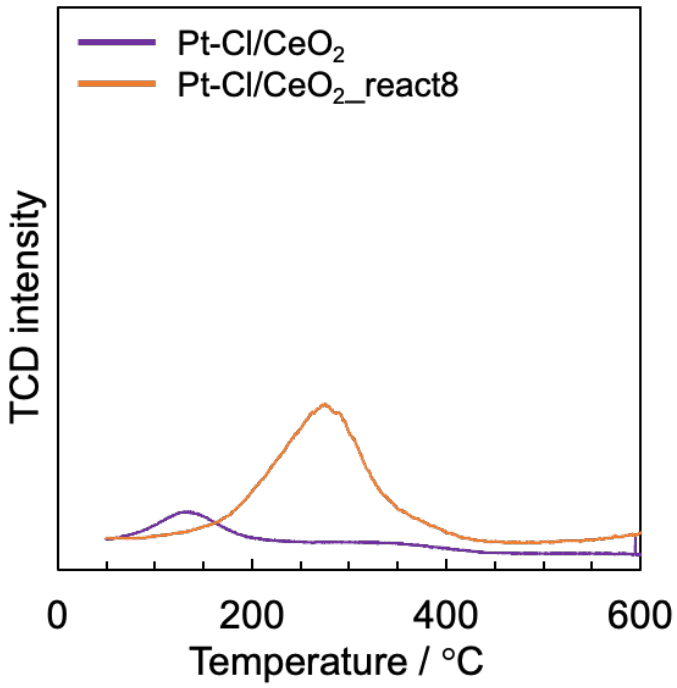

Figure 3. TPD profiles of Pt-Cl/CeO_2 catalysts fresh and after the 8th run.

Reactivation method of HCl-treatment gave an obvious recovery of activity in the catalytic isomerization reaction, and no recovery of activity was achieved for the used catalysts only treated with a calcination at 500 °C (Table 1). In addition, no significant changes were observed in CO-pulse detection, revealing that no significant obvious agglutination of supported Pt species occurred after reacting for 8 times. Thus, reduction of the active Pt species in high valence should be the dominant reason for the deactivation. Furthermore, although no obvious byproducts were detected from the GC results, we infer that the trace alcohol compounds produced from the inevitable hydrolysis of esters should be a reductant for the reduction of Pt species in the reaction.

Table 1 Discussion on the reusability and reactivation of the Pt-Cl/CeO_2[a]

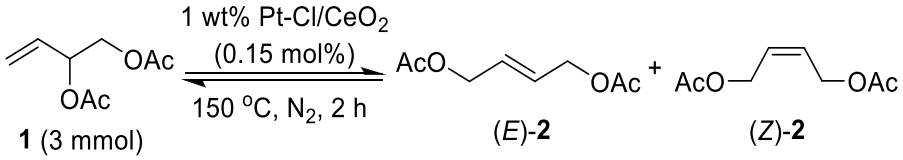

Entry	Run	Conv. (%)[a]	Yield (%)[b]	
			(*E*)-**2**	(*Z*)-**2**
1	1st	64	57	4
2	8th	41	39	trace
3[c,d]	calcination	39	37	trace
4[d,e]	HCl treatment	58	54	2

[a]Reaction scale was 3 mmol. [b]Determined by GC analysis with tridecane as internal standard. [c]The catalyst after the 8th run was calcined at 500 °C. [d]1 mmol scale. [e]The catalyst after the 8th run was treated by HCl and a following calcination at 500 °C.

Afterwards, Pt L_{III}-edge XAFS spectra were collected and analyzed to investigate the fine structure of the catalysts after the 8th run. Pt L_{III}-edge X-ray absorption near edge structure (XANES) spectra of the Pt-Cl/CeO_2 catalysts as prepared and after the 8th run were compared with Pt foil as the reference (Fig. 4a). The reduction of the supported Pt species was uncovered by observing the decrease in intensity of the used catalysts through the characteristic peak, the white line[23]. In addition, phase-uncorrected radial structure functions (RSFs) for the discussed catalysts were also analyzed (Fig. 4b), and the peaks at approximately 1.65 Å attributing to the Pt–O coordination and the peaks at approximately 1.95 Å attributing to the Pt–Cl coordination were observed in both the fresh and used catalysts with the reference peaks of PtO_2 and K_2PtCl_6. After comparing the changes over RSFs, the intensity of Pt–O coordination decreased more significantly than the Pt–Cl coordination after the 8th run. No obvious peaks around 2.60 Å and 2.85 Å were observed, which should attribute to the Pt–Pt coordination and the Pt–O–Pt coordination, respectively, revealing the unobvious agglutination. Thus, the oxidation state is a significant factor for the catalytic activities of the catalysts, and the Pt–Cl coordination is more stable than the Pt–O

coordination. Moreover, the reactivated catalysts after HCl-treatment-calcination were also analyzed using Pt L_{III}-edge XAFS spectra, and the structural parameters of the catalysts were analyzed through EXAFS curve-fitting (Table 2). In the XANES spectra, an enhancement in oxidation was observed by comparing the white lines of the used catalysts and the used catalyst with reactivation treatment (Fig. 4c). The increase in the intensity of Pt–O coordination should account for the reactivation, and the relatively low intensity in the region of Pt–Cl coordination and the enhanced intensity in the region Pt–Pt coordination revealed a little agglutination of supported Pt species after the reactivation treatment, which should be caused by the post-calcination at 500 °C (Fig. 4d).

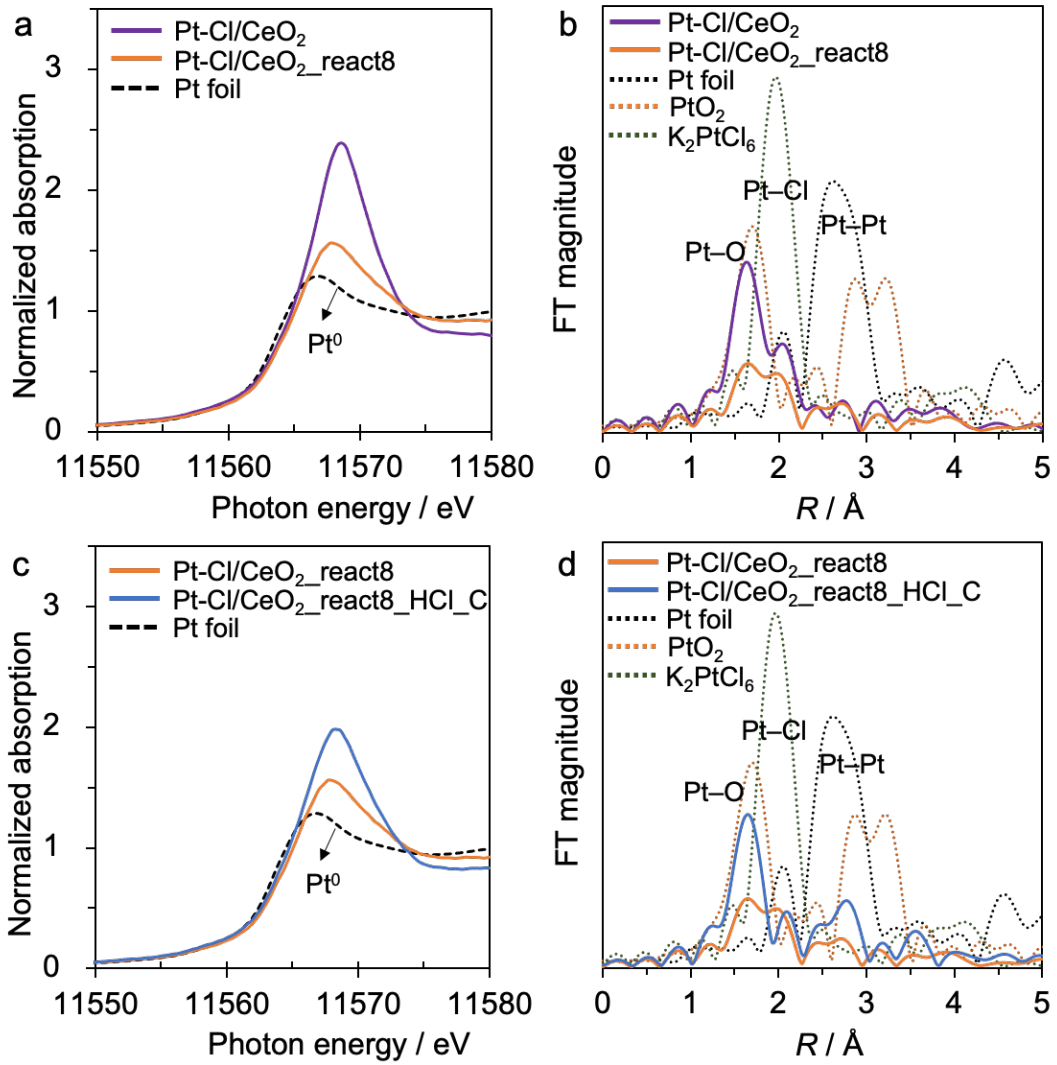

Figure 4. (a) Pt L_{III}-edge XANES spectra, (b) RSFs, and (c) Pt L_{III}-edge XANES spectra, (d) RSFs of Pt-Cl/CeO_2 catalysts after the 8th run and reactivated.

Table 2. EXAFS fitting results and of Pt-Cl/CeO_2 in different situation.[a]

Catalyst	Scattering path	*CN*[b]	*R* (Å)[c]	σ^2 (Å^2)[d]	*R*-factor[f]
Pt foil	Pt–Pt	12[e]	2.76 ± 0.002	0.004 ± 0.0002	0.001
$Na_2Pt(OH)_6$	Pt–O	6[e]	2.00 ± 0.006	0.002 ± 0.0008	0.002
K_2PtCl_6	Pt–Cl	6[e]	2.32 ± 0.004	0.002 ± 0.0004	0.004
Pt-Cl/CeO_2_fresh	Pt–O	4.69 ± 0.53[g]	1.99 ± 0.012	0.002 ± 0.001	0.003
	Pt–Cl[h]	1.31 ± 0.53[g]	2.32 ± 0.009	0.001 ± 0.002	
Pt-Cl/CeO_2_	Pt–O	2.75 ± 0.76	2.03 ± 0.032	0.009 ± 0.007	0.005
react1	Pt–Cl[h]	1.95 ± 0.92	2.31 ± 0.015	0.007 ± 0.005	
Pt-Cl/CeO_2_	Pt–O[h]	2.15 ± 0.54	2.04 ± 0.032	0.006 ± 0.004	0.010
react8	Pt–Cl[h]	1.91 ± 0.90	2.31 ± 0.020	0.010 ± 0.007	
Pt-Cl/CeO_2_	Pt–O[h]	4.38 ± 1.04[g]	2.01 ± 0.011	0.004 ± 0.002	0.020
8th_HCl_C	Pt–Cl[h]	1.62 ± 1.04[g]	2.31 ± 0.060	0.019 ± 0.009	

[a] k^3: *k*-range = 3–12 Å^{-1}. Intrinsic loss factor, S_0^2=0.77(Pt–O), 0.82(Pt–Cl), and 0.80(Pt–Pt). *r*-range=1.8–3.2, 1.0–2.0, 1.0–2.5, and 1.0–2.5 Å for Pt foil, PtO_2, $Na_2Pt(OH)_6$, and Pt catalysts, respectively. [b] Coordination number. [c] Bond length. [d] Debye-Waller factor. [e] Fixed. [f] Goodness-of-fit index. [g] Total coordination numbers were fixed to 6. [h] ΔE_0 was fixed to the value of reference samples (Pt–O: 15.57 eV, Pt–Cl:13.15 eV).

Pt-Cl/CeO_2 and Pt-Cl/ZrO_2 showed similar Pt oxidation state and Pt–Cl coordination [11]. In this section, we analyzed the used catalysts with XAFS and conducted reusing test under the same condition to compare their reusability (Fig. 5). Partial reduction of Pt species and decrease in the intensity of Pt–O coordination was observed for the Pt-Cl/CeO_2 catalysts, which were recycled from the first run (Fig. 5a and 5b). However, no obvious decrease in yield could be found during the 4-run reusing test (Fig. 5c). In addition, almost completely reduced Pt species were observed in the XANES spectra for the used Pt-Cl/ZrO_2 catalysts (Fig. 5d). In the RSFs spectra, the intensities of Pt–O coordination and Pt–Cl coordination were drastically decrease, which were seems to be replaced by the Pt–Pt coordination (Fig. 5e). The strong signal of Pt–Pt coordination uncovered the reduction and agglutination of the Pt species supported by ZrO_2. Meanwhile, the results of structure analysis were consistent with the drastic degradation in the reusing test (Fig. 5f).

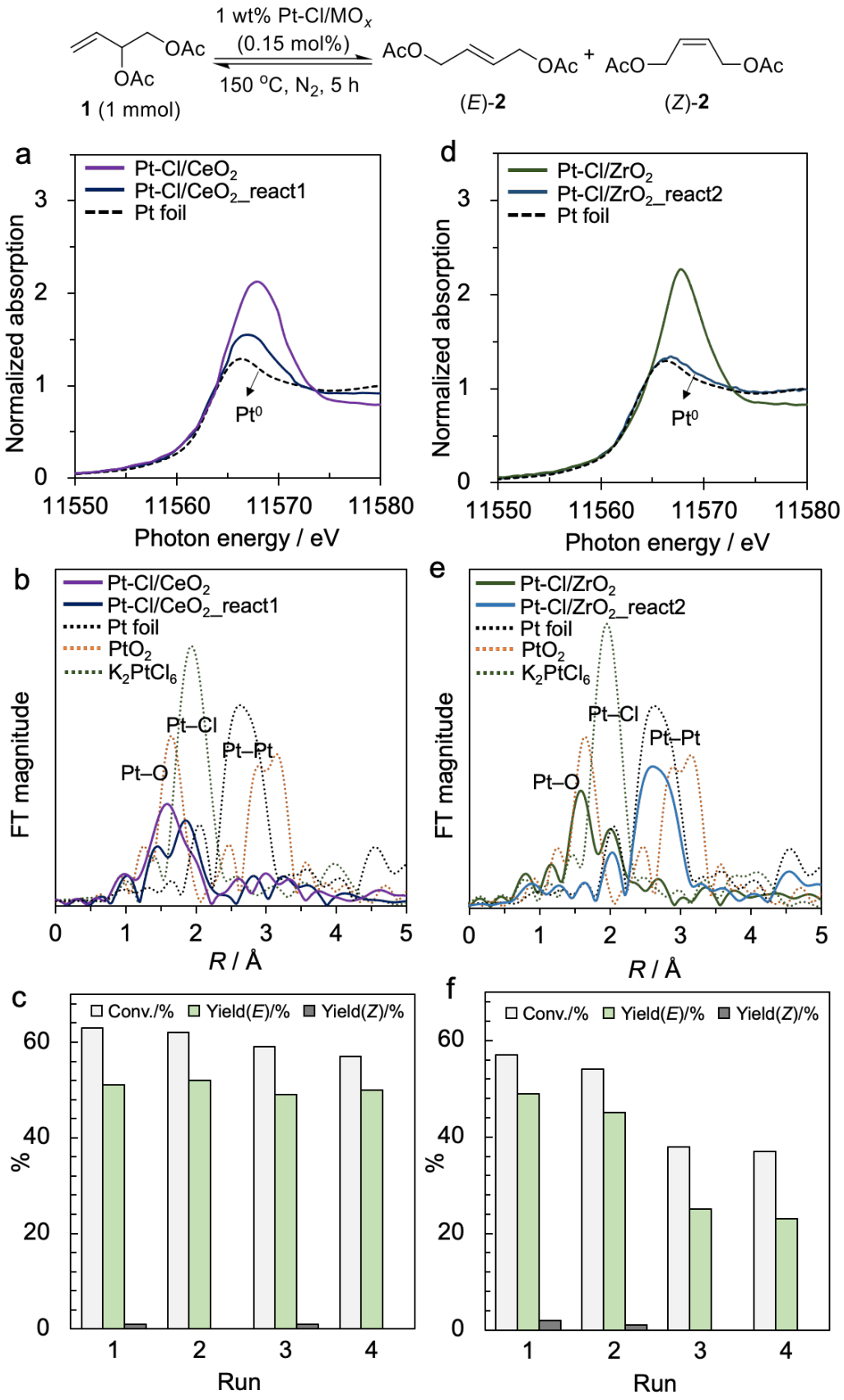

Figure 5. (a) Pt L_{III}-edge XANES spectra, (b) RSFs, and (c) reusing result of Pt-Cl/CeO_2. (d) Pt L_{III}-edge XANES spectra, (e) RSFs, and (f) reusing result of Pt-Cl/ZrO_2.

The reusability of Pt-Cl/Al_2O_3 was also discussed with two kinds of Al_2O_3 supports, γ-Al_2O_3 (JRC-ALO-9) and θ-Al_2O_3 (JRC-ALO-10). XAFS analysis was performed for the fresh Pt-Cl/Al_2O_3(9) and Pt-Cl/Al_2O_3(10) catalysts, and a relatively high oxidative state of Pt species in Pt-Cl/Al_2O_3(10) was observed (Fig. 6).

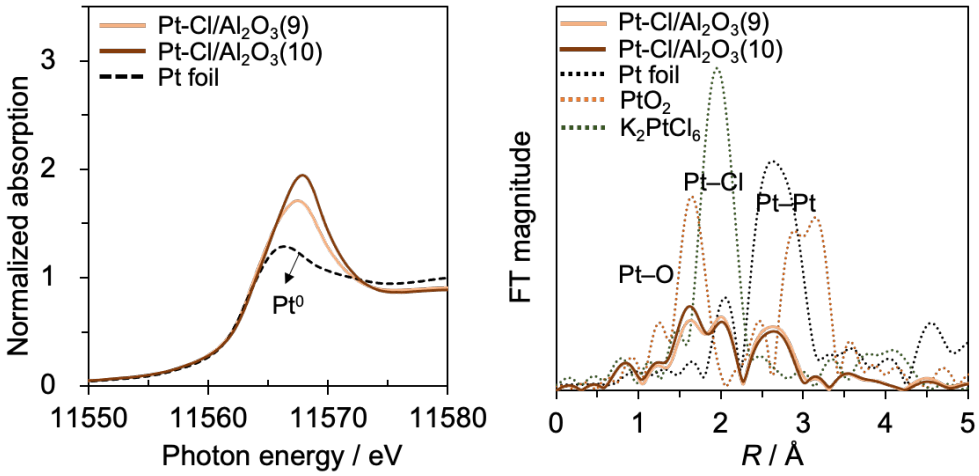

Figure 6. (a) Pt L_{III}-edge XANES spectra of Pt-Cl/Al_2O_3(9) and Pt-Cl/Al_2O_3(10). (b) RSFs of Pt-Cl/Al_2O_3(9) and Pt-Cl/Al_2O_3(10).

In the reusing test, a drastic degradation in reaction activity was observed when using the Pt-Cl/Al_2O_3(10) catalysts (Fig. 7f). However, only a moderate decrease in reaction results occurred when using the Pt-Cl/Al_2O_3(9) catalysts (Fig. 7c). In addition, the XANES spectra of the used catalyst showed that Pt-Cl/Al_2O_3 catalysts are easy to be reduced (Fig. 7a and 7d). On the other hand, drastic decreases in the intensities of Pt–O coordination were also observed in RSFs (Fig. 7b and 7e). Through the curve-fitting of the EXAFS spectra, the relatively great reusability of Pt-Cl/Al_2O_3(9) catalysts should be related to the relatively high Pt–Cl coordination number (Table 3), which was significant for the catalytic activity. Based on the above results, Pt-Cl/Al_2O_3 seems unsuitable for further optimized as industrial catalysts for this kind of reaction. Among the metal oxide supports discussed in this study, CeO_2 supported Pt catalysts provided superior performance both in the catalytic activity and reusability. This could be attributed to the relatively strong metal-support interaction between Pt species and CeO_2.

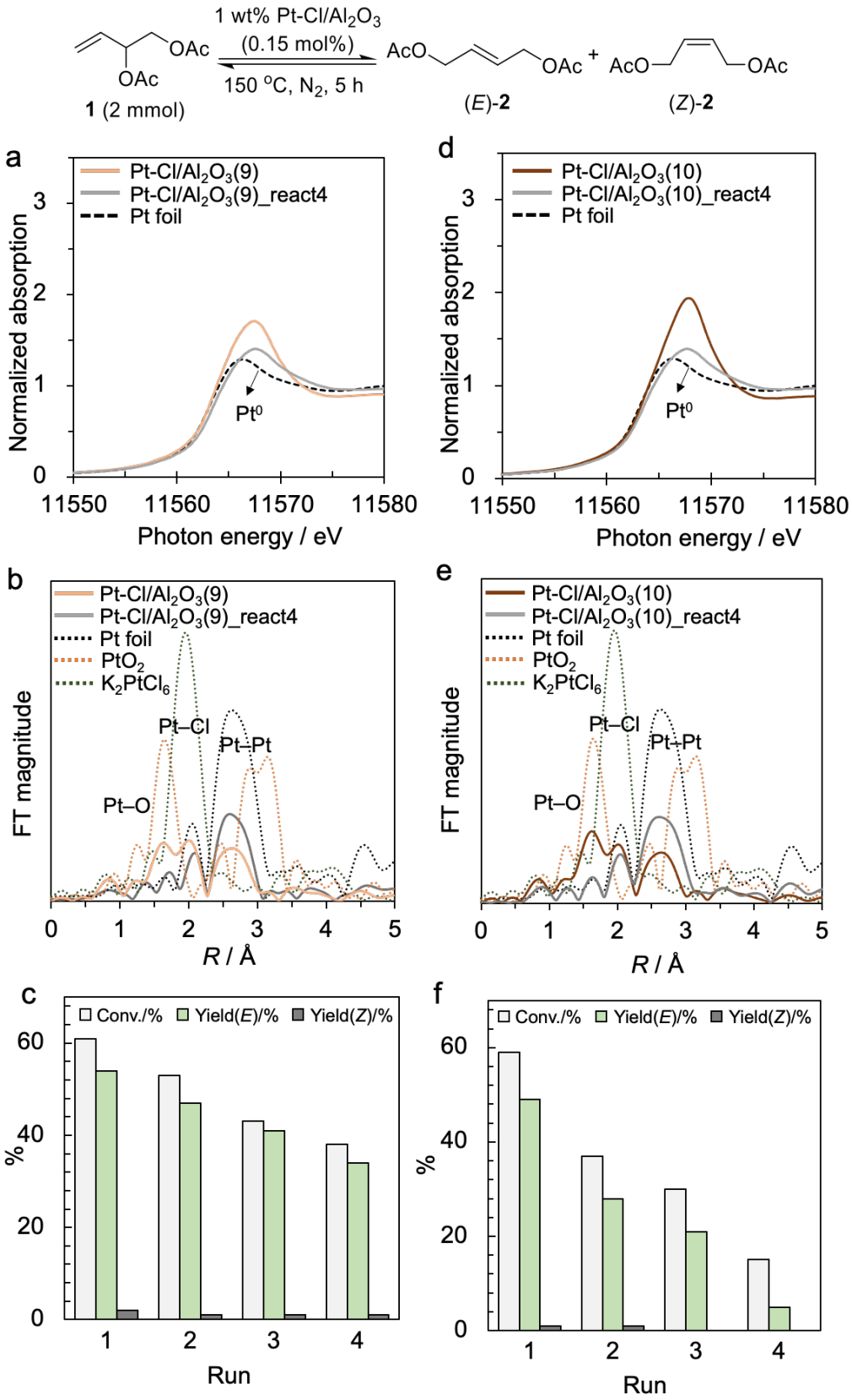

Figure 7. (a) Pt L_{III}-edge XANES spectra, (b) RSFs, and (c) reusing result of Pt-Cl/Al_2O_3(9). (d) Pt L_{III}-edge XANES spectra, (e) RSFs, and (f) reusing result of Pt-Cl/Al_2O_2(10).

Table 3. EXAFS fitting results of Pt/MO_x.[a]

Catalyst	Scattering path	*CN*[b]	*R* (Å)[c]	σ^2 (Å^2)[d]	*R*-factor[f]
Pt foil	Pt–Pt	12[e]	2.76 ± 0.002	0.004 ± 0.0002	0.001
$Na_2Pt(OH)_6$	Pt–O	6[e]	2.00 ± 0.006	0.002 ± 0.0008	0.002
K_2PtCl_6	Pt–Cl	6[e]	2.32 ± 0.004	0.002 ± 0.0004	0.004
Pt-Cl/CeO_2_fresh	Pt–O	4.69 ± 0.53[g]	1.99 ± 0.012	0.002 ± 0.001	0.003
	Pt–Cl[h]	1.31 ± 0.53[g]	2.32 ± 0.009	0.001 ± 0.002	
Pt-Cl/ZrO_2	Pt–O	4.82 ± 0.90[g]	1.99 ± 0.025	0.003 ± 0.001	0.012
	Pt–Cl[h]	1.18 ± 0.90[g]	2.30 ± 0.015	0.0001 ± 0.005	
Pt-Cl/Al_2O_3(9)[I]	Pt–O[h]	2.34 ± 0.89	2.02 ± 0.014	0.004 ± 0.003	0.013
	Pt–Cl[h]	1.05 ± 0.62	2.30 ± 0.010	0.002 ± 0.004	
	Pt–Pt[h]	4.48 ± 1.79	2.76 ± 0.006	0.006 ± 0.002	
Pt-Cl/Al_2O_3(10)[I]	Pt–O[h]	2.99 ± 1.16	2.01 ± 0.015	0.004 ± 0.003	0.020
	Pt–Cl[h]	0.95 ± 0.79	2.32 ± 0.014	0.002 ± 0.005	
	Pt–Pt[h]	4.74 ± 2.55	2.77 ± 0.009	0.007 ± 0.003	

[a] k^3: *k*-range = 3–12 Å^{-1}. Intrinsic loss factor, S_0^2=0.77(Pt–O), 0.82(Pt–Cl), and 0.80(Pt–Pt). *r*-range=1.8–3.2, 1.0–2.0, 1.0–2.5, and 1.0–2.5 Å for Pt foil, PtO_2, $Na_2Pt(OH)_6$, and Pt catalysts, respectively. [b] Coordination number. [c] Bond length. [d] Debye-Waller factor. [e] Fixed. [f] Goodness-of-fit index. [g] Total coordination numbers were fixed to 6. [h] ΔE_0 was fixed to the value of reference samples (Pt–O: 15.57 eV, Pt–Cl:13.15 eV, Pt–Pt:9.68 eV). [I] *r*-range=1.0–3.0 Å, *k*-range = 3–13 Å^{-1}.

Spectral analyses were carried out using the XAFS analysis software of Athena and Artemis. In the curve-fitting analysis, backscattering amplitude, phase shift, and mean free path of the photoelectrons were calculated by FEFF6 and then the other parameters, including the number of neighboring atoms, the interatomic distance between the adsorbed atom to the neighboring atom, the Debye-Waller factor, and absorption edge energy, were treated as fitting parameters. The intrinsic loss factors were obtained by curve-fitting analysis of the EXAFS data of reference samples, Pt foil, PtO_2 and $Na_2Pt(OH)_6$, respectively.

Through the above investigation, it was found that the Pt–O coordination of the supported Pt catalysts is easier to be reduced than the Pt–Cl coordination, and this

usually affect their catalytic efficiency. In addition, it was also uncovered that the Pt–Cl coordination play a significant role in the reaction and govern the upper limit of the catalytic efficiency. Fortunately, both Pt–O coordination and Pt–Cl coordination were reduced moderately when using the catalysts supported by CeO_2, and they were proved by the XAFS measurement of Pt-Cl/CeO_2 reused in different cycles. Besides, a relatively stable state of the supported Pt species may form during the reusing, and it could effectively prevent the catalysts from further deactivation (Fig. 8).

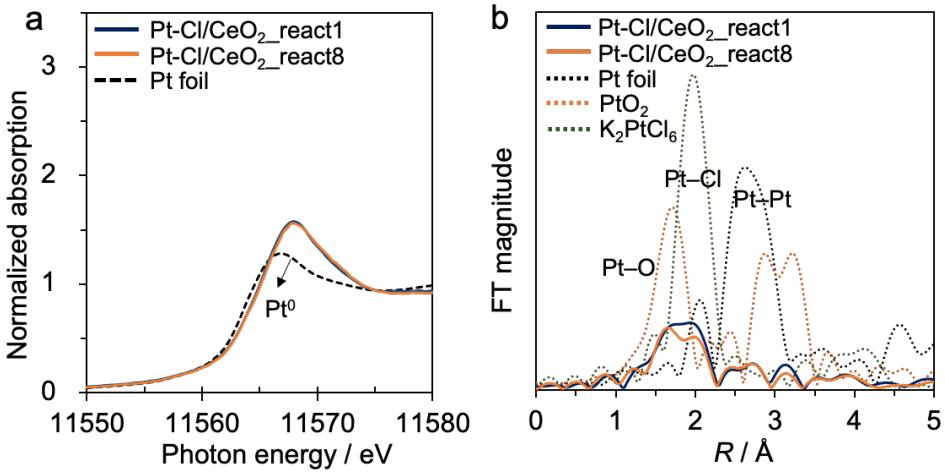

Figure 8. (a) Pt L_{III}-edge XANES spectra and (b) RSFs of the used Pt-Cl/CeO_2 catalysts recycled from the first run and the 8th run.

3.4. Conclusion

In conclusion, we carried out investigation on the reusability and deactivation mechanism of metal oxides supported Pt catalysts in the isomerization of 3,4-DABE. The results showed that it is peasible to reactivate the catalysts and recover the high catalytic activities by treating the deactivated catalysts with 0.1 mol% HCl solution. Among the metal oxides supported Pt catalysts investigated, Pt-Cl/CeO_2 catalysts showed the best reusability, and it should be related to the highly dispersed stable Pt species protected by the CeO_2. XAFS measurements were mainly utilized to learn the deactivation of the catalysts and revealed that the reduction of active PtO_xCl_y species should be the dominant reason for the deactivation. In addition, the XAFS analysis of Pt-Cl/CeO_2 reused in different cycles also uncovered one of the reasons for the great

reusability of Pt-Cl/CeO_2 that a stable state could form during the reuse. This research has provided an example for analyzing the deactivation pathway for supported Pt catalysts and reactivating their activities. The investigation method to understand the deactivation mechanism and the reactivation strategy will be a valuable reference for the further application of supported catalysts.

3.5. References

[1] C.-Y. Ahn, J.E. Park, S. Kim, O.-H. Kim, W. Hwang, M. Her, S.Y. Kang, S.B. Park, O.J. Kwon, H.S. Park, Y.-H. Cho, Y.-E. Sung, Chem. Rev. 121 (2021) 15075–15140.

[2] S. Matsumoto, Catal. Today 90 (2004) 183–190.

[3] Y. Shi, Z. Li, J. Wang, R. Zhou, Appl. Catal. B Environ. 286 (2021) 119936.

[4] N. Kaylor, R.J. Davis, J. Catal. 367 (2018) 181–193.

[5] A. Glotov, A. Vutolkina, M. Artemova, N. Demikhova, E. Smirnova, E. Roldugina, A. Stavitskaya, E. Ivanov, S. Egazar'yants, V. Vinokurov, Appl. Catal. A Gen. 603 (2020) 117764.

[6] Q. Sun, S. Wang, H. Liu, ACS Catal. 9 (2019) 11413–11425.

[7] X. Wang, Y. Liu, X. Liang, Green Chem. 20 (2018) 2894–2902.

[8] X. Xing, C. Xu, B. Chen, C. Li, S.C.Virgil, R.H. Grubbs, J. Am. Chem. Soc. 140 (2018) 17782–17789.

[9] A. Scarso, M. Colladon, P. Sgarbossa, C. Santo, R.A. Michelin, G. Strukul, Organometallics 29 (2010) 1487–1497.

[10] R.G. Pearson, J. Am. Chem. Soc. 107 (1985) 6801–6806.

[11] Q.-A. Huang, A. Haruta, Y. Kumamoto, H. Murayama, E. Yamamoto, T. Honma, M. Okumura, H. Nobutou, M. Tokunaga, Appl. Catal. B Environ. 296 (2021) 120333.

[12] A.M. Zawisza, S. Bouquillon, J. Muzart, Eur. J. Org. Chem. 2 (2007) 3901–3304.

[13] N. Marion, R. Gealageas, S.P. Nolan, Org. Lett. 9 (2007) 2653–2656.

[14] Y. Lu, Z. Zhang, H. Wang, Y. Wang, Appl. Catal. B Environ. 292 (2021) 120162.

[15] Y. Lou, F. Jiang, W. Zhu, L. Wang, T. Yao, S. Wang, B. Yang, B. Yang, Y. Zhu, X. Liu, Appl. Catal. B Environ. 291 (2021) 120122.

[16] Z. Zhang, T. Mamba, Q.-A. Huang, H. Murayama, E. Yamamoto, T. Honma, M. Tokunaga, Mol. Catal. 475 (2019) 110502.

[17] Y. Oh, H. Noh, H. Park, H. Han, T.-B. Nguyen, Catal. Today 352 (2020) 329–336.

[18] N. Kapil, T. Weissenberger, F. Cardinale, P. Trogadas, T.A. Nijhuis, M.M. Nigra, M.-O. Coppens, Angew. Chem. Int. Ed. 60 (2021) 18185–18193.

[19] T. Ishida, T. Honma, K. Nakada, H. Murayama, T. Mamba, K. Kume, Y. Izawa, M. Utsunomiya, M. Tokunaga, J. Catal. 374 (2019) 320–327.

[20] H.O. Otor, J.B. Steiner, C. García-Sancho, A.C. Alba-Rubio, ACS Catal. 10 (2020) 7630–7656.

[21] N. Yuan, A. Gudmundsson, K.P.J. Gustafson, M. Oschmann, C.-W. Tai, I. Persson, X. Zou, O. Verho, E.G. Bajnóczi, J.-E. Bäckvall, ACS Catal. 11 (2021) 2999–3008.

[22] F. Cabello Galisteo, R. Mariscal, M. López Granados, J.L.G. Fierro, R.A. Daley, J.A. Anderson, Appl. Catal. B Environ. 59 (2005) 227–233.

[23] M. Brown. R.E. Peierls, E.A. Stern, Phys. Rev. B 15 (1977) 738–744.

Chapter 4.
Engineering active and stable Au/ZrO_2 catalysts for isomerization of allylic esters: a practical application of gold catalysis

4.1. Introduction

The high activities of nano-scale gold catalysts were discovered for the oxidation of CO and the hydrochlorination respectively by Haruta et al. and Hutchings et al. in the 1980s[1,2]. The catalytic activity of Au strongly depends on the size and contact structure of gold nanoparticles[3]. When the gold was prepared as supported nanoparticles (NPs), excellent performance could be obtained[4,5]. Since then, supported gold catalysts have been explored for valuable reaction development[6]. Applications of supported gold catalyst in redox reactions were widely discussed, such as propylene epoxidation[7,8], oxidation of alcohols[9,10], and selective hydrogenation[11,12]. Meanwhile, several studies on the activity of their Lewis acid function were also reported[13–15]. On the other hand, the practical application of gold catalysis was still under developing[16]. To the best of out knowledge, two supported gold catalysts are commercially employed in the chemical industry: Carbon-supported Au catalyst for the hydrochlorination of acetylene to vinyl chloride[17], which could avoid the use of highly toxic $HgCl_2$ catalyst, and the supported core-shell $AuNiO_x$ catalyst for the oxidative esterification of methacrolein to methyl methacrylate[18]. The ongoing development of new applications of gold catalysis has been expected to tackle significant environmental and economic issues.

In the last decade, the development of sustainable chemistry and clean production has become an essential direction in the field of heterogeneous catalysis and resource chemistry, and a lot of attention has been paid to the efficient conversion of biomass derivatives and the captured carbon dioxide, promising technologies for the environmental society[19–22]. Before this society is realized, addressing the current problems in the existing chemical production process could still reap environmental and economic benefits. For example, sustainable production of C4 chemicals is significant in the industry. C4 derivatives, like tetrahydrofuran (THF) and butane-1,4-diol (1,4-BG) are important raw materials to produce polyester and polyether, and they are produced million tons/year globally. However, in an essential C4 chemical reaction route from buta-1,3-diene[23], there is a byproduct but-3-ene-1,2-diyl diacetate (3,4-

DABE), an isomer of but-2-ene-1,4-diyl acetate (1,4-DABE) which is a valuable intermediate for the synthesis of 14BG and THF (Fig. 1). Most of the 3,4-DABE waste is currently treated by combustion, causing environmental problems. Therefore, developing efficient catalysts for the isomerization of 3,4-DABE into 1,4-DABE will be beneficial to low-carbon society and economy. Since the isomerization of allylic esters is reversible, even if the demands for butane-1,2-diol (1,2-BG) and 3,4-DABE increase significantly in the future, this catalytic process can easily realize the transformation of 1,4-DABE to 3,4-DABE.

Catalytic isomerization of allylic esters has been developed with several homogeneous catalysts via the soft Lewis acid mechanism or the π-allyl mechanism [24,25]. In the recent year, we demonstrated for the first time that PtO_xCl_y/CeO_2 can act as a heterogeneous soft Lewis acid catalyst and high activity was observed in the isomerization of allylic esters under solvent-free conditions[26]. We further proved that the reduction of the Pt species cause deactivation, although the activity could be recovered by reactivation[27]. Both homogeneous and heterogeneous Au catalysts have been developed for their soft Lewis acid functions[28–30], including the metal oxide supported Au NPs catalysts[31,32]. Supported Au NPs catalysts were firstly discussed in our previous research as a comparison of supported platinum catalysts, and the catalytic activity was two orders of magnitude lower than that of the supported Pt catalysts[26]. Ishida et al. prepared hydroxyapatites (HAPs) supported Au catalysts with strong metal-support interaction (SMSI) under oxidative atmosphere and found the catalytic activities for isomerization of 3,4-DABE correlated well with the cationic properties of Au ($Au^{\delta+}$)[33].

Moreover, it has been proved that precise engineering of supported Au catalysts has could effectively realize high stability and activity and contact structure or atmosphere could also regulate the catalytic performance[34,35]. We developed Na-salt-modified Au/*m*-ZrO_2 catalysts, and they showed activity and stability in the intramolecular cyclization of alkynoic acids, a soft Lewis acid reaction[36]. However, the decomposition of the contact structure limited the durability of the Au/ZrO_2 and

thus the further application. Considering the ambient condition of the supported Au catalyst could also affect the electronic states of the supported gold catalysts and their performance[37], we envisaged that regulation of the local gas-phase environment will be a promising method for developing highly active and stable gold catalysts for the practical application.

In this research, we reported a facile solvent-free methodology for isomerization of allylic esters with supported Au NPs catalysts, which showed superior catalytic activity and stability. Koros-Nowak criterion test and reaction condition modulation were performed to optimize the catalytic efficiency. Catalysts with high loading amount of gold showed a better catalytic efficiency for per gold atom, and partial pressure of oxygen for the reaction produced an essential effect on the performance of supported Au NPs catalysts in both batch and flow reactions. The oxygen atmosphere could facilitate the formation and thus the maintenance the of $Au^{\delta+}$ component, which is the active specie with soft Lewis acid property. Lifetime and stability of the optimized catalyst were evaluated by a 14-day flow reaction in the scale of kilogram, and no obvious deactivation occurred. The Au/*m*-ZrO_2 catalysts demonstrate a promising activity and stability over the efficient conversion and utilization of C4 derivatives, and we hope this practical technology will be applied industrial process soon and promote the development of industrial gold catalysis.

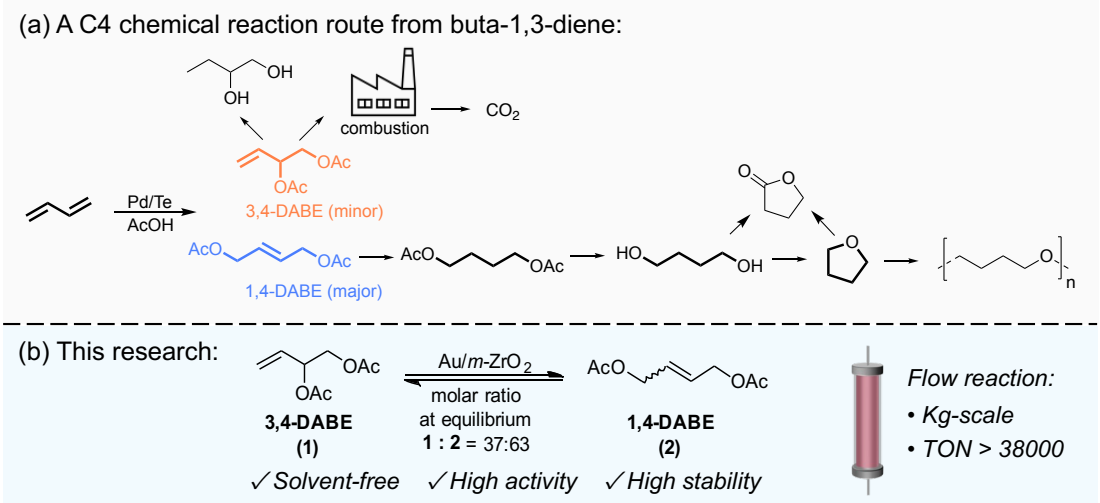

Figure 1. (a) A C4 chemical reaction route from buta-1,3-diene. (b) this research.

4.2. Experimental

4.2.1. Materials

$HAuCl_4 \cdot 4H_2O$ was purchased from Tanaka Precious Metals Co., Ltd. Metal oxides Al_2O_3 (JRC-ALO-9), Nb_2O_5 (JRC-NBO-1), MgO (JRC-MGO-4, 2000A), CeO_2 (JRC-CEO-3), TiO_2 (JRC-TIO-17), and *m*-ZrO_2 (JRC-ZRO-8, monoclinic) were reference catalysts obtained from the Catalysis Society of Japan. *a*-ZrO_2 (NND, amorphous) and *m*-$ZrO_2(SO_4)$ (3%) was purchased from Daiichi Kigenso Kagaku Kogyo Co., Ltd. *t*-ZrO_2 (SZ61152, tetragonal) was purchased from Saint-Gobain Co., Ltd. But-3-ene-1,2-diyl diacetate were purchased from Sigma Aldrich, Ltd. and but-2-ene-1,4-diyl diacetate was obtained from Mitsubishi Chemical Co., Ltd. All chemicals were used without further treatment.

4.2.2. Preparation of catalysts

The optimized Au/ZrO_2 catalyst was prepared by deposition-precipitation method (DP) as reported[36]. *m*-ZrO_2 (1g, powder) was added to distilled water (50 mL) and keep stirring for 10 min. An aqueous solution (25 mL) with $(NH_4)_2CO_3$ (2.4 g) was prepared and added to the suspension. Then, the aqueous solution of $HAuCl_4 \cdot 4H_2O$ (3 mM, 50 mL) was dropped to it slowly within 30 min, and the mixture was stirred for 4 h. After filtration, the solid was washed with hot water (70 °C, 200 mL), and dried in air at 70 °C overnight. The calcination process was performed in air at 200 °C for 1 h and directly used for catalytic reactions without further treatment. The other catalysts discussed in this research were prepared in the same method with differences in support, precursor amount and calcination temperature.

4.2.3. Characterization

High-angle annular dark-field scanning transmission electron microscopy (HAADF-STEM) images were performed with a JEOL JEM-ARM200F operated at 200 kV. The loading amounts of prepared catalysts were detected by microwave plasma atomic emission spectrometry (MP-AES) on Agilent 4100 MP-AES. The crystalline structures of the catalysts were measured with Powder X-ray diffraction (PXRD) using a Rigaku MiniFlex600 equipped with a Cu K_α radiation source. The properties of the

surface species were analyzed by X-ray photoelectron spectroscopy (XPS) using a Shimadzu-AXIS-165 spectrometer equipped with an Al K_α radiation source at pressure below 10^{-8} Pa. The obtained binding energies were calibrated to the C 1s peak at 284.8 eV. XPS profiles were further analyzed using XPSPEAK41 software. The local structures of Au NPs were analyzed by the Au L_{III}-edge X-ray absorption fine structure (XAFS) spectra collected at the BL14B2 beamline of SPring-8 (Hyogo, Japan). Diffuse reflectance infrared Fourier transform (DRIFT) spectra were recorded using a JASCO FT/IR-6100 V system equipped with a heat chamber. The powder sample was pretreated at 150 °C for 1 h in a N_2 flow (50 mL min^{-1}) and then exposed to 10 vol% CO in He (40 mL min^{-1}) at −175 °C. After the Au sites were saturated with CO, N_2 (50 mL min^{-1}) was introduced, and O_2 (10 mL min^{-1}) was also introduced to investigate the effect of oxygen. All the spectra were collected at −175 °C. DRIFT spectra were obtained by subtracting the background spectrum.

The results of the benchmark reaction including the calculation of conversions and yields of the compounds were detected by gas chromatography (GC) using an Agilent GC 6850 Series II equipped with a flame ionization detector (FID) and a J&W HP-1 column with tridecane as an internal standard. The ^1H and ^{13}C NMR spectra of the substrates were obtained using the JEOL JNM-ECS400 spectrometer.

4.2.4. General procedure for the catalytic reactions

A screw cap vial was charged with the prepared catalyst, substrate, and a magnetic stirring bar. Then the reaction mixture was stirred at 150 °C. The mixture was filtered after reaction, and the filtrate was analyzed by GC using tridecane as an internal standard. In a reusing experiment, the same procedure was repeated. After each run, the catalysts were washed with Et_2O and dried under vacuum condition for 3 h. For the discussion on reaction atmosphere, an autoclave was used, and filled with target gas (O_2, Air, 6% O_2/N_2, N_2) to a total pressure of 0.5 MPa. Absolute pressures were used in this study.

4.2.5. Continuous flow reactions

Flow reaction for isomerization of but-2-ene-1,4-diyl diacetate was performed by

a flow reactor (EYELA, Flow Factory, FFX-1000G). The stainless column (Φ10×50 mm) bed reactor was packed with 2.5 wt% Au/*m*-ZrO_2 (0.4 g) catalyst and sea sand. The column was set vertically in a downward flow mode. The reaction mixture was collected and analyzed by GC using tridecane as an internal standard.

4.3. Results and discussion

4.3.1. Screening and optimization of the active catalyst

In this research, isomerization of 3,4-DABE(**1**) to 1,4-DABE(**2**) was chose as the benchmark reaction to screen the active catalysts. This reaction was a reversible reaction, and the equilibrium between the 3,4-DABE and 1,4-DABE was 37/63[24], so there is an upper limit to the yield. Since the supported gold nanoparticles have been proved to be soft Lewis acid catalysts in our previous studies[33,36]. Hence, we directly performed catalyst screening with metal oxides supported gold nanoparticles in the preliminary discussion, due to the stability of metal oxides. The activities of heterogeneous gold catalyst supported by several metal oxides was evaluated (Table 1, entries 1–6). Monoclinic zirconium oxide (*m*-ZrO_2) supported gold catalysts showed a yield around 58% in this reaction, which was better than those of the other catalysts. Under the same reaction condition, Au catalysts using amorphous zirconium oxide (*a*-ZrO_2) or the tetragonal zirconium oxide (*t*-ZrO_2) only produced 1,4-DABE in low yields (entries 7 and 8). In addition, the acidity-enhanced zirconium oxide support SO_4-ZrO_2 was also tested (entry 9), and the yield was not as high as that of *m*-ZrO_2. Au/*m*-ZrO_2 catalysts calcined under H_2 atmosphere showed a yield below 50% (entry 10), which was lower than that of the catalysts calcined under air. Moreover, a low yield around 6% was obtained when perform the reaction under Ar atmosphere (entry 11), supporting the essential role of oxygen in this reaction. Moreover, reaction at a low catalyst equivalent was discussed, and a turnover number (TON) of 680 was achieved (entry 12). No products were detected when using the *m*-ZrO_2 as the catalyst (entry 13).

Table 1. Catalyst screening results over isomerization of 3,4-DABE.

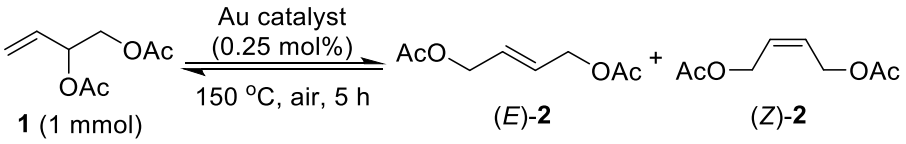

Entry	Catalyst	Conv./%[a]	Yield/%[a]		TON
			(E)	(Z)	
1	Au/Al_2O_3	24	12	trace	48
2	Au/Nb_2O_5	4	n.d.	n.d.	–
3	Au/MgO	5	n.d.	n.d.	–
4	Au/CeO_2	18	12	1	52
5	Au/TiO_2	41	33	2	140
6	Au/m-ZrO_2	61	52	6	232
7	Au/a-ZrO_2	15	8	1	36
8	Au/t-ZrO_2	20	16	1	68
9	Au/m-$ZrO_2(SO_4)$	40	36	2	152
10[b]	Au/m-ZrO_2	53	45	4	196
11[c]	Au/m-ZrO_2	8	6	trace	24
12[d]	Au/m-ZrO_2	37	32	2	680
13[e]	m-ZrO_2	9	n.d.	n.d.	–

[a]Determined by GC analysis using tridecane as an internal standard. [b]Calcined under hydrogen atmosphere at 300 °C. [c]Performed under Ar atmosphere. [d]Au amount: 0.05 mol%, 24 h. [e]Catalyst: 20 mg.

The sizes of supported gold nanoparticles are thought to affect their catalytic activities, and the particle sizes usually changed along with the calcination temperature[36]; therefore, the effect of calcination temperature was discussed. (Fig. 2a). Superior reaction activity was obtained when using Au/*m*-ZrO_2 calcined under 200 °C. The XRD intensities of Au 111 were extremely weak when calcined under 200 °C (Fig. 2b), supporting the formation of small Au NPs, and this may boost the preeminent activity.

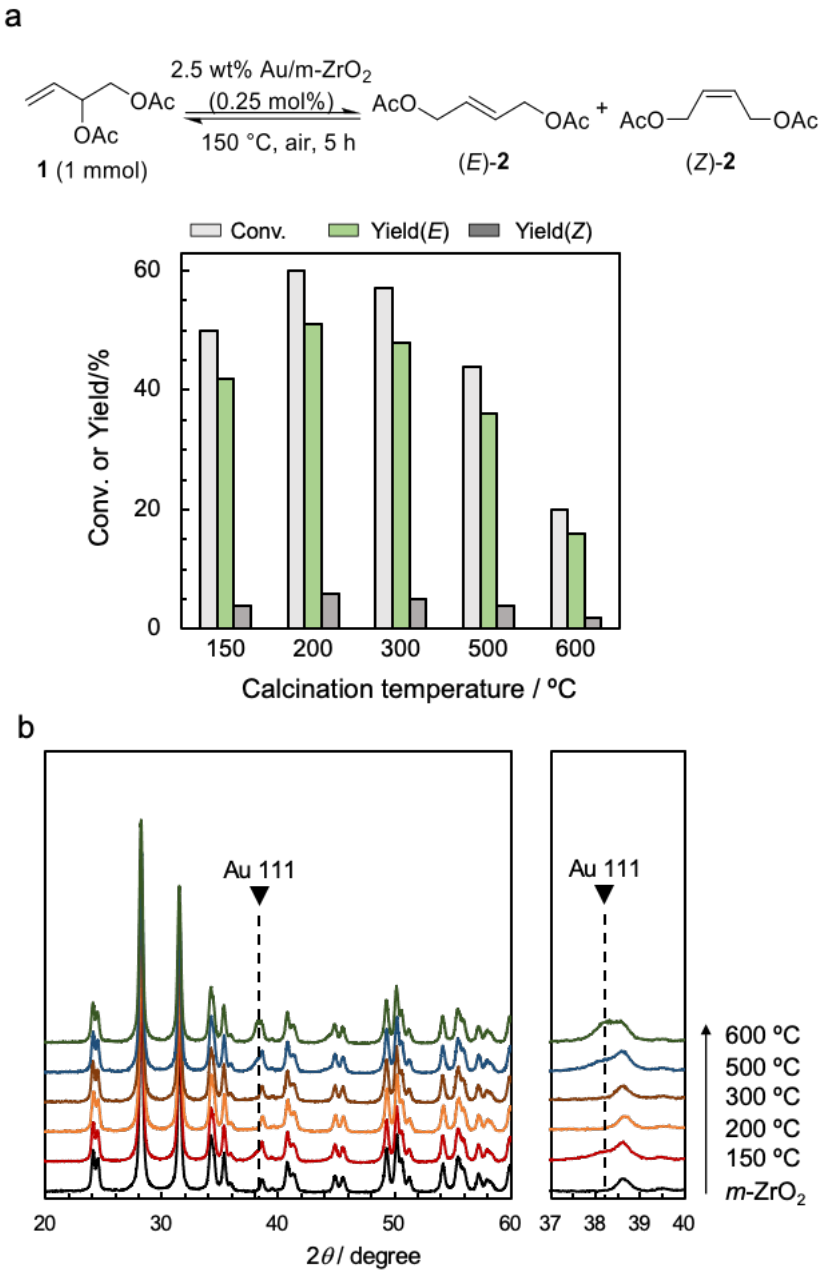

Figure 2. (a) Au/*m*-ZrO_2 calcined under different temperatures. (b) XRD patterns of the Au/*m*-ZrO_2 catalysts calcined at different temperatures.

In addition, the optimization on the loading amount was carried out based on the constant Au amount and the constant weight (Fig. 3a and 3b). Au/*m*-ZrO_2 with low Au loading amount afforded low catalytic efficiency, and the yield increased with the augment of the loading amount. Meanwhile, the catalyst adding amount based on the Au equivalent was also discussed using the 0.35 wt% Au/*m*-ZrO_2 and 2.5 wt% Au/*m*-ZrO_2. A decline in yield was observed when Au equivalent exceeded 0.15 mol%, using the 0.35 wt% Au/*m*-ZrO_2. This possibly due to the low stirring efficiency (Fig 3c).

Besides, a continuous increase in yield was achieved with the increase in gold equivalent when the 2.5 wt% Au/*m*-ZrO_2 was used (Fig. 3d). Based on the above results and taking the cost and reactivity of catalyst into consideration, the optimized catalyst was determined as 2.5 wt% Au/*m*-ZrO_2 in this research. Furthermore, time course of the concentration of each compound over the optimized catalyst was determined (Fig. 4), which fit the character of a reversible reaction.

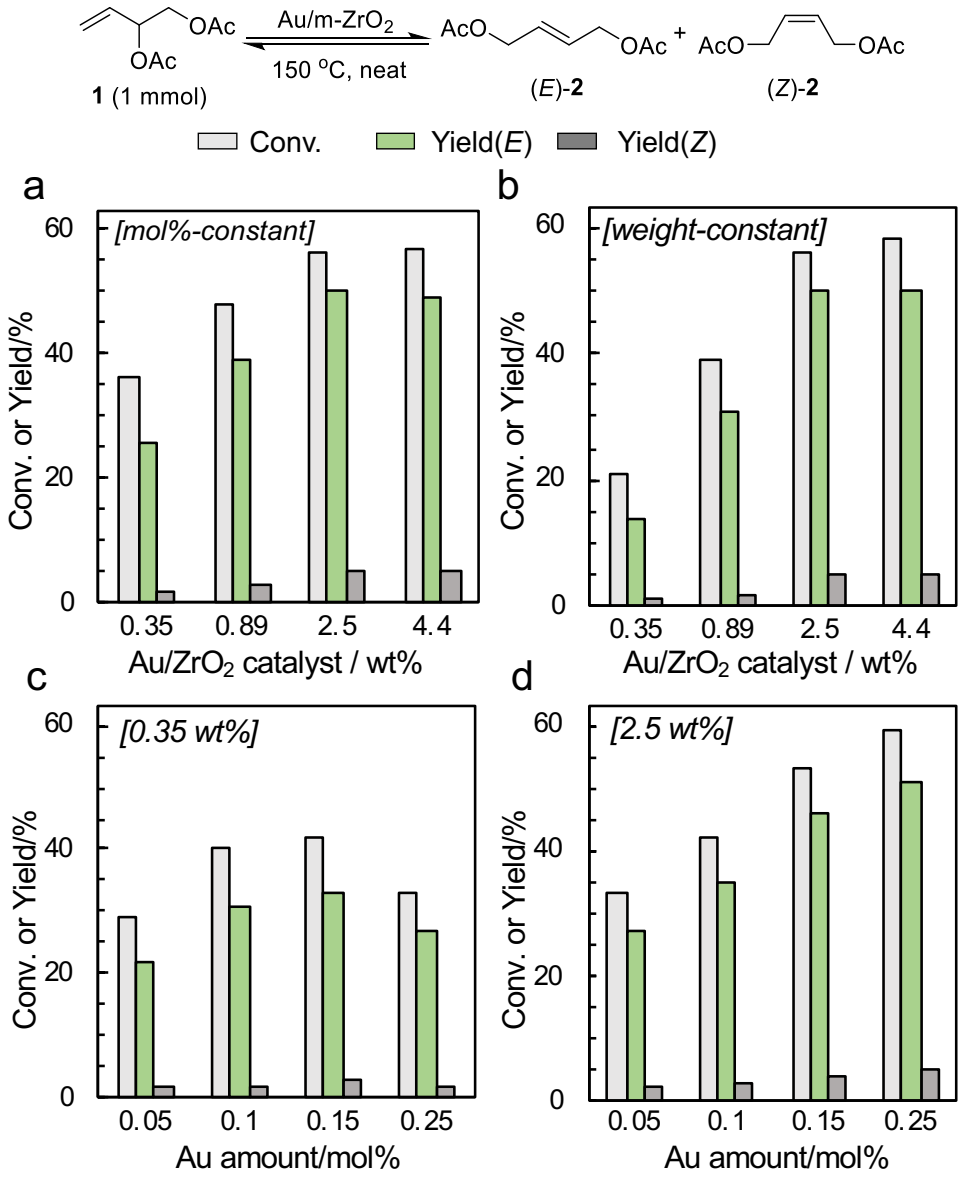

Figure 3. (a) Results of different Au loading amount with constant Au mol% in 0.25. (Koros-Nowak criterion test) (b) Results of different Au loading amount with constant weight in 20 mg. (c) Results of different Au amount with 0.35 wt% Au/*m*-ZrO_2. (d) Results of different Au amount with 2.5 wt% Au/*m*-ZrO_2.

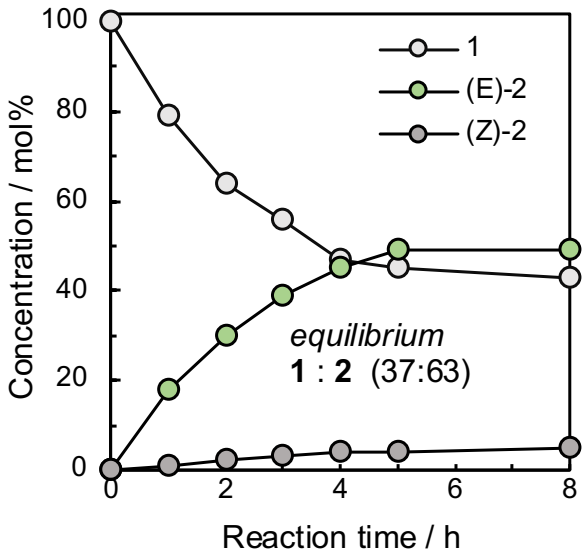

Figure 4. Time course of the reaction.

In addition, reaction temperature was also discussed with the optimized Au/*m*-ZrO_2, and the appropriate temperature around 150 °C was obtained (Table 2).

The smaller particle size usually provides more active sites considering the active sites on the surface or perimeter of supported nanoparticles. Here, we measured the particle sizes of the optimized catalyst with HAADF-STEM, and well dispersed and uniform Au NPs were observed (fig. 5). The average size of the Au NPs was around 2.3 nm.

Table 2. Effect of the reaction temperature.

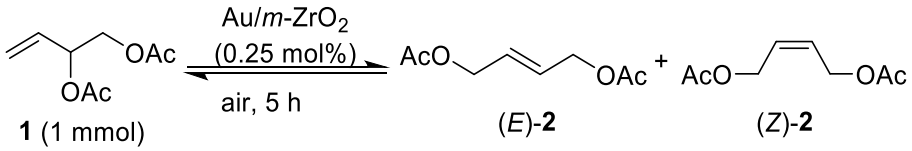

Entry	Temp./°C	Conv./%[a]	Yield/%[a]	
			(E)	(Z)
1	90	5	1	trace
2	120	17	13	1
3	150	55	49	4
4	180	44	38	3

[a]Determined by GC analysis using tridecane as an internal standard.

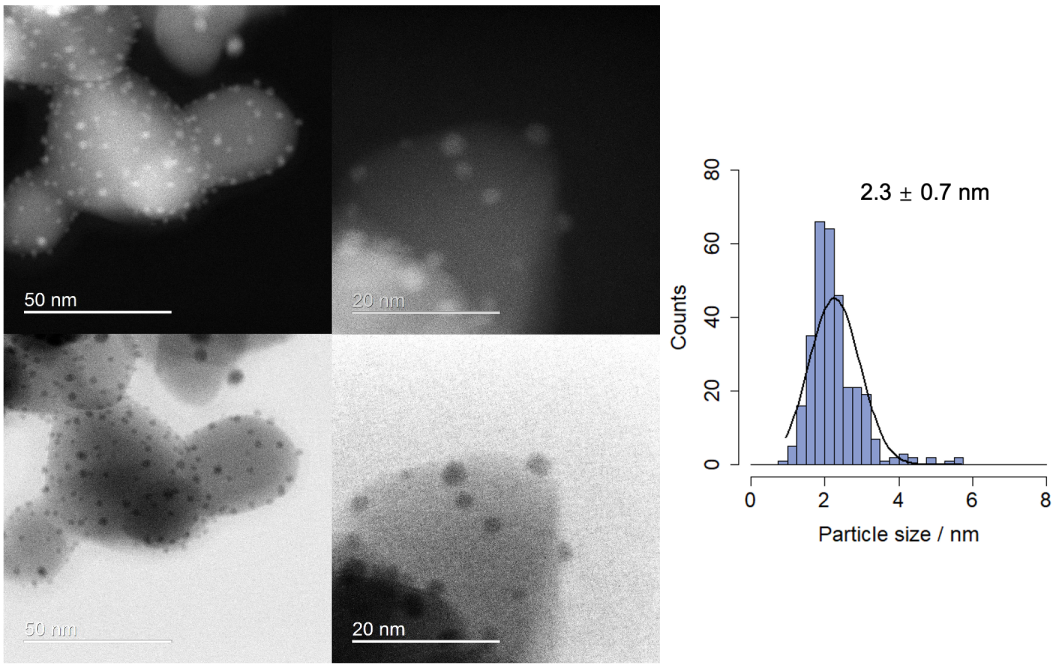

Figure 5. HAADF-STEM image and the histogram of the particle sizes.

XRD was also performed to investigate the crystal size of Au NPs, and almost no obvious peak from Au (111) was observed when compared with that of *m*-ZrO_2, showing the Au NPs were in small sizes (fig. 6). In fact, the peak of Au (111) was also partially overlapped with *m*-ZrO_2 (120).

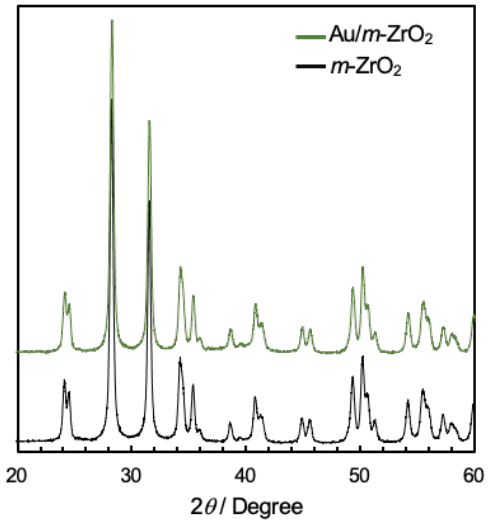

Figure 6. XRD patterns of of Au/*m*-ZrO_2 and *m*-ZrO_2.

Deposition-precipitation method (DP) is a conventional route to prepare supported Au NPs catalyst. However, when the catalyst is calcined at a relatively low temperature, residual $Au^{\delta+}$ species could be detected. The optimized catalysts were also analyzed by XAFS with the reference samples of the Au foil and Au_2O_3. The Au L_{III}-edge X-ray

absorption near edge structure (XANES) spectra showed that the Au species in the Au/*m*-ZrO_2 are mainly in zero valence. Besides, the slight difference from the zero-valent Au foil also indicates the presence of residual oxidation states (fig. 7a). After analyzing the radial structure functions, a relatively low coordinating intensity was observed when it was compared with Au foil, supporting the small sizes of Au NPs in this catalyst (fig. 7b).

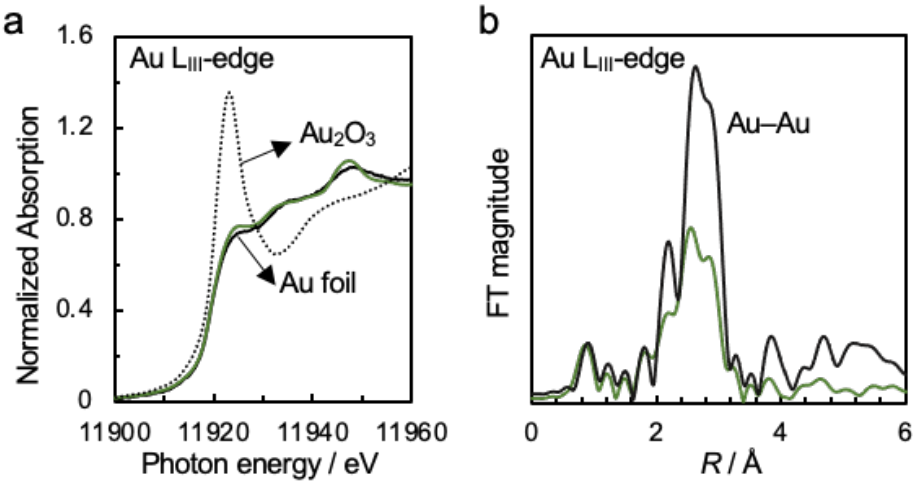

Figure 7. (a) Au L_{III}-edge XANES spectra and (b) radial structure functions of Au/*m*-ZrO_2.

Additionally, XPS analysis was performed to investigate the chemical states of the surface species. According to the Au 4f spectra, Au species in the optimized Au/m-ZrO_2 catalysts were principally in the Au^0 state (83.5 eV, Au $4f_{7/2}$; 87.2 eV, Au $4f_{5/2}$), and a pair of peaks attributable to components from $Au^{\delta+}$ (84.5 eV, Au $4f_{7/2}$; 88.2 eV, Au $4f_{5/2}$) were also observed (fig. 8)[38]. Considering the essential role of oxygen species during reaction, we inferred that residual $Au^{\delta+}$ or the generated $Au^{\delta+}$ through the surface-oxidation on the of Au NPs should be the dominant active sites during this kind of reaction.

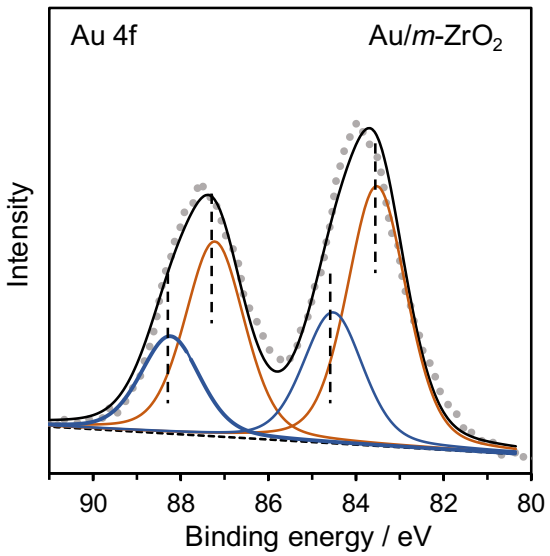

Figure 8. Au 4f XPS profiles of Au/*m*-ZrO_2.

Moreover, CO-DRIFT measurement was performed to investigate to surface species and the effect of oxygen atmosphere, and the shift of the peaks from 2096 cm^{-1} to 2102 cm^{-1} verified the generation of $Au^{\delta+}$ with the existence of oxygen atmosphere (fig. 9).

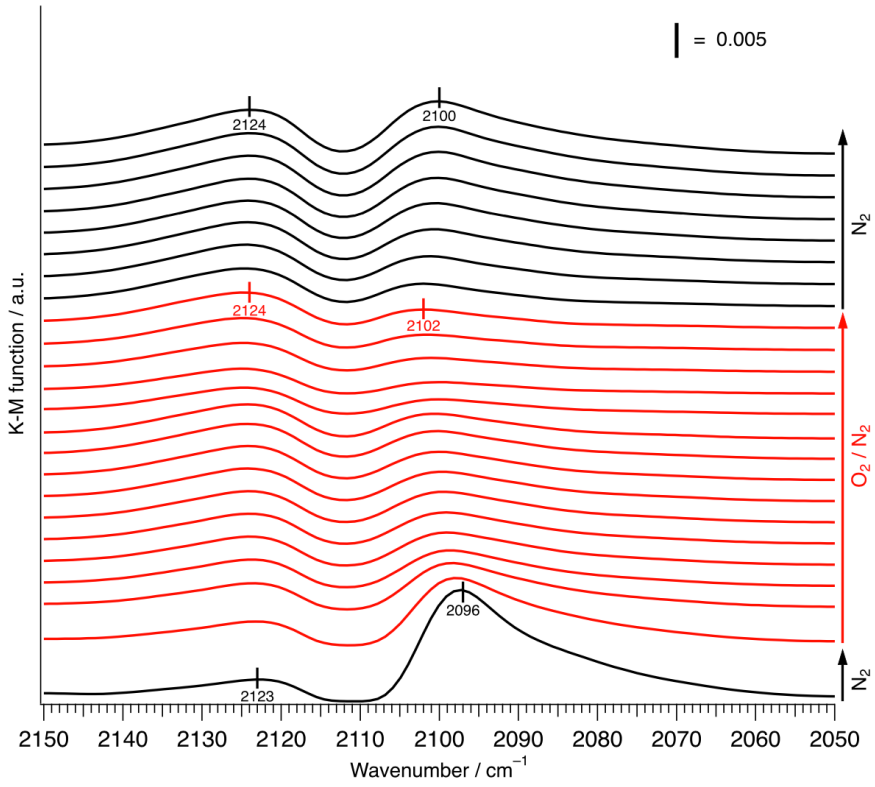

Figure 9. CO-DRIFT spectra of Au/*m*-ZrO_2 under changed atmosphere.

4.3.2. Effect of reaction atmosphere

Through the above catalyst screening and optimization process, this reaction has proceeded under air atmosphere instead of the previous research under N_2. Due to the interaction between oxygen and Au NPs, we discussed the effect of reaction pressure of air atmosphere (fig. 10a). Enhanced reaction efficiency was observed when the reaction pressure was increased to more than 0.3 MPa. This revealed the positive effect of air pressure for this reaction, but whether the partial pressure of oxygen is a factor was not clear. Thus, we evaluated the atmosphere with different oxygen partial pressure (fig. 10b). The reaction using N_2 only showed a yield below 5%, a yield of 35% was obtained even under atmosphere containing oxygen in 6%. As expected, higher yields were detected when the reaction atmosphere with higher oxygen partial pressures was discussed, showing that the existence of oxygen in reaction atmosphere should act as an essential role in this kind of reaction.

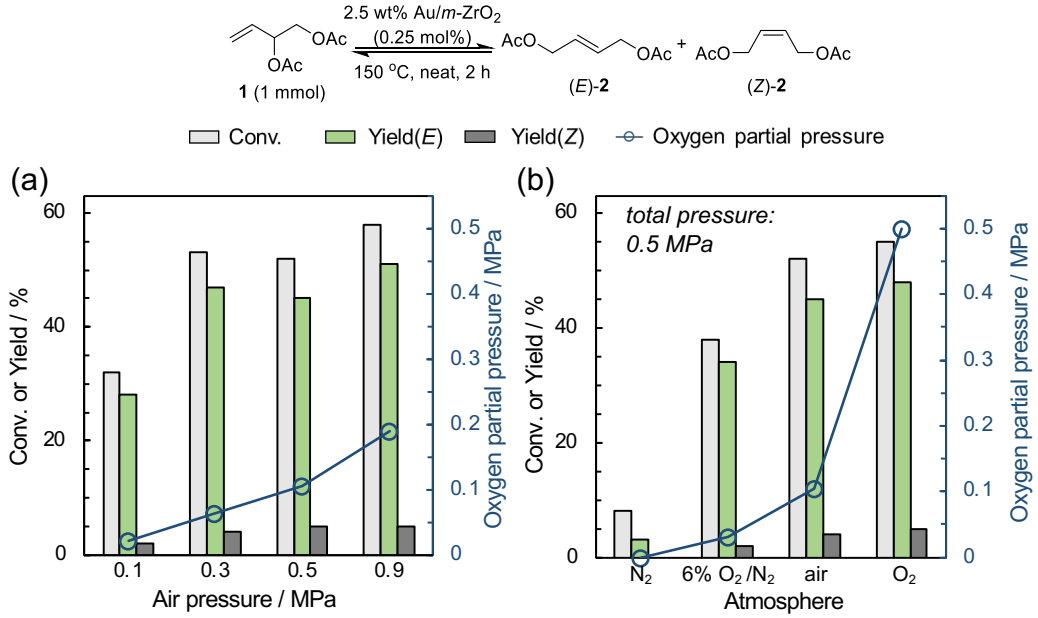

Figure 10. Discussion on reaction atmosphere over the optimized Au/*m*-ZrO_2 catalysts. (a) Absolute pressures of air. (b) Different partial pressure of oxygen. Reaction conditions: 2.5 wt% Au 0.25 mol%, 150 °C, 2 h.

4.3.3. Reusability and stability

The application of this catalytic reaction is significant for the emission reduction and the goal of carbon neutral for the high atomic efficiency and solvent-free reaction.

Thus, the reusability and stability of the Au/*m*-ZrO_2 catalysts become valuable evaluation indexes. Notably, the optimized Au/m-ZrO_2 showed great reusability for the isomerization of 3,4-DABE, and almost no obvious deactivation in yields were detected even used for eight catalytic runs (fig. 11a). Besides, the recycled catalysts after the 8th run were analyzed by HAADF-STEM (fig. 11b), and an average particle size of 3.8 nm was determined (fig. 11c). Compared with the fresh catalysts and other practical application of Au NPs catalysts, the aggregation of Au NPs and the resulting deactivation were not obvious. This result support the optimized Au/*m*-ZrO_2 have the potential to be a long-life industrial catalyst.

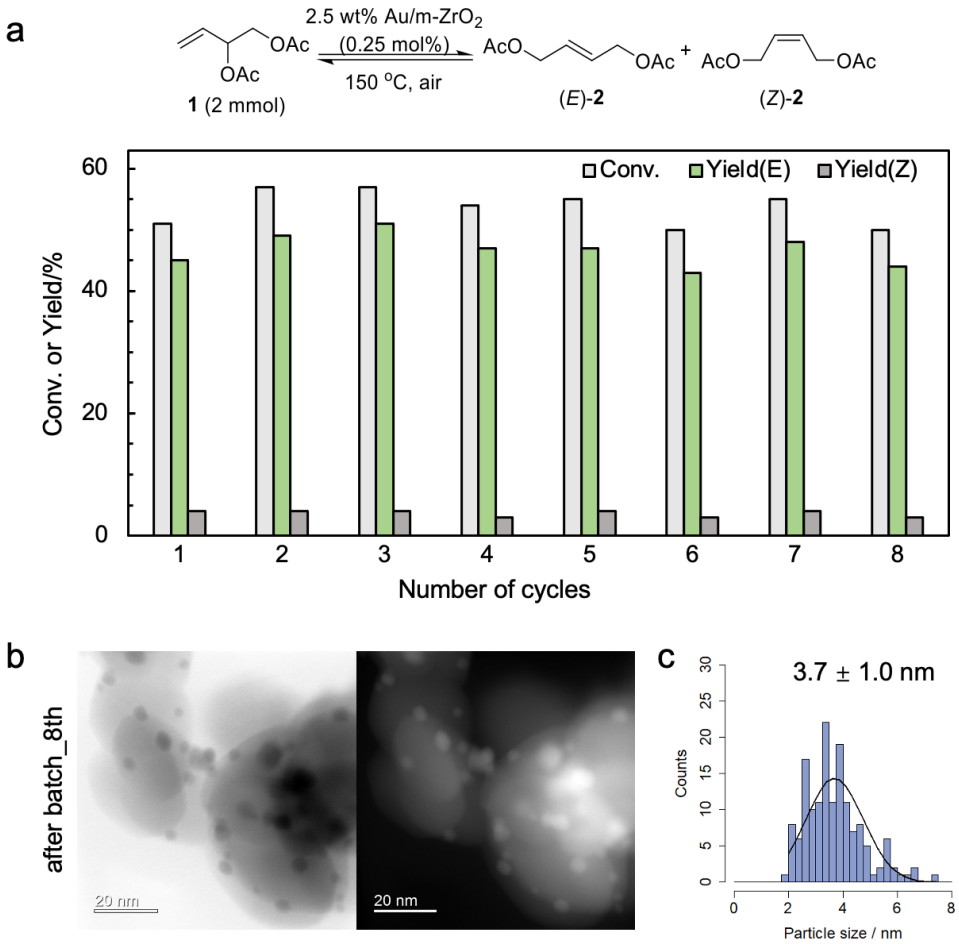

Figure 11. Reusability of the optimized Au/m-ZrO_2 for the catalytic isomerization of 3,4-DABE. (a) Results for a 10-run reusing test by batch reaction. (b) HAADF-STEM images of the catalysts after the 8th run and (c) the histogram of the particle sizes.

Furthermore, to evaluate the long-time stability and the practical catalytic

efficiency, we conducted a continuous reaction test based on a laboratory fixed-bed flow reactor (fig. 12b). Here, we executed a 7-cycle test with different reaction conditions in 14 days, obtaining a total TON more than 38000 (fig. 12a). To our excitement, no significant decrease in yield was confirmed during each cycle. Effect of oxygen partial pressure was confirmed between the cycle 1 and cycle 2. Besides, only slight changes in activity were observed at different oxygen flow rates by comparing the cycle 3–5. When the reaction temperature was raised, the enhancement in reaction efficiency could be observed. Additionally, the discussion on the feed rate showed that even if the rate was increased to three times, the catalytic efficiency was still stable.

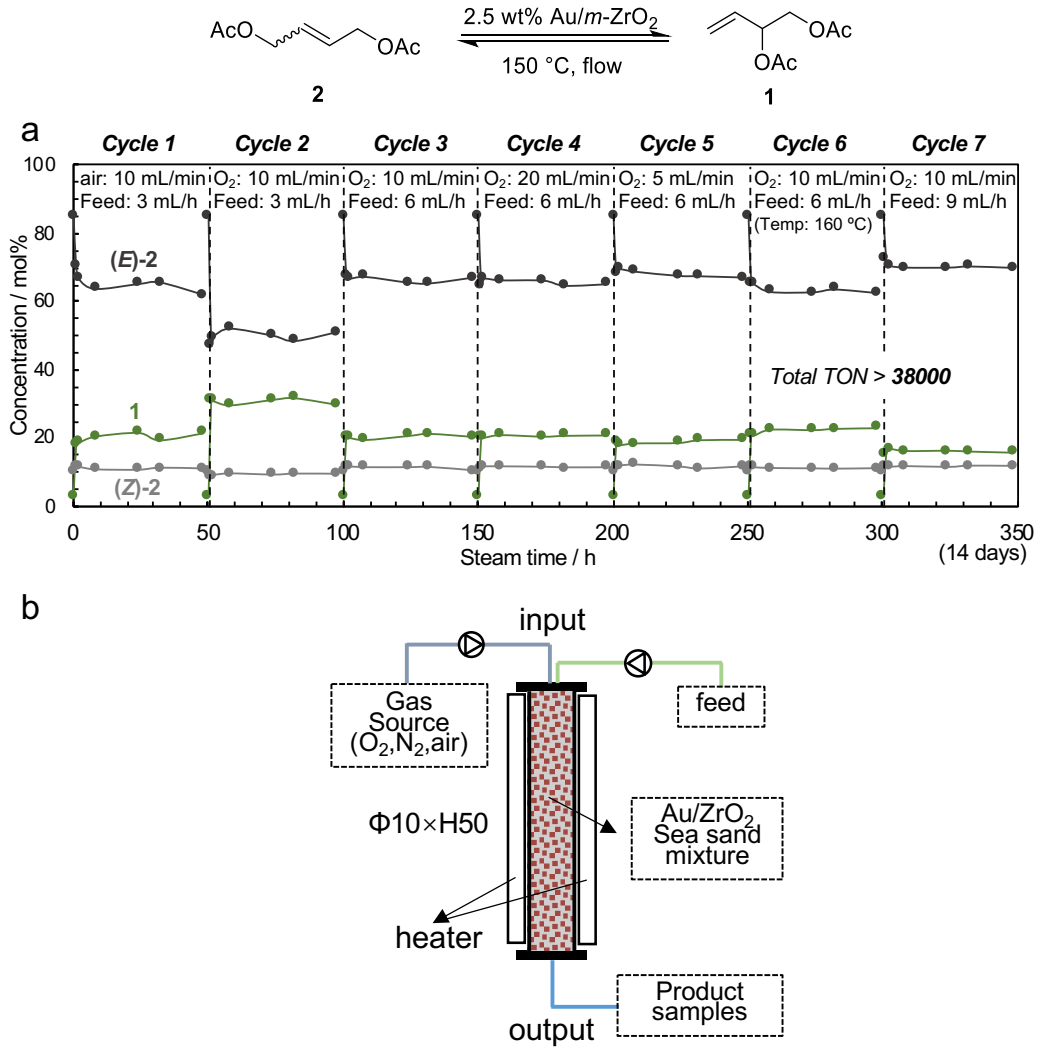

Figure 12. Evaluation the stability of the optimized Au/m-ZrO_2 using the continuous-flow reactor. (a) result of flow reaction for 7 cycles in 14 days. (b) Illustration of continuous-flow reaction.

We analyzed the morphology and particle sizes of the recycled catalysts (fig. 13a), and the average particle diameter only increased to 3.7 nm, which was smaller that of the recycled catalysts in batch reaction (fig. 13b). In addition, small amount of agglutinated Au NPs were still observed after the long-time reaction, because the agglutination of Au NPs is inevitable. The increase of particle diameter did not lead to the sharp decline of catalyst activity, which may be caused by the sufficient contact and activation between oxygen and the catalysts in the flow reactor. The above results will provide an important basis for the industrial application of the heterogeneous Au catalysis.

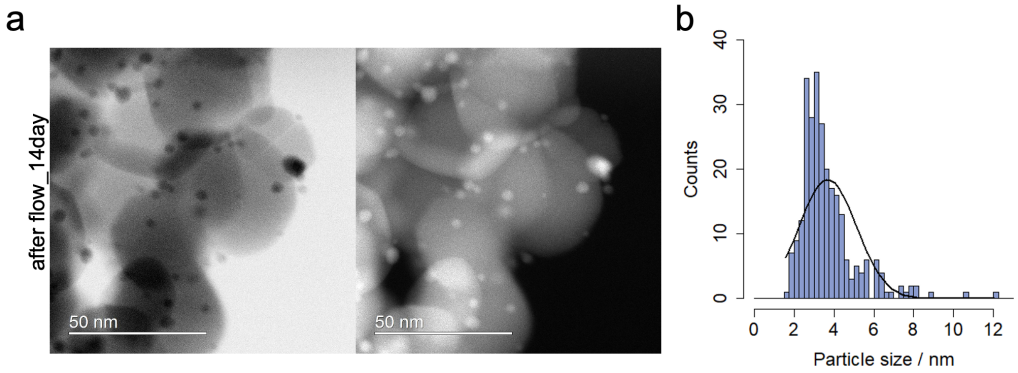

Figure 13. (a) HAADF-STEM images of the catalysts after the flow reaction and (b) the histogram of the particle sizes.

Moreover, the recycled catalysts from the flow reaction were also evaluated through the batch reactions of both directions, and only slight decrease in yields were observed (fig. 14). This leads to the belief that the optimized Au/m-ZrO_2 catalysts are available to keep its activity for at least thousands of hours in this reaction.

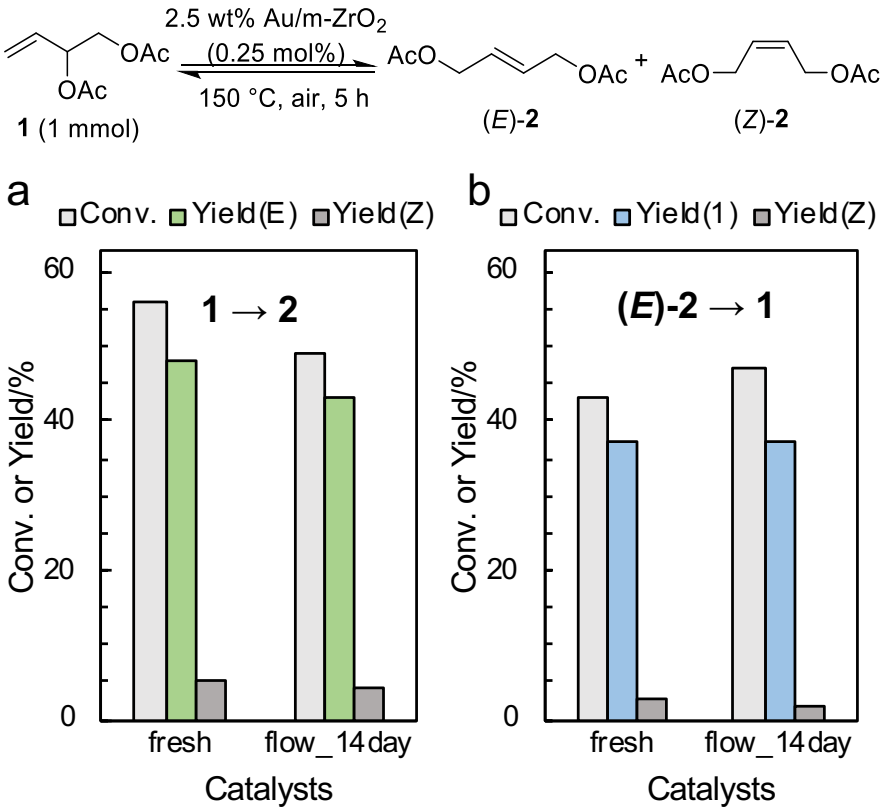

Figure 14. Evaluation of activities of the catalysts after 14-day flow reaction by the Reversible isomerization of 3,4-DABE and 1,4-DABE.

In addition, the recycled catalysts from the 8-run batch reaction and 14-day flow reaction were also analyzed by the XPS, compared with the fresh catalysts. Although no significant deactivation was observed in the reaction result, the $Au^{\delta+}$ species on the catalysts decreased over reaction time (fig. 15). The reasons may be that the agglutination of the Au NPs leads to the decrease of $Au^{\delta+}$ on their surface. Besides, the direct reduction of $Au^{\delta+}$ on the Au NPs should also be an important reason. Indeed, due to the existence of oxygen during the reaction, the $Au^{\delta+}$ can still be continuously generated on the surface of Au NPs and keep the high catalytic activity.

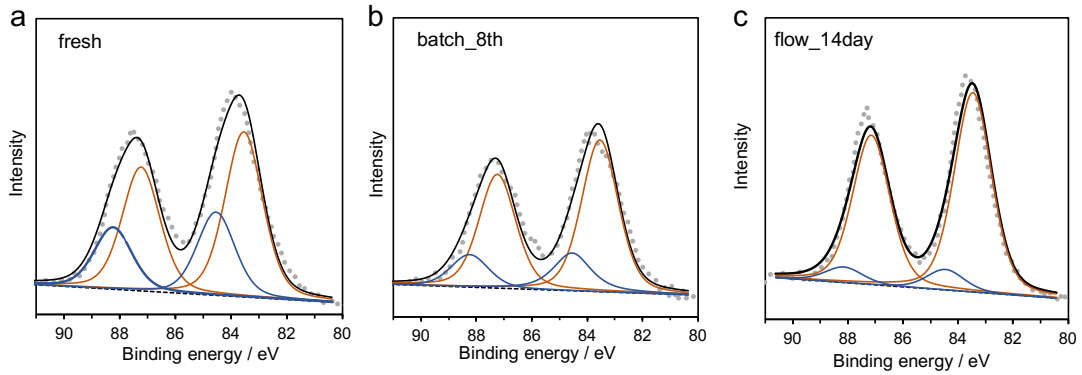

Figure 15. Au 4f XPS profiles of the Au/m-ZrO_2. (a) fresh. (b) after the 8th run in batch reaction. (c) after a 14-day flow reaction.

4.3.4. Investigation on substrate scopes and reaction mechanism

With the optimized catalyst and reaction condition, a substrate scope of allylic acetates and allylic benzoates was investigated (Table 2). When the substrate with phenyl group was tested, a yield of 33% was detected (entry 1). A yield of 38% was achieved when using linalyl acetate derived from tertiary alcohols, and almost no obvious steric effect existed during the reaction (entry 2). Besides, the substrate with the pentyl showed a yield of 46% (entry 3). Additionally, during the investigation on allylic benzoates, the presence of the electron-withdrawing nitryl or electron-donating methoxy group on the phenyl resulted in quite different results (entry 4–6). An enhanced yield was observed when discussed the methoxy group. However, A limited yield of 15% was obtained when it contained the nitryl group. Moreover, we also investigated the steric effects through the allylic benzoate with a 2,4,6-trimethylphenyl group (entry 7). Beyond our expectation, a relatively higher yield at 58% was received even when it was compared with that of the active Pt catalysts. This revealed that the electron effect produces a deeper impact than the steric effect in Au/*m*-ZrO_2 catalyzed isomerization of allylic benzoates. The theoretical maximum yields for the equilibria have not been investigated for each substrate, but they can be evaluated with the result in our previous report.

Table 3. Catalytic isomerization of allylic acetates and allylic benzoates.

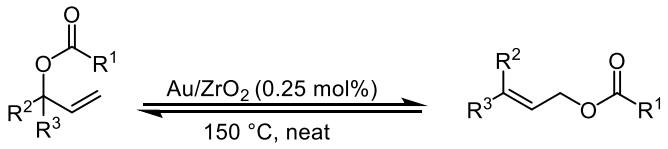

1b–h (1 mmol) **2b–h**

Entry	Substrate	Product	Conv. (%)[b]	Yield (%)[b]
1[c]	**1b** R^1 = Me, R^2 = H, R^3 = Ph	**2b**	36[d]	33[d]
2	**1c** R^1 = Me, R^2 = Me, R^3 = C_6H_{11}	**2c**	41	38
3	**1d** R^1 = Me, R^2 = H, R^3 = C_5H_{11}	**2d**	48[d]	46[d]
4	**1e** R^1 = Ph, R^2 = H, R^3 = C_5H_{11}	**2e**	46	43
5	**1f** R^1 = 4-NO_2-C_6H_5, R^2 = H, R^3 = C_5H_{11}	**2f**	19	15
6	**1g** R^1 = 4-MeO-C_6H_5, R^2 = H, R^3 = C_5H_{11}	**2g**	54	50
7	**1h** R^1 = 2,4,6-Me_3-C_6H_3, R^2 = H, R^3 = C_5H_{11}	**2h**	61	58

[a]Reaction conditions: 2.5 wt% Au/m-ZrO_2 (0.25 mol%), 150 °C, 8 h, under air. [b]Determined by ^{1}H NMR analysis using mesitylene as an internal standard. [c]5 h. [d]Determined by GC analysis using tridecane as an internal standard.

To determine the reaction mechanism, we performed a simple controlling experiment and distinguished whether the reaction belonged to the π-allyl mechanism or soft Lewis acid mechanism. Here, pentanoic acid was added to the reaction system with Au/ZrO_2 catalysts. A relatively low yields of (*E*)-2a and (*Z*)-2a were obtained after the reaction, and no exchange of acetic acid group was observed (fig. 16a). Based on the above results, we proposed that the catalytic isomerization of allylic esters over Au/ZrO_2 should in a soft Lewis acid mechanism. Initially, the presence of oxygen promotes the generation of surface $Au^{\delta+}$ species, which increase the soft Lewis acidity

of the supported Au NPs. Subsequently, the alkene moiety in allylic esters acting as soft Lewis base coordinate to the surface $Au^{\delta+}$. A transition state of the hexatomic ring state on Au NPs is formed through the attack to electrophilic carbon by C=O. Then, hexatomic ring opens, following with the generation of isomer allylic ester (fig. 16b).

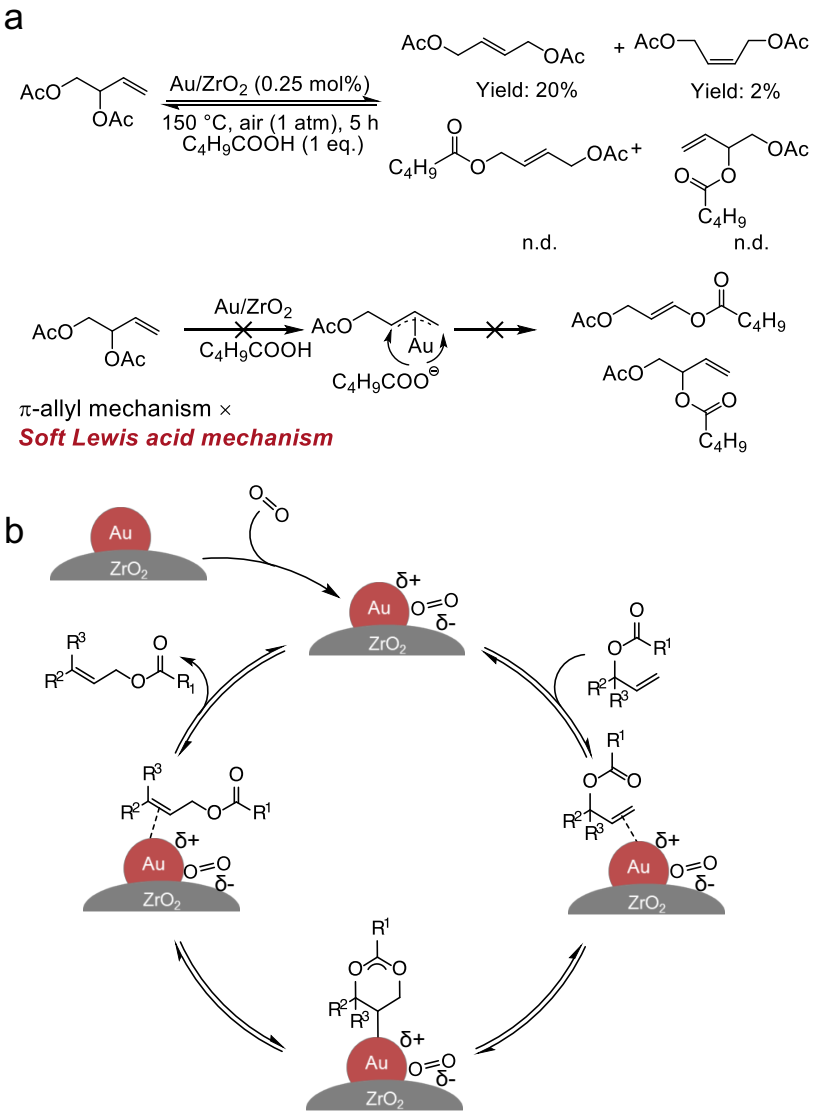

Figure 16. (a) Investigation of reaction mechanism. (b) Proposed reaction mechanism of isomerization of allylic esters over Au/m-ZrO_2 with the existence of oxygen.

Finally, we compared the catalytic activity of Au/*m*-ZrO_2 with previously reported results for rearrangement reaction of allylic acetates (Table 4). For the catalyst Au/Mg0.1SrHAP calcined under oxygen, a TON value of 204 could be realized after 24 h. In this research, a TON value of 232 for 5 h and a TON value of 680 for 24 h was obtained. Furthermore, a total TON more 38,000 was also be realized through a 14-day

flow reaction.

Table 4. Comparison of the catalytic activity of Au catalysts for the isomerization of allylic esters.

Catalyst	Au loading/wt%	Au amount/mol%	Time/h	Yield[a]/%	TON	Ref.
[(IPr)AuCl]/$AgBF_4$[b]	–	3 mol%	12	95	32	[25]
Au/ZrO_2	1.0	0.15 mol%	2	11	73	[26][d]
Au/Mg0.1SrHAP	1.0	0.25 mol%	5	34	136	[33]
Au/Mg0.1SrHAP	1.0	0.25 mol%	24	51	204	[33]
Au/*m*-ZrO_2	2.5	0.25 mol%	5	58	232	This work
Au/*m*-ZrO_2	2.5	0.05 mol%	24	34	680	This work
Au/*m*-ZrO_2[c]	2.5	–	336	–	>38,000	This work

[a] Total yield of the *E* and *Z* isomers. [b] Reaction conditions: 1-phenylallyl acetate as a substrate (1 mmol), catalyst (3 mol%), $AgBF_4$ (2 mol%), 1,2-dichloroethane (5 mL), and refluxing in an oil bath for 12 h. [c] flow reaction. [d] our previous report.

4.4. Conclusions

Catalytic isomerization of allylic esters with zirconia supported Au NPs is demonstrated to be simple and efficient. It offers a new practical application to the gold catalysis in the transformation between 3,4-DABE and 1,4-DABE, valuable intermediates of butanediol or THF. This reaction can be well operated under an environmentally friendly solvent-free condition, and optimal catalysts can also maintain high activity and stability. Koros-Nowak test and reaction condition modulation are conducted to optimize the catalytic efficiency. In addition to the catalyst with high loading amount of gold showing better efficiency with respect to per gold atom, partial pressure of oxygen for the reaction reveals an essential effect on the performance of supported Au NPs catalysts in both batch and flow reactions. The local oxygen atmosphere shows modifying function to the surface of the supported Au NPs and is considered to facilitate the formation and thus the maintenance the of $Au^{\delta+}$ component, which is the active specie with soft Lewis acid property. Furthermore, a total TON of more than 38,000 are available by flow reaction with the total scale up to kilogram. Meanwhile, there is no obvious deactivation despite slight agglutination of Au NPs, confirming that this catalytic system is highly suitable for the further industrial application. Moreover, we hope the strategies and the catalysts discussed in this

research could promote the application of the technologies in green chemistry and heterogeneous catalysis.

4.5. References

[1] M. Haruta, T. Kobayashi, H. Sano, N. Yamada, *Chem. Lett.* 16 (1987) 405–408.

[2] B. Nkosi, N. J. Coville, G. J. Hutchings, *J. Chem. Soc. Chem. Commun.,* 1 (1988) 71–72.

[3] T. Ishida, T. Murayama, A. Taketoshio, M. Haruta, *Chem. Rev.* 120 (2020) 464–525.

[4] G. J. Hutchings, *ACS Cent. Sci.* 4 (2018) 1095–1101.

[5] T. Ishida, H. Koga, M. Okumura, M. Haruta, *Chem. Rec.* 2016, **16**, 2278–2293.

[6] A. Corma, H. Garcia, *Chem. Soc. Rev.* 37 (2008) 2096–2126.

[7] T. Hayashi, K. Tanaka, M. Haruta, *J. Catal.* 178 (1998) 566–575.

[8] B. Taylor, J. Lauterbach, W. N. Delgass, *Appl. Catal. A Gen* 291 (2005) 188–198.

[9] T. Mitsudome, A. Noujima, T. Mizugaki, K. Jitsukawa, K. Kaneda, *Adv. Synth. Catal.* 351 (2009) 1890–1896.

[10] A. Buonerba, S. Impemba, A. D. Litta, C. Capacchione, S. Milione, A. Grassi, *ChemSusChem* 11 (2018) 3139–3149.

[11] T. Mitsudome, M. Yamamoto, Z. Maeno, T. Mizugaki, K. Jitsukawa, K. Kaneda, *J. Am. Chem, Soc.* 137 (2015) 13452–13455.

[12] C. C. Torres, V. A. Jiménez, C. H. Campos, J. B. Alderete, R. Dinamarca, T. M. Bustamente, B. Pawelec, *Mol. Catal.* 447 (2018) 21–27.

[13] A. Corma, P. Concepción, I. Domínguez, V. Forné, M. J. Sabater, *J. Catal.* 251 (2007) 39–47.

[14] Y. Yamane, X. Liu, A. Hamasaki, T. Ishida, M. Haruta, T. Yokoyama, M. Tokunaga, *Org. Lett.* 11 (2009) 5162–5165.

[15] S. Liang, L. Hammond, B. Xu, G. B. Hammond, *Adv. Synth. Catal.* 358 (2016) 3313–3318.

[16] R. Cirminna, E. Falletta, C. D. Pina, J. H. Teles, M. Pagliaro, *Angew. Chem. Int. Ed.* 55 (2016) 14210–14217.

[17] P. Johnston, N. Carthey, G. J. Hutchings, *J. Am. Chem. Soc.* 137 (2015) 14548–14557.

[18] K. Suzuki, T. Yamaguchi, K. Matsushita, C. Iitsuka, J. Miura, T. Akaogi, H. Ishida, *ACS Catal.* 3 (2013) 1845–1849.

[19] J. Ma, N. Sun, X. Zhang, N. Zhao, F. Xiao, W. Wei, Y. Sun, *Catal. Today* 148 (2009) 221–231.

[20] I. Sullivan, A. Goryachev, I. A. Digdaya, X. Li, H. A. Atwater, D. A. Vermaas, C. Xiang, *Nat. Catal.* 4 (2021) 952–958.

[21] D. J. Liu, E. Y. X. Chen, *Green Chem.* 16 (2014) 964–981.

[22] L. Wang, F. S. Xiao, *Green Chem.* 17 (2015) 24–39.

[23] Y. Izawa and T. Yokoyama, in Liquid phase aerobic oxidation catalysis: Industrial applications and academic perspectives, ed. S. S. Stahl and P. L. Alsters, Wiley, Hoboken, USA, 2016, pp. 159–171.

[24] S. Bouquillon, J. Muzart, *Eur. J. Org. Chem.* 17 (2001) 3301–3305.

[25] N. Marion, R. Gealageas, S. P. Nolan, *Org. Lett.* 9 (2007) 2653–2656.

[26] Q. A. Huang, A. Haruta, Y. Kumamoto, H. Murayama, E. Yamamoto, T. Honma, M. Okumura, H. Nobutou, M. Tokunaga, *Appl. Catal. B Environ.* 296 (2021) 120333.

[27] Q. A. Huang, H. Murayama, E. Yamamoto, T. Honma, M. Tokunaga, *Catal. Today*, 2022, in press. (doi: 10.1016/j.cattod.2022.06.007)

[28] X. Z. Shu, S. C. Nguyen, Y. He, F. Oba, Q. Zhang, C. Canlas, G. A. Somorjai, A. P. Alivisatos, F. D. Toste, *J. Am. Chem. Soc.* 137 (2015) 7083–7086.

[29] D. Liu, Q. Nie, R. Zhang, M. Cai. *Adv. Synth. Catal.* 360 (2018) 3940–3948.

[30] L. C. Lee, Y. Zhao, *ACS Catal.* 4 (2014) 688–691.

[31] A. D. Litta, A. Buonerba, A. Casu, A. Falqui, C. Capacchione, A. Franconetti, H. Garcia, A. Grassi, *J. Catal.* 400 (2021) 71–82.

[32] M. Sengupta, A. Bag, S. Das, A. Shukla, L. N. S. Konathala, C. A. Naidu, A. Bordoloi, *ChemCatChem*, 8 (2016) 3131–3130.

[33] A. Nakayama, R. Sodenaga, Y. Gangarajula, A. Taketoshi, T. Murayama, T. Honma, N. Sakaguchi, T. Shimada, S. Takagi, M. Haruta, B. Qiao, J. Wang, T. Ishida, *J. Catal.* 410 (2022) 194–205.

[34] N. Kapil, T. Weissenberger, F. Cardinale, P. Trogadas, T. A. Nijhuis, M. M. Nigra, M. O. Coppens, *Angew. Chem. Int. Ed.* 60 (2021) 18185–18193.

[35] K. Xia, T. Yatabe, K. Yonesato, T. Ybe, S. Kikkawa, S. Yamazoe, A. Nakata, K. Ymaguchi, K. Suzuki, *Angew. Chem. Int. Ed.* 61 (2022) e202205873.

[36] Q. A. Huang, T. Ikeda, K. Haruguchi, S. Kawai, E. Yamamoto, H. Murayama, T. Ishida, T. Honma, M. Tokunaga, *Appl. Catal. A Gen* 643 (2022) 118765.

[37] F. Neatu, Z. Li, R. Richards, P. Y. Toullec, J. P. Genêt, K. Dumbuya, J. M. Gottfried, H. P. Steinrück, V. I. Pârvulescu, V. Michelet, *Chem. Eur. J.* 14 (2008) 9412–9418.

[38] J. Huang, W. L. Dai, K. Fan, J. Catal. 266 (2009) 228–235.

Chapter 5.
Intramolecular cyclization of alkynoic acid catalyzed by Na-salt-modified Au nanoparticles supported on metal oxides

5.1. Introduction

Enol lactones occur extensively in nature and exhibit high bioactivity and are useful for the synthesis of pharmaceuticals and other complex natural molecules[1,2]. Catalytic intramolecular cyclization of alkynoic acids into enol lactones is one of the most promising methods owing to its high atom efficiency and step economy, which is in line with the principles of green chemistry and the standards in the sustainable development goals (SDGs)[3–5].

In the recent decades, numerous metal catalysts for the intramolecular cyclization of alkynoic acids, such as Au[6–9], Pd[10–13], Ag[14–16], Pt[17], Rh[18], Ir[18], Ru[19], and Ni[20], have been reported. In recent years, developments in Au and Pd catalysts have provided reliable and effective tools for improving the reaction. An extremely high turnover number (approximately 10^6) was obtained using the Pd complex catalyst reported by Domínguez et al [21]. Conversely, several heterogeneous Pd catalysts for this reaction were reported to result in relatively low activity. Ramón et al. demonstrated that Pd(II) oxide impregnated on magnetite can act as a versatile and active catalyst for the intramolecular cyclization of alkynoic acids[22]. Additionally, Bäckvall et al. developed heterogeneous catalysts where Pd was immobilized on aminopropyl (AmP) functionalized siliceous mesocellular foam (MCF) and successfully applied in the intramolecular cyclization of alkynoic acids[23]. Subsequently, they established the active species of the developed catalyst as the immobilized Pd(II) species, and using in situ X-ray absorption spectroscopy (XAS) investigated the deactivation process[24]. The results showed that the essential base triethylamine promotes the reduction of Pd(II) to metallic Pd NPs. Therefore, the unstable active species of heterogeneous Pd catalysts would limit this prospect.

Moreover, Au complex catalysts were widely investigated for use in intramolecular cyclization of alkynoic acids (Figure 1a). Michelet and Cadierno et al. reported that both Au(I) and Au(III) complexes with sulfonated NHC ligands are active in the aforementioned reaction[6]. In addition, Nolan et al. developed a dinuclear NHC-Au(I) catalyst and realized high reaction efficiency[25]. Meanwhile, methods with heterogeneous Au catalysts were developed for the intramolecular cyclization of

alkynoic acids mainly in the immobilization forms (Figure 1b). Michelet et al. developed a zeolite beta-NH4+ supported Au(III) catalyst for this reaction and proposed the deactivation process as the reduction of Au(III) species[26,27]. In addition, Toste et al.19 immobilized the Au(I) complex on SBA-15 and achieved reliable reusability[28]. Because the Au species in the oxidation state is unstable and easily reduced, Bäckvall et al. reduced the Au(I) thiolates immobilized in the pores of MCF proved the activity of zero-valent Au species[29]. However, the complex preparation process and rapid deactivation reveal the deficiency of this species and were therefore significant focal points for this research. Besides, the deactivation of the reported Au catalysts can be attributed to the reduction of Au(I) or (III) species; however, the real reasons for the poor reusability of the Au(0) species remain unclear.

Sustainable synthesis of fine chemicals is significant in the industry; hence, the development of reusable and stable heterogeneous catalysts for the required type of reaction is valuable. Our group is dedicated to the study of this subject and has reported several reactions with metal oxide-supported Au catalysts[30,31], as well as supported Pd catalysts[32,33]. We also developed a simple impregnation method for preparing supported small Au NPs on most of the supports[34]. Instead of the immobilization of metal complexes, we recently focused on the method of element modification and are committed to solving several existing problems. We previously reported that Cl-modification over Pt/CeO2 boosted excellent activity for the isomerization of allylic esters[35].

In this study, the essential role of Na-modification for the catalytic intramolecular cyclization of alkynoic acids is uncovered. Na species like NaOH and Na_2CO_3 were widely used to synthesize Au NPs or Au precursors from $HAuCl_4 \cdot nH_2O$[36–38]. For instance, Na species were used in previous reports on heterogeneous Au catalysts shown in Figure 1b. Trace amounts of Na species might disturb the nuclear active sites and have adverse effects[39]. In contrast, the addition of alkali metal like sodium for promotion effects was also reported. Several of its functions, such as stabilizing atomically dispersed noble metal species[40–42], facilitating the activation of both

surface OH groups and chemisorbed oxygen[43–46], and acting as immobilized base on the surface of the catalysts, determined[47–50]. We modified the prepared Au/m-ZrO_2 with Na_2CO_3 and disclosed the positive and significant role of Na salts on the intramolecular cyclization of alkynoic acids (Figure 1c). Therefore, a stable, reusable, and reactivable catalytic system was successfully achieved.

Herein, we report the catalytic intramolecular cyclization of alkynoic acids with Na-modified Au(0)/m-ZrO_2, and enhancement in the turnover frequency (TOF) by more than one order of magnitude achieved after the addition of Na salts. The optimized Na-Au/m-ZrO_2 shows stability, reusability, and reactivating ability, addressing the questions and limitations left unresolved in previous research. The X-ray photoelectron spectroscopy (XPS) results uncovered the effects of the Na species on the surface of the catalysts. Even negatively charged Au^0 NPs can facilitate the reaction, supporting the deactivation drives from the leaching of Na species rather than the reduction of Au. Following in-depth analysis of the kinetics and reaction mechanism, we, for the first time, clearly demonstrate kinetics of catalytic intramolecular cyclization of alkynoic acid substrate over supported Au^0 NPs. Additionally, the reaction is determined to be zero-order in substrate and the active sites are identified on the surface of the supported Au NPs. The rate-determining step of the reaction is presumed to be protodeauration with kinetic isotope effects. We proposed that Na salts in this case act as a base and might accelerate the addition of carboxylic acid to alkyne, thus changing the rate-determining step. Furthermore, yields of more than 98% and TON above 9000 were obtained during the continuous flow reaction, showing that this catalytic system can be a promising green method in fine chemical synthesis.

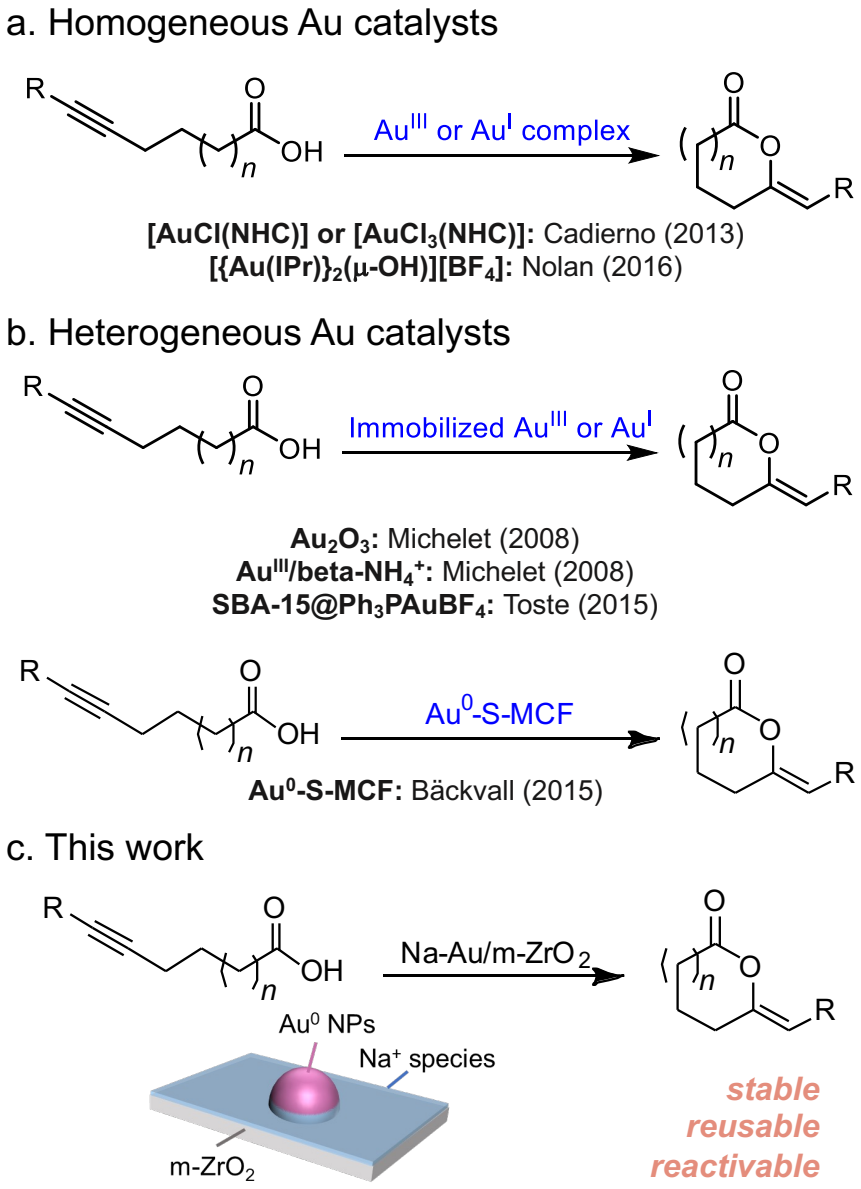

Figure 1. Previously reports on intramolecular cyclization of alkynoic acids over (a) homogeneous Au catalysts and (b) heterogeneous Au catalysts, and (c) this work.

5.2. Experimental

5.2.1. Materials

$HAuCl_4 \cdot 4H_2O$ was purchased from Tanaka Kikinzoku Kogyo K.K. Commercially available chemicals were supplied by FUJIFILM Wako Pure Chemical Corp. or Tokyo Chemical Industry. 5-Hexynoic acid was purified by distillation before use, and the other reagents were used without purification. *m*-ZrO_2 (JRC-ZRO-4, monoclinic structure) and *am*-ZrO_2 (JRC-ZRO-6, amorphous structure) were reference catalysts

obtained from the Catalysis Society of Japan. *t*-ZrO_2 (SZ61152, tetragonal structure), CeO_2 (HS), SiO_2 (CARiACT Q-10), carbon (Tokusen Shirasagi), TiO_2 (anatase, PC-111), and WO_3 were purchased from Saint-Gobain K.K., Daiichi Kigenso Kagaku Kogyo Co., Ltd., Fuji Silysia Chemical Ltd., Mitsubishi Corporation Life Sciences Ltd., Titan Kogyo Ltd., and FUJIFILM Wako Pure Chemical Corp, respectively.

5.2.2. Catalyst Preparation

Preparation of supported Au NP catalysts by an impregnation (IP) method

A convenient impregnation method using chloride-free and water-soluble Au complex Au–(*β*-ala) was employed to prepare the small nanoparticles[34].

The Au complex precursor (Au: 10 mg) was dissolved in distilled water (The amount of distilled water used for different supports was as follows: Au/ZrO_2: 0.2 mL, Au/WO_3: 0.4 mL, Au/C: 0.5 mL, Au/SiO_2 and Au/TiO_2: 1.0 mL). The support powder (990 mg) was added to the solution of Au complex in a mortar, and the mixture was stirred for 20 min at room temperature (approx. 25 °C). After impregnation, the solid was heated to 300 °C for 30 min and calcined for 30 min with air atmosphere. The catalysts obtained were directly used for catalytic reactions without further treatment. The targeted Au loading of all the catalysts prepared in this study was 1 wt%. The Au/m-ZrO_2 catalyst prepared by the impregnation method was written as Au/m-ZrO_2 (IP).

Preparation of Au/m-ZrO_2 catalysts by a deposition–precipitation (DP) method

m-ZrO_2 (1.0 g) was added to distilled water (50 mL) and stirred continuously for 10 min. An aqueous solution (25 mL) with $(NH_4)_2CO_3$ (2.4 g) that had been previously prepared was added to the suspension. Then drops of $HAuCl_4 \cdot 4H_2O$ (3 mM, 50 mL) aqueous solution were added slowly over a period of 30 min and the mixture was stirred for 4 h at room temperature (approx. 25 °C). After collection by filtration, the solid was washed with hot water (70 °C, 200 mL), and dried in air at 70 °C overnight. The calcination process was the same as that in the impregnation method. The Au/*m*-ZrO_2 catalyst prepared by the DP method was written as Au/*m*-ZrO_2. Au loading amount of prepared Au/m-ZrO2_DP was 0.9 wt%, as determined by microwave plasma atomic emission spectrometry (MP-AES).

Alkali metal modification of Au/*m*-ZrO_2

Na-Au/m-ZrO_2 catalysts were prepared by a post-modification of Au/m-ZrO_2 with alkali metal salts (1 M) via grinding (1500 rpm). Subsequently, all the catalysts were dried at room temperature under a vacuum condition for 6 h. In addition, MgO/*m*-ZrO_2 was prepared based on a previously reported method[51]. Then, the Au/MgO/*m*-ZrO_2 catalysts were prepared by the DP method described above.

5.2.3. Catalyst characterization

High-angle annular dark-field scanning transmission electron microscopy (HAADF-STEM) images were obtained using a JEOL JEM-ARM200F microscope operated at 200 kV. The loading amount of Au for the prepared catalysts were detected using MP-AES on Agilent 4100 system. The crystalline structure and size of gold nanoparticles were measured via powder X-ray diffraction (PXRD) using a Rigaku MiniFlex600 equipped with a Cu Kα radiation source. The properties of the surface species were analyzed via XPS using a Shimadzu-AXIS-165 spectrometer equipped with Al Kα radiation at a pressure below 10^{-8} Pa. The obtained binding energies were calibrated to the C 1s peak at 284.8 eV. XPS spectra were further analyzed using XPS PEAK41 software. The local structures of Au nanoparticles were analyzed using Au L_{III}-edge X-ray absorption fine structure (XAFS) spectra collected at the BL14B2 beamline of SPring-8 (Hyogo, Japan)[52]. Diffuse reflectance infrared Fourier transform (DRIFT) spectra were recorded using JASCO FT/IR-6100 V equipped with a heat chamber. The powder sample was pretreated in an air flow (50 mL min^{-1}) at 250 °C for 1 h, and then exposed to 10 vol% CO in He (40 mL min^{-1}) at −180 °C for 35 min. DRIFT spectra were obtained by subtracting the background spectrum. After Au sites had been saturated with CO, a flow of N_2 (30 mL min^{-1}) was performed, and the spectra were collected at −180 °C. The yields of the compounds discussed in this paper were determined by ^{1}H NMR spectra using a JEOL JNM-ECS400 spectrometer. Besides, ^{1}H and ^{13}C NMR spectra of the substrates were also analyzed on a JEOL JNM-ECS400 spectrometer.

5.2.4. Catalytic test

A screw cap vial was charged with a supported Au catalyst and a magnetic stirring bar, then an anhydrous solvent, alkynoic acid was added under N_2 flow. The reaction tube was sealed, and the mixture was stirred at 50 °C. After the reaction, the mixture was cooled to room temperature (approx. 25 °C) and centrifuged. The supernatant of the reaction mixtures was analyzed using ^{1}H NMR after adding mesitylene as the internal standard. In the reusing experiments, the reaction was subjected to the same process as normal. After the reaction, the used catalyst was washed using Et_2O twice and dried in a vacuum for 3 h before reusing.

5.2.5. Flow Reaction

A column reactor (diameter: 10 mm, Length: 50 mm) was packed with Au/*m*-ZrO_2 (0.4 g, Au: 0.018 mmol) mixed with 2.6 g sea sand. In addition, cotton was fitted at each end. A mixture CH_2Cl_2 solution with mesitylene (0.1 M), 5-hexynoic acid **1a** (1.0 M), and pre-dissolved Na_2CO_3 (0.5 mol%) was continuously pumped into the column reactor in a rate of 0.05 mL/min. The column was set vertically in a downward flow method. A fraction of the mixture was collected from the exit of the column every few hours or overnight. The yields were determined by ^{1}H NMR analyses.

5.3. Results and Discussion

We examined the catalytic activity with the metal oxide-supported Au NP catalysts prepared by the simple impregnation (IP) method developed in our previous research[31], in which a chloride-free and water-soluble complex Au–(*β*-ala) was used as the precursor. This method has been established to have the ability to prepare stable and small Au nanoparticles on most of the supports.

Among the prepared catalysts, *m*-ZrO_2- and SiO_2-supported Au NPs produced **2a** in 100% yields (Table 1, entries 1−4).

Their reuse performance is presented in Tables 2 and 3, and the results reveal the superior reusability of Au/*m*-ZrO_2 in this reaction, comparing with that of Au/SiO_2. In contrast, Au/TiO_2 and Au/WO_3 only exhibited low yields (entries 5 and 6), and Au/C

and Au/CeO_2 even showed almost no yields (entries 7 and 8). Additionally, because the different crystalline structures of zirconium oxides have in recent decades been reported to have notable effects on catalytic reactions[53–55], we discuss three kinds of zirconium oxides: amorphous (*am*-ZrO_2), tetragonal (*t*-ZrO_2), monoclinic (*m*-ZrO_2). Compared with the high catalytic activity of Au/*m*-ZrO_2, trace **2a** was detected after the reaction when Au/*am*-ZrO_2 (entry 9) was used, and only 21% yield was obtained over the Au/*t*-ZrO2 (entry 10). The different behavior of *m*-ZrO_2 might be attributed to differences in acidic/basic properties as well as the concentrations of hydroxyl group on the surface [56,57].

Table 1. Intramolecular cyclization of **1a** using supported Au NP catalysts prepared by the impregnation method[a]

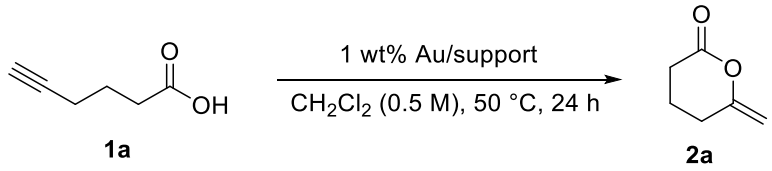

1a **2a**

Entry	Catalyst	Au amount/mol%	Yield/%[b]	TOF/h^{-1}
1	Au/SiO_2	0.1	100	42
2	Au/SiO_2	0.05	100	83
3	Au/*m*-ZrO_2	0.1	100	42
4	Au/*m*-ZrO_2	0.05	100	83
5	Au/TiO_2	1.0	14	1
6	Au/WO_3	1.0	42	2
7	Au/C	0.2	trace	–
8	Au/CeO_2	1.0	n.d.	–
9	Au/*am*-ZrO_2	0.1	trace	–
10	Au/*t*-ZrO_2	0.1	21	9

[a]Reaction conditions: **1a** (0.3 mmol), 1 wt% Au/support (0.05–1 mol%), CH_2Cl_2 (0.6 mL), 50 °C, 24 h, under N_2. [b]Determined by ^1H NMR analysis using mesitylene as an internal standard.

Table 2. Reusing test of Au/*m*-ZrO_2 (IP) in the catalytic intramolecular cyclization of **1a**[a]

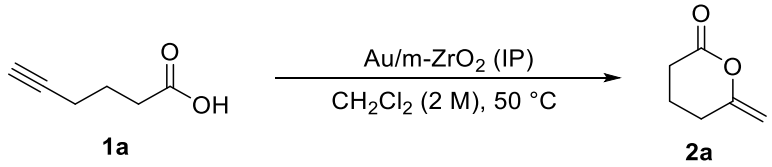

1a **2a**

Entry	Run	Yield/%[b]
1	1st	100
2	2nd	100
3	3rd	100
4	4th	100
5	5th	100
6	6th	87
7	7th	75
8	8th	69

[a]Reaction conditions: **1a** (3 mmol), 1 wt% Au/*m*-ZrO_2 (IP) (Au 0.2 mol%), CH_2Cl_2 (1.5 mL), 50 °C, 24 h, under N_2. [b]Determined by ^{1}H NMR analysis using mesitylene as an internal standard.

Table 3. Reusing test of Au/SiO_2 (IP) in the catalytic intramolecular cyclization of **1a**[a]

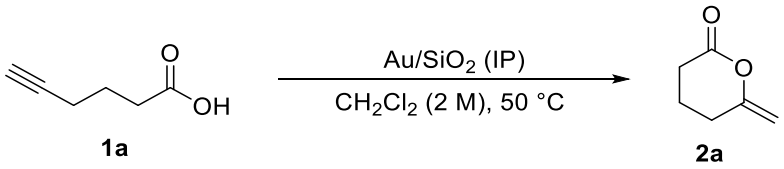

1a **2a**

Entry	Run	Yield/%[b]
1	1st	100
2	2nd	89
3	3rd	86
4	4th	76

[a]Reaction conditions: **1a** (3 mmol), 1 wt% Au/SiO_2 (IP) (Au 0.2 mol%), CH_2Cl_2 (1.5 mL), 50 °C, 24 h, under N_2. [b]Determined by ^{1}H NMR analysis using mesitylene as an internal standard.

Because the catalytic activity of supported Au NPs usually depends on the sizes of Au NPs[58,59]; therefore, the particle size distribution of the prepared catalysts Au/*m*-ZrO_2 (IP) was measured by HAADF-STEM. The result shows a uniform distribution of particles with an average size of 2.4 nm (Fig. 2a). The size of Au NPs in Au/SiO_2 (IP) was also calculated to be 3.1 nm by XRD (Fig 3).

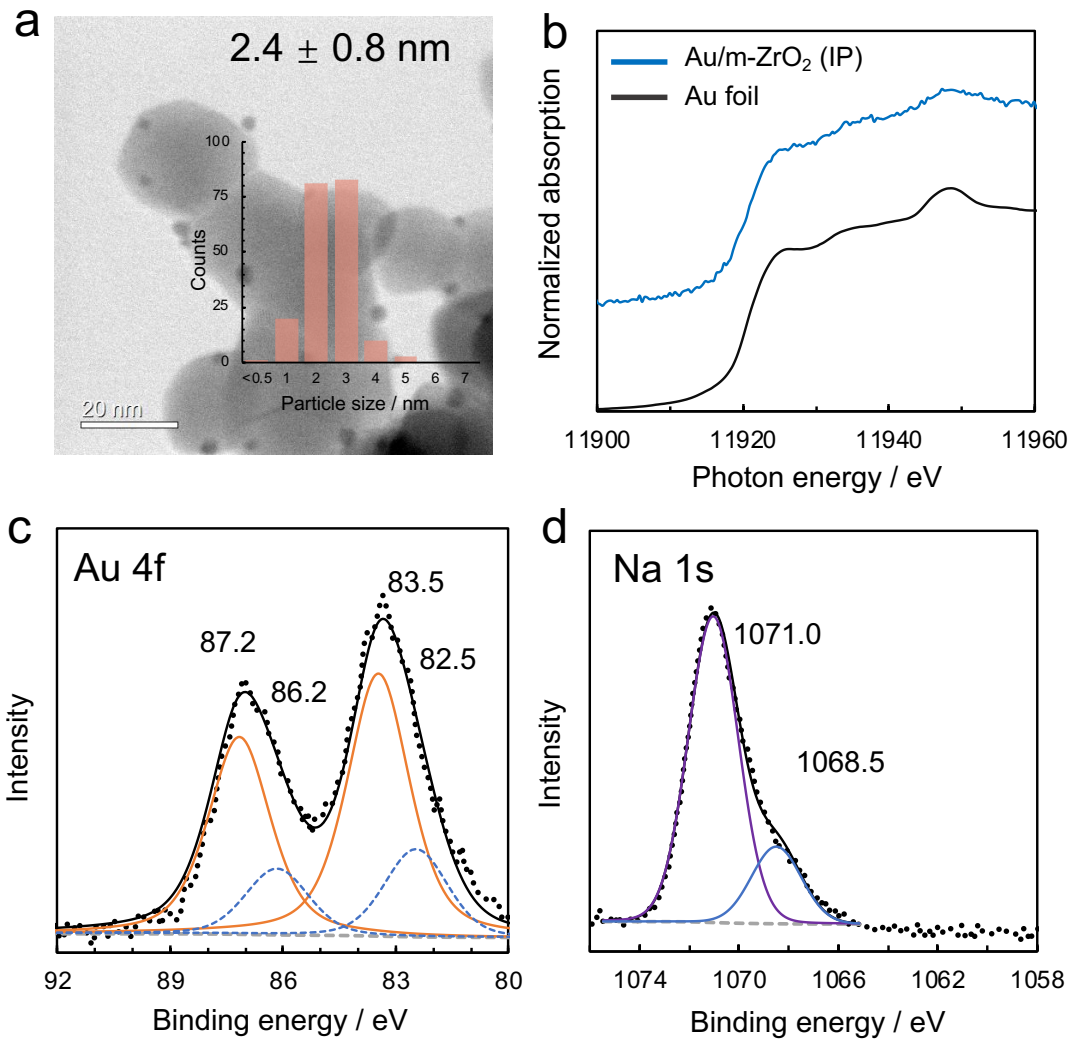

Figure 2. Characterization results of Au/*m*-ZrO_2 (IP). (a) BF-STEM image, (b) Au L_{III}-edge XANES spectra, (c) Au 4f XPS spectra, and (d) Na 1s XPS spectra.

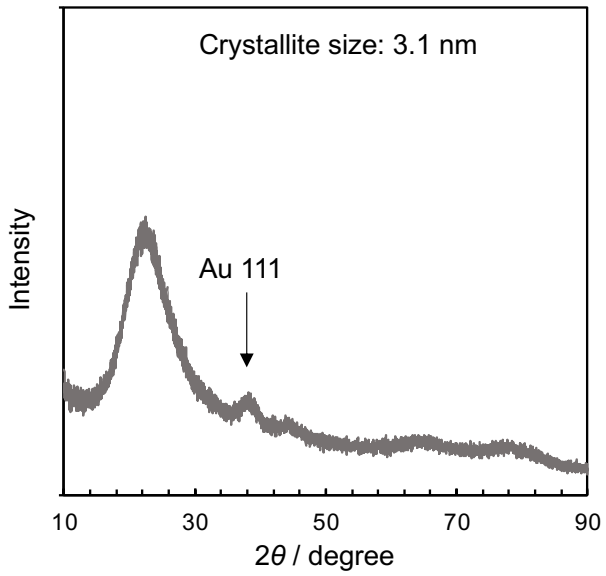

Figure 3. XRD pattern of Au/SiO_2 (IP).

In addition, the prepared Au catalysts were analyzed by XAFS, and Au L_{III}-edge X-ray absorption near edge structure (XANES) spectra attested the presence of Au^0 NPs in the catalysts with the reference sample of Au foil (Fig. 2b). Moreover, XAFS analysis of the Au^0 NPs supported by *t*-ZrO_2 and SiO_2 were conducted (Fig. 4), and their XANES spectra, k^3-weighted EXAFS oscillations, and radial structure functions were also compared, showing zero-valence of the supported Au NPs.

XPS was performed to analyze the chemical state of surface species. In the Au 4f spectra, Au species on the surface of the catalyst were primarily Au^0 state with binding energy of 83.5 eV (Au $4f_{7/2}$) and 87.2 eV (Au $4f_{5/2}$) (Fig. 2c)[60–62]. Furthermore, a couple of peaks of 82.5 eV (Au $4f_{7/2}$) and 86.2 eV (Au $4f_{5/2}$) was observed after fitting the curve, which were relatively low for normal supported Au NPs and possibly contributed to the negatively charged Au^0 particles ($Au^{\delta-}$)[63,64]. Therefore, we inferred the possible presence of elements acting as electron donors around the supported Au NPs. Meanwhile, during the surveying sweeps, an evident signal around 1071.0 eV was observed, which should belong to the 1s peak of Na[65]. The Na 1s XPS profile is shown in Figure 2d, and the peak in a relatively low binding energy (1068.5 eV) may be derived from the Na^+ bonded to oxygen in the transition metal oxide[66],

such as ZrO_2. Indeed, the residual basic counterion of the Na cation would act as an electron-donating ligand and cause the negative charge of Au species. Besides, the Na salts could trigger the reaction by deprotonating the carboxylic acid and then facilitate the addition of carboxylic acid group to alkynes. The source of Na would be the NaOH reagent used in the preparation process of Au–(β-ala) complex. In the preparation process of Au NPs catalysts, bases or reducing agents containing Na salts are often used in large quantities, and the complete removal of these Na species from the surface of the catalyst is usually difficult, thus affecting the catalytic reactions[39,67].

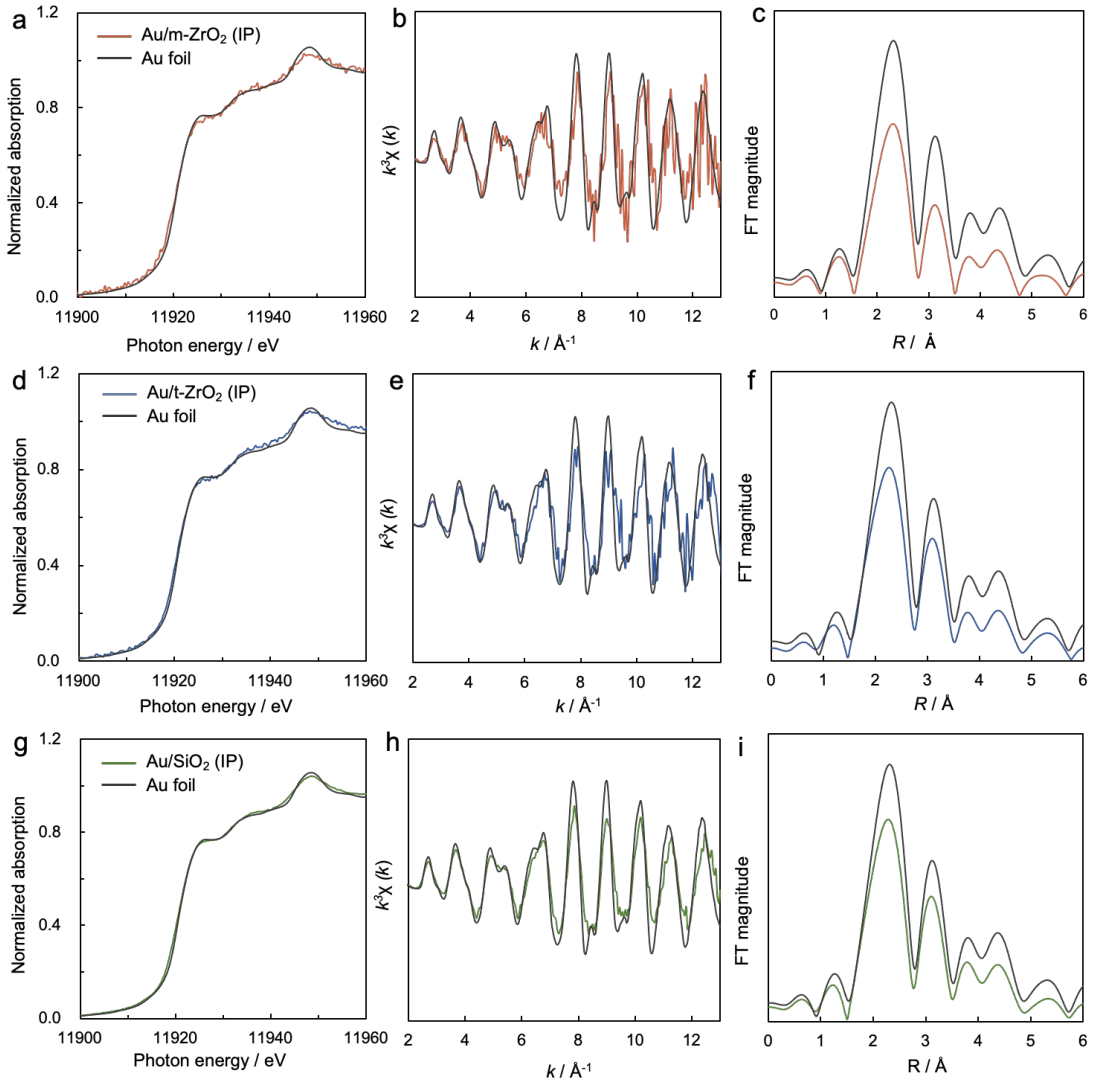

Figure 4. Results of XAFS analysis of Au/*m*-ZrO_2, (IP) Au/*t*-ZrO_2, and (IP) Au/SiO_2 (IP). (a) Au L_{III}-edge XANES spectra, (b) k^3-weighted EXAFS oscillations, and (c) radial structure functions (k = 2–10 $Å^{-1}$).

To remove the influence of the residual Na species and clarify the active sites of the Au/*m*-ZrO_2 (IP) catalyst, a normal Au/*m*-ZrO_2 catalyst prepared by the deposition precipitation (DP) method was discussed. Considering that the Na salts should play the role of bases, an analysis on the intramolecular cyclization of **1a** over Au/*m*-ZrO_2 with the addition of a normal base Na_2CO_3 was performed (Table 4). Only low yield and TOF were obtained when using the Au/*m*-ZrO_2 prepared by the Na-free DP method (entry 1). After directly adding the Na_2CO_3 to the catalyst or the reaction system, the TOF turned up to 153 h^{-1} and 157 h^{-1}, respectively (entries 3 and 4), which were higher than the 130 h^1 of Au/*m*-ZrO_2 (IP) (entry 7). Meanwhile, organic base triethylamine was added to the reaction and contributed to a TOF of 163 h^1, demonstrating the essential role of base to this reaction (entry 5). Moreover, the amount of Au was investigated; a TOF exceeding 100 h^1 could still be achieved under Au 0.01 mol% and a stable TOF was achieved if the Au amount was not too low (entries 6 and 8). Among the Na-added Au/*m*-ZrO_2 catalyst, the Na-Au/*m*-ZrO_2 prepared by grinding yielded the highest TOF (250 h^1) (entry 9), which may be due to the improved distribution of the Na salts achieved by grinding[68]. Additionally, a Na-modified *m*-ZrO_2 was prepared and no generation of **2a** was detected (entry 10). In addition, reaction under air atmosphere was also investigated, and a TOF of 223 h^1 was obtained.

Table 4. Intramolecular cyclization of **1a** over Au/*m*-ZrO_2 prepared or treated by different methods[a]

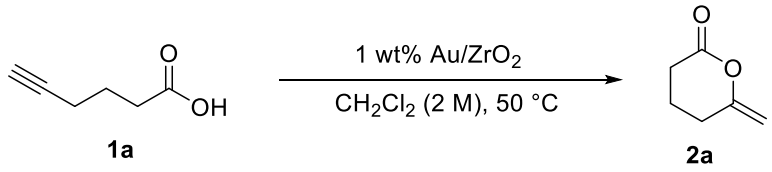

1a **2a**

Entry	Catalyst	Method	Time/h	Yield/%[b]	TOF/h^{-1}
1	Au/m-ZrO_2	Au DP	24	8	7
2	Na-Au/m-ZrO_2	Au DP, Na_2CO_3 (IP)	24	100	83
3	Na-Au/m-ZrO_2	Au DP, Na_2CO_3 (IP)	6	46	153
4	Au/m-ZrO_2	Au DP, Na_2CO_3 (addition)	6	47	157
5	Au/m-ZrO_2	Au DP, Et_3N (addition)	6	49	163
6[c]	Na-Au/m-ZrO_2	Au DP, Na_2CO_3 (IP)	24	25	104
7	Au/m-ZrO_2 (IP)	Au IP	2	52	130
8[d]	Na-Au/m-ZrO_2	Au DP, Na_2CO_3 (IP)	2	63	158
9[d]	Na-Au/m-ZrO_2	Au DP, Na_2CO_3 (grinding)	2	100	250
10[e]	Na/m-ZrO_2	Na_2CO_3 (IP)	6	n.d.	–
11[f]	Na-Au/m-ZrO_2	Au DP, Na_2CO_3 (grinding)	2	89	223

[a]Reaction conditions: **1a** (1 mmol), Au/m-ZrO_2 (0.05 mol%), alkali metal salts or base (0.4 mol%), CH_2Cl_2 (0.5 mL), 50 °C, N_2. [b]Determined by ^1H NMR analysis using mesitylene as an internal standard. [c]Au amount was 0.01 mol%, alkali metal salts was 0.09 mol%. [d]Au amount was 0.2 mol%, alkali metal salt amount was 1.7 mol%. [e]Catalyst weight was 40 mg. [f]Reaction atmosphere was air.

The advantage of Na salt modification by the grinding process was further discussed using Na_2CO_3 and a more stable Na salt, Na_3PO_4 (Table 5). Similar results were obtained for the modification methods, and it reveals that Na-Au/*m*-ZrO_2 catalysts prepared by grinding are more active than those prepared by impregnation.

Table 5. Effect of bases and modification methods for Na-Au/*m*-ZrO_2 catalysts[a]

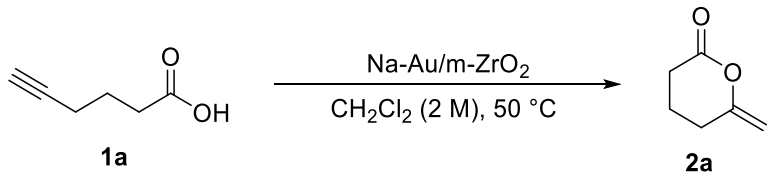

1a

1 mmol

2a

Entry	Na source	Modification method	Yield/%[b]	TOF/h^{-1}
1	NaOH	residual species	52	130
2	Na_2CO_3	impregnation	63	158
3	Na_3PO_4	impregnation	60	150
4	Na_2CO_3	grinding	100	250
5	Na_3PO_4	grinding	100	250
6[c]	Na_2CO_3	grinding	50	250
7[c]	Na_3PO_4	grinding	47	235

[a]Reaction conditions: **1a** (1 mmol), 1 wt% Na-Au/*m*-ZrO_2 (Au 0.2 mol%, Na 1.7 mol%), CH_2Cl_2 (0.5 mL), 50 °C, 2 h, N_2. [b]Determined by ^1H NMR analysis using mesitylene as an internal standard. [c]Reaction time was 1 h.

Afterwards, other Na salts and carbonates of K, Cs, and Li were used to undertand the effects of alkali metals and their counter anions (Table 6). Under the same grinding process, Na_2CO_3 showed higher activity than K_2CO_3, Cs_2CO_3, and Li_2CO_3 (entries 2−5). This revealed the high basicity of salts might lower the Lewis acidity of the supported Au NPs, and the Na salts could supply the opportune basicity. Catalytic activity of Au/*m*-ZrO_2 modified with Na_2CO_3 or Na_3PO_4 salt was inferior to that of the others (entries 6−9). Because the Na salts can be dissolved in the reaction conditions to some extent, the effects of the insoluble base of hydrotalcite and MgO were evaluated in this reaction, which gave very low yields (entries 10 and 11).

Table 6. Intramolecular cyclization of **1a** over Au/m-ZrO_2 modified with different basic species[a]

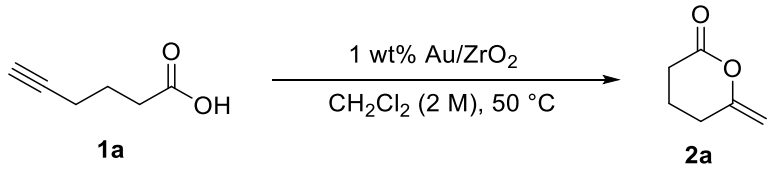

1a **2a**

Entry	Catalyst	Modification	Yield/%[b]	TOF/h^{-1}
1	Au/m-ZrO_2	–	7	18
2	Na-Au/m-ZrO_2	Na_2CO_3	100	250
3	K-Au/m-ZrO_2	K_2CO_3	81	203
4	Cs-Au/m-ZrO_2	Cs_2CO_3	51	128
5	Li-Au/m-ZrO_2	Li_2CO_3	36	90
6	Na-Au/m-ZrO_2	Na_3PO_4	100	250
7	Na-Au/m-ZrO_2	NaOH	91	228
8	Na-Au/m-ZrO_2	$NaHCO_3$	70	175
9	Na-Au/m-ZrO_2	NaCl	31	78
10	Au/m-ZrO_2	Hydrotalcite[c]	n.d.	–
11	Au/MgO/m-ZrO_2	MgO	n.d.	–

[a]Reaction conditions: **1a** (1 mmol), 1 wt% Au/m-ZrO_2 (Au: 0.2 mol%, alkali metal salts: 1.7 mol%), CH_2Cl_2 (0.5 mL), 50 °C, 2 h, N_2. [b]Determined by ^{1}H NMR analysis using mesitylene as an internal standard. [c]The weight was 4 mg.

Furthermore, based on the optimized catalyst and reaction condition, the effect of the solvent was also discussed, and a higher reaction efficiency was obtained when using CH_2Cl_2 as the solvent than those using the others (Table 7). Meanwhile, a secondary result (TOF = 158 h^{-1}) can be achieved even under neat conditions.

Table 7. Effect of solvents catalytic intramolecular cyclization of **1a**[a]

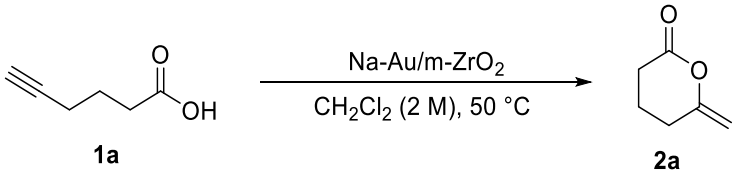

1a

1 mmol

2a

Entry	Solvent	Yield/%[b]	TOF/h^{-1}
1	neat	63	158
2	CH_2Cl_2	100	250
3	$CHCl_3$	56	140
4	Toluene	52	130
5	MeCN	43	108
6	CH_2Cl_2[c]	88	220

[a]Reaction conditions: **1a** (1 mmol), 1 wt% Na-Au/m-ZrO_2 (Au 0.2 mol%, Na 1.7 mol%), CH_2Cl_2 (0.5 mL), 50 °C, 2 h, N_2. [b]Determined by ^1H NMR analysis using mesitylene as an internal standard. [c]Non-purified CH_2Cl_2.

To further uncover the function of Na modification, the effect of the Na loading amount was investigated using Na_2CO_3 (Fig. 5). Na-free 1 wt% Au/m-ZrO_2 catalyst confirmed by the Na 1s XPS analysis showed a TOF of 18 h^{-1} (Fig. 6), which could be considered as the basic value for the following comparison. When the Na loading amount increased to 0.4 mol%, a TOF of 118 h^{-1} was obtained. For the 0.9 mol% one, more than 10-fold enhancement was observed in catalytic activity. However, as the loading amount increased from 1.7 mol% to 3.4 mol%, no significant change was observed in TOF. The above results reveal that a significant enhancement effect can be realized even if a small amount of Na species is added to the Au/*m*-ZrO_2 catalysts. In addition, the enhancement effect becomes steady after the Na loading amount over 1 wt% (1.7 mol%, Na/Au > 9), which may imply surface modification with Na salts, becomes saturated. Moreover, when the catalyst is loaded with a relatively excess amount of Na species, the catalytic efficiency should begin to be limited by the number of active sites from Au NPs.

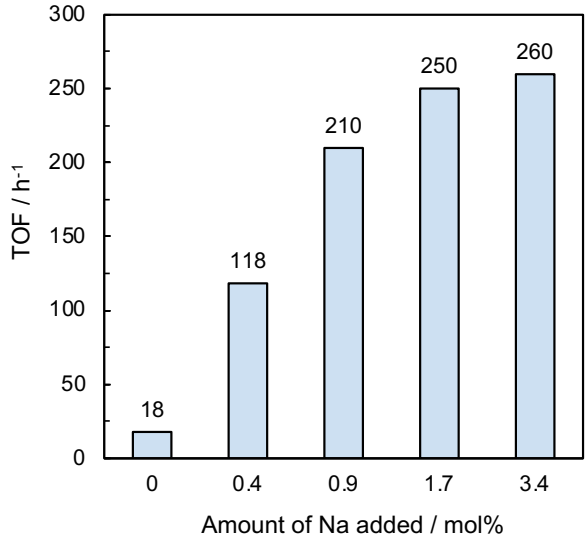

Figure 5. Investigation of the influence of Na loading amount on the catalytic intramolecular cyclization of **1a**.

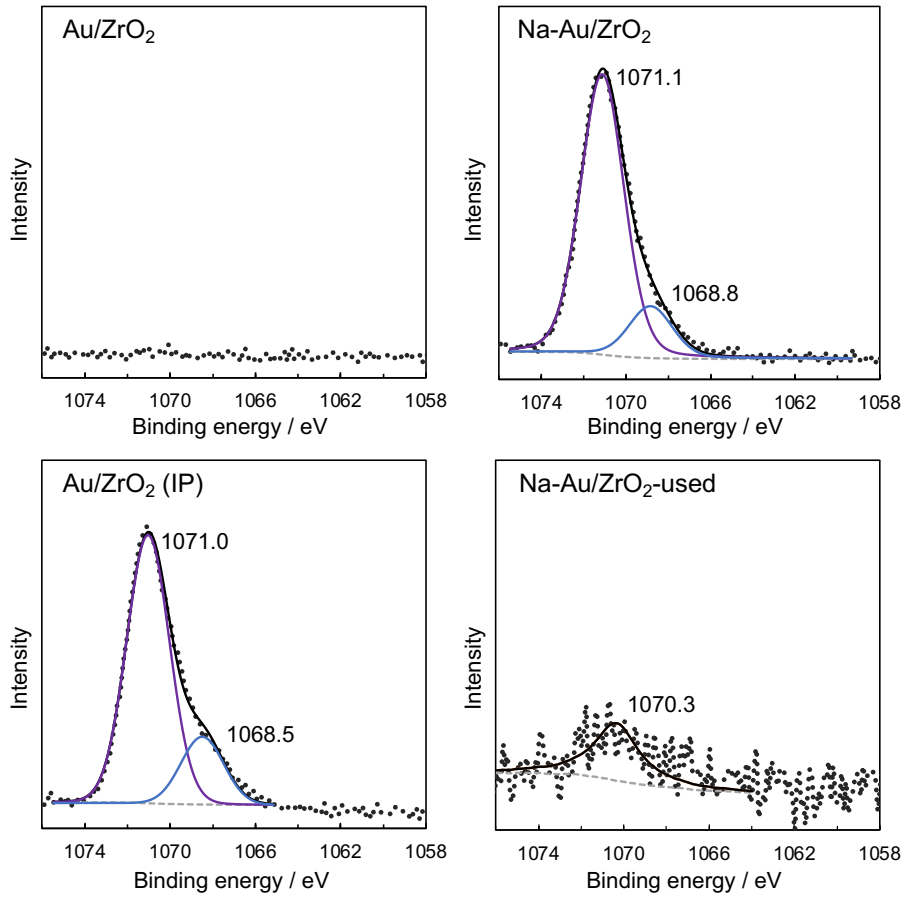

Figure 6. Na 1s XPS spectra of Au/m-ZrO_2, Na-Au/*m*-ZrO_2, Au/*m*-ZrO_2 (IP), and Na-Au/*m*-ZrO_2-used (after the 4th run).

A reusing test was carried out using the optimized Na-Au (1:1 wt%)/*m*-ZrO_2 to investigate its reusability (Table 8). High yields could be maintained until the second run, and a steep drop was observed during the third run, which is attributed to the leaching of Na species (Fig. 6).

Table 8. Reusing test of the Na-Au/m-ZrO_2[a]

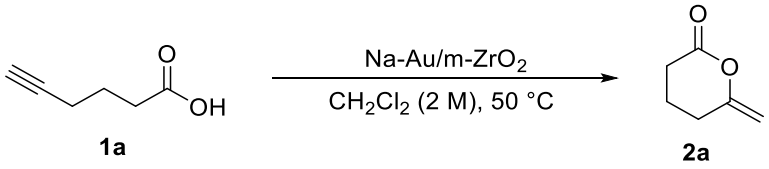

1a 2a

Entry	Run	Na addition	Yield/%[b]
1	1st	Na_2CO_3	100
2	2nd	–	100
3	3rd	–	94
4	4th	–	46
5[c]	5th	Na_2CO_3	100

[a]Reaction conditions: **1a** (1 mmol), 1 wt% Au/m-ZrO_2 (Au 0.05 mol%, Na 0.4 mol%), CH_2Cl_2 (0.5 mL), 50 °C, 24 h, under N_2. [b]Determined by ^{1}H NMR analysis using mesitylene as an internal standard. [c]Na_2CO_3 addition (0.4 mol%) was performed again.

Following the later addition of Na_2CO_3 to the recycled catalyst, the yield returned to the same level as that of the fresh catalyst. This reveals that the active sites of Au NPs can remain active until reused four times. In addition, replenishing the loss of the Na species should achieve stable and multiple reuses. To confirm the catalytic system developed in this research could be a reliable green synthesis route for further application, we conducted this reaction with a continuous flow reactor. In the first 24 h, the yield remained above 98%, and there was almost no significant deterioration (Fig. 7).

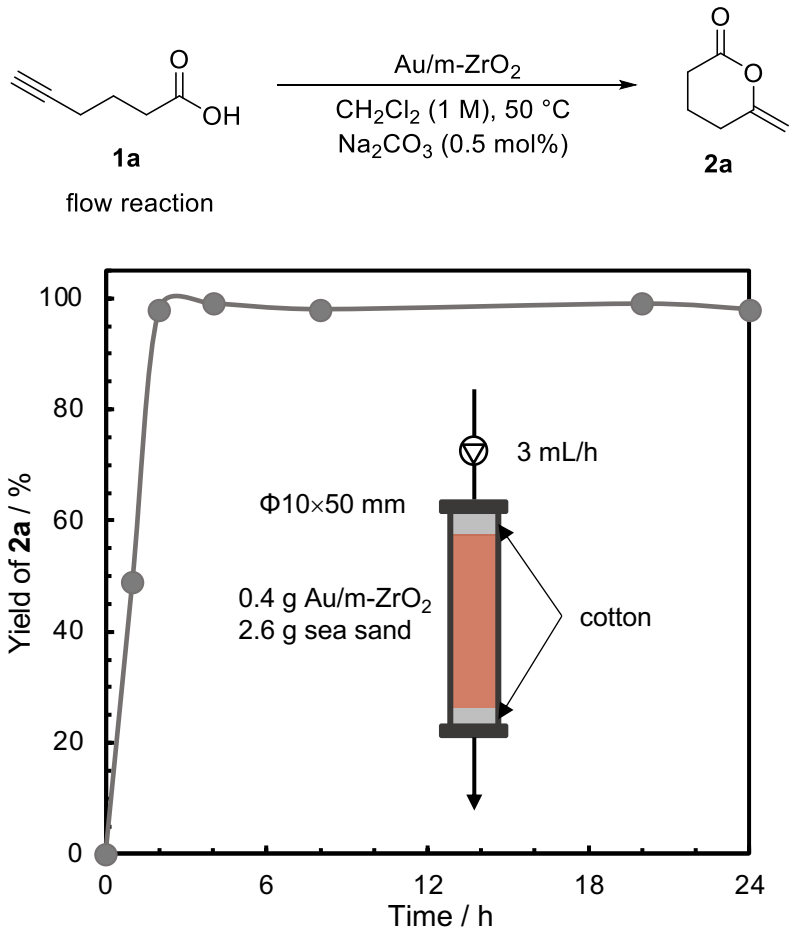

Figure 7. Relationship between yield and time in the continuous synthesis of **2a** using a flow reactor.

After a continuous flow reaction of 72 h, a total TON above 9000 was achieved (Table 9). This should be the highest TON of heterogeneous Au catalysts for the intramolecular cyclization of **1a**, and the feasibility in flow synthesis also provides significant reference for synthesizing these compounds using a green method.

Table 9. Continuous flow synthesis of **2a** with Na-modified Au/m-ZrO_2[a]

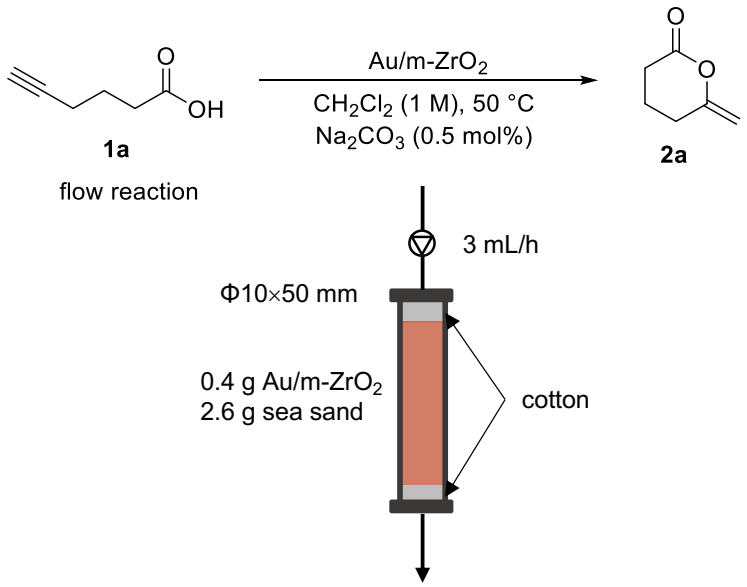

Entry	Reaction time/h	Yield/%[b]
1	0	0
2	1	49
3	2	98
4	4	99
5	8	98
6	20	99
7	24	98
8	28	95
9	32	92
10	44	87
11	48	85
12	52	84
13	56	86
14	68	85
15	72	94

[a]Reaction conditions: 1 wt% Au/m-ZrO_2 (400 mg), **1a** (23.2 g), CH_2Cl_2 (210 mL), Na_2CO_3 (110 mg), mesitylene, 50 °C, flow rate: 0.05 mL/min. [b]Determined by ^1H NMR analysis using mesitylene as an internal standard.

Moreover, the catalysts recycled from the continuous flow reaction were investigated by XRD, and the slightly increased intensity in the region of Au (111) phase showed the agglutination of Au NPs was a reason for the decrease in yield during a long time reaction (Fig. 8).

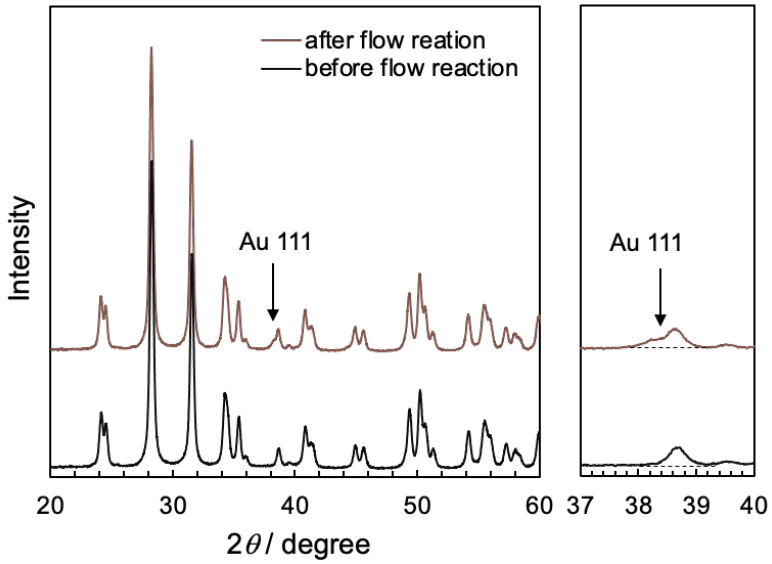

Figure 8. XRD patterns of the fresh catalyst and the used catalyst after flow reaction.

XAFS analysis was used to confirm the changes in chemical valence states of gold nanoparticles after the addition of Na_2CO_3 for the optimized Na-Au/*m*-ZrO_2 (Fig. 9). No visible change was observed in XANES spectra, revealing that the active species of both the catalysts should be the zero-valent Au NPs. Furthermore, XRD was also performed over the *m*-ZrO_2, Au/*m*-ZrO_2, and Na-Au/*m*-ZrO_2 (Fig. 10). The loading of Au NPs and the Na salts evidently causes no changes in the reflecting peaks, verifying that the Au NPs and Na salts were highly dispersed.

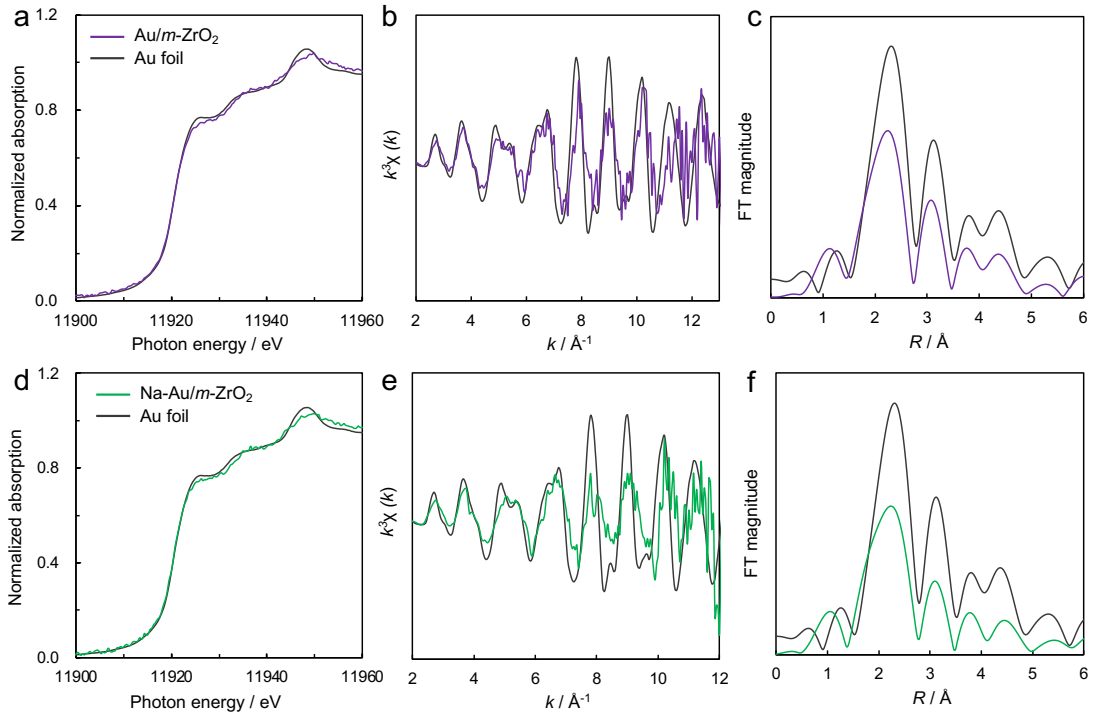

Figure 9. XAFS analysis of Au/*m*-ZrO_2 and Na-Au/*m*-ZrO_2. (a) Au L_{III}-edge XANES spectra, (b) k^3-weighted EXAFS oscillations, and (c) radial structure functions (k = 2–10 $Å^{-1}$).

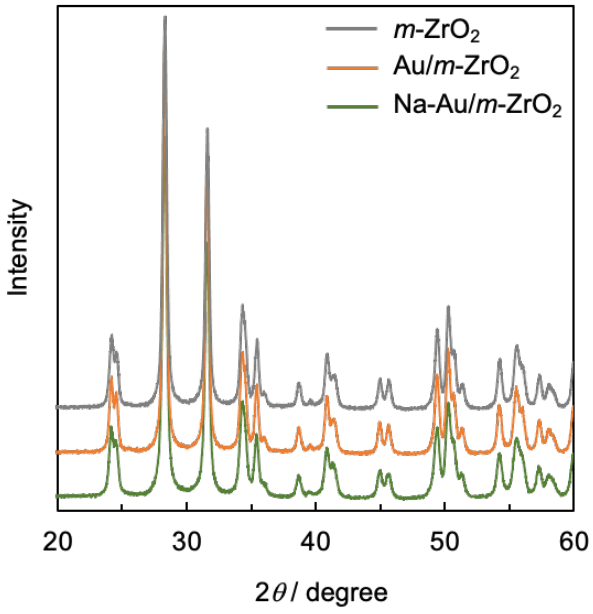

Figure 10. XRD patterns of Au/*m*-ZrO_2 and Na-Au/*m*-ZrO_2 with *m*-ZrO_2 as the reference.

Au 4f XPS profile of the Na-free Au/*m*-ZrO_2 was also collected and analyzed via peak deconvolution (Fig. 11a). Au species on the *m*-ZrO_2 were primarily in the Au^0 (83.5 eV, Au $4f_{7/2}$; 87.2 eV, Au $4f_{5/2}$) with components from $Au^{\delta+}$ (84.5 eV, Au $4f_{7/2}$; 88.2 eV, Au $4f_{5/2}$)[69–72]. After the addition of Na salts to the catalysts, the peaks belonging to $Au^{\delta+}$ disappeared and a couple of negatively charged peaks were observed in 82.5 eV (Au $4f_{7/2}$) and 86.2 eV (Au $4f_{5/2}$) (Fig. 11b), which exhibited the same binding energy as that of the $Au^{\delta-}$ species illustrated in Figure 2.

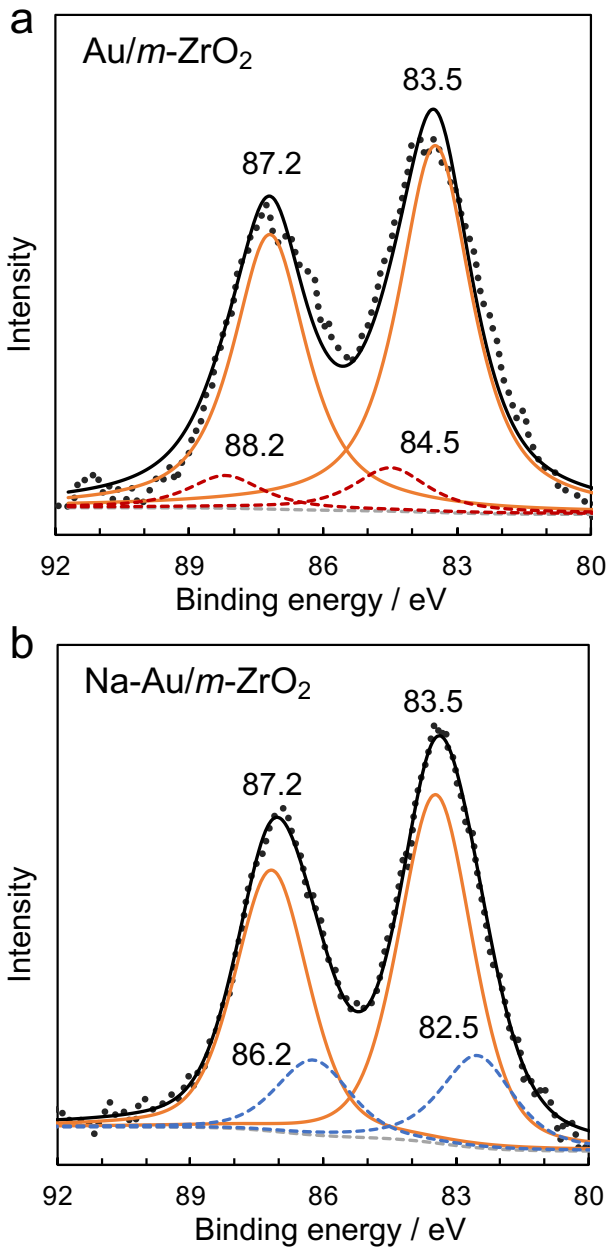

Figure 11. Au 4f XPS spectra of (a) Au/*m*-ZrO_2, and (b) Na-Au/*m*-ZrO_2.

The catalyst recycled from the reusing test was also analyzed; apart from the Au^0 species in 83.5 eV (Au $4f_{7/2}$) and 87.2 eV (Au $4f_{5/2}$), a couple of relatively weak peaks were observed in 82.5 eV (Au $4f_{7/2}$) and 86.2 eV (Au $4f_{5/2}$) (Fig. 12). Therefore, the relationship between $Au^{\delta-}$ species and Na species was confirmed by contrasting the Au 4f and Na 1s XPS spectra. Na salts added to the Au/*m*-ZrO_2 act as an electron donor and account for the negatively charged Au species.

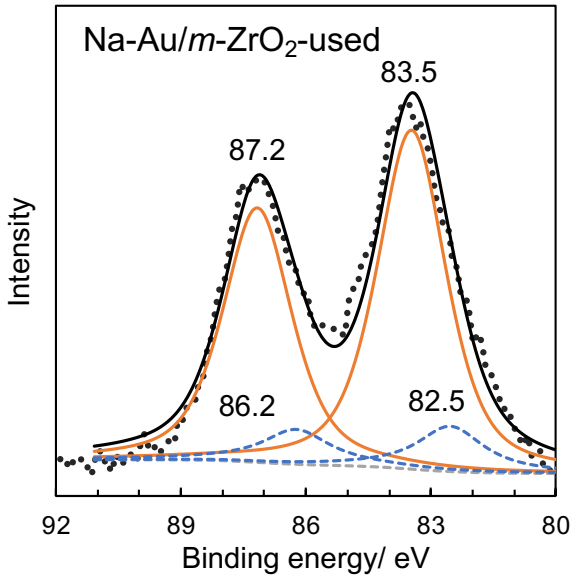

Figure 12. Au 4f XPS spectra of Na-Au/*m*-ZrO_2-used (after the 4th run).

To elucidate the role of Na salts on the Au/*m*-ZrO_2, XPS spectra of Zr 3d were also investigated (Fig. 13). The Zr 3d peaks of the catalysts containing Na species shifted by 0.2 eV to lower binding energy compared with those of the Na-free Au/*m*-ZrO_2 and used Na-Au/*m*-ZrO_2 catalysts. This can be considered as the negative charge effect from the Na salt, revealing the adhesion of Na species on the surface of *m*-ZrO_2 and the strong interaction between *m*-ZrO_2 and Na species. Moreover, the further reduced Zr species (178.5 eV, Zr $3d_{5/2}$; 180.9 eV, Zr $3d_{3/2}$) in Au/*m*-ZrO_2 (IP) catalysts might be related to the partial reduction of *m*-ZrO_2 caused by the existence of Na species during the calcination[35].

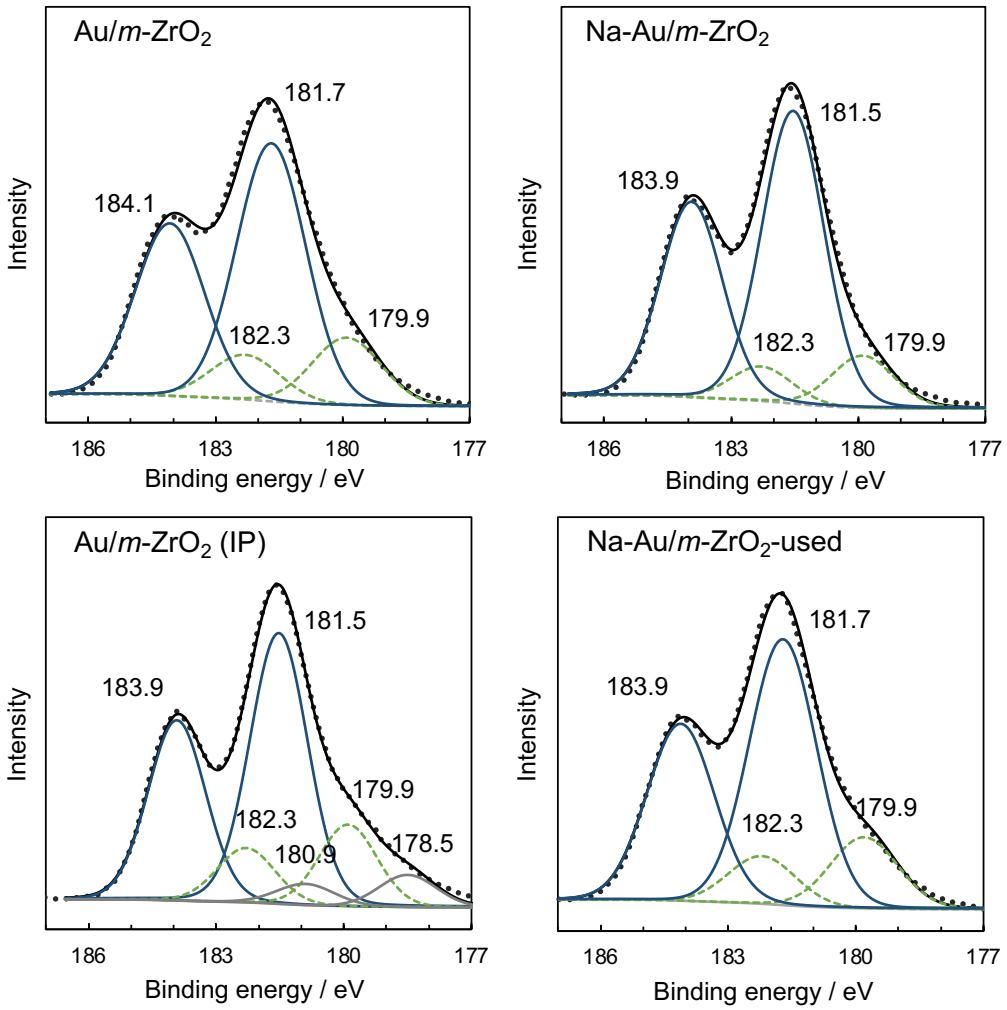

Figure 13. Zr 3d XPS spectra of Au/*m*-ZrO_2, Na-Au/*m*-ZrO_2, Au/*m*-ZrO_2 (IP), and Na-Au/*m*-ZrO_2-used (after the 4th run).

Meanwhile, CO-DRIFT analysis was also used to characterize the surface species of Au NPs (Fig. 14). Compared with the spectrum of support *m*-ZrO_2, peaks belonging to both Au^0-CO and $Au^{\delta-}$-CO were observed from the Na-containing Au/*m*-ZrO_2 catalysts[64,73,74]. This is consistent with the XPS spectra. Therefore, although it was reported that supported $Au^{\delta+}$ species is active for the intramolecular cyclization of alkynoic acids, considering the results in this study, reduced Au species may also be active, and the addition of Na salts should play the key role during the catalytic reaction.

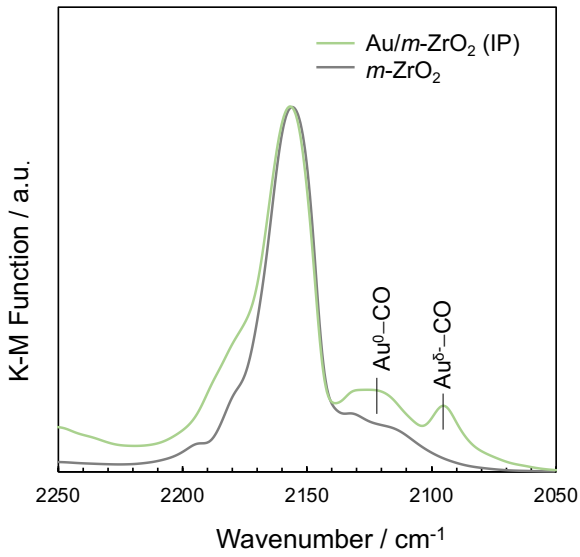

Figure 14. CO-DRIFT measurements of *m*-ZrO_2 and Au/*m*-ZrO_2 (IP).

The maximum reaction efficiency was proved to be limited by the number of active sites; therefore, clarifying active sites is significant. Initially, calcination process was controlled and thus catalysts with different Au particles sizes were obtained (Fig. 15a–d). When the calcination temperature was 500 °C, only mild aggregation occurred, compared with the sample at 300 °C. However, an average size above 10 nm was observed with the calcination temperature of 600 °C. Subsequently, these catalysts with Na salt modification were used in a group of kinetic investigations (Fig 15e). Based on the results in the time course of the yield over the Na-Au/*m*-ZrO_2 catalysts with different Au particles sizes, a linear relationship between yield and reaction time was found. Thus, this reaction should be a zero-order in substrate. Afterwards, we tried to calculate and fit the kinetic data in relation to the model of active Au atoms on surface area or the model of active Au atoms on interface perimeter. The data of the catalytic reaction are highly consistent with the model of active Au atoms on surface area (Fig. 15f)[72], rather than the model of interface perimeter[75,76]. This is the first time that a clear kinetic demonstration of catalytic intramolecular cyclization of alkynoic acid substrate has been achieved on supported Au^0 NPs, and the following two important points are confirmed. The reaction is zero-order in substrate and the active sites are on the surface of the supported Au NPs. This will provide valuable reference for the development of additional green reactions over supported Au NPs catalysts in the future.

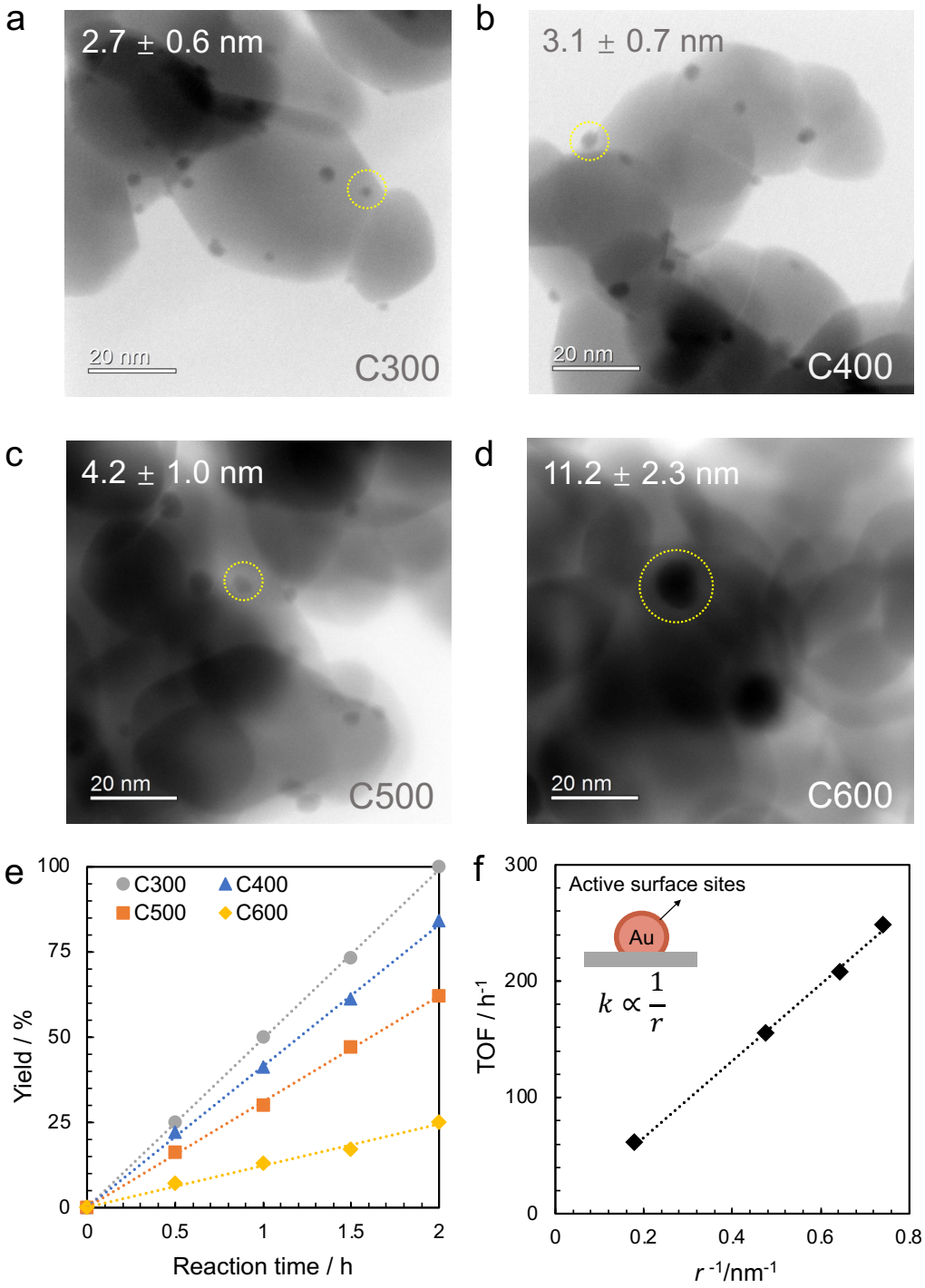

Figure 15. Investigation of the reaction kinetics and active sites of the catalyst. BF-STEM images of Na-Au/m-ZrO_2 calcined at (a) 300 °C (C300), (b) 400 °C (C400), (c) 500 °C (C500), and (d) 600 °C (C600). (e) Time course of the yields over catalysts with different particle sizes. (f) Relationship between the average particle size and TOF in the intramolecular cyclization of **1a** (*k* represents the reaction rate and *r* is the average radius of Au NPs).

The substrate scope was also investigated under the optimized reaction conditions. The Na-Au/*m*-ZrO_2 catalysts also provided satisfactory reaction activity for the intramolecular cyclization of other alkynoic acids (Table 10).

Table 10. Intramolecular cyclization of alkynoic acids catalyzed by Na-Au/*m*-ZrO_2[a]

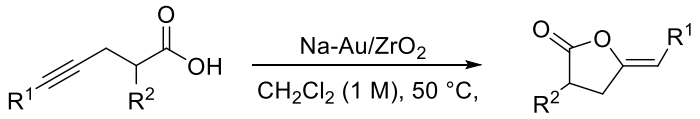

1b–d (1 mmol) **2b–d**

Entry	Substrate		Product		Yield[b]/%
1	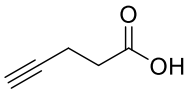	**1b**	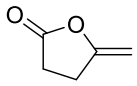	**2b**	100 92[d]
2	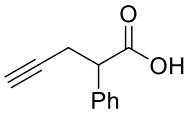	**1c**	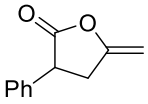	**2c**	100 91[d]
3[c]	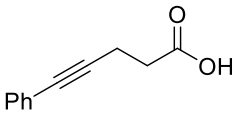	**1d**	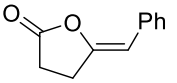	**2d**	94
4[c]	R^1=4-MeO-C_6H_5 R^2=H	**1e**	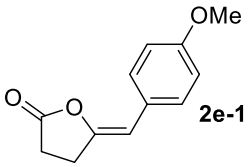	**2e-1**	70
			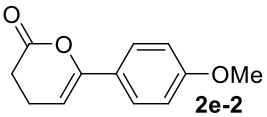	**2e-2**	30
5[c]	R^1=4-F_3C-C_6H_5 R^2=H	**1f**	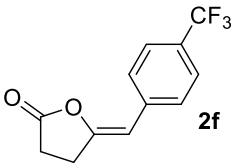	**2f**	68[e]

[a]Reaction conditions: substrate (1 mmol), 1 wt% Na-Au/m-ZrO_2 (Au 0.2 mol%, Na 1.7 mol%), CH_2Cl_2 (1 mL), 50 °C, 5 h, N_2. [b]Determined by ^{1}H NMR analysis using mesitylene as an internal standard. [c]Reaction scale was 0.5 mmol. [d]Isolated yield. [e]Reaction time was 24 h.

Yields as high as 100% were detected when 4-pentynoic acid (**1b**) and 2-phenyl-4-pentenoic acid (**1c**) were tested. A relatively low yield of 94% was obtained in the conversion of 5-phenyl-4-pentynoic acid (**1d**) without any noticeable formation of byproducts. Moreover, the presence of electron-donating methoxy in phenyl at the end

of the alkyne(1**e**) was also evaluated, and a yield of 70% for the pentatomic ring product and 30% for the hexatomic ring product was detected. On the other hand, the presence of electron-withdrawing trifluoromethyl (1**f**) only provided a relatively low yield of 68%, showing the distinct electron effect from the substrates.

Considering the property of Au^0 NPs and previous reports about similar reactions over homogeneous Au(I) catalysts, the rate-determining step of the intramolecular cyclization of alkynoic acids over supported Au0 NPs catalysts could be considered as the addition of carboxylic acid to alkyne or the protodeauration[77,78]. To address this uncertainty, an isotopic effect investigation was performed to confirm the rate-determining step of this reaction. Under the same reaction conditions used above, a deuterated substrate RCOOD **1a-*d*$_1$** which was treated with CD_3OD, only gave a yield of 16% for **2a** and 8% for **2a-*d*$_1$** (Scheme 1), and the formation of **2a** should be derived from the incompletely deuterated substrate. On the contrary, a significant yield of 91% was detected when using the substrate treated by the normal methanol in a same process. This result proves the reaction is of zero-order with respect to substrate concentration. Here, we simply calculated the k_H/k_D by dividing the yield of 91% (without deuterium) with the yield of 8% (with deuterium). Therefore, a kinetic isotopic effect (KIE) was observed in this research, and a large KIE value (k_H/k_D = 11.4) should be related to the quantum tunneling effect[79].

Scheme 1. Isotope effect on the protodeauration step in the catalytic intramolecular cyclization of **1a-*d*$_1$** over Na-Au/m-ZrO_2.

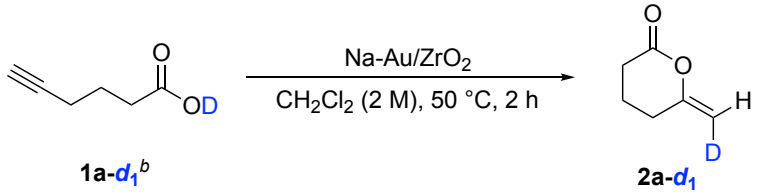

1a-*d*$_1$[b] **2a-*d*$_1$**

Conv.: 25% (total)[c]
Yield: 24% (total)[c], 16% (**2a**)[c], 8% (**2a-*d*$_1$**)[c]

[a]Reaction conditions: **1a-*d*$_1$** (1 mmol), 1 wt% Na-Au/m-ZrO_2 (Au 0.2 mol%, Na 1.7 mol%), CH_2Cl_2 (0.5 mL), 50 °C, 2 h, under N_2. [b]Treated with CD_3OD (see details in supporting information). [c]Determined by ^1H NMR analysis using mesitylene as an internal standard.

This result reveals that the rate-determining step of this reaction over Na-Au/m-ZrO_2 catalyst should be the protodeauration. The Na species on the surface of the catalyst likely act as bases and promote the nucleophilic attack of the carboxylic acid, thereby accelerating the addition of carboxylic acid to alkynes.

In addition, an isotopic effect investigation using a substrate with an alkynyl Csp-D bond was also carried out on the stereoselectivity of the protonation process (Scheme 2). This proved that the generation of the Z configuration product is favorable, the configuration of which is the same as in the cyclization of alkynoic acids using homogeneous Au(I) catalysts[25].

Scheme 2. Investigation on the stereoselectivity of protonation.

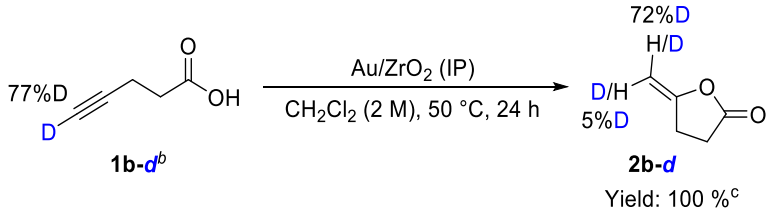

[a]Reaction conditions: **1b-*d*** (1 mmol), 1 wt% Au/m-ZrO_2 (prepared by IP method, Au 0.1 mol%, residual sodium), CH_2Cl_2 (0.5 mL), 50 °C, 24 h, under N_2. [b]Treated with *tert*-BuLi and D_2O at –78 °C. [c]Determined by ^1H NMR analysis using mesitylene as an internal standard.

Based on the above results and analysis, a proposed catalytic cycle for the intramolecular cyclization was present (Scheme 2): (i) coordination of either the alkyne or the carboxylate to the surface of Au0 NPs and activation of the substrate by deprotonation with add of Na species; (ii) addition of carboxylic acid to alkyne and thus the intramolecular cyclization; (iii) protodeauration of vinyl gold intermediate.

Scheme 2. Proposed reaction mechanism of the intramolecular cyclization of alkynoic acids over Na-Au/ZrO_2 catalysts.

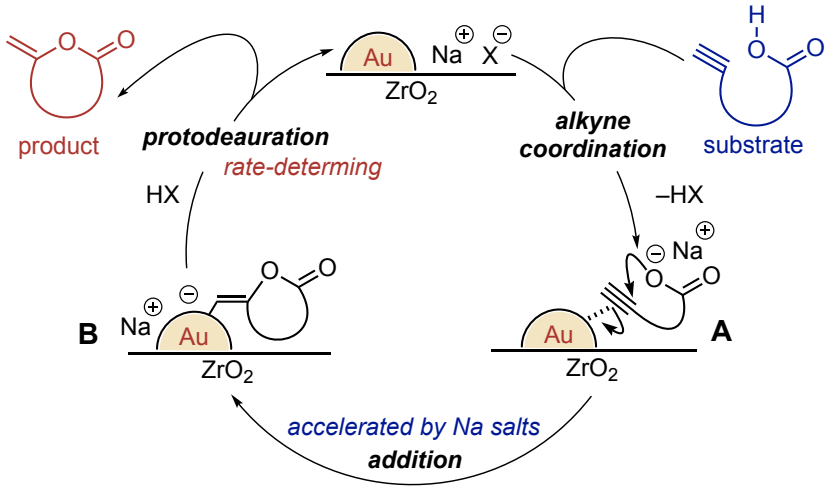

5.4. Conclusion

In conclusion, we demonstrated that the atomically efficient intramolecular cyclization of alkynoic acids could be realized even over the supported Au^0 NPs catalysts modified by sodium salts, which is a very stable and simple catalyst compared to the current ones. More than one order of magnitude of enhancement in the reaction efficiency was achieved by adding the Na_2CO_3 even below 1 mol%. The effects of the Na species on the surface of the catalysts were also investigated based on XPS. Even negatively charged Au0 NPs can facilitate the reaction. This study also conducted the analysis on kinetics. We, for the first time, provide a clear kinetic demonstration of the catalytic intramolecular cyclization of alkynoic acid substrate over supported Au0 NPs. The reaction is zero-order in substrate concentration and the active sites are on the surface of the supported Au NPs. The rate-determining step of the reaction is presumed to be protodeauration with the isotopic discussion. In addition, we proposed that the most desirable role of Na salts was accelerating the addition of carboxylic acid to alkyne and changed the rate-determining step. Furthermore, continuous yields of more than 98% and TON above 9000 were obtained during the flow reaction, verifying that this catalytic system can be a promising green method in the synthesis of fine chemicals. Moreover, the essential role of Na and the uncovered active sites on the surface of

nanoparticles could map out the strategies for the design of catalyst composition and active sites.

5.5. References

[1] R. Wu, J. Li, Y. Wang, Z. Quan, Y. Su, C. Huo, Adv. Synth. Catal. 362 (2019) 3436–3440.

[2] Y. Ogawa, M. Kato, I. Sasaki, H. Sugimura, J. Org. Chem. 83 (2018) 12315–12319.

[3] X. F. Wu, H. Neumann, M. Beller, Chem. Rev. 113 (2013) 1–35.

[4] R. A. Sheldon, Chem. Soc. Rev. 41 (2012) 1437–1451.

[5] D. E. Resasco, B. Wang, D. Sabatini, Nat. Catal. 1 (2018) 731–735.

[6] E. Tomás-Mendivil, P. Y. Toullec, J. Borge, S. Conejero, V. Michelet, V. Cadierno, ACS Catal. 3 (2013) 3086–3098.

[7] S. Bhakta, T. Ghosh, Asian J. Org. Chem. 10 (2021) 496–505.

[8] V. Cadierno, Catalysts 10 (2020) 1206.

[9] M. J. Rodríguez-Álvarez, C. Vidal, J. Díez, J. García-Álvarez, Chem. Commun. 50 (2014) 12927–12929

[10] N. Nebra, J. Monot, R. Shaw, B. Martin-Vaca, D. Bourissou, ACS Catal. 3 (2013) 2930–2934.

[11] G. Hamasaka, Y. Uozumi, Chem. Commun. 50 (2014) 14516–14518.

[12] E. Tomás-Mendivil, P. Y. Toullec, J. Díez, S. Conejero, V. Michelet, V. Cardierno, Org. Lett. 14 (2012) 2520–2523

[13] J. García-Álvarez, J. Díez, C. Vidal, Green Chem. 14 (2012) 3190–3196

[14] V. Dalla, P. Pale, New J. Chem. 23 (1999) 803–805.

[15] P. Pale, J. Chuche, Tet. Lett. 28 (1987) 6447–6448.

[16] V. Dalla, P. Pale, Tet. Lett. 35 (1994) 3525–3528.

[17] D. Ke, N. Á. Espinosa, S. Mallet-Ladeira, J. Monot, B. Martin-Vaca, D. Bourissou, Adv. Synth. Catal. 358 (2016) 2324–2331.

[18] M. Viciano, E. Mas-Marzá, M. Sanaú, E. Peris, Organometallics 25 (2006) 3063–3069.

[19] M. Jiménez-Tenorio, M. C. Puerta, P. Valerga, F. J. Moreno-Dorado, F. M. Guerra, G. M. Massanet, Chem. Commun. 22 (2001) 2324–2325.

[20] I. Takei, Y. Wakebe, K. Suzuki, Y. Enta, T. Suzuki, Y. Mizobe, M. Hidai, Organometallics 22 (2003) 4639–4641.

[21] N. Conde, R. SanMartin, M. T. Herrero, E. Domínguez, Adv. Synth. Catal. 358 (2016) 3283–3292.

[22] B. Saavedra, J. M. Pérez, M. J. Rodríguez-Álvarez, J. García-Álvarez, D. J. Ramón, Green Chem. 20 (2018) 2151–2157.

[23] A. Nagendiran, O. Verho, C. Haller, E. V. Johnston, J. E. Bäckvall, J. Org. Chem. 79 (2014) 1399–1405.

[24] N. Yuan, A. Gudmundsson, K. P. J. Gustafson, M. Oschmann, C. W. Tai, I. Persson, X. Zou, O. Verho, É. G. Bajnóczi, J. E. Bäckvall, ACS Catal. 11 (2021) 2999–3008.

[25] D. Gasperini, L. Maggi, S. Dupuy, R. M. P. Veenboer, D. B. Cordes, A. M. Z. Slawin, S. P. Nolan, Adv. Synth. Catal. 2016, 358, 3857–3862.

[26] P. Y. Toullec, E. Genin, S. Antoniotti, J.-P. Genêt, V. Michelet, Synlett 5 (2008) 707–711.

[27] F. Neaţu, Z. Li, R. Richards, P. Y. Toullec, J.-P. Genêt, K. Dumbuya, J. M. Gottfried, H. P. Steinrück, V. I. Pârvulescu, V. Michelet, Chem. Eur. J. 14 (2008) 9412–9418.

[28] X. Z. Shu, S. C. Nguyen, Y. He, F. Oba, Q. Zhang, C. Canlas, G. A. Somorjai, A. P. Alivisatos, F. D. Toste, J. Am. Chem. Soc. 137 (2015) 7083–7086.

[29] K. Eriksson, O. Verho, L. Nyholm, S. Oscarsson, J. E. Bäckvall, European J. Org. Chem. 2015 (2015) 2250–2255.

[30] Y. Yamane, X. Liu, A. Hamasaki, T. Ishida, M. Haruta, T. Yokoyama, M. Tokunaga, Org. Lett. 11 (2009) 5162–5165.

[31] T. Ishida, S. Aikawa, Y. Mise, R. Akebi, A. Hamasaki, T. Honma, H. Ohashi, T. Tsuji, Y. Yamamoto, M. Miyasaka, T. Yokoyama, M. Tokunaga, ChemSusChem 8 (2015) 695–701.

[32] Z. Zhang, T. Mamba, E. Yamamoto, H. Murayama, T. Ishida, T. Honma, T. Fujitani, M. Tokunaga, Appl. Catal. B Environ. 246 (2019) 100–110.

[33] Z. Zhang, T. Mamba, Q. A. Huang, H. Murayama, E. Yamamoto, T. Honma, M. Tokunaga, Mol. Catal. 475 (2019) 110502.

[34] H. Murayama, T. Hasegawa, Y. Yamamoto, M. Tone, M. Kimura, T. Ishida, T. Honma, M. Okumura, A. Isogai, T. Fujii, M. Tokunaga, J. Catal. 353 (2017) 74–80.

[35] Q. A. Huang, A. Haruta, Y. Kumamoto, H. Murayama, E. Yamamoto, T. Honma, M. Okumura, H. Nobutou, M. Tokunaga, Appl. Catal. B Environ. 296 (2021) 120333.

[36] Y. Zhang, J. Zhang, B. Zhang, R. Si, B. Han, F. Hong, Y. Niu, L. Sun, L. Li, B. Qiao, K. Sun, J. Huang, M. Haruta, Nat. Commun. 11 (2020) 1–10.

[37] T. Ishida, T. Murayama, A. Taketoshi, M. Haruta, Chem. Rev. 120 (2020) 464–525.

[38] M. Sankar, Q. He, R. V. Engel, M. A. Sainna, A. J. Logsdail, A. Roldan, D. J. Willock, N. Agarwal, C. J. Kiely, G. J. Hutchings, Chem. Rev. 120 (2020) 3890–3938.

[39] N. Nikolopoulos, R. G. Geitenbeek, G. T. Whiting, B. M. Weckhuysen, J. Catal. 2021, 396, 136–147.

[40] R. Qin, L. Zhou, P. Liu, Y. Gong, K. Liu, C. Xu, Y. Zhao, L. Gu, G. Fu, N. Zheng, Nat. Catal. 2020, 3, 703–709.

[41] C. Zhang, F. Liu, Y. Zhai, H. Ariga, N. Yi, Y. Liu, K. Asakura, Angew. Chem. Int. Ed. 51 (2012) 9628–9632.

[42] L. X. Dien, T. Ishida, A. Taketoshi, D. Q. Truong, Chinh, H. Dang, T. Honma, T. Murayama, M. Haruta, Appl. Catal. B Environ. 241 (2019) 539–547.

[43] C. Xiao, L. L. Wang, R. V. Maligal-Ganesh, V. Smetana, H. Walen, P. A. Thiel, G. J. Miller, D. D. Johnson, W. Huang, J. Am. Chem. Soc. 135 (2013) 9592–9595.

[44] Y. Li, X. Chen, C. Wang, C. Zhang, H. He, ACS Catal. 8 (2018) 11377–11385.

[45] C. Zhang, Y. Li, Y. Wang, H. He, Environ. Sci. Technol. 48 (2014) 5816–5822.

[46] J. M. Pigos, C. J. Brooks, G. Jacobs, B. H. Davis, Appl. Catal. A Gen. 319 (2007) 47–57.

[47] H. J. Eom, M. S. Kim, D. W. Lee, Y. K. Hong, G. Jeong, K. Y. Lee, Appl. Catal. A Gen. 493 (2015) 149–157.

[48] V. Mishra, J. K. Cho, S. H. Shin, Y. W. Suh, H. S. Kim, Y. J. Kim, Appl. Catal. A Gen. 487 (2014) 82–90.

[49] S. Liu, S. Huang, L. Guan, J. Li, N. Zhao, W. Wei, Y. Sun, Microporous Mesoporous Mater. 102 (2007) 304–309.

[50] T. S. Nguyen, S. He, G. Raman, K. Seshan, Chem. Eng. J. 299 (2016) 415–419.

[51] M. A. Isaacs, C. M. A. Parlett, N. Robinson, L. J. Durndell, J. C. Manayil, S. K. Beaumont, S. Jiang, N. S. Hondow, A. C. Lamb, D. Jampaiah, M. L. Johns, K. Wilson, A. F. Lee, Nat. Catal. 3 (2020) 921–931.

[52] H. Oji, Y. Taniguchi, S. Hirayama, H. Ofuchi, M. Takagaki, T. Honma, J. Synchrotron Radiat. 19 (**2012**) 54–59.

[53] Y. Wang, H. Gao, J. Phys. Chem. B 121 (2017) 2132–2141.

[54] C. M. Wang, K. N. Fan, Z. P. Liu, J. Am. Chem. Soc. 129 (2007) 2642–2647.

[55] X. Zhang, H. Wang, B. Q. Xu, J. Phys. Chem. B 109 (2005) 9678–9683.

[56] J. Li, J. Chen, W. Song, J. Liu, W. Shen, Appl. Catal. A Gen. 334 (2008) 321–329.

[57] P. M. De Souza, R. C. Rabelo-Neto, L. E. P. Borges, G. Jacobs, B. H. Davis, U. M. Graham, D. E. Resasco, F. B. Noronha, ACS Catal. 5 (2015) 7385–7398.

[58] C. D'Agostino, G. Brett, G. Divitini, C. Ducati, G. J. Hutchings, M. D. Mantle, L. F. Gladden, ACS Catal. 7 (2017) 4235–4241.

[59] S. Chen, L. Luo, Z. Jiang, W. Huang, ACS Catal. 5 (2015) 1653–1662.

[60] Z. Li, C. Zhu, H. Wang, Y. Liang, H. Xin, S. Li, X. Hu, C. Wang, Q. Zhang, Q. Liu, L. Ma, ACS Sustain. Chem. Eng. 9 (2021) 6355–6369.

[61] S. Zhu, Y. Xue, J. Guo, Y. Cen, J. Wang, W. Fan, ACS Catal. 6 (2016) 2035–2042.

[62] X. Zhang, H. Shi, B. Q. Xu, Catal. Today 122 (2007) 330–337.

[63] N. Liu, M. Xu, Y. Yang, S. Zhang, J. Zhang, W. Wang, L. Zheng, S. Hong, M. Wei, ACS Catal. 9 (2019) 2707–2717.

[64] A. M. Abdel-Mageed, A. Klyushin, A. Rezvani, A. Knop-Gericke, R. Schlögl, R. J. Behm, Angew. Chem. Int. Ed. 58 (2019) 10325–10329.

[65] H. Xie, J. Lu, M. Shekhar, J. W. Elam, W. N. Delgass, F. H. Ribeiro, E. Weitz, K. R. Poeppelmeier, ACS Catal. 3 (2013) 61–73.

[66] S. Ivanova, E. Zhecheva, R. Kukeva, D. Nihtianova, L. Mihaylov, G. Atanasova, R. Stoyanova, ACS Appl. Mater. Interfaces 8 (2016) 17321–17333.

[67] M. Khawaji, D. Chadwick, Catal. Today 334 (2019) 122–130.

[68] S. A. Kondrat, G. Shaw, S. J. Freakley, Q. He, J. Hampton, J. K. Edwards, P. J. Miedziak, T. E. Davies, A. F. Carley, S. H. Taylor, C. J. Kiely, G. J. Hutchings, Chem. Sci. 3 (2012) 2965–2971.

[69] J. Huang, W. L. Dai, K. Fan, J. Catal. 266 (2009) 228–235.

[70] J. Radnik, C. Mohr, P. Claus, Phys. Chem. Chem. Phys. 5 (2003) 172–177.

[71] B. Weng, K. Q. Lu, Z. Tang, H. M. Chen, Y. J. Xu, Nat. Commun. 9 (2018) 1543.

[72] X. Meng, Y. Zhang, Z. Li, H. Wang, S. Zhang, Ind. Eng. Chem. Res. 58 (2019) 8506–8516.

[73] M. Sterrer, M. Yulikov, E. Fischbach, M. Heyde, H. P. Rust, G. Pacchioni, T. Risse, H. J. Freund, Angew. Chem. Int. Ed. 45 (2006) 2630–2632.

[74] B. Yoon, H. Häkkinen, U. Landman, A. S. Wörz, J. M. Antonietti, S. Abbet, K. Judai, U. Heiz, Science 307 (2005) 403–407.

[75] T. Fujitani, I. Nakamura, A. Takahashi, ACS Catal. 10 (2020) 2517–2521.

[76] M. Kotobuki, R. Leppelt, D. A. Hansgen, D. Widmann, R. J. Behm, *J. Catal.* 264 (2009) 67–76.

[77] T. J. Brown, D. Weber, M. R. Gagné, R. A. Widenhoefer, J. Am. Chem. Soc. 134 (2012) 9134–9137.

[78] W. J. Ramsay, N. A. W. Bell, Y. Qing, H. Bayley, J. Am. Chem. Soc. 140 (2018) 17538–17546.

[79] K. Mori, Y. Futamura, S. Masuda, H. Kobayashi, H. Yamashita, Nat. Commun. 10 (2019) 1–10.

Chapter 6.
Effect of the structure of metal oxide support on the activity of supported Au nanoparticles in soft Lewis acid catalysis

6.1. Introduction

Supported Au catalysts were widely developed started from the 1980s by the revolutionary independent researches of Haruta and Hutchings[1,2]. It was discovered that small Au nanoparticles (NPs) supported by metal oxides (MO_x) showed great catalytic activity for the CO oxidation[3]. In addition, supported Au NPs with the size below 5 nm were obtained by coprecipitation or deposition-precipitation method[4,5], and such Au NPs can provide superior catalytic activities in various reactions. Thus, these discoveries triggered developments of supported Au NPs catalysts for many types of reactions such as the normal hydrogenation and oxidation reactions[6,7]. Small Au NPs could show not only the effect of the increased number of surface Au sites, but also the changed chemical properties of surface Au atoms. In addition, It was also reported that as the size of Au NPs, the continuous valence bands of the bulk metal begin to separate in a discrete state, similar to semiconductor oxides[8].

On the other hand, the catalytic activity of supported Au catalysts strongly depends on the kind of support [9]. Selecting a suitable support to stabilize the small NPs and to form an optimal contact structure between Au and the support is significant. For different reactions, the electronic state of the supported Au NPs can be regulated by adjusting the type of the support, thus to achieve the optimization of the reaction[10,11]. In addition, the structure like vacancies on the support also affect the catalytic activities [12,13]. Moreover, there is also a sabatier principle in the interaction between supported Au NPs and supports. Too strong of an interaction is demonstrated to trigger Ostwald ripening; however, too weak of an interaction stimulates particle migration and agglutination[14]. Furthermore, it was also reported that the catalytic activity of supported Au NPs could be regulated through changing the particle size of ZnO, and this was explained by an electronic modification of Au interface perimeter sites due to the electronic metal-support interactions (EMSIs)[15]. Meanwhile, the Au NP catalysts supported by ZrO_2 with large particle size or small specific surface area also showed better activity than that by ZrO_2 with small particle size or large specific surface area[16].

In recent decades, supported Au NPs have been developed as soft Lewis acid catalyst and discussed for the hydration, hydroamination, isomerization, and cyclization of alkynes or alkenes[17–21]. Au NPs supported by various metal oxides were discussed in these researches, and the effect of metal oxides was demonstrated significant. Since the specific surface area or the particle size of the metal oxide also affect the catalytic activities, we attempted to control the particle size or specific surface area of the metal oxides to improve the catalytic activity of the Au NPs supported by them.

Herein, we found a practical method for regulating and optimizing the activities of metal-oxide supported Au NP catalysts. Its effect was investigated in the multiple reactions based on the soft Lewis acid function of Au NPs. By comparing the relationship between specific surface areas and catalytic activities of the prepared metal-oxide supported Au NP catalysts, the catalysts with smaller specific surface area showed better catalytic activity. This tread was obtained in the soft Lewis acid reactions, including isomerization, cyclization, and hydroamination reactions. In addition, after increasing the Au load densities and comparing their catalytic efficiencies. There is no sufficient evidence to prove that the high activity of Au NPs supported by metal-oxides with low specific surface areas comes from the reduced mass transfer limitation. In addition, XPS spectra reveal that the Au NPs supported by the metal-oxides with low specific surface areas tend to have higher binding energy, revealing that more $Au^{\delta+}$ species should form on their surfaces.

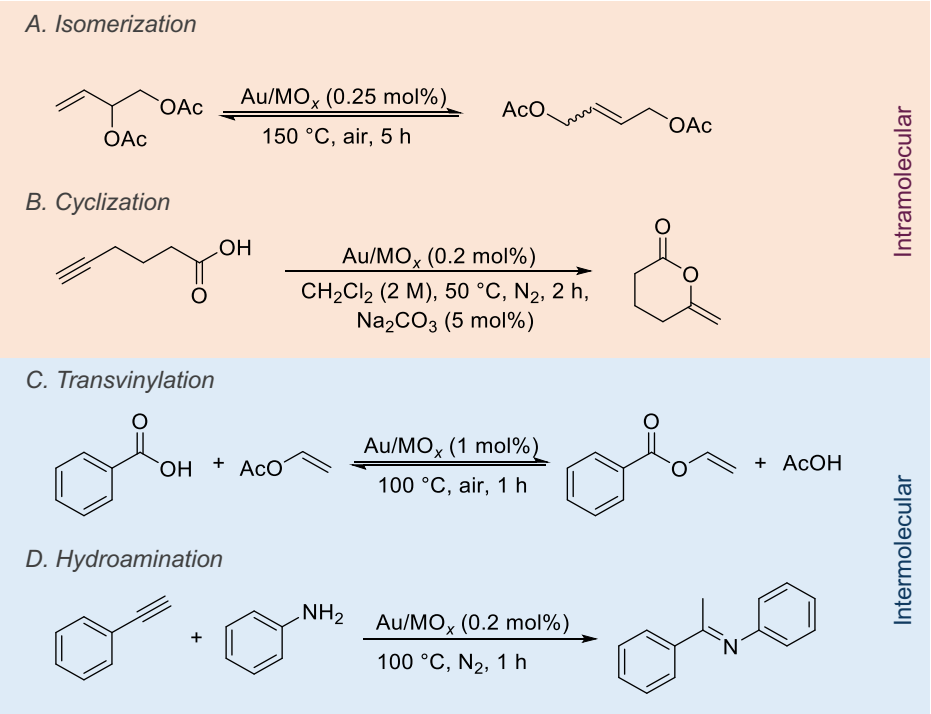

Figure 1. (a) Isomerization of allylic esters, (b) cyclization of alkynoic acid, (c) transvinylation of carboxylic acid, and (d) hydroamination of alkyne.

6.2. Experimental

6.2.1. Materials

$HAuCl_4 \cdot 4H_2O$ was purchased from Tanaka Precious Metals Co., Ltd. But-3-ene-1,2-diyl diacetate were purchased from Sigma Aldrich, Ltd., and but-2-ene-1,4-diyl diacetate was obtained from Mitsubishi Chemical Co., Ltd. 5-Hexynoic acid, aniline, benzoic acid, ethenyl acetate, were purchased from FUJIFILM Wako Pure Chemical Corp. Ethynylbenzene was purchased from Tokyo Chemical Industry Co., Ltd. 5-Hexynoic acid and aniline were purified by distillation before use, and the other reagents were used as received.

ZrO_2 (NND) was reference catalyst obtained from the Catalysis Society of Japan, and commercial ZrO_2 supports (SZ series) were purchased from Saint-Gobain Co., Ltd. CeO_2 (JRC-CEO-1) and CeO_2 (JRC-CEO-3) were obtained from the Catalysis Society of Japan. TiO_2 (JRC-TIO-17, P25) was obtained from the Catalysis Society of Japan, TiO_2 (STR-100N) was purchased from Sakai Chemical Industry Co., Ltd., and TiO_2 (ST-01) was purchased from Ishihara Sangyo Kaisha, Ltd. Al_2O_3 (JRC-ALO-9) and

Al_2O_3 (JRC-ALO-10) were reference catalyst obtained from the Catalysis Society of Japan, and Al_2O_3 (α-Al_2O_3) was purchased from FUJIFILM Wako Pure Chemical Corp.

6.2.2. Preparation of catalysts

Annealing treatment was used to controlling the crystallite sizes of the chose metal oxides, and thus changing their specific surface area. The temperature was raised at a rate of 15 °C min^{-1}, and the materials were then annealed at air atmosphere with the specified temperature for 3 hours.

Metal oxide supported Au NPs catalysts were prepared by deposition-precipitation method (DP) as reported[20]. Support (1g) was added to distilled water (50 mL) and keep stirring for 10 min. An aqueous solution (25 mL) with $(NH_4)_2CO_3$ (2.4 g) was prepared and added to the suspension. Then, the aqueous solution of $HAuCl_4 \cdot 4H_2O$ (3 mM, 50 mL) was dropped to it slowly within 30 min, and the mixture was stirred for 4 h. After filtration, the solid was washed with hot water (70 °C, 200 mL), and dried in air at 70 °C overnight. The calcination process was performed in air at 200 °C for 1 h and directly used for catalytic reactions without further treatment. All catalysts have a target Au loading of 3 wt%, unless otherwise specified. The bead catalysts were prepared by the same method from the bead supports without breaking into powders, and stirred using sealing mixer UZU.

6.2.3. Characterization

High-angle annular dark-field scanning transmission electron microscopy (HAADF-STEM) images were performed with a JEOL JEM-ARM200F operated at 200 kV. The loading amounts of prepared catalysts were detected by microwave plasma atomic emission spectrometry (MP-AES) on Agilent 4100 MP-AES. The crystalline structures of the catalysts were measured with Powder X-ray diffraction (PXRD) using a Rigaku MiniFlex600 equipped with a Cu K_α radiation source. The properties of the surface species were analyzed by X-ray photoelectron spectroscopy (XPS) using a Shimadzu-AXIS-165 spectrometer equipped with an Al K_α radiation source at pressure below 10^{-8} Pa. The obtained binding energies were calibrated to the C 1s peak at 284.8 eV. XPS profiles were further analyzed using XPSPEAK41 software. The specific surface areas were measured using an automatic adsorption instrument BELSORP-Max

(MicrotracBEL) and were calculated by the Brunauer–Emmet–Teller (BET) method. All samples were degassed at 100 °C for 3 h before measuring the adsorption isotherms of N_2 at –190 °C.

The results of the isomerization and transvinylation including the calculation of conversions and yields of the compounds were detected by gas chromatography (GC) using an Agilent GC 6850 Series II equipped with a flame ionization detector (FID) and a J&W HP-1 column. The yields of the products for the cyclization and hydroamination were determined by 1H NMR spectroscopy (JEOL JNM-ECS400 spectrometer).

6.2.4. General procedure for the catalytic isomerization reaction

A screw cap vial was charged with the prepared catalyst, substrate, and a magnetic stirring bar. Then the reaction mixture was stirred at 150 °C. The mixture was filtered after reaction, and the filtrate was analyzed by GC using tridecane as an internal standard.

6.2.5. General procedure for the catalytic cyclization reaction

A screw cap vial with a magnetic stirring bar was charged with the prepared catalyst and Na_2CO_3. Then, an anhydrous solvent and the alkynoic acid were added under N_2 flow. The reaction tube was sealed, and the mixture was stirred at 50 °C. After the reaction, the mixture was cooled to room temperature and centrifuged. The supernatant of the reaction mixture was analyzed by ^{1}H NMR spectroscopy after the addition of mesitylene as the internal standard.

6.2.6. General procedure for the catalytic hydroamination reaction

A screw cap vial with a magnetic stirring bar was charged with the prepared catalyst. Then, aniline and ethynylbenzene were added under N_2 flow. The reaction tube was sealed, and the mixture was stirred at 100 °C. After the reaction, the mixture was cooled to room temperature and centrifuged. The supernatant of the reaction mixture was analyzed by ^{1}H NMR spectroscopy after the addition of 1,3,5-trimethoxybenzene as the internal standard.

6.2.7. General procedure for the catalytic transvinylation reaction

Benzoic acid, vinyl acetate, catalyst, and a magnetic stirring bar were placed in a screw capp vial. The reaction was carried out in air at 100 °C with stirring. After the reaction, the reaction solution was analyzed by GC using tridecane as an internal standard.

6.2.8. Continuous flow reactions

Flow reaction for isomerization of but-2-ene-1,4-diyl diacetate was performed by a flow reactor (EYELA, Flow Factory, FFX-1000G). The stainless column (Φ10×50 mm) bed reactor was packed with catalyst and sea sand. The column was set vertically in a downward flow mode. The reaction mixture was collected and analyzed by GC using tridecane as an internal standard.

6.3. Results and Discussion

6.3.1. Study on the ZrO_2 support

In order to better understand the universality of the influence of supports on soft Lewis acid catalysis, commercial supports were used for preliminary discussion in this study. SZ31164 (monoclinic-ZrO_2) and NND (amorphous-ZrO_2) were annealed under different temperatures, and the changed on crystalline was analyzed by XRD (Fig. 2). Because the monoclinic is stable state for ZrO_2, only the increases in crystalline sizes were observed for SZ31164. Meanwhile, both changes in crystalline phases and sizes were observed for NND.

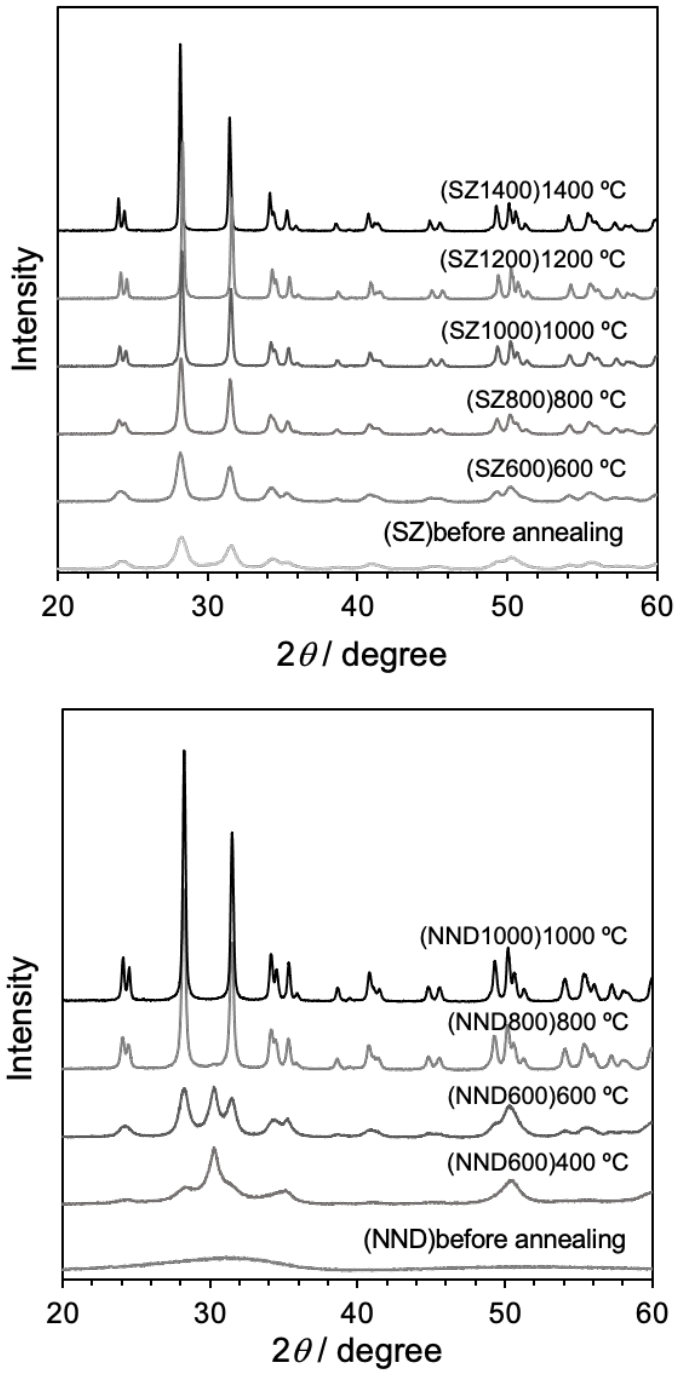

Figure 2. XRD pattern of ZrO_2 annealed at different temperature from (a) SZ31164 and (b) NND.

Due to the support might contain organic impurities, they will decompose at high temperature and affect the catalyst activity. Some commercial ZrO_2 supports with different crystalline phases and sizes were also used as reference in this research and analyzed by XRD (Fig. 3).

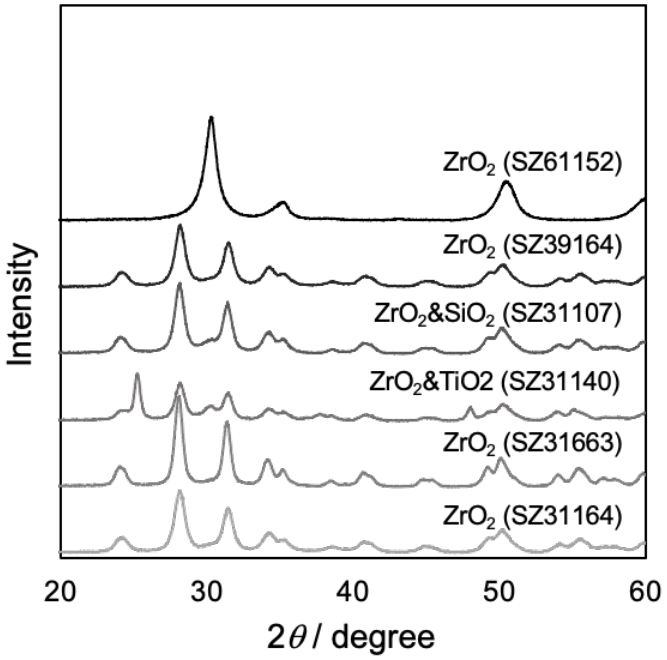

Figure 3. XRD pattern of SZ series supports.

The sizes of the supported Au NPs usually affect their catalytic activities. Therefore, while investigating the influence of other factors on the catalytic activity, it is necessary to prepare Au NPs of the same size as possible. HAADF-STEM was performed to compare the morphology and measure the average particle sizes of the supported Au NPs. For the catalysts prepared from the SZ31164 annealed at different temperatures, the average diameters of Au NPs prepared on the supports were around 2.5 nm except for the support annealed at 1400 °C (Fig. 4).

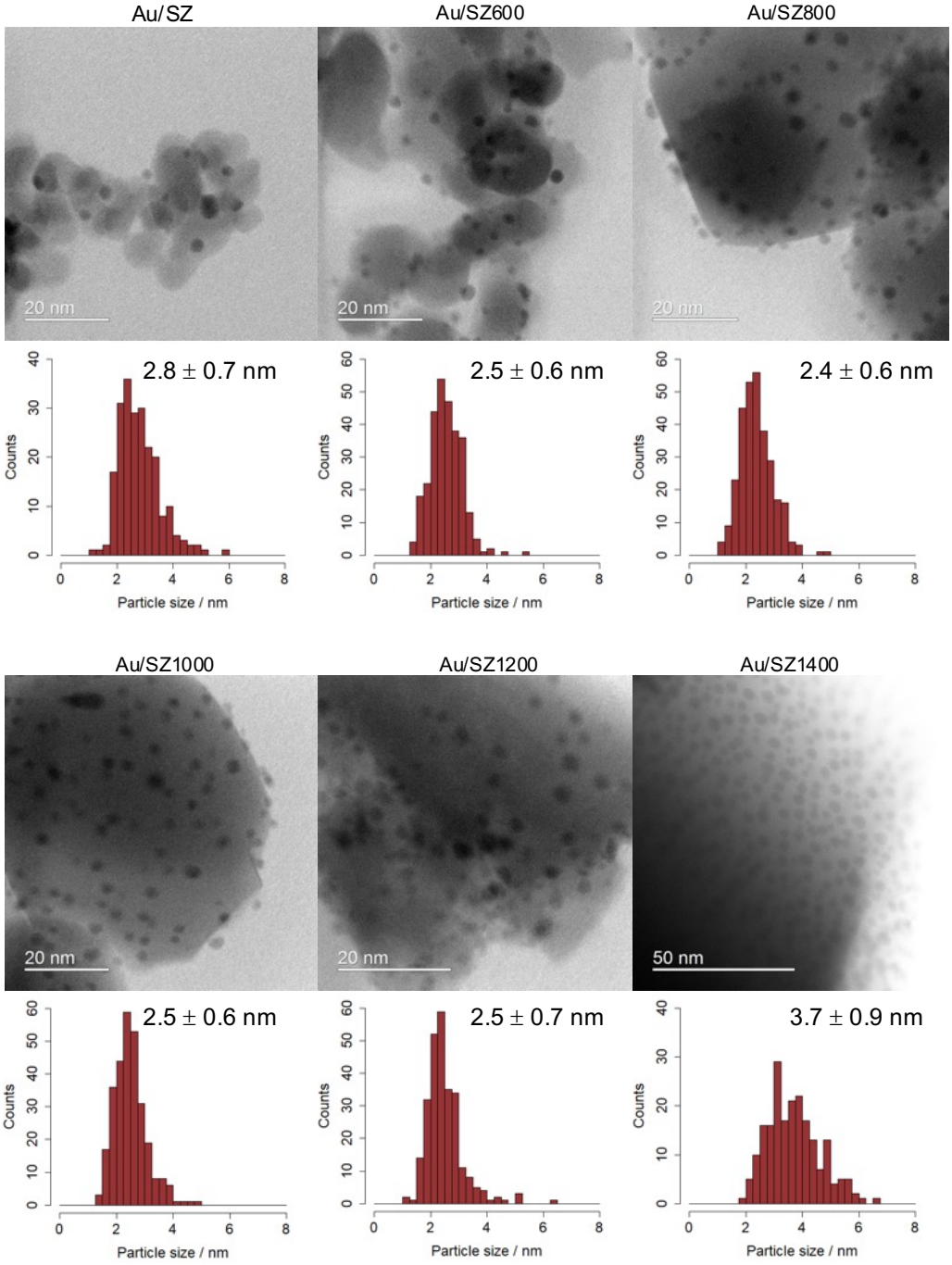

Figure 4. BF-STEM images and histogram of particle sizes of Au/ZrO_2 catalysts prepared from the SZ31164 with different annealing temperatures.

Additionally, morphology and the average particle sizes of Au/ZrO_2 catalysts prepared from NND with different annealing temperatures were also measured by HAADF-STEM (Fig. 5). Because the presence of Au NPs was not observed on the unannealed NND-supported gold catalyst, its average particle size was not counted. The average particle sizes of Au NPs on these catalysts were around 2.2 nm.

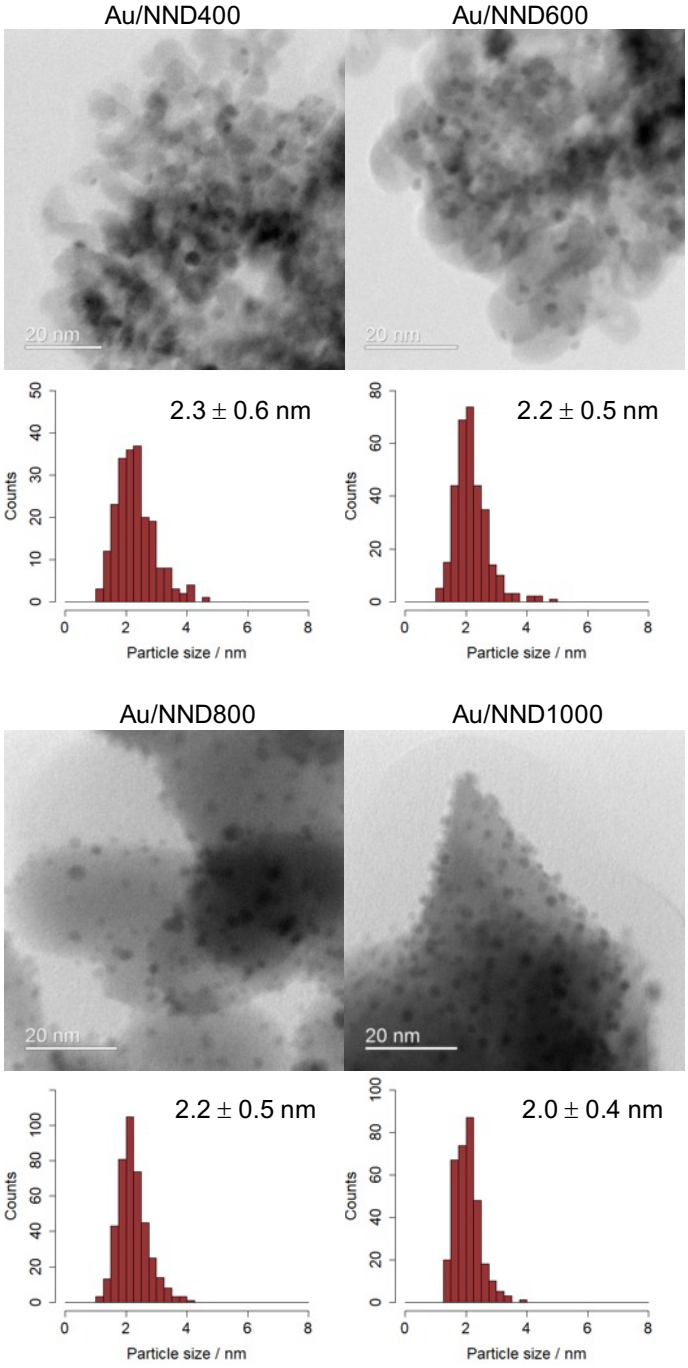

Figure 5. BF-STEM images and histogram of particle sizes of Au/ZrO_2 catalysts prepared from the NND with different annealing temperatures.

The average sizes for the gold nanoparticles of catalysts prepared from unannealed SZ series commercial supports were also measured by HAADF-STEM (Fig. 6). The sizes of the Au NPs on the pure ZrO_2 supports were still around 2.5 nm. However, the sizes of Au NPs on the metal oxide mixtures were increased greatly.

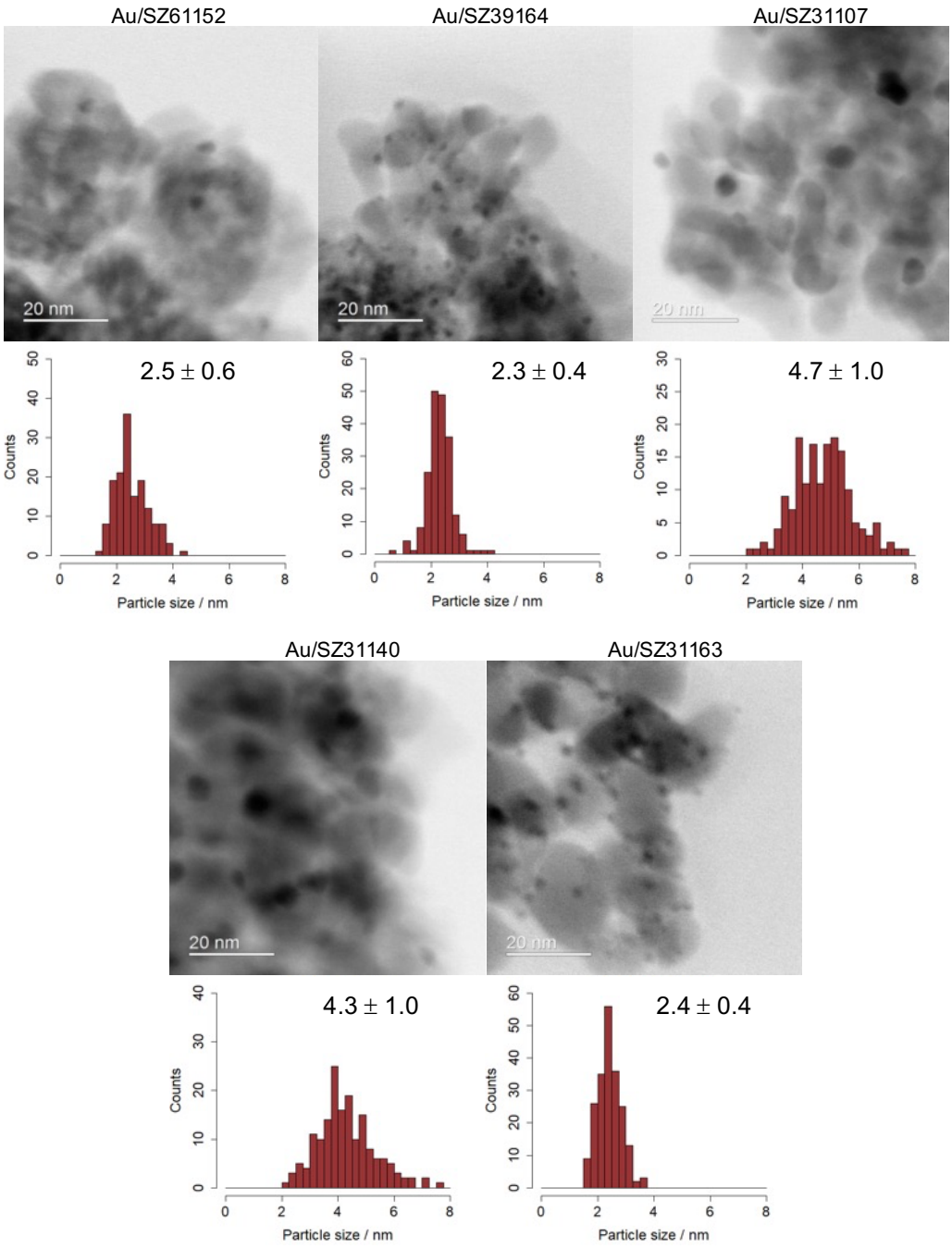

Figure 6. BF-STEM images and histogram of particle sizes of Au/ZrO_2 catalysts prepared from the SZ series supports.

Through the above discussion, a total of 16 Au/ZrO_2 catalysts with different support properties were prepared, and their Au loading amount, specific surface area, and average particle size were listed together (Table 1).

Table 1. Basic properties of Au/ZrO_2 catalysts.

Entry	Catalyst	Au loading amount[a]/wt%	S_{BET}[b]/$m^2\ g^{-1}$	Au NP size /nm
1	Au/SZ	2.5	94.3	2.8 ± 0.7
2	Au/SZ600	2.5	48.2	2.5 ± 0.6
3	Au/SZ800	2.5	20.1	2.4 ± 0.6
4	Au/SZ1000	2.6	10.8	2.5 ± 0.6
5	Au/SZ1200	2.1	2.2	2.5 ± 0.7
6	Au/SZ1400	1.0	0.9	3.7 ± 0.9
7	Au/NND	2.6	296.4	–
8	Au/NND400	2.5	150.6	2.3 ± 0.6
9	Au/NND600	2.6	73.8	2.2 ± 0.5
10	Au/NND800	2.0	11.9	2.2 ± 0.5
11	Au/NND1000	1.4	3.7	2.0 ± 0.4
12	Au/SZ61152	2.6	136.8	2.5 ± 0.6
13	Au/SZ39164	2.5	109.0	2.3 ± 0.4
14	Au/SZ31107	2.4	92.4	4.7 ± 1.0
15	Au/SZ31140	2.4	81.4	4.3 ± 1.0
16	Au/SZ31163	2.4	52.5	2.4 ± 0.4

[a] Determined by MP-AES. [b] Calculated by the images of HAADF-STEM.

To investigate the effects of these different supports on the activity of supported Au NPs in the soft Lewis acid catalyzed reaction, the intramolecular isomerization and cyclization reactions were used preferentially for evaluation. Initially, the catalytic activities of these catalysts were evaluated by the isomerization of 3,4-DABE (Table 2). It can be roughly observed from the reaction results that the annealing of the supports enhances the catalytic activity. Meanwhile, the catalytic activities of these catalysts were also evaluated by the cyclization of 5-hexynoic acid (Table 3), and a same trend was also be observed.

Table 2. Results of Au/ZrO_2 catalysts over the isomerization reaction of allylic esters.

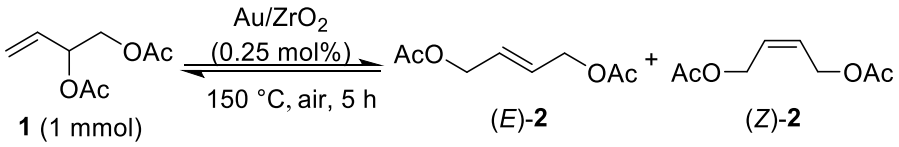

Entry	Catalyst	Conv.[a]/%	Yield(E)[a]/%	Yield(Z)[a]/%	TON
1	Au/SZ	37	33	2	140
2	Au/SZ600	51	45	3	192
3	Au/SZ800	55	47	4	204
4	Au/SZ1000	58	52	4	224
5	Au/SZ1200	58	51	4	220
6	Au/SZ1400	47	41	3	176
7	Au/NND	15	8	trace	32
8	Au/NND400	22	15	1	64
9	Au/NND600	43	37	3	160
10	Au/NND800	57	49	4	212
11	Au/NND1000	57	50	4	216
12	Au/SZ61152	29	22	1	92
13	Au/SZ39164	39	33	2	140
14	Au/SZ31107	22	18	1	76
15	Au/SZ31140	32	27	2	116
16	Au/SZ31163	48	43	3	184

[a] Determined by GC analysis using tridecane as an internal standard.

Table 3. Results of Au/ZrO_2 catalysts over the cyclization reaction of alkynoic acid.

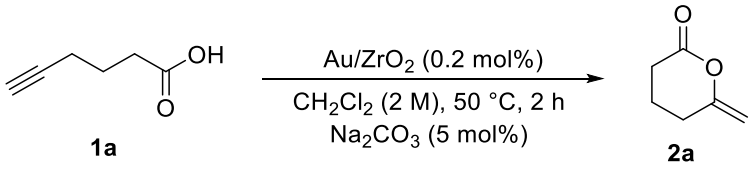

1a

1mmol

2a

Entry	Catalyst	Yield/%	TON
1	Au/SZ	29	145
2	Au/SZ600	64	320
3	Au/SZ800	75	375
4	Au/SZ1000	82	410
5	Au/SZ1200	72	360
6	Au/SZ1400	75	375
7	Au/NND	n.d.	–
8	Au/NND400	2	10
9	Au/NND600	30	150
10	Au/NND800	80	500
11	Au/NND1000	70	350
12	Au/SZ61152	4	20
13	Au/SZ39164	13	65
14	Au/SZ31107	34	170
15	Au/SZ31140	28	140
16	Au/SZ31163	42	210

[a] Determined by NMR analysis using mesitylene as an internal standard.

Afterwards, to better understand and investigate the above results, we conducted a further comparative study over the above data. The specific surface areas of the supports are large variables in the annealing treatment of the supports; therefore, the relationship between the specific surface area and the catalytic activities was mainly investigated here. In addition, because in the commercial supports of SZ series, SZ31107 and SZ31140 are mixtures of ZrO_2 and SiO_2 and TiO_2, respectively; the effect of metal oxide mixing of SZ series is preferentially discussed (Fig. 7).

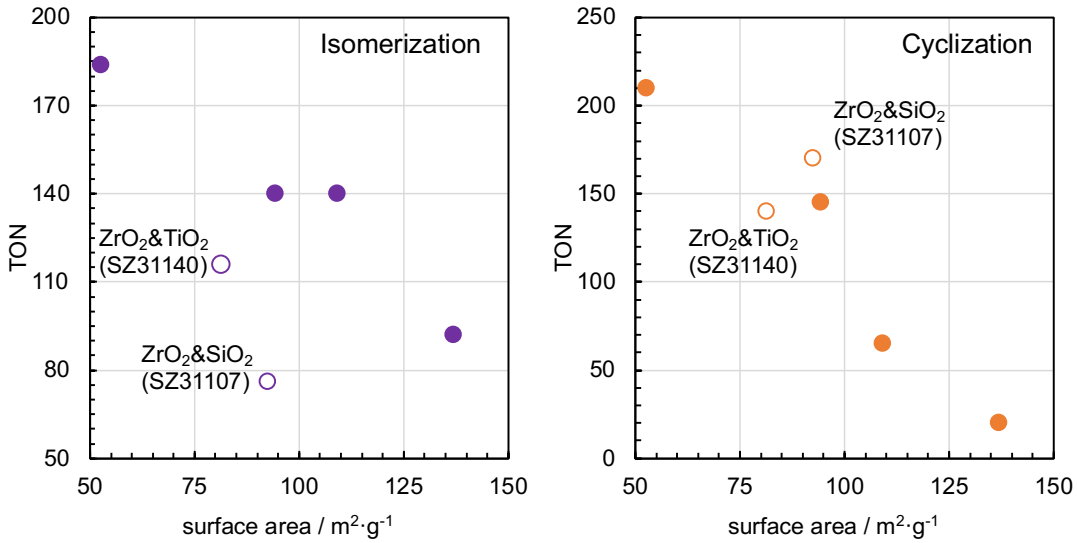

Figure 7. Relationship between TON and specific surface area of Au/ZrO_2 catalysts prepared from commercial SZ series.

Except for commercial supports containing TiO_2 or SiO_2 component, supported Au NPs catalysts prepared from these commercial supports of SZ series showed linear relationship between relationship between turnover number (TON) and specific surface area both in isomerization reaction and cyclization reaction. These results reveal that the catalytic activities of the supported gold nanoparticles prepared from the metal oxide supports with low specific surface area is higher than those of the catalysts prepared from the same kind of metal oxide supports with high specific surface area.

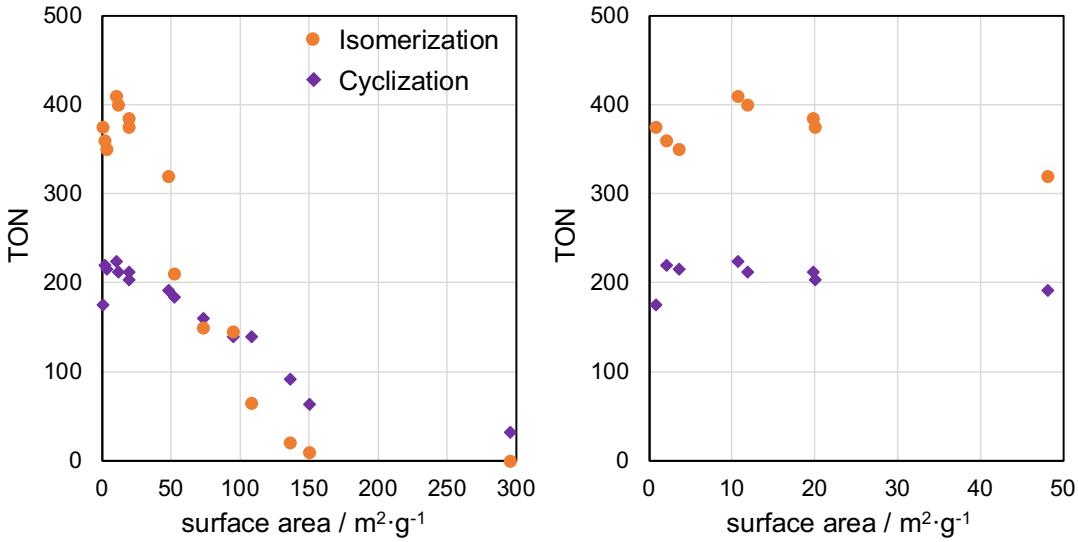

Figure 8. Relationship between TON and specific surface area of Au/ZrO_2 catalysts prepared from ZrO_2 supports.

In addition, all the samples except SZ31140 and SZ31107, which are not pure ZrO_2, were analyzed for the relationship between specific surface area and TON (Fig. 8). The trend observed in catalysts prepared from SZ series support was observed in all the supported Au NPs catalysts prepared from ZrO_2 discussed in this research. However, this trend stagnated when the specific surface area was low (below 10 m^2/g), which may be due to the Au NPs tended to agglutinate when the loading density is high, thus affecting the catalytic activity.

Considering that the reduced specific surface is conducive to reducing the mass transfer limitation, Au/ZrO_2 catalysts with Au loading amount were evaluated (Fig. 9). The changes in yield were observed in the isomerization reaction, but not occurred in the cyclic reaction. Therefore, the phenomenon discussed here seems to be independent of the mass transfer limitation, and changes in isomerization reaction should be due to the changes in stirring efficiencies under neat condition.

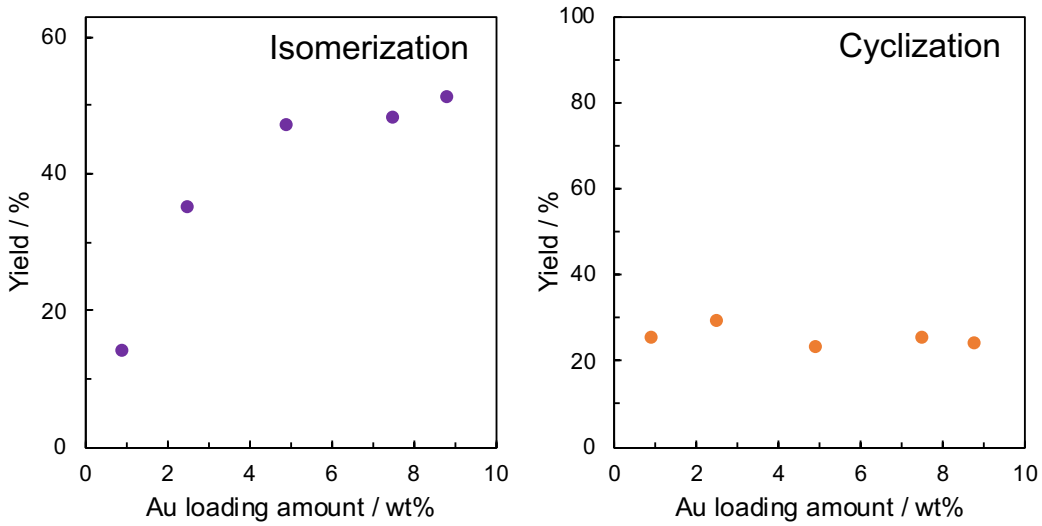

Figure 9. Discussion on mass transfer limitation in isomerization and cyclization reaction. (Isomerization: Au 0.25 mol%; Cyclization: Au 0.20 mol%)

6.3.2. Study on the multiple metal oxide supports and reactions

Because enhanced catalytic activities have been obtained by controlling the specific surface area of the ZrO_2 support, and CeO_2, Al_2O_3, and TiO_2 were normal metal oxide supports for the supported Au catalysts, the effect of support structure was also investigated among the Au/CeO_2, Au/Al_2O_3, and Au/TiO_2. In addition, hydroamination

and transvinylation were used to evaluate the catalytic activities of these catalysts as well as the isomerization and cyclization.

Four kinds of oxides were annealed at different temperatures to change their morphologies and structures, and a total of sixteen different supports samples were obtained. Then, all of them are prepared as supported Au NP catalysts under the same condition (Table 4).

Table 4. Number of the discussed catalysts and the detailed information about the corresponding metal oxide supports.

Entry	Catalyst	Support	Annealing temperature/°C
1	Au/ZrO_2-1	NND	400
2	Au/ZrO_2-2	SZ31164	–
3	Au/ZrO_2-3	SZ31164	600
4	Au/ZrO_2-4	SZ31164	1000
5	Au/CeO_2-1	JRC-CEO-1	–
6	Au/CeO_2-2	JRC-CEO-3	–
7	Au/CeO_2-3	JRC-CEO-3	1000
8	Au/CeO_2-4	JRC-CEO-3	1200
9	Au/TiO_2-1	ST-01	–
10	Au/TiO_2-2	STR-100N	–
11	Au/TiO_2-3	P25	–
12	Au/TiO_2-4	STR-100N	1000
13	Au/Al_2O_3-1	JRC-ALO-9	–
14	Au/Al_2O_3-2	JRC-ALO-9	1000
15	Au/Al_2O_3-3	JRC-ALO-10	–
16	Au/Al_2O_3-4	Wako (015-13001)	–

Afterwards, XRD pattern of these catalysts was collect and compared in the group of same metal oxide (Fig. 10). Changes in crystal structures were observed in the metal oxides, except the CeO_2. In addition, the high-temperature crystalline phases could keep

relatively stable structures, and their narrow FWHM indicated their larger crystalline sizes.

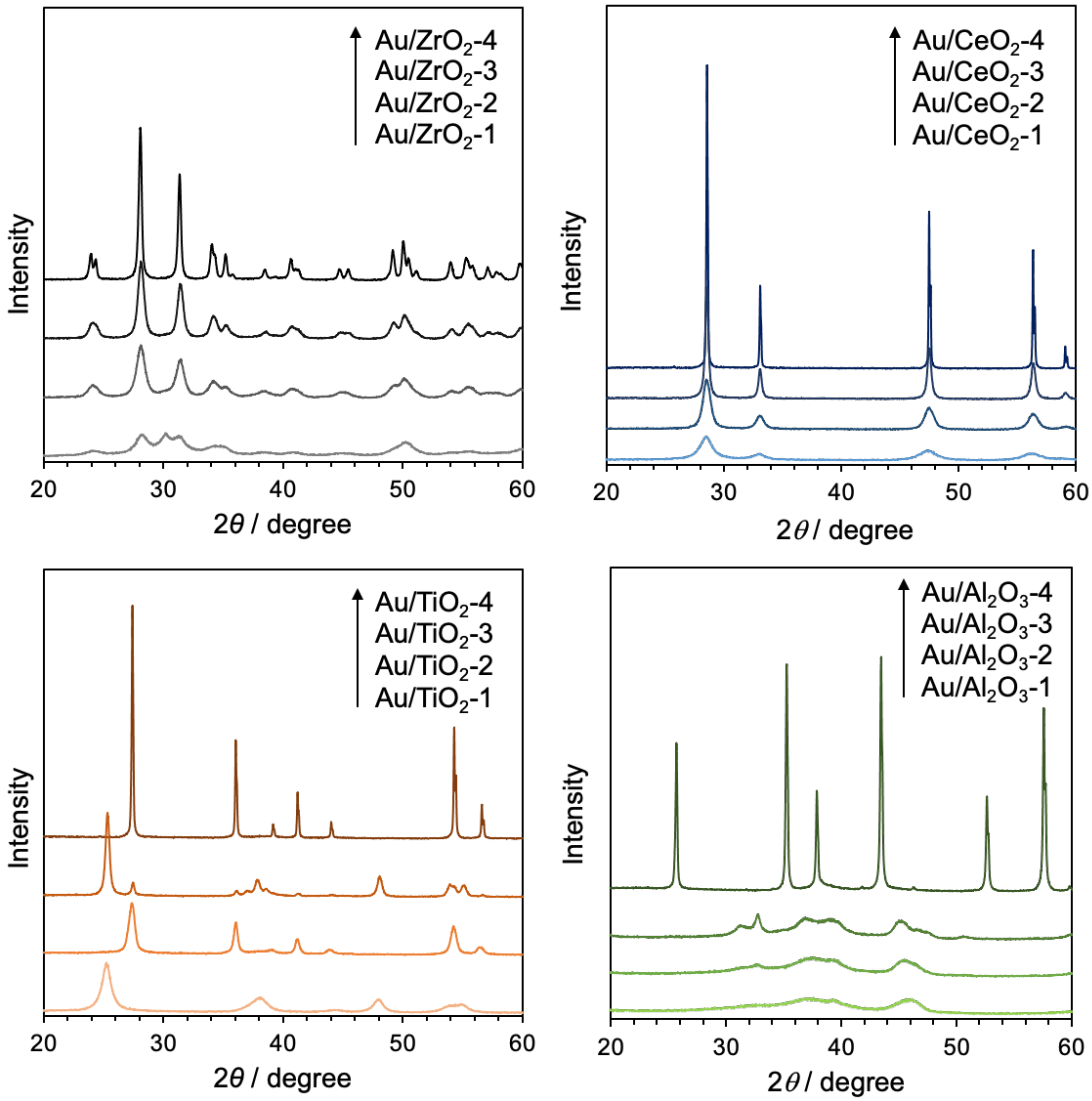

Figure 10. XRD pattern of the Au/MO_x catalysts list in table 4.

The uniform distribution and the small Au NPs can be demonstrated by XRD by detecting whether there is an obvious peak at around 38.4° attributed to Au 111. No distinct peaks from Au NPs were obtained in Au/CeO_2. However, there are serious interference of other peaks in the spectra of Au/ZrO_2, Au/TiO_2, and Au/Al_2O_3. Therefore, HAADF-STEM measurement was performed to confirm whether the average particle sizes are small and similar (Fig. 11–13). The results showed that similar Au NPs could be well prepared on metal oxides with various morphologies.

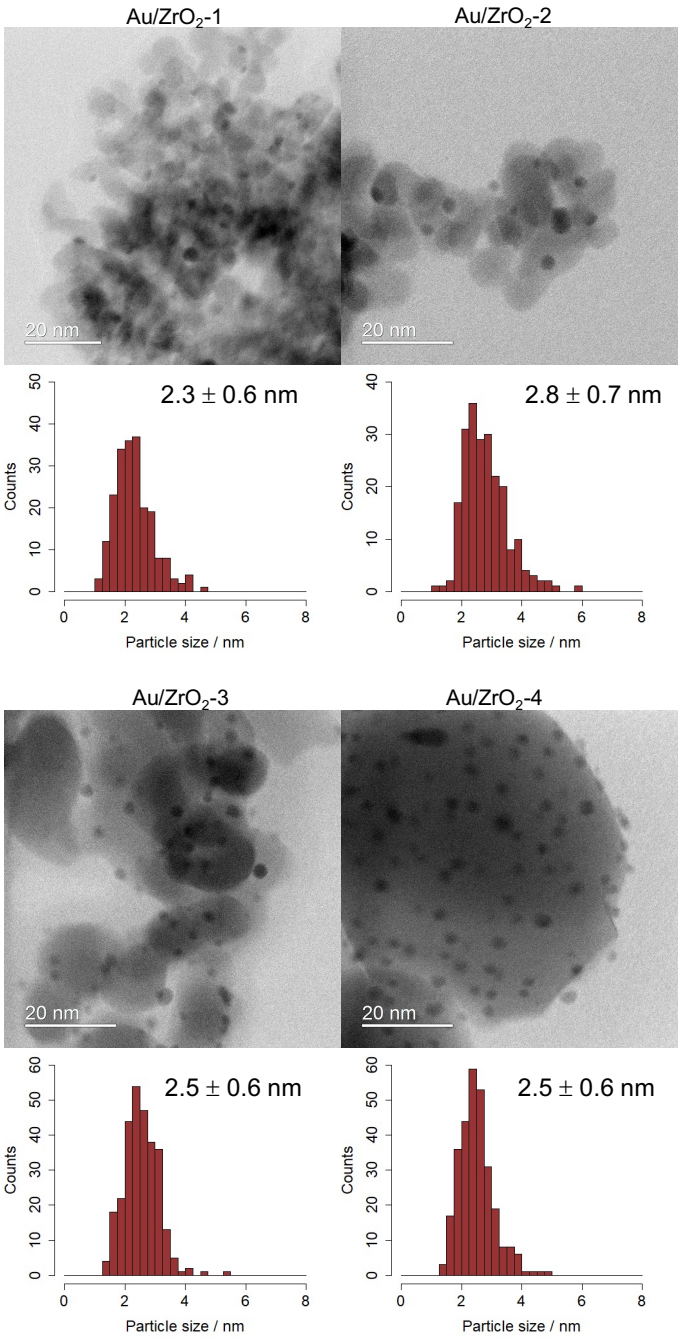

Figure 11. BF-STEM images and histogram of particle sizes of Au/ZrO_2-n catalysts.

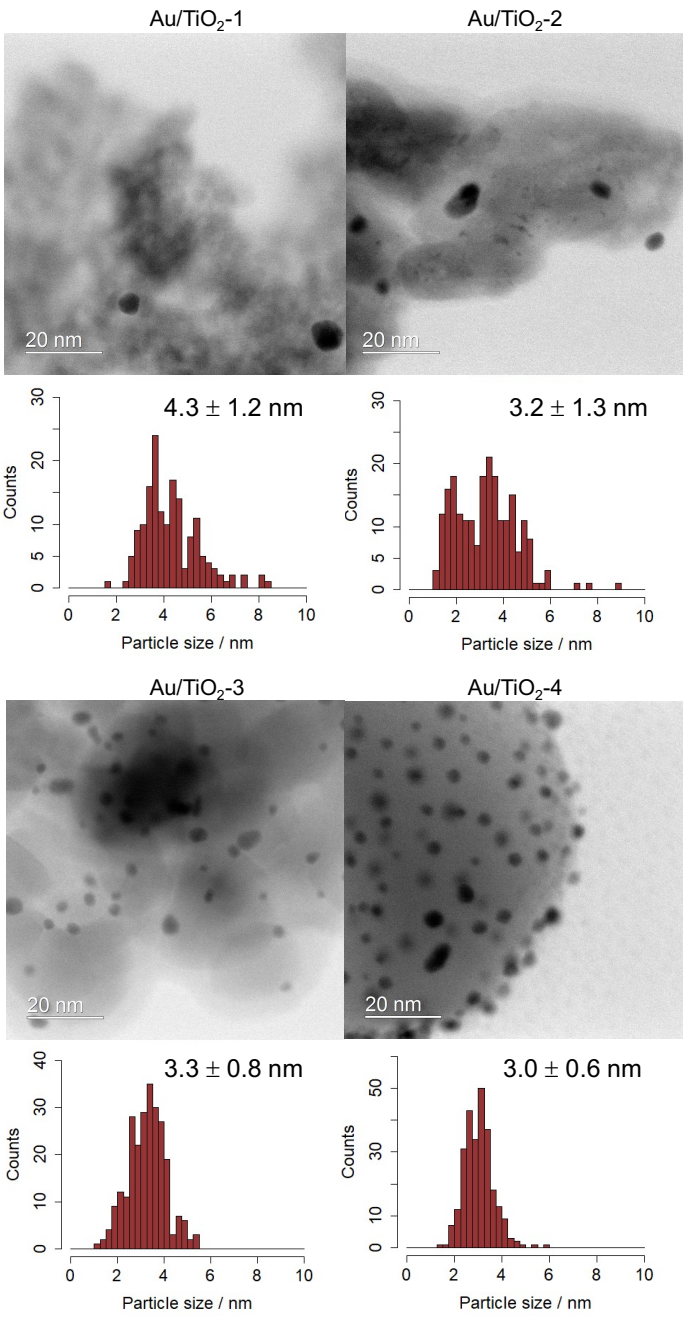

Figure 12. BF-STEM images and histogram of particle sizes of Au/TiO_2-n catalysts.

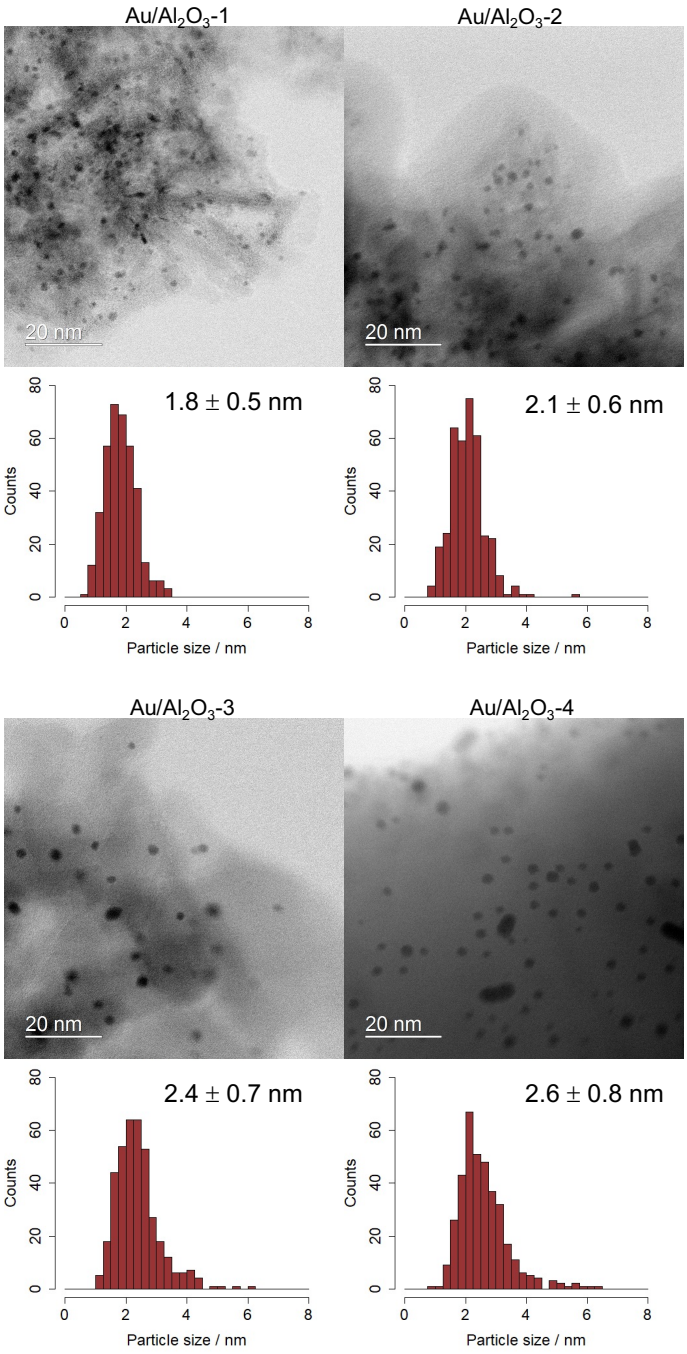

Figure 13. BF-STEM images and histogram of particle sizes of Au/Al_2O_3-n catalysts.

Au loading amounts of discussed Au/MO_x catalysts were determined using MP-AES, and their specific surface areas were measured by BET method. Basic properties of the Au/MO_x with a total of sixteen different supports were concluded and listed together (Table 5). The specific surface areas of the catalysts were mainly in the range of 3–220 m^2/g.

Table 5. Basic properties of discussed Au/MO_x catalysts.

Entry	Catalyst	Au loading amount[a]/wt%	S_{BET}[b]/m^2 g^{-1}	Au NP size[b]/nm
1	Au/ZrO_2-1	2.5	150.6	2.3 ± 0.6
2	Au/ZrO_2-2	2.5	94.3	2.8 ± 0.7
3	Au/ZrO_2-3	2.5	48.2	2.5 ± 0.6
4	Au/ZrO_2-4	2.1	10.8	2.5 ± 0.6
5	Au/CeO_2-1	2.6	149.2	< 5[c]
6	Au/CeO_2-2	2.8	70.8	< 5[c]
7	Au/CeO_2-3	2.2	27.6	< 5[c]
8	Au/CeO_2-4	1.0	3.2	< 5[c]
9	Au/TiO_2-1	2.7	213.6	4.3 ± 1.2
10	Au/TiO_2-2	2.1	79.8	3.2 ± 1.3
11	Au/TiO_2-3	2.5	49.9	3.3 ± 0.8
12	Au/TiO_2-4	1.4	5.4	3.0 ± 0.6
13	Au/Al_2O_3-1	2.5	203.6	1.8 ± 0.5
14	Au/Al_2O_3-2	2.6	155.6	2.1 ± 0.6
15	Au/Al_2O_3-3	2.3	109.9	2.4 ± 0.7
16	Au/Al_2O_3-4	1.4	4.6	2.6 ± 0.8

[a] Determined by MP-AES. [b] Calculated by the images of HAADF-STEM. [c] Estimated by XRD.

Initially, isomerization of 3,4-DABE was used to evaluate the catalytic activities of the prepared Au/MO_x (Table 6). For the catalysts prepared from different metal oxides, the Au NPs supported by metal oxides in high-temperature crystalline phases or with low specific areas provided higher TONs than those of the metal oxides in low-temperature crystalline phases or with large specific areas. High TONs could be obtained if the supported Au NP catalysts were prepared using metal oxides with specific surface areas below 10 m^2/g.

Table 6. Results of Au/MO_x catalysts over the isomerization reaction of allylic esters.

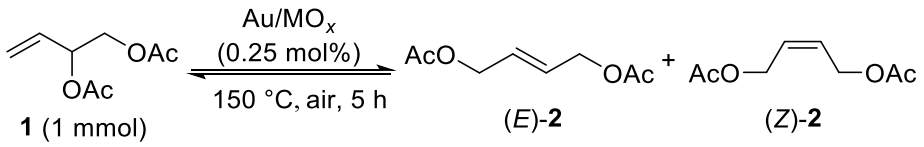

Entry	Catalyst	Conv.[a]/%	Yield(E)[a]/%	Yield(Z)[a]/%	TON
1	Au/ZrO_2-1	22	15	1	64
2	Au/ZrO_2-2	37	33	3	140
3	Au/ZrO_2-3	51	45	3	192
4	Au/ZrO_2-4	58	52	4	224
5	Au/CeO_2-1	7	1	trace	4
6	Au/CeO_2-2	18	12	1	52
7	Au/CeO_2-3	34	28	2	120
8	Au/CeO_2-4	47	41	3	176
9	Au/TiO_2-1	9	3	trace	12
10	Au/TiO_2-2	18	13	1	56
11	Au/TiO_2-3	35	29	2	124
12	Au/TiO_2-4	52	45	3	192
13	Au/Al_2O_3-1	24	12	trace	48
14	Au/Al_2O_3-2	36	24	1	100
15	Au/Al_2O_3-3	38	33	2	140
16	Au/Al_2O_3-4	55	47	4	204

[a] Determined by GC analysis using tridecane as an internal standard.

Cyclization of 5-hexynoic acid was also used to evaluate the catalytic activities (Table 7). Except the reaction with Au/CeO_2 catalysts, the trend of increasing catalytic activity with decreasing specific surface area of the supports was also observed. The reaction with Au/CeO_2 was found to proceed only by the catalysts with the lowest specific surface area (Au/CeO_2-4).

Table 7. Results of Au/MO_x catalysts over the cyclization reaction of alkynoic acid.

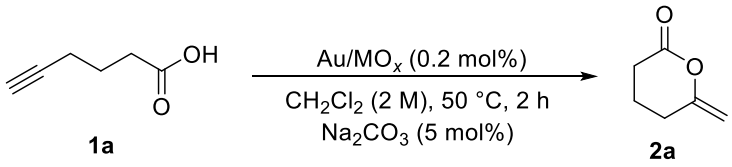

1a
1mmol

2a

Entry	Catalyst	Yield/%	TON
1	Au/ZrO_2-1	2	10
2	Au/ZrO_2-2	29	145
3	Au/ZrO_2-3	64	320
4	Au/ZrO_2-4	82	410
5	Au/CeO_2-1	n.d.	-
6	Au/CeO_2-2	trace	-
7	Au/CeO_2-3	trace	-
8	Au/CeO_2-4	41	205
9	Au/TiO_2-1	15	75
10	Au/TiO_2-2	33	165
11	Au/TiO_2-3	72	360
12	Au/TiO_2-4	89	445
13	Au/Al_2O_3-1	3	15
14	Au/Al_2O_3-2	5	25
15	Au/Al_2O_3-3	16	80
16	Au/Al_2O_3-4	60	300

[a] Determined by NMR analysis using mesitylene as an internal standard.

Reaction tests of hydroamination of ethynylbenzene and aniline were also performed to investigate the phenomenon in intermolecular reaction (Table 8). Great trend was observed when using the Au/ZrO_2 and Au/TiO_2 catalysts. In addition, in the reaction with Au/CeO_2 and Au/Al_2O_3 catalysts, sharp increase in catalytic activity occurred using the catalysts with the lowest specific surface areas, and only low

catalytic activities could be obtained using the catalysts with relatively large specific surface areas.

Table 8. Results of Au/MO_x catalysts over the hydroamination reaction.

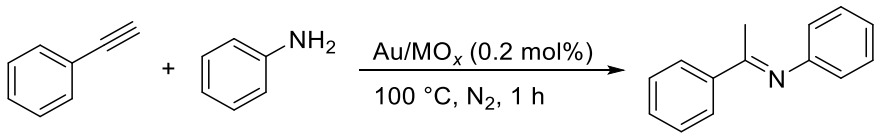

Entry	Catalyst	Yield/%	TON
1	Au/ZrO_2-1	n.d.	–
2	Au/ZrO_2-2	4	20
3	Au/ZrO_2-3	46	230
4	Au/ZrO_2-4	56	280
5	Au/CeO_2-1	1	5
6	Au/CeO_2-2	1	5
7	Au/CeO_2-3	1	5
8	Au/CeO_2-4	12	60
9	Au/TiO_2-1	14	75
10	Au/TiO_2-2	33	165
11	Au/TiO_2-3	60	300
12	Au/TiO_2-4	66	330
13	Au/Al_2O_3-1	7	35
14	Au/Al_2O_3-2	4	20
15	Au/Al_2O_3-3	3	15
16	Au/Al_2O_3-4	54	270

[a] Determined by NMR analysis using trimethoxybenzene as an internal standard.

Moreover, transvinylation of benzoic acid and ethenyl acetate was conducted using these catalysts as another example of intermolecular reaction (Table 8). Unlike the reactions described above, no clear relationship between the specific surface area and the catalytic activity of the catalyst could be observed.

Table 8. Results of Au/MO_x catalysts over the transvinylation reaction.

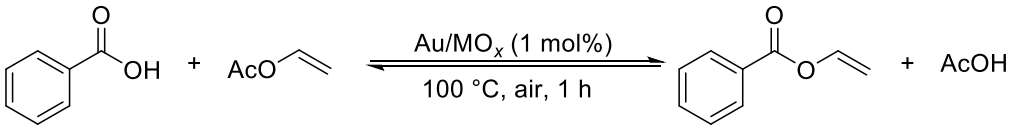

0.5 mmol 1 mL

Entry	Catalyst	Conv.[a]/%	Yield[a]/%	TON
1	Au/ZrO_2-1	23	14	14
2	Au/ZrO_2-2	32	24	24
3	Au/ZrO_2-3	63	56	56
4	Au/ZrO_2-4	56	47	47
5	Au/CeO_2-1	16	7	7
6	Au/CeO_2-2	67	63	63
7	Au/CeO_2-3	62	54	54
8	Au/CeO_2-4	45	37	37
9	Au/TiO_2-1	10	3	3
10	Au/TiO_2-2	27	20	20
11	Au/TiO_2-3	16	8	8
12	Au/TiO_2-4	15	8	8
13	Au/Al_2O_3-1	59	37	27
14	Au/Al_2O_3-2	19	10	10
15	Au/Al_2O_3-3	13	6	6
16	Au/Al_2O_3-4	8	trace	–

[a] Determined by GC analysis using tridecane as an internal standard.

Furthermore, the results of the above four reactions and the relationships between their TONs and specific surface areas are summarized (Fig. 14). It is easy to find that the catalysts with low specific surface area show superior catalytic activities in isomerization reaction, cyclization reaction, and hydroamination reaction. Therefore, the catalyst supported Au NP catalysts supported by metal oxides with low specific surface areas seems to have better catalytic efficiency in gold atoms. However, the

reason for the different results in transvinylation reaction is still unclear, and it should be further discussed.

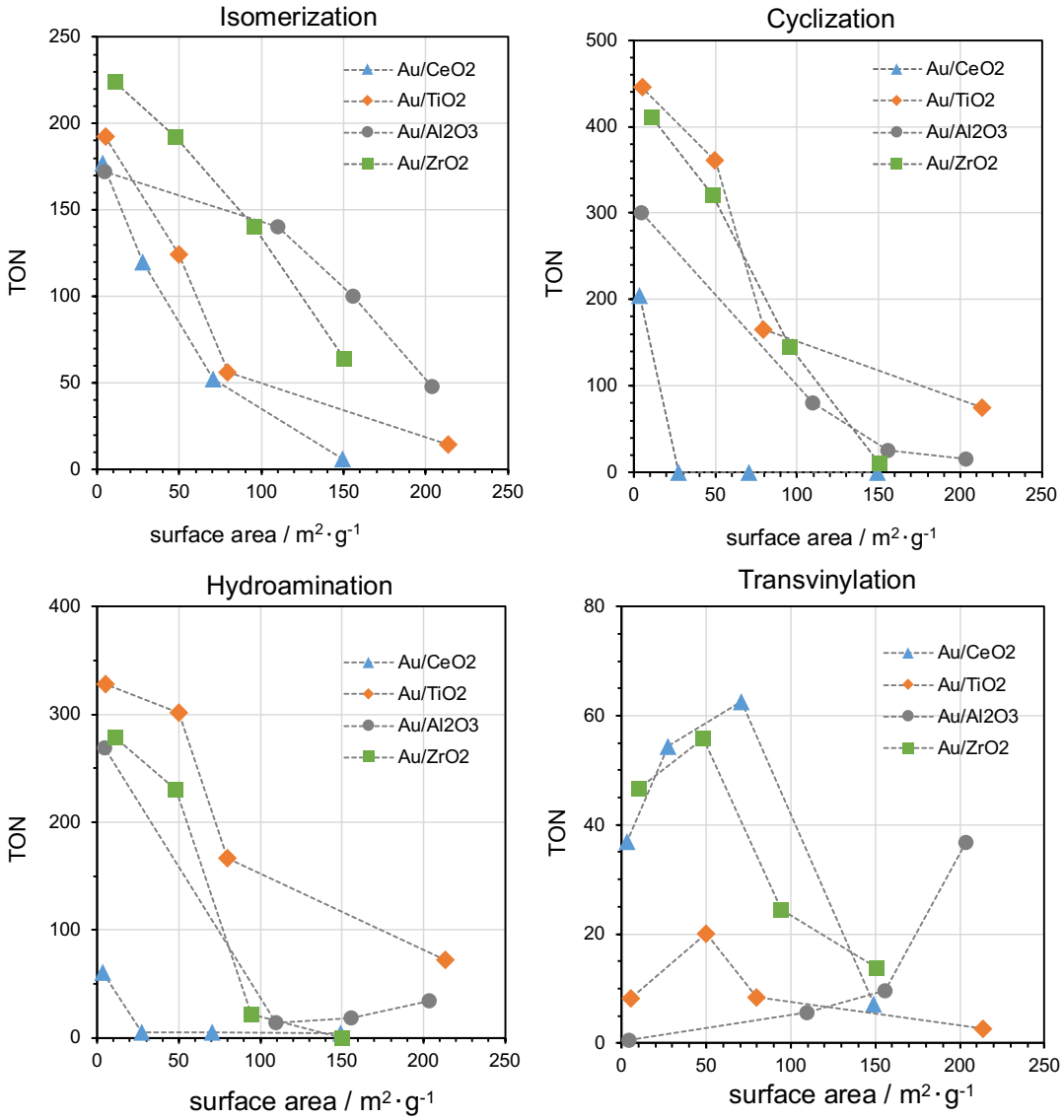

Figure 14. Summary of the reaction results of Au/MO_x catalysts in isomerization, cyclization, hydroamination, and transvinylation.

6.3.4. Characterizations of the prepared Au/MO_x catalysts.

To understand the reasons for the results obtained above, characterizations, such as N_2 adsorption/desorption and XPS spectra were performed over the prepared catalyst. Compared with the pore size distributions of the catalysts with relatively low activities, almost no pores could be observed on the catalysts with good catalytic activity (Fig. 15). Therefore, unlike the phenomenon in most catalytic reactions, the abundance of

pores brought negative effects in soft Lewis acid reactions using supported Au NP catalysts.

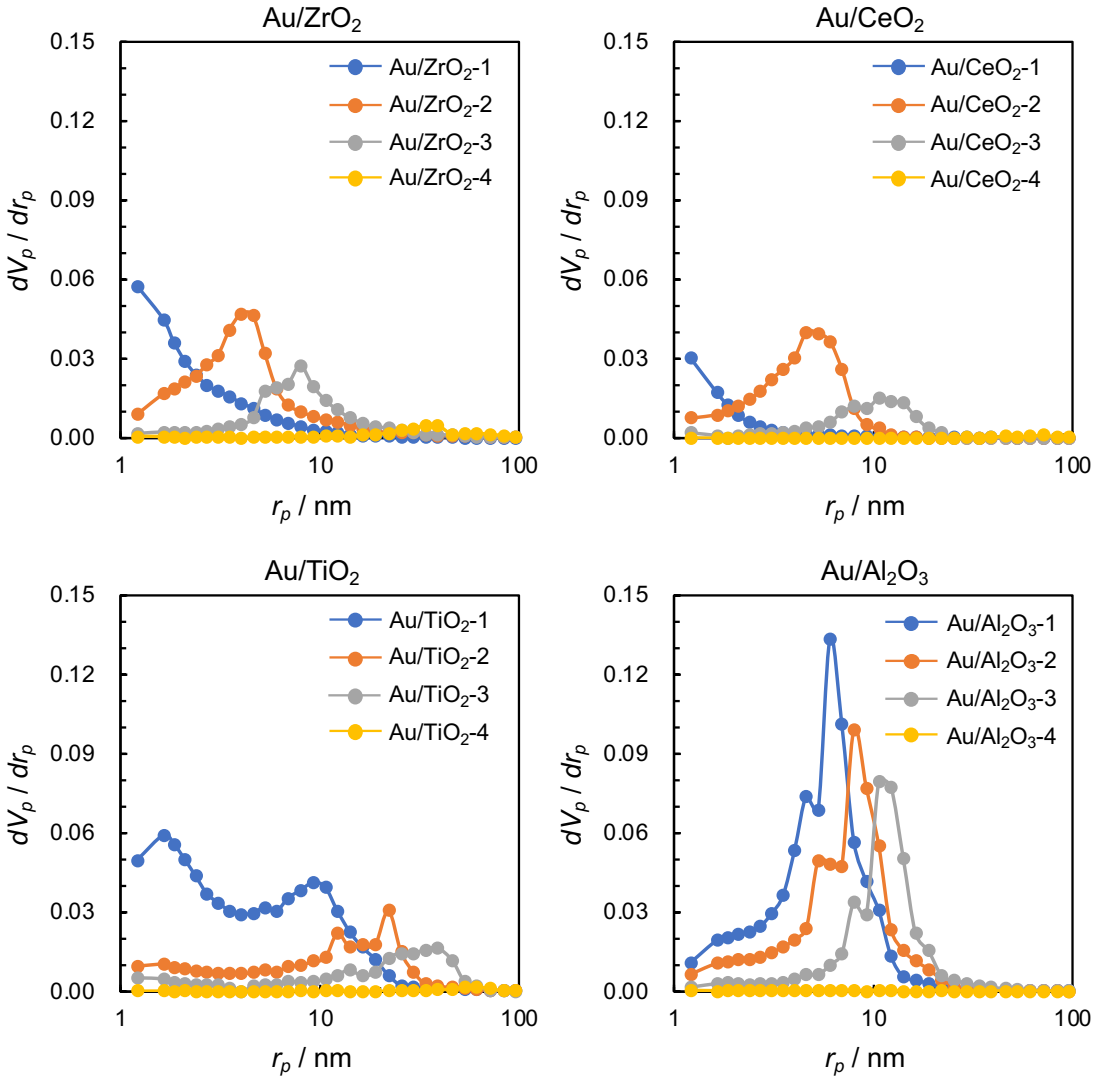

Figure 15. Pore size distributions of the prepared Au/MO_x catalysts.

In addition, the electron states of the prepared Au/MO_x catalysts were collected and analyzed by XPS measurement (Fig. 16). In the Au 4f XPS spectra, the catalysts prepared by the supports with small specific surface areas showed a higher binding energy. To some extent, the metal-oxide supports in high-temperature crystalline phases with low specific surface areas should bring a positive charging effect on the supported Au NPs, and thus enhance the soft Lewis acidity.

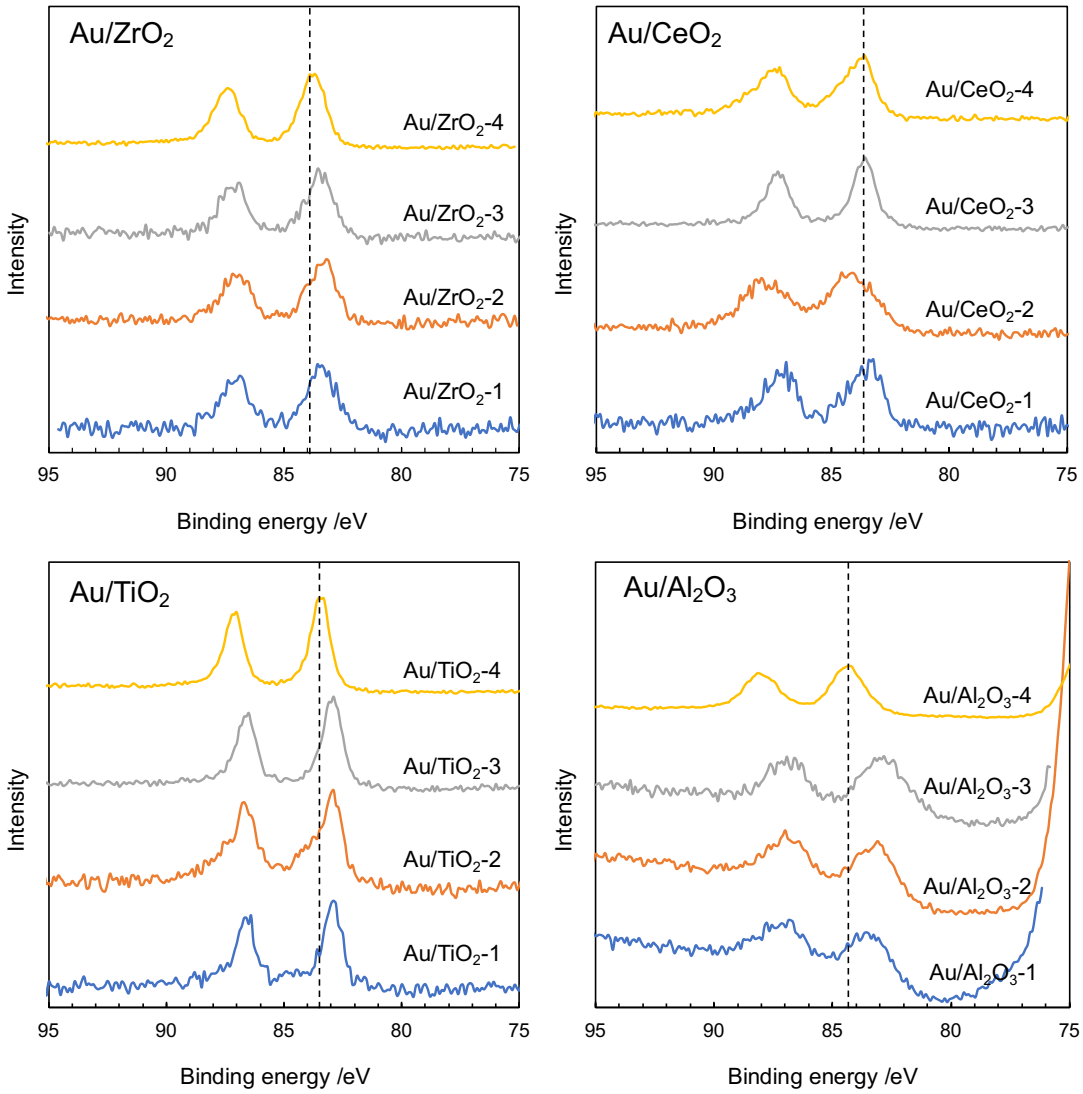

Figure 16. Au 4f XPS spectra of the prepared Au/MO_x catalysts.

6.3.4. Application in preparing industrial catalysts

Isomerization of 3,4-DABE is a practical reaction in chemical industry and developing industrial catalysts for this reaction is significant. Normally, the industrial catalysts are usually prepared using the supported in the shape of bead. Based on the above findings, if the catalytic activity can be improved through the annealing treatment of metal-oxide supports, it will bring pratical value for the performance-enhancement of industrial catalysts. Thus, we discussed the annealing effect on the bead support of ZrO_2 and evaluated the catalytic activities in isomerization reaction using the prepared Au/ZrO_2 (bead) (Table 9). Enhancements in the activities were achieved through the

annealing treatments of supports, and a superior result was obtained when the annealing temperature was 1000 °C (entry 4).

Table 9. Results of Au/ZrO_2 catalysts (bead) over the isomerization reaction of allylic esters.

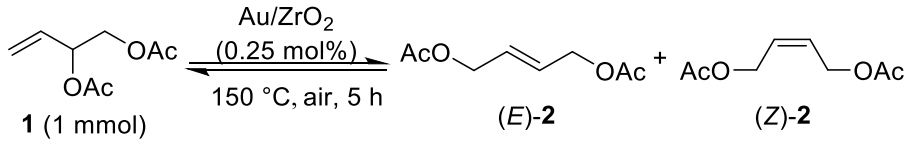

Entry	Catalyst[a]	Conv.[b]/%	Yield(E)[b]/%	Yield(Z)[b]/%
1	2.1 wt% Au/SZ (bead)	28	25	1
2	1.9 wt% Au/SZ600 (bead)	46	39	3
3	1.6 wt% Au/SZ800 (bead)	50	44	4
4	1.1 wt% Au/SZ1000 (bead)	53	45	5
5	0.5 wt% Au/SZ1200 (bead)	46	39	4

[a] Support: SZ31164 in the shape of bead; target Au loading amount: 3wt%. [b] Determined by GC analysis using tridecane as an internal standard.

Furthermore, to evaluate the stability of the prepared catalysts, a continuous reaction test based on a laboratory fixed-bed flow reactor was conducted (Fig. 17). A 4-cycle test with different reaction conditions was executed in 7 days, obtaining a total TON more than 8000. In addition, no significant decrease in yield was confirmed during each cycle.

Additionally, the morphology and particle sizes of the recycled catalysts were analyzed using the fresh catalysts as a reference (Fig. 18). The average particle diameter increased from 3.1 nm to 3.2 nm after the 7-day flow reaction. This result should provide an effective method for enhancing the performance of supported Au catalysts.

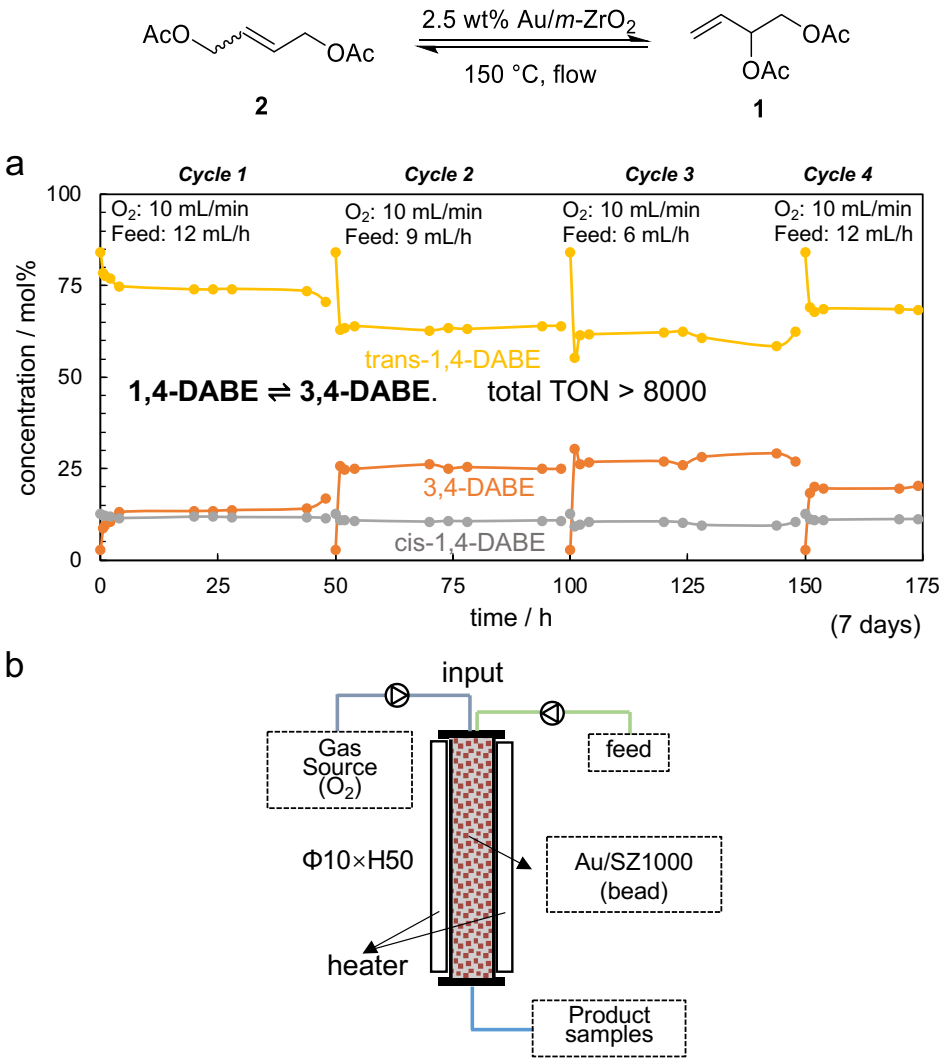

Figure 17. Evaluation the stability of the Au/ZrO_2 (bead) using the continuous-flow reactor. (a) result of flow reaction for 4 cycles in 7 days. (b) Illustration of continuous-flow reaction.

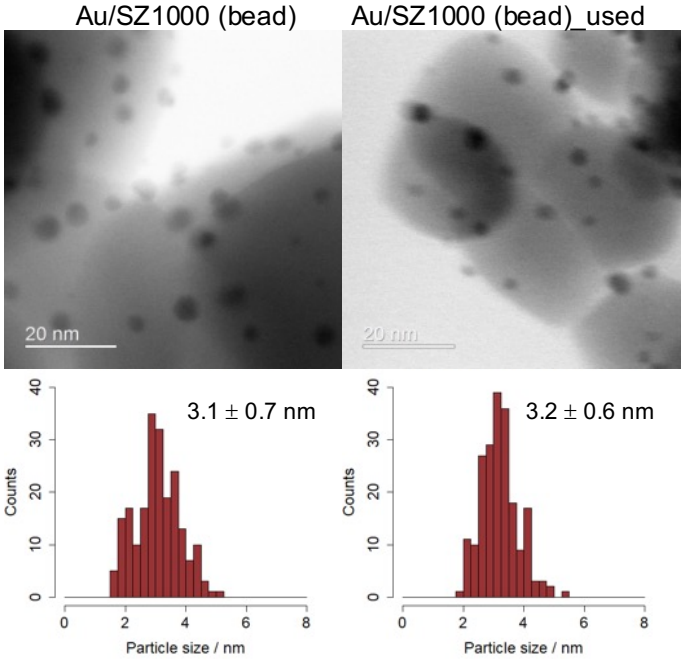

Figure 18. BF-STEM images and of histogram of the particle sizes of the catalysts before and after the flow reaction.

6.4. Conclusion

In conclusion, a practical method for regulating and optimizing the activities of metal-oxide supported Au NP catalysts was developed and investigated, and its effect was verified in the multiple reactions based on the soft Lewis acid function of Au NPs. By comparing the relationship between specific surface areas and catalytic activities of the prepared metal-oxide supported Au NP catalysts, the catalysts with smaller specific surface area showed better catalytic activity. This tread was observed in intramolecular and intermolecular reactions based on the soft Lewis acid function, including isomerization, cyclization, and hydroamination reactions. The effect of surface area shrinkage on mass transfer was also discussed, it was conducted by simply increasing the load densities and comparing their catalytic efficiencies. There is no sufficient evidence to prove that the high activity of Au NPs supported by metal-oxides with low specific surface areas comes from the reduced mass transfer limitation. By comparing the influence of different metal-oxide supports in different specific surface areas on the catalytic activities of the supported Au NPs, changing the specific surface area of the

congeneric metal oxide is even significant than changing the metal oxides. In addition, XPS spectra reveal that the Au NPs supported by the metal-oxides with low specific surface areas tend to have higher binding energy, that is, more $Au^{\delta+}$ species should form on their surfaces. Moreover, this method was successfully applied to enhance the activities of supported Au NP catalyst in the shape of beads and showed practical application value for the industrial catalysts.

6.5. References

[1] M. Haruta, T. Kobayashi, H. Sano, N. Yamada, Chem. Lett. 16 (1987) 405–408.

[2] G. Hutchings, J. Catal. 96 (1985) 292–295.

[3] M. Haruta, N. Yamada, T. Kobayashi, S. Ijima, J. Catal. 115 (1989) 301–309.

[4] M. Khoudiakov, M. C. Gupta, S. Deevi, Appl. Catal. A Gen 291 (2005) 151–161.

[5] J. E. Bailie, H. A. Abdullah, J. A. Anderson, C. H. Rochester, N. V. Richardson, N. Hodge, J. G. Zhang, A. Burrows, C. J. Kiely, G. J. Hutchings, Phys. Chem. Chem. Phys. 3 (2001) 4113–4121.

[6] C. Milone, R. Ingoglia, G. Neri, A. Pistone, S. Galvagno, Appl. Catal. A Gen 211 (2011) 251–257.

[7] T. Mitsudome, M. Yamamoto, Z. Maeno, T. Mizugaki, K. Jitsukawa, K. Kaneda, J. Am. Chem. Soc. 137 (2015) 13452–13455.

[8] A. Taketoshi, M. Haruta, Chem. Lett. 43 (2014) 380–387.

[9] T. Ishida, T. Murayama, A. Taketoshi, M. Haruta, Chem. Rev. 120 (2020) 464–525.

[10] H. Miura, T. Toyomasu, H. Nishio, T. Shishido, Catal. Sci. Technol. 12 (2022) 1109–1116.

[11] S. Zhu, Y. Xue, J. Guo, Y. Cen, J. Wang, W. Fan, ACS Catal. 6 (2016) 2035–2042.

[12] M. Okumura, J. M. Coronado, J. Soria, M. Haruta, J. C. Conesa, J. Catal. 203 (2001) 168–174.

[13] J. Strunk, K. Kähler, X. Xia, M. Comotti, F. Schüth, T. Reinecke, M. Muhler, 359 (2009) 121–128.

[14] S. Hu, W. X. Li, Science 374 (2021) 1360–1365.

[15] S. Chen, A. M. Abdel-Mageed, C. Mochizuki, T. Ishida, T. Murayama, J. Rabeah, M. Parlinska-Wojtan, A. Brückner, R. J. Behm, ACS Catal. 11 (2021) 9022–9033.

[16] Y. Zhang, M. Okumura, X. Hua, A. Sonoura, H. Su, H. Nobutou, X. Sun, L. Sun, F. Xiao, C. Qi, J. Catal. 401 (2021) 188–199.

[17] Y. M. Liu, L. He, M. M. Wang, Y. Cao, H. Y. He, ChemSusChem 5 (2012) 1392–1396.

[18] A. Corma, P. Concepción, I. Domínguez, V. Fornés, M. J. Sabater, J. Catal. 251 (2007) 39–47.

[19] Q. A. Huang, A. Haruta, Y. Kumamoto, H. Murayama, E. Yamamoto, T. Honma, M. Okumura, H. Nobutou, M. Tokunaga, Appl. Catal. B Environ. 296 (2021) 120333.

[20] Q. A. Huang, T. Ikeda, K. Haruguchi, S. Kawai, E. Yamamoto, H. Murayama, T. Ishida, T. Honma, M. Tokunaga, 643 (2022) 118765.

[21] A. Nakayama, R. Sodenaga, Y. Gangarajula, A. Taketoshi, T. Murayama, T. Honma, N. Sakaguchi, T. Shimada, S. Takagi, M. Haruta, B. Qiao, J. Wang, T. Ishida, J. Catal. 410 (2022) 194–205.

Chapter 7.
One-pot synthesis of THF from but-2-ene-1,4-diyl acetate (1,4-DABE) over bifunctional rhodium silica-alumina catalysts

7.1. Introduction

Tetrahydrofuran (THF) is a common raw material used in in the production of poly tetramethylene ether glycol (PTMEG), a component of polyurethane and a great industrial solvent used in Vinyl chloride (PVC), pharmaceuticals and coatings. THF was mainly a product of the petrochemical industry, and about million tons of THF are produced annually. On the other hand, with the deepening of the research on biomass in recent years, the methods using biomass resources have also been developed, and furfural was used as the main raw material[1,2]. In addition, a synthesis method of THF from 1,4-anhydroerythritol (1,4-AHERY), a dehydration product of biomass-derived erythritol was also reported[3]. Although there are many specific processes for the mass production, most are based on C4 base chemicals. For example, in the current Mitsubishi Chemical Corporation (MCC) method[4,5], a four-step process from buta-1,3-diene was used (Fig. 1a). In the process, the buta-1,3-diene was first transformed to but-3-ene-1,2-diyl diacetate (1,4-DABE) through acetoxylation, and subsequent hydrogenation, hydrolysis, and condensation take place to obtain the final product. The yield of each step is relatively high, but the complex process, high investment, and large amounts of wastewater limit the sustainability of the process. Therefore, in addition to using more environmentally friendly raw materials like biomass, sustainable improvements and innovations in existing processes are also of great value. In the MCC method, if the multi-step process of THF could be replaced by a one-pot synthesis, huge economic and environmental benefits could be achieved.

One-pot synthesis method in catalysis requires the catalysts to provide multiple functions simultaneously[6,7]. Considering the unit step in the current MCC method, the acid function and hydrogenation function of catalysts should play dominant roles; thus, bifunctional heterogeneous catalysts need to be developed. The general concept of bifunctional heterogeneous catalysis is that there are two distinct types of active sites that function in tandem. Normally, the two sites are expected to catalyze different steps within an overall reaction. In principle, the two sites could participate in the same step, for example, acting on different parts of the adsorbed reactant molecule, as in a

consistent reaction [8]. In fact, bifunctional catalysts have been widely researched in various direct synthesis of valued-added chemicals, such as hydrodeoxygenation[9,10], hydroisomerization[11,12], and dehydrocyclization[13,14].

A typical model of bifunctional catalysts was metal species supported by zeolites or mesoporous materials with rich porosities and acidities [15–18]. Noble metals (Pt, Pd, Ru, Rh) and transition metals (Ni, Co, Fe) were widely used as active hydrogenation centers, and even show great efficiencies under low metal loadings. Therefore, supported bifunctional catalysts should consist of active metal nanoparticles with hydrogenation capacities and supports of zeolite or mesoporous materials. In addition, the synergistic effect of metal and zeolite/mesoporous materials over bifunctional catalysts was normally existed and the adjustment to specific chemical reaction pathway could enhance the conversion and the selectivity of final products. [19–22].

Herein, a direct one-pot synthesis method of THF from 1,4-DABE was realized using bifunctional catalysts Rh^0/Al-MCM-41 (Fig. 1b). A yield around 60% was obtained using the optimized catalysts, and another main product was butane-1,4-diyl diacetate (1,4-DAB) in a yield around 30%, which could be further used in the synthesis of THF. The characterization over the catalysts showed that supported Rh nanoparticles (NPs) were in small sizes and highly dispersed. In addition, a synergistic effect in the acidity occurred, the loading of Rh NPs enhanced the strong acid sites.

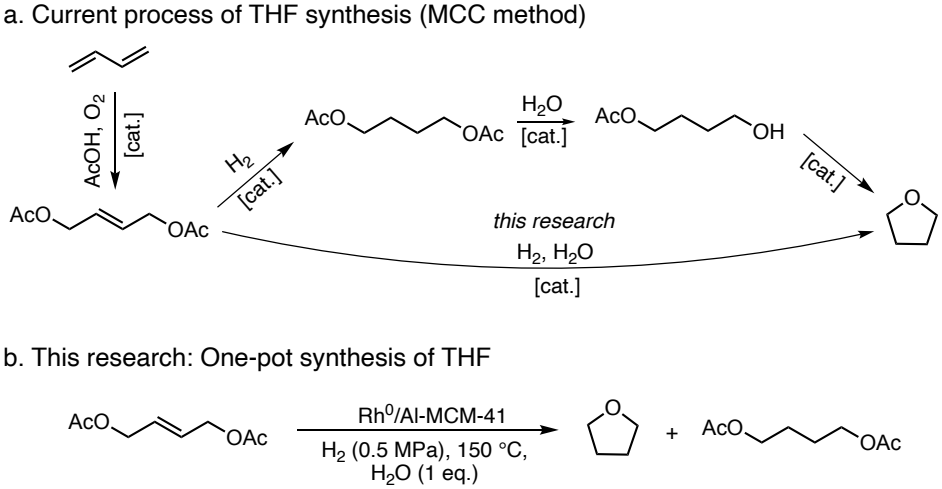

Figure 1. The current MCC process (a) and the new one-pot process (b) to THF synthesis.

7.2. Experimental

7.2.1. Materials

Rhodium(III) chloride trihydrate ($RhCl_3 \cdot 3H_2O$) and ruthenium(III) chloride trihydrate ($RuCl_3 \cdot 3H_2O$) were purchased from Sigma Aldrich Ltd. Chloroplatinic acid hexahydrate ($H_2PtCl_6 \cdot 6H_2O$) was purchased from Furuya Metal Co., Ltd. Palladium nitrate ($Pd(NO_3)_2$) were purchased from Tanaka Precious Metals Co., Ltd. Nickel(II) nitrate hexahydrate ($Ni(NO_3)_2 \cdot 6H_2O$), Cobalt(II) nitrate hexahydrate ($Co(NO_3)_2 \cdot 6H_2O$), and Iron(III) nitrate enneahydrate ($Fe(NO_3)_3 \cdot 9H_2O$) were purchased from FUJIFILM Wako Pure Chemical Corp.

Al-MCM-41 and Mont-K10 were purchased from Sigma Aldrich Ltd. Al_2O_3 (JRC-ALO-10), Nb_2O_5 (JRC-NBO-1), and MgO (JRC-MGO-4, A2000) were reference catalysts supplied by the Catalysts Society of Japan. HS690 was purchased from Daiichi Kigenso Kagaku Kogyo Co., Ltd. SiO_2 (CARiACT Q-10) was purchased from Fuji Silysia Ltd. 1,4-DABE was provided by Mitsubishi Chemical Corporation and used as received. Hydrotalcite was purchased from FUJIFILM Wako Pure Chemical Corp.

7.2.2. Preparation of catalysts

Supported catalysts with a loading of 1 wt% were generally prepared by the impregnation method. The precursor was dissolved in distilled water (The amount of distilled water used for different supports was as follows. Mont-K10: 0.5 mL; Al-MCM-41: 1 mL; Al_2O_3: 1.5 mL; SiO_2: 1.5 mL; HS690: 1 mL; Nb_2O_5: 0.5 mL; Hydrotalcite: 1 mL; MgO: 0.5 mL). The support power (1.0 g) was added to the solution, and the mixture was stirred for 20 min at room temperature. After the impregnation was completed, residual distilled water was removed by drying at 70 °C overnight. The catalysts were calcined at 400 °C for 2 h. Then they were reduced in a flow of H_2 (20 mL/min) at 300 °C for 1 h. The obtained catalysts were directly used for catalytic reactions without further treatment.

In the preparation of Pt/Al-MCM-41 and Pd/Al-MCM-41, H_2PtCl_6 aqueous

solution (Pt: 20 g/L; 505 μL) or $Pd(NO_3)_2$ aqueous solution (Pd: 200 g/L, 51 μL) was diluted in 1 mL distilled water. Al-MCM-41 (1.0 g) was added to the aqueous solution, and the following procedures were the same as those of the general method.

Ni/Al-MCM-41, Co/Al-MCM-41, and Fe/Al-MCM-41were prepared by the same method, and changed temperatures of 600 °C, 300 °C, and 600 °C were used in the reduction process, respectively, which were determined by the temperature-programmed reduction of H_2 (H_2-TPR)

7.2.3. Characterization

High-angle annular dark-field scanning transmission electron microscopy (HAADF-STEM) images were performed with a JEOL JEM-ARM200F. H_2-TPR was performed by a BELCAT instrument equipped with a thermal conductivity detector (TCD). Temperature-programmed desorption of NH_3 (NH_3-TPD) was measured by a BELCAT instrument equipped with a BELMASS quadrupole mass spectrometer. 200g catalyst was placed in a glass tube and pretreated at 250 °C for 1 h under a He flow. The adsorption of NH_3 was performed at 100 °C for 1 h with a flow 5% NH_3 in He at 50 mL/min. Then a flow of He at 50 mL/min was performed at 100 °C for 1 h. During the test, the samples were heated to 800 °C at 10 °C /min, under a He flow of 50 mL/min. The mass spectrometer for NH_3 desorption was collected by m/z = 17.

Conversions and yields of the compounds discussed were detected by gas chromatography (GC) using an Agilent GC 6850 Series II instrument equipped with a flame ionization detector (FID) and a J&W HP-1 column. GC mass spectrometry (GC-MS) analysis was performed to determine the products using a Shimadzu GCMS-QP2010 SE.

7.2.4. General Procedure for the Catalytic Reactions

A mini-autoclave (10 mL) was charged with 1,4-DABE (1 mmol), catalysts (50 mg), distilled water (1 mmol), and a magnetic stirring bar. Then, the autoclave was purged and filled with H_2 until the pressure reached 0.5 MPa, and then stirred at 150 °C for 24 h. After the reaction, the mixture was filtered, and the filtrate was analyzed by GC using tridecane as an internal standard.

7.3. Results and conclusions

In the catalyst screening section, mesoporous materials supported Ru NPs was examined (Table 1, entries 1–6). High conversions were obtained when using these catalysts, and a yield of 50% was achieved over the Ru/Mont-K10 catalysts for 48 h. However, limited yields of THF were obtained with the Ru/Al_2O_3 and Ru/SiO_2, which should be caused by the relatively low acidities compared with those of Ru/Mont-K10 and Ru/Al-MCM-41. In addition, supported Rh NPs catalysts were also investigated (entries 7–9), and Rh/Al-MCM-41 showed a yield of 55%.

Table 1. Catalyst screening for the one-pot synthesis of THF from 1,4-DABE.

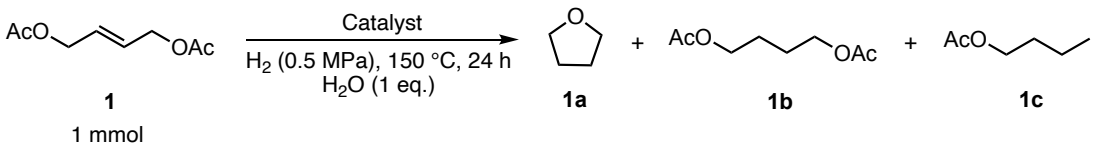

1 (1 mmol) → **1a** + **1b** + **1c**

Entry	Catalyst	Conv.[a]/%	Yield(**1a**)[a]/%	Yield(**1b**)[a]/%	Yield(**1c**)[a]/%
1	Ru/Mont-K10	>99	29	33	12
2[b]	Ru/Mont-K10	>99	50	10	17
3	Ru/Al-MCM-41	>99	28	41	13
4[b]	Ru/Al-MCM-41	>99	33	21	15
5	Ru/Al_2O_3	91	3	49	18
6	Ru/SiO_2	96	n.d.	50	26
7	Rh/Mont-K10	>99	20	29	23
8	Rh/Al-MCM-41	99	55	33	9
9[c]	Rh/Al-MCM-41	98	21	37	14
10	Pt/Al-MCM-41	99	12	25	33
11	Pd/Al-MCM-41	97	1	12	7
12	Ni/Al-MCM-41	>99	33	7	12
13	Co/Al-MCM-41	>99	7	13	12
14	Fe/Al-MCM-41	98	11	22	13

[a] Determined by GC analysis using tridecane as an internal standard.

[b] Reaction time: 48h

[c] Catalyst: 25 mg

Moreover, other metals, such as Pt, Pd, Ni, Co, and Fe with reduction capacities were also examined based on the Al-MCM-41 support (entries 10–14). However, only low yields were obtained with Pt/Al-MCM-41 and Pd/Al-MCM-41 catalysts. On the other hand, Ni/Al-MCM-41 provided a yield of THF in 33%, which was higher than that of Ru/Al-MCM-41. No satisfactory yields were obtained when the Co/Al-MCM-41 and Fe/Al-MCM-41 were tested. In addition to the target product THF and intermediate 1,4-DAB, a byproduct butyl acetate (BUA) was also detected. The highest selectivity of THF AND 1,4-DAB was realized with the Rh/Al-MCM-41 among the examined catalysts.

Because of the great yield of Rh/Al-MCM-41 in the initial screening, a further investigation on the supports was conducted (Table 2). Considering the properties of the supports, the high strong Brønsted acidity and high specific surface area seem to facilitate the reaction. In addition, no production of THF was detected when using the catalysts prepared from basic supports.

Table 2. Results of the one-pot synthesis from 1,4-DABE using Rh NPs on different supports.

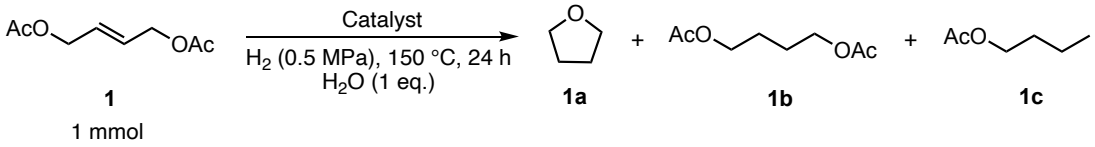

1 (1 mmol) **1a** **1b** **1c**

Entry	Catalyst	Conv.[a]/%	Yield(**1a**)[a]/%	Yield(**1b**)[a]/%	Yield(**1c**)[a]/%
1	Rh/Al-MCM-41	99	55	33	9
2	Rh/Mont-K10	>99	20	29	23
3	Rh/HS690	99	17	31	15
4	Rh/Nb_2O_5	99	13	20	23
5	Rh/Hydrotalcite	>98	n.d.	9	13
6	Rh/MgO	98	n.d.	27	23

[a] Determined by GC analysis using tridecane as an internal standard.

Because the Rh/Al-MCM-41 showed superior activity in this one-pot synthesis of THF from 1,4-DABE. The morphology and particle size distribution of the optimized

Rh/Al-MCM-41 catalysts were measured by HAADF-STEM (Fig. 2). A narrow distribution of Rh NPs within 0.5 to 2 nm reveals that the Rh NPs were high dispersed on the surface of Al-MCM-41, and the average particle size was 1.3 nm.

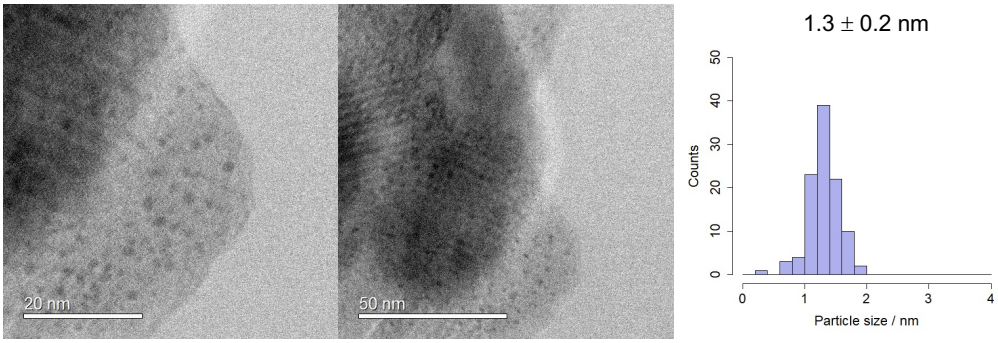

Figure 2. BF-STEM images and histograms of the particle sized of Rh/Al-MCM-41.

Afterwards, the effect of hydrogen pressure in the one-pot synthesis of THF was investigated with Rh/Al-MCM-41 (Fig. 3). A hydrogen pressure of 0.5 MPa brought the best THF yield and selectivity within the pressure range from 0.1 to 5.0 MPa. The results showed that a yield a 51% could be obtained even under 0.1 MPa. In addition, with the increase of hydrogen pressure, the yields of THF and 1,4-DAB decreased to a certain extent. On the contrary, the yield of byproduct BUA decreased along with the increased hydrogen pressure.

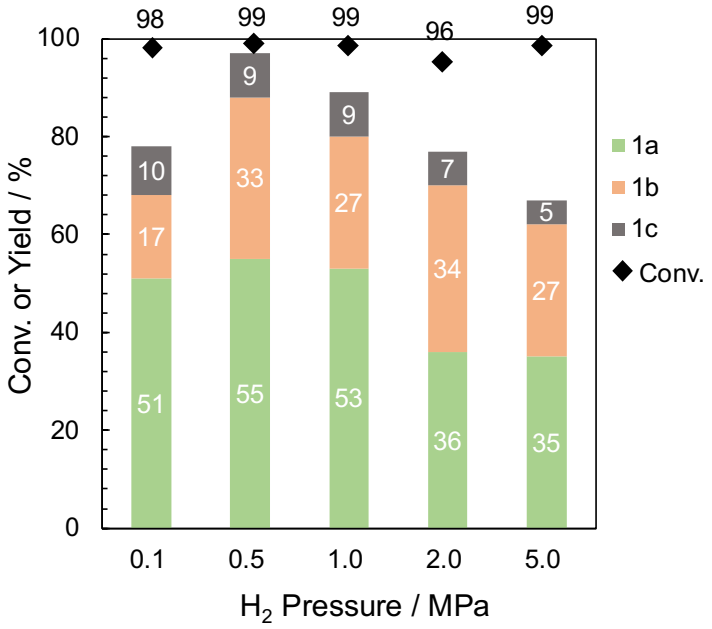

Figure 3. Effect of hydrogen pressures (relative pressure).

In addition, discussion on the reaction temperatures was carried out to further optimize the reaction condition (Table 3). At a reaction temperature of 30 °C, 90% yield of 1,4-DAB was obtained, and no THF was detected. When the reaction temperature increased to 100 °C, the production of THF was still not detectable. Moreover, at a reaction temperature of 170 °C, 60 % yield of THF was achieved. It was discovered that the hydrogenation of 1,4-DABE could occur around room temperature, and the hydrolysis and condensation should require a high reaction temperature.

Table 3. Effect of reaction temperatures in the one-pot synthesis of THF from 1,4-DABE using Rh/Al-MCM-41.

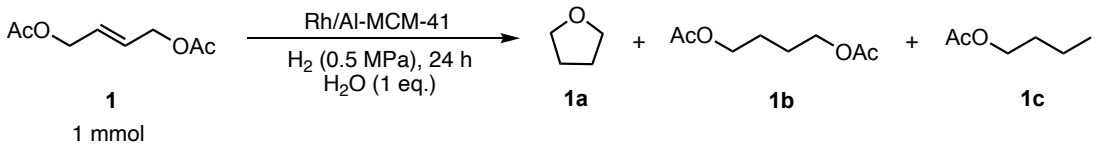

Entry	Temperature/°C	Conv.[a]/%	Yield(**1a**)[a]/%	Yield(**1b**)[a]/%	Yield(**1c**)[a]/%
1	30	99	n.d.	90	6
2	100	92	n.d.	49	19
3	150	99	55	33	9
4	170	98	60	13	13

[a] Determined by GC analysis using tridecane as an internal standard.

Because the hydrogenation reaction was relatively easy to go, compared with the following hydrolysis and condensation, a discussion was performed to optimize the Rh loading amount to determine if the loading amount can be reduced to improve the atomic efficiency and cost of the noble metal (Fig. 4). When the Rh loading amount was 0.25 wt%, the conversion was relatively low, and a yield of only 18% for THF was obtained. With the Rh loading amount increasing to 1.0 wt%, the yield of THF increased up to 55%. Similar results were available when the Rh loading amount was 1.0 wt% and 2.0 wt%. As the Rh loading amount further increased to 4.0 wt%, decrease in THF yield was observed. These results reveal that the high yield of THF should be related to the synergistic effect from Rh NPs and the Al-MCM-41support. The supported Rh NPs

not only acted on the hydrogenation process, but also promotes the hydrolysis and condensation.

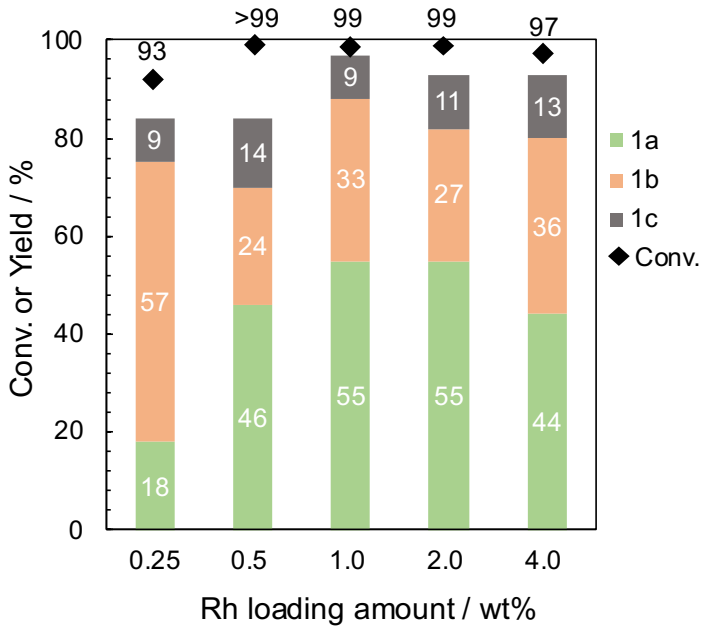

Figure 4. Discussion on the Rh loading amounts in the one-pot synthesis of THF from 1,4-DABE using Rh/Al-MCM-41.

Furthermore, a NH_3-TPD measurement was performed on the Rh/Al-MCM-41 catalysts with various Rh loading amounts to investigate the effect of acid sites in this reaction (Fig. 5). In the result of reference sample Al-MCM-41, two peaks of NH_3 desorption were observed at the weak and strong acid sites. With the loading of Rh NPs, the NH_3 desorption peaks at high temperatures, which were considered strong acid sites, shifted to higher temperatures, and no obvious changes occurred at low temperatures, which were considered weak acid sites. This revealed that the loading of Rh NPs promoted the enhancement of acidity at the strong acid site. However, the great reaction results of 1 wt% and 2 wt% Rh/Al-MCM-41 and the relative bad reaction results of 0.25 wt%, 0.5 wt% and 4 wt% Rh/Al-MCM-41 further support that an opportune strong acid site was significant in this reaction.

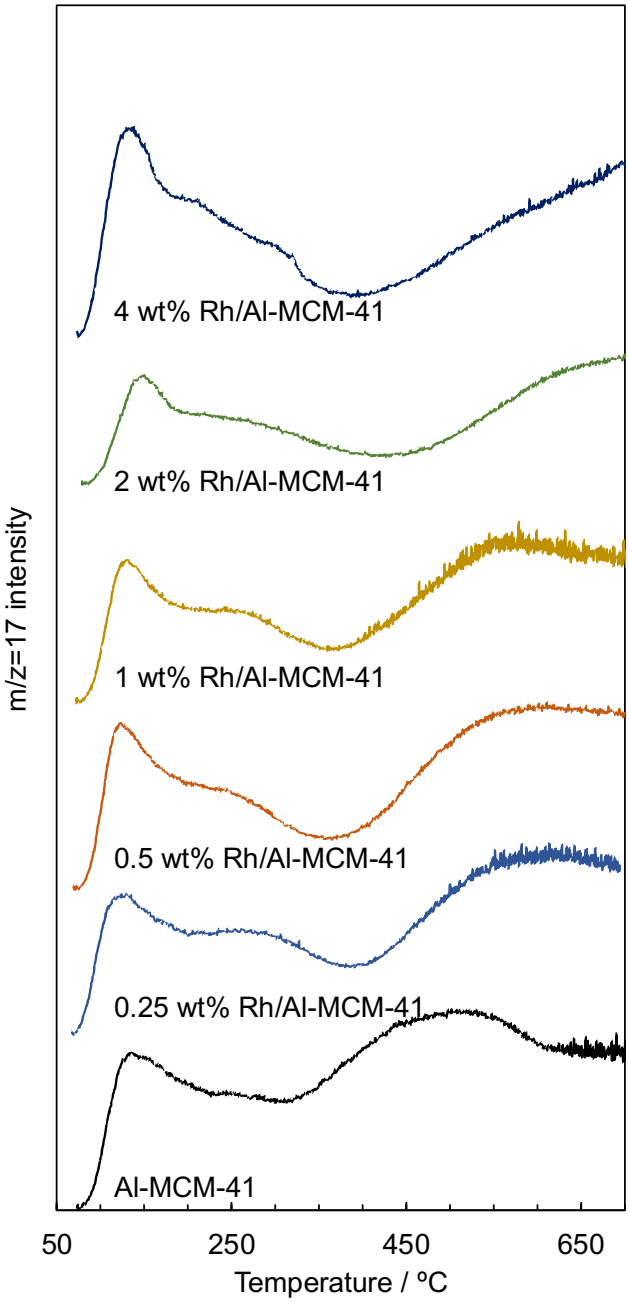

Figure 5. NH_3-TPD profiles of Rh/Al-MCM-41 with different Rh loading amounts (m/z=17).

7.4. Conclusion

In conclusion, a direct one-pot synthesis method of THF from 1,4-DABE was developed over bifunctional catalysts Rh^0/Al-MCM-41 (Fig. 1b). A maximum yield around 60% was obtained using the optimized catalysts, and another main product was 1,4-DAB in a yield around 30%, which was an intermediate in the synthesis of THF.

The characterization over the catalysts showed that supported Rh NPs were in small sizes and highly dispersed. In addition, a synergistic effect in the acidity was discovered, and the loading of Rh NPs enhanced the strong acid sites.

7.5. Reference

[1] X. Li, P. Jia, T. Wang, ACS Catal. 6 (2016) 7621–7640.

[2] P. Khemthong, Chakrit Yimsukanan, T. Narkkum, A. Srifa, T. Witoon, S. Pongchaiphol, S. Kiatphuengporn, K. Faungnawakij, Biomass and Bioenergy 148 (2021) 106033.

[3] N. Ota, M. Tamura, Y. Nakagawa, K. Okumura, K. Tomishige, Angew. Chem. 127 (2015) 1917–1920.

[4] M. Misono, Appl. Catal. 64 (1990) 1–30.

[5] Y. Izawa, T. Yokoyama, 1,4-Butanediol from 1,3-Butadiene, (2016) 159–171.

[6] M. J. Climent, A. Corma, S. Iborra, Chem. Rev. 111 (2011) 1072–1133.

[7] R. Calmanti, M. Selva, A. Perosa, Green Chem. 23 (2021) 1921–1941.

[8] A. M. Robinson, J. E. Hensley, J. W. Medlin, ACS Catal. 6 (2016) 5026–5043.

[9] X. Wu, Q. Sun, H. Wang, J. Han, Q. Ge, X. Zhu, Catal. Today 355 (2020) 43–50.

[10] S. Kim, E. Kwon, Y. T. Kim, S. Jung, H. J. Kim, G. W. Huber, J. Lee, Green Chem. 21 (2019) 3715–3743.

[11] W. Wang, C. J. Liu, W. Wu, Catal. Sci. Technol. 9 (2019) 4162–4187.

[12] Y. Tan, W. Hu, Y. Du, J. Li, Appl. Catal. A Gen 611 (2021) 117916.

[13] S. Kasipandi, J. W. Bae, Adv. Mater. 31 (2019) 1803390.

[14] J. Fling, I. Wang, J. Catal. 130 (1991) 577–587.

[15] R. Otomo, T. Yokoi, J. N. Kondo, T. Tatsumi, Appl. Catal. A Gen 470 (2014) 318–326.

[16] Y. Ji, Z. Zhao, D. Xiao, Q. Han, H. Chen, K. Gong, K. Chen, X. Han, X. Bao, G. Hou, Nat. Catal. 5 (2022) 594–604.

[17] K. K. Sharma, T. Asefa, Angew. Chem. Int. Ed. 46 (2007) 2879–2882.

[18] F. X. Zhu, W. Wang, H. X. Li, J. Am. Chem. Soc. 133 (2011) 11632–11640.

[19] Y. Shi, E. Xing, K. Wu, J. Wang, M. Yang, Y. Wu, Catal. Sci. Technol. 7 (2017) 2385–2415.

[20] M. V. Bykova, D. Y. Ermakov, V. V. Kaichev, O. A. Bulavchenko, A. A. Saraev, M. Y. Lebedev, V. A. Yakovlev, Appl. Catal. B Environ. 113 (2012) 296-307.

[21] R. N. Olcese, M. Bettahar, D. Petitjean, B. Malaman, F. Giovanella, A. Dufour, Appl. Catal. B Environ. 115 (2012) 63-73.

[22] N. T. T. Tran, Y. Uemura, S. Chowdhury, A. Ramli, Appl Catal A Gen 512 (2016) 93-100.

Concluding Remarks

In this doctoral thesis, the author systematically studied the soft Lewis acid function in supported noble metal nano-catalysts for sustainable synthesis.

In chapter 1, general introduction of the soft Lewis acid catalysis and the development of supported noble metal catalysts was conducted. It was pointed out that the sustainable synthesis could be realized by the application of active and stable heterogeneous catalysts.

In chapter 2, Pt/CeO_2 with residual chloride was proved to act as soft Lewis acids and facilitate the efficient isomerization of allylic esters.

In chapter 3, reusability and deactivation mechanism of this Pt catalysts were investigated, and a great reactivation method was also developed.

In chapter 4, a facile solvent-free methodology was developed for isomerization of allylic esters with supported Au NPs catalysts, which showed superior catalytic activity and stability. Lifetime and stability of the optimized catalyst were evaluated by a 14-day flow reaction in the scale of kilogram, and no obvious deactivation occurred.

In chapter 5, a sustainable catalytic system for the intramolecular cyclization of alkynoic acids by using Na-salt-modified Au NPs supported on monoclinic ZrO_2 was realized, and the positive and significant role of the Na salt in this reaction was disclosed.

In chapter 6, a practical method for regulating and optimizing the activities of metal-oxide supported Au NP catalysts was well investigated. The catalysts with smaller specific surface area showed better catalytic activity, and this tread was obtained in the soft Lewis acid reactions, including isomerization, cyclization, and hydroamination reactions

In chapter 7, one-pot synthesis of THF was also developed to further enhance the sustainability of the C4 synthesis process.

These works highlighted that supported noble metal catalysts could be used as active and stable soft Lewis acid catalyst in multiple valuable reaction, and their activities could be controlled and optimized, and even be reactivated.

Acknowledgment

I would like to express my deepest appreciation to all those who helped me to complete this thesis. A special gratitude I give to my supervisors, Prof. Makoto Tokunaga, Associate Prof. Haruno Murayama and Assistant Prof. Eiji Yamamoto who provided me with the chance to study at Kyushu University and supported me for carrying out my research smoothly. I also want to acknowledge the help and care from all the students in Tokunaga Lab.

I would like to thank Dr. Tetsuo Honma for his guidance about XAFS measurements and result in analysis. I also want to express my thanks to Prof. Mitsutaka Okumura and Prof. Tamao Ishida for their collaboration on DFT calculation and CO-DRIFT measurements, respectively. In addition, I want to thank Mitsubishi Chemical Corporation for the financial support of the research on isomerization reaction.

My gratitude also extends to all the professors, secretaries, and students in the Advanced Graduate Course on Molecular Systems for Devices.

Finally, I would like to express my gratitude to my family members and my friends for their kind encouragement and support.

List of Publication

[1] Z Zhang, T Mamba, **Q.-A Huang**, H Murayama, E Yamamoto, T Honma, M Tokunaga, The Additive Effect of Amines on the Dihydroxylation of Buta-1,3-diene into Butenediols by Supported Pd Catalyst, Mol. Catal., 2019, 475, 110502.

[2] **Q.-A Huang**, A Haruta, Y Kumamoto, H Murayama, E Yamamoto, T Honma, M Okumura, H Nobutou, M Tokunaga, Pt/CeO_2 with Residual Chloride as Reusable Soft Lewis Acid Catalysts: Application to Highly Efficient Isomerization of Allylic Esters, Appl. Catal. B Environ., 2021, 296, 120333.

[3] **Q.-A Huang**, T Ikeda, K Haruguchi, S Kawai, E Yamamoto, H Murayama, T Ishida, T Honma, M Tokunaga, Intramolecular Cyclization of Alkynoic Acid Catalyzed by Na-salt-modified Au Nanoparticles Supported on Metal Oxides, Appl. Catal. A Gen, 2022, 643, 118765.

[4] **Q.-A Huang**, H Murayama, E Yamamoto, T Honma, M Tokunaga, Investigation of Reusability and Deactivation Mechanism of Supported Platinum Catalysts in the Practical Isomerization of Allylic Esters, Catal. Today, 2023, 410, 215–221.

[5] **Q.-A Huang**, H Murayama, E Yamamoto, A. Nakayama, T Ishida, T. Honma, M Tokunaga, Engineering Active and Stable Au/ZrO_2 Catalysts for Isomerization of Allylic Esters: A Practical Application of Gold Catalysis, (in preparation)

[6] **Q.-A Huang**, H Murayama, E Yamamoto, M Tokunaga, Effect of the Structure of Metal Oxide Support on the Activity of Supported Au Nanoparticles in Soft Lewis Acid Catalysis, (in preparation)

[7] **Q.-A Huang**, M. Takaki, H Murayama, E Yamamoto, M Tokunaga, L. X. Dien, T. Ishida, T. Honma, N. V. Tzouras, T. Scattolin, S. P. Nolan, Supported Gold

Nanoparticles Prepared from NHC-Au Complex Precursors as Reusable Heterogeneous Catalysts, (in preparation)

[8] **Q.-A Huang**, H Murayama, E Yamamoto, M Tokunaga, One-pot Synthesis of THF from But-2-ene-1,4-diyl acetate (1,4-DABE) over Bifunctional Rhodium Silica-alumina Catalysts, (in preparation)